# DEVELOPMENT AND VALIDATION OF A SPATIAL PREDICTION MODEL FOR FORENSIC GEOGRAPHICAL PROVENANCING OF HUMAN REMAINS

A thesis submitted to the

**School of Chemistry**

of the

**University of East Anglia**

in partial fulfilment of the requirements for the degree of

**Doctor of Philosophy**

By

**Robert Geoffrey Posey**

November 2011

# Abstract

The number of human remains found annually that are still unidentified after investigation using conventional means is unacceptable. The main objective of this thesis has been to develop a set of new forensic human identification tools that will help to reduce the number of remains that go unidentified each year. Stable and radiogenic isotopes and trace elements found in human tissue can provide a chemical 'history' of an individual's origin and migration during life. This information may prove invaluable in a forensic investigation. Application of isotopic and elemental intelligence for forensic human identification is in its infancy and to date there are no validated published spatial prediction isotope models (isoscapes) for human tissue other than for hair [1]. In this study, a collection (adult) human teeth originating from 5 countries (Iran, Iraq, Oman, UAE and Yemen) in the Middle East were analysed for their oxygen and strontium isotopic and trace elemental composition. The results yield information about the spatial isotopic variation in the Middle East and show great potential for isotopic and trace element information as a forensic tool. The major fruits of this thesis are: the derivation of a model describing the relationship between drinking water and tooth enamel carbonate oxygen isotope compositions, and the development of new tooth enamel oxygen and strontium isoscapes for the Middle East. A multivariate trace element model has also been produced for the Middle East. All the models have been shown to improve the likelihood of identifying the origin of human remains, particularly when the methods are combined. Also investigated in this thesis is a new probabilistic approach for the presentation of spatial isotopic data that will greatly facilitate the presentation of isotopic evidence in the courtroom.

*Destitutus ventis, remos adhibe*

If the wind will not serve, take to the oars.

*Latin Proverb*

# Acknowledgements

The last three and a half years have been draining, tiring, emotional and mentally exhausting. In short, they have been the best years of my life. I have a lot of people to thank for not only getting me through these tough years but for making them so much damn fun. I hope I can do them justice in this short section of my thesis.

Firstly to my family. Thank you for always being there for me. You have fed me, clothed me, housed me and financed me. We have laughed together and cried together and we have got through some tough times stronger than we started. Most of all you have been there when I needed you most. I am lucky enough to have a big family: parents and step parents, an amazing sister, step siblings and adopted siblings, grandparents and step grandparents. I cherish you all and hope that I make you proud. I couldn't have done it without you all.

Of course, I have been at the University of East Anglia now for over seven years and Norwich has become home for me thanks to my second family - the friends that I have made in Norwich over the years. We have had so many amazing adventures together that I would need to write another book to mention them all. In fact my circle of friends is probably a psychology thesis waiting to happen! Hannah and Paul, we have known each other almost 8 years now and I don't think we have ever had an argument. You guys are the best friends that I could ask for. You have always been there to make me smile and we have had some great times together. Not living near you guys is going to be the worst thing about leaving Norwich. Emma, I couldn't have done this without you. Steph, you

crazy, crazy American. You are awesome. Thank you for all the laughs, the drunken nights out, the drunken nights in and generally just making my life so much more fun for the last three and a bit years. To all the other great friends that I have made over the past seven years, I love you all.

Finally I want to thank all those people who made this research possible and who have supported me both inside and outside the lab. Jurian, thank you for giving me the chance to do this PhD. I greatly appreciate the advice and support you have offered over the last 4 or so years. I hope that everything goes well for you in New Zealand and maybe I shall see you over there in the future. Henriette, without you I don't think any of us would have got any results! Thank you for being a great lab manager and for always being there with a smile and friendly advice when we needed it. You were truly the heart of the CFP. To Hilary, Ana, Scotty and all of the undergraduate students who have worked with and around me during my PhD. Thank you for making the CFP a great place to come and work. It has not always been the calmest of working environments (especially when the instruments were playing up) but it has always been fun. It has been a pleasure working with you all. Alina, thank you for all of your help with the stable isotope measurements. I think of all my PhD I have enjoyed learning stable isotope geochemistry the most. Also thank you for being a patient supervisor and for trawling through pages of my thesis for me. Andrew, thank you for your help and advice, particularly in these last months. You have really helped to focus me during the last stage of this thesis, when my motivation and energy have been at their lowest. Thanks to Graham for all his help with the laser ablation work. Khudooma, thank you for access to the teeth samples, without them there would be no thesis. Thank you IsoMAP, for kindly funding my attendance at the Isoscapes conference this year. Thank you to the EPSRC for funding this project. Thank you to Wolfram and Paul for their invaluable feedback during my viva and for helping me craft the final thesis. Finally thank you to the UEA, I shall miss you but after 7 years it is time for me to 'Do Different'.

# Contents

# List of Tables

# List of Figures

# Chapter 1

# Introduction

## 1.1 Unidentified human remains: ‘A mass disaster over time’

At the end of 2010, the bodies of 989 individuals found in the UK over the past 60 years remained unidentified by conventional means [4].

The requirement for additional research into forensic human identification has been highlighted in the past decade by a number of mass disasters that have shocked the world. The terrorist attack on the World Trade Centre on September 11, 2001 left 2,749 dead, 1,100 of whom remain unidentified after the forensic effort ended in 2005 [5]. More recently, the devastating Tohoku earthquake that hit Japan in March 2011 claimed 15,642 lives with 5,001 missing or unaccounted for [6]. With losses like these occurring in isolated disasters, it is easy to overlook the scale of the problem occurring every day. According to the National Policing Improvement Agency - Missing Persons Bureaus [7], around 15 new unidentified body cases are recorded each month in the UK. A short study by Cattaneo [8], illustrated that from eight European countries (Denmark, Finland, Greece, Ireland, Portugal, Luxembourg, Spain and Germany), of the 3035 cases involving unidentified human remains between 1994 - 1998 almost one third (807) of the individuals remain

unidentified. Nancy Ritter [9], suggests that in the US alone there are more than 40,000 sets of human remains held in evidence rooms that cannot be identified by 'conventional means'.

The reason for the high number of human remains that are unidentified globally can be attributed to a number of confounding factors. Forensic resources and personnel involved in the identification of human remains are overwhelmed by the number of cases [8, 9, 10]. Commonly used techniques such as DNA, fingerprinting and comparison of dental records rely heavily on reference databases such as the Combined DNA Index System (CODIS) in the US and the National DNA database in the UK. These databases are heavily biased towards convicted criminals hence a large number of unidentified remains do not appear in the databases. DNA evidence may also become degraded with time and become unmeasurable. This is particularly true if the individual has been buried for a long period of time as is often the case in mass graves from war crimes such as those from the Spanish Civil War.

Identification is further complicated by the fact that the majority of the modern human population has access to international transportation which has led to diverse multicultural populations in many countries around the world. Keeping track of such rapidly changing populations is near impossible and unidentified remains can no longer be assumed to have originated locally, or even nationally in a great number of cases. Of course it is often the relatives who suffer worse when a family member goes missing or when a body cannot be identified from a mass disaster. They are left not knowing whether their loved one will return or if they will ever be given a proper burial. In criminal cases it is very difficult to prosecute when the victim cannot be identified, hence justice cannot be served.

Analysis of stable and radiogenic isotope composition and trace element concentrations in human tissue can provide forensic investigators with additional information that may prove vital in the identification of unknown remains. Due to chemical and environmental processes that shall be discussed later in this thesis, the isotopic and trace element composition of human tissue varies spatially across the globe so that analysis of these signals

may allow an unknown individual to be linked to a geographic region.

## 1.2 Research objectives

The number of human remains found annually, that remain unidentified is unacceptable and highlights the need for the development of new forensic tools. Therefore the main objective of this thesis is to produce a new forensic tool for the identification of origin of unidentified remains. This new tool shall be based on the isotopic and elemental composition of human tooth enamel.

In order to achieve this objective, this thesis aims to determine the extent to which it is possible to predict the origin of unidentified human remains based on the oxygen and strontium isotope and trace element 'fingerprint' stored in tooth enamel. This is not a novel question in itself, as strontium and oxygen isotopes in particular have been used for over a decade in archaeological studies to identify migration patterns of ancient populations ([11, 12, 13], see Chapters 2 and 3). However the application and the methods of data analysis used in this thesis offer an innovative approach to the provenancing of modern human remains. Only a handful of studies have attempted to apply these techniques to modern humans and those based on ancient populations are generally limited to small geographical regions. This thesis aims to answer some of the questions that are not answered by these previous studies and provide the first example of a spatial prediction model based on the isotopic and trace element composition (isoscape, [14]) of modern human tooth enamel. Most previous examples in the forensic literature have been based on individual case studies, focused on a small geographical area [15, 16, 17, 18]. These studies have mainly compared values measured in the sample of interest to a number of reference samples from possible locations of origin, selected based on forensic intelligence. There are currently no published spatial models for the prediction of origin of human tissue except for $\delta^{18}$O and $\delta$D in human hair from the US [1].

This thesis attempts to examine the spatial isotopic and elemental variation in tooth enamel

samples from the Middle East and to use the information gathered to produce the first spatial exclusion models (isoscapes, [14]) for the determination of origin of unidentified human remains in the study region. This is an area of interest for a number of reasons that will be discussed further in Section 1.6. The thesis will also consider the way in which isotopic and trace element data are presented. Until recently isotopic information gathered in a forensic investigation has been used for intelligence purposes but is not necessarily presented in court. This study will use statistical methods currently being employed for the tracking of bird migration [19, 20] in order to transform spatial isotopic data into spatial probability of origin. By presenting isotopic evidence as a probability or likelihood it is more likely to be understood by a jury and is therefore more likely to be admissible in a court of law. This is the first example of a 'probability landscape' being produced to present isotopic data from human bone and tooth material.

## 1.3 Research assumptions

A number of assumptions have been made when producing the various spatial models presented in this thesis. These will be covered in the relevant chapters. However a number of general assumptions have to be made that cover the extent of this thesis and may apply to other isotopic and elemental studies of human remains.

The main difficulty that arises from the provenancing of modern human tissue samples based on the isotopic and trace element analysis is that these signals are determined by the diet consumed by an individual. In today's developed modern society, particularly in the western world where people have convenient access to food in supermarkets, individuals have a much wider choice of food products than they did just 100 years ago. Non-local foods, imported foods and mass produced foods are now all commonly available to the modern consumer thanks to improved transportation and food preservation methods. As will be discussed further in Section 1.5.1 consumption of non-local food products could lead to a significant shift in isotopic composition of human tissue, limiting the extent to

which an isotopic signature could be linked to a geographical region. The scale of the isotopic shift will depend largely on the proportion of non-local food consumed and will be different for different cultural populations (see Section 1.5.1).

For the purpose of this study, an assumption has been made that the main source of hydration of the sampled individuals, including water for washing and food preparation, will have come mainly from local water sources and that at least a proportion of the diet consumed will have originated locally. The validity of this assumption should be fairly easy to determine as if individuals are not consuming local water and food then one would expect no spatial pattern in the isotopic or elemental values.

The second assumption is that due to the Middle East teeth samples being modern, they will not have undergone any diagenesis that may alter analytical measurements and that any surface contamination has been removed by the sample pre-treatment. This is a reasonable assumption as none of the samples used in this study have ever been buried or submerged in a reactive aqueous environment so there has been no opportunity for contamination or secondary mineralisation that has been shown to lead to a change in isotopic or elemental composition in archaeological samples [21].

A third assumption is that the location of origin provided by the sampled individuals is accurate and that the individuals did not travel from this region for a significant period of time during their childhood. All individuals who donated samples were asked to fill in some personal information by Al Na'imi [22] and it has to be assumed that the information provided is accurate. This is an assumption that has to be made in any study utilising spatial data derived from human samples. As with all forensic studies, a good chain of custody for the samples can reduce the chance of error. Outliers in the data may provide some indication of inaccurate spatial data for known samples.

## 1.4 Research hypotheses

Based on the overall research objectives and assumptions, a number of hypothesis will be tested during the scope of this thesis:

1. The $\delta^{18}$O isotopic composition of human tooth enamel carbonate is directly related to the $\delta^{18}$O isotopic composition of local drinking water and therefore should prove a viable method for the determination of origin of an individual.

2. It is predicted that current isoscape models of the $\delta^{18}$O isotopic composition of precipitation may not sufficiently explain the variation in the Middle East due to limited data for this region.

3. The $^{87}$Sr/$^{86}$Sr isotopic composition of human tooth enamel is directly related to the $^{87}$Sr/$^{86}$Sr composition of an individuals diet which in turn is related to the $^{87}$Sr/$^{86}$Sr composition of the source region based on underlying soil and geology. Hence $^{87}$Sr/$^{86}$Sr composition of an individuals tooth enamel should offer an indication of their origin assuming that the majority of their diet was sourced locally.

4. Trace elements are transfered from underlying geology into the food chain. These trace elements can be incorporated into human tissue through dietary sources. Hence it should be possible to differentiate between modern human populations consuming diets from different regions based on trace element concentration.

5. The oxygen and strontium isotope and trace element concentration models can be used to exclude regions of unlikely origin for an unknown individual. By combining each of these ‘exclusion layers’ into a multi-layer ‘sieving’ probabilistic model it should be possible to significantly reduce the area of possible origin of an individual therefore increasing the likelihood that an individual can be identified as shown in Figure 1.

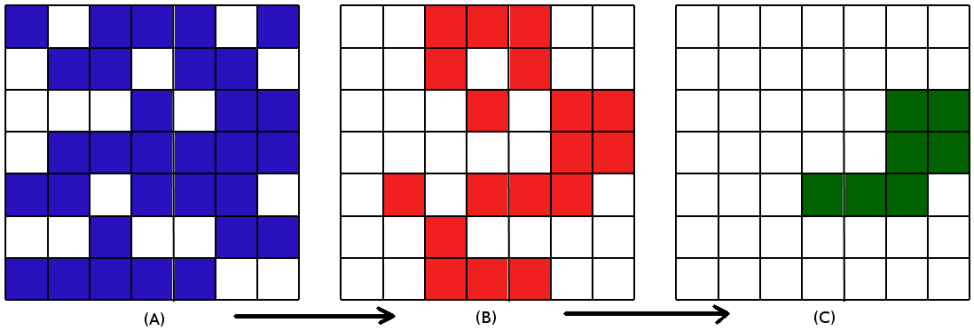


Figure 1: An illustration of a multi-layer exclusion ‘sieving’ model where each layer A-C reduce the possible area of origin of an individual.

## 1.5 The elemental and isotopic ‘fingerprint’ in human tissue

The phrase ‘you are what you eat’ has become almost cliché in modern western culture: a term used to describe the importance of healthy eating for a healthy body. From a chemical perspective this phrase is not far from the truth, with diet being the main source of nutrients for the growth of human tissue. A number of archaeological studies in particular have been able to take advantage of this to determine the dietary habits of ancient civilisations. For the purpose of this thesis, it is not ‘what you eat’ that is important but ‘you are **where** you eat’. Chemical signatures in food vary spatially across the globe due to a number of environmental, chemical and geological factors. That ‘signature’ can become incorporated into human tissue so that if the spatial variation of that chemical signal is understood, it could be used to deduce where that human tissue originated. This thesis is concerned with oxygen and strontium isotope composition and trace element concentrations of human tooth enamel: the factors leading to the spatial variation of these chemical systems will be discussed in Chapters 2,3 and 4.

Within the tissues of the human body is a wealth of spatial chemical information dating from early childhood through to present day that can be of vital significance to the identification of unidentified remains. Blood, urine and body water are in constant chemical equilibrium with an individuals diet, with a turnover time of hours to a few days and can

be used to give an indication of an individuals most recent movements. Hair and nail contain a chemical record of between 14 days up to 20 months [15] and can be used to track recent migration of modern individuals [23]. Hair and nail have been mostly used in modern cases due to the non-invasive nature of sampling. Inorganic material such as the bio apatite in bone and teeth offers an insight into an individuals past migrations but are only useful in cases involving the identification of a deceased individual due to the invasive nature of sampling. As such there are very few reports of bone or teeth being used in modern forensic cases although the archaeological literature is relatively rich (e.g. [24, 16, 13] etc.). Bone is in constant equilibrium with body water but takes approximately 5 - 10 years for full turnover in trabecular bones (i.e. rib) and around 25 years for full turnover in long bones (i.e. femur). Hence bone offers a good indication of an individuals later migrational history. Human tooth enamel forms during early childhood ($\sim$ 0 - 14 years [25]) and can offer chemical information on the geographical origin of an individual. It is tooth enamel that shall be the main focus of this study, although the methods used to produce spatial prediction models of an individuals origin in the later chapters of this thesis are transferable to any tissue.

### 1.5.1 The effect of modern 'supermarket' diet on the isotopic composition of human tissue

The isotopic composition of a human population at a given location is determined by the food and water that they consume. A number of archaeological studies have been able to use stable and radiogenic isotopes to successfully identify migrants in a given population as the majority of food and water consumed within those populations would be locally sourced due to the limited availability of imported foodstuffs [13, 24, 26, 11, 16]. However, in our modern 21st century population, internationally imported foodstuff has become readily available thanks to globalisation [27] and the improved accessibility of supermarkets. In one of the most influential papers concerning strontium isotopic composition of human skeletal material Beard and Johnson [28] state that 'in the case of humans,

the utility of using Sr isotopes to infer geographic information is probably more difficult than it was just two or three decades ago, because of increased national and international diversity of Ca (and Sr) sources in food’. As will be discussed further in this section, the extent to which ‘supermarket culture’ has limited the usefulness of oxygen and strontium isotope analysis in human provenancing studies is largely dependent on the proportion of non-local foodstuff consumed which in turn is dependent on the population being considered.

The proportion of imported foods consumed by humans is highest in economically developed regions such as the United States, Western Europe and Japan [29] and therefore it would be expected that the isotopic signal of human populations in these regions would be the most diluted from that found in local food and water.

The majority of stable isotope studies on human tissue have focused on populations from the United States of America. Due to the vast geographical scale of the US, one would expect the average food miles (i.e. the distance from field to fork) of the general human population to be large, even for foodstuff grown within the country. The US Department of Agriculture (USDA) [30] have shown that the average food miles for a product in the US is 619 miles. This is largely due to the spatial distribution of growing regions within the US. For example the majority of sugar cane that is proccessed into sweet products originates in the southern states, Florida, Louisiana and Texas while the majority of corn is grown in the Corn belt in the Mid-West states. Therefore one would not expect to see a correlation between the isotopic composition of foodstuff in an individuals average diet and the isotopic composition of local drinking water. A number of studies have shown that this is indeed the case. O’Brien and Wooller [31] have shown that the $\delta^{18}$O and $\delta^{2}$H isotopic composition of the average human diet between two geographically distinct US populations, East Greenbush (NY) and Fairbanks (AK) were statistically indistinguishable. The average $\delta^{18}$O isotopic composition of food products for the two regions were $26\pm6$ ‰ and $24\pm7$ ‰ but the range of isotopic compositions of food products was large (3.0 - 32.4 ‰). A study on the isotopic composition of food products from the US by

Chesson *et al* [32] yielded a similar national average oxygen isotopic composition (22.1 and 22.6 ‰ for supermarket bought food vs. restaurant bought food respectively) although again the author concludes that there is significant difference between the isotopic compositions of food types (i.e. dairy, carbohydrates, meat). These results support the existance of an US 'continental supermarket' culture. Another study by Ehleringer *et al* [1] assumed that the isotopic composition of the human diet across the US could be considered to be the same due to the existence of this 'continental supermarket' culture and applied a value of 26 ‰ for the $\delta^{18}$O isotope composition of diet although they concluded that the precision of the model produced in this study was limited by scatter around this dietary value.

Despite the evidence that there is no spatial differentiation in the isotopic composition of food stuff in the United states, the studies of Ehleringer *et al* [1] and O'Brien and Wooller [31] still succeeded in differentiating between individuals from different regions in the US due to the maintained relationship between local drinking water and hair keratin. This suggests that the volume of locally consumed water is still significant. O'Brien used a two member mixing model with local drinking water and average food composition as the two inputs to determine that approximately 27% and 36% of oxygen and hydrogen found in human hair is incorporated from locally sourced drinking water. Ehleringer produced linear regression models between the oxygen and hydrogen isotope composition of hair vs. drinking water (Figure 2) and a first order interpretation of these results suggest 35% and 27% of oxygen and hydrogen in hair respectively is incorporated from locally sourced drinking water. Ehleringer *et al* used these results as the basis of a mechanistic model for the prediction of $\delta^{18}$O and $\delta^{2}$H in human hair that successfully describes 85 % of the observed isotopic variation.

In a similar study based on individuals from Asia, Thompson *et al* [34] derived linear regression models between the oxygen and hydrogen isotope composition of hair vs. drinking water (Figure 2) and a first order interpretation of these results suggest 40% and 42% of oxygen and hydrogen in hair respectively is incorporated from locally sourced drinking

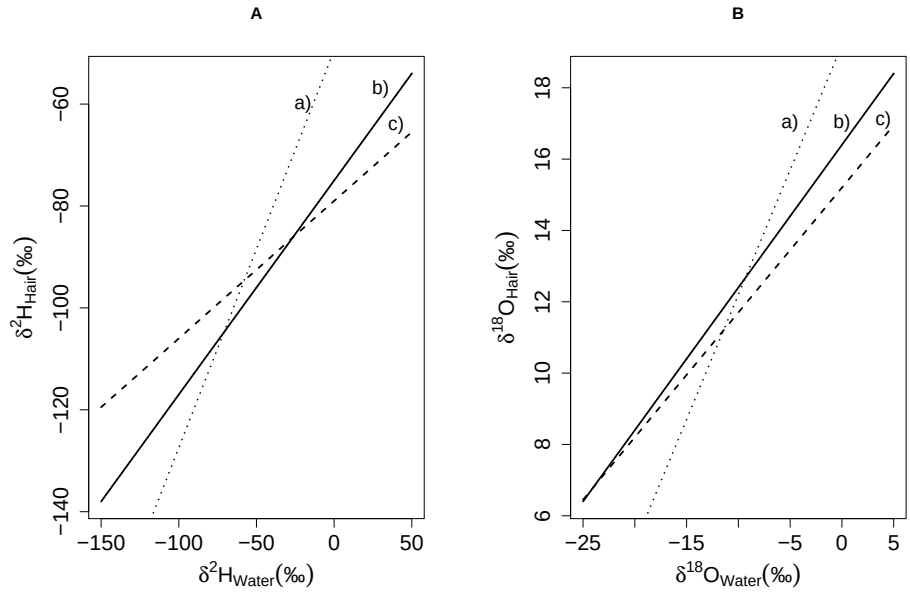


Figure 2: The relationship between drinking water and human hair A) $\delta^2$H (a)y=0.78x-49.5 [33], b) y=0.42x-75 [34] and c) y=0.27x-79 [1]) and B) $\delta^{18}$O (a) y=0.70x+19.2 [33], b) y=0.40x+16.4 [34] and c) y=0.35x+15.2 [1]) isotopic composition reported in the literature

water. Clearly a higher proportion of locally sourced food and water is consumed in Asia compared to the US population and this is to be expected due to the lower proportion of imported foods consumed in these countries [34]. Using new model parameters it was calculated that an average of 15 % of human diet comes from locally produced foodstuff. Bowen *et al* [33] present data from geographically isolated indigenous populations collected during the 1930’s-50’s. Due to the isolation of these populations from the developed world it would be assumed that the majority of food and water consumed would be locally sourced. The results suggested that approximately 70% and 78% of oxygen and hydrogen found in the hair keratin was incorporated from local drinking water (Figure 2). It was calculated that approximately 60-80% of foodstuff was locally sourced. This study also highlighted the danger of misinterpreting information from populations consuming a high marine diet as the isotopic composition of hair is significantly enriched in the heavy isotopes of oxygen and hydrogen in this case.

### 1.5.2 The development and composition of human teeth

It is useful to briefly consider the biology of human teeth. Pye and Croft [25] provide a good, basic introduction for forensic geoscientists. Most humans grow two sets of teeth during their lifetime. The first set, known as the deciduous (baby) teeth start to develop during gestation and are generally fully grown between the age of 2 to 6. The deciduous dentition comprises 20 teeth. The deciduous teeth are generally lost between the ages of 6 to 14 years and replaced with a second set, known as the permanent (adult) teeth, comprising 32 teeth. Each tooth consists of two main features, the crown and the root (Figure 3).

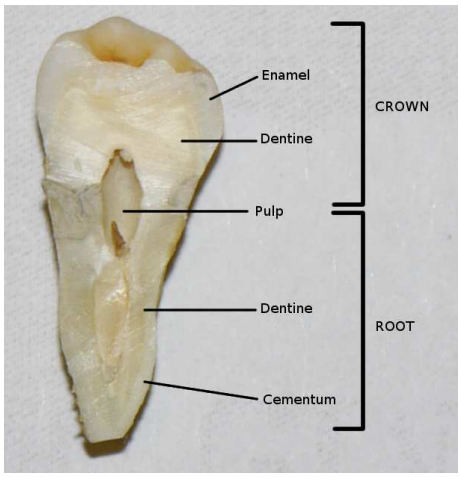


Figure 3: A photo of the internal structure of a human tooth with the major components labeled.

The crown is the section of the tooth that is visible above the gum and is comprised of a hard outer layer of enamel with a softer inner layer of dentin. The root comprises a cementum outer layer with a dentin inner layer. A pulp cavity runs through the centre of each tooth containing blood vessels that supply oxygen and minerals for the healthy development of the tooth. Tooth enamel dentin and cementum are all composed mainly of the mineral apatite (carbonate-hydroxy apatite) which has the general formula $[Ca_{10}(PO_4)_6(OH)_2]$ but is more accurately represented by the formula $[(Ca,Na,Mg,[])(PO_4, HPO_4, CO_3)(OH,F,Cl,CO_3,O,[])]$ [35] due to the substitution of the phosphate and hydroxide moieties with ions of similar charge and radius such as carbonate and fluoride.

Trace element ions are able to substitute into the calcium coordination site of the mineral. Tooth enamel is the hardest substance in the human body, composed of 96 - 97 % inorganic mineral apatite [36]. Enamel is generally fully formed by the age of 14 [25] and is not subject to exchange after formation due to its high stability making it a good indicator of dietary inputs during the early stages of an individuals life and may therefore provide information about their origin.

#### 1.5.2.1 The effect of tooth type on isotopic and elemental composition of enamel

Crown mineralisation of human permanent teeth (other than the second and third molars) begins intra-utera and continues into the early years of childhood with completion at around 3-5 years of age. Second and third molars being formation later in childhood and continue to mineralise up to the ages of $\sim$7 and $\sim$16 years of age respectively [36]. Isotopic or elemental composition of tooth enamel in incisors, canines and first molars may be altered by the effect of the mothers diet during pregnancy, consumption of breast milk as an infant, diet during weening and early childhood physiology as well as the isotopic composition of local water and dietary sources. As such second and third molars are the tooth of choice in previous studies [16, 15]. Obtaining suitable second and third molars for large scale studies is challenging and as such the tooth collection used in this study is a collection including incisors, canines and premolars, while only 66 % of the collection are the more suitable second and third molars. While this is not ideal, the dataset produced by this collection will be invaluable for future research. Care will be taken to ensure that data from non molar teeth is not significantly different from molars of similar geographical origin.

## 1.6 Case study: The Middle East

A collection of modern human teeth (referred to hence forth as the 'Middle East Collection') , gathered during the Masters study of Khudooma Said Al Na'imi [37], was

provided by the University of Lancashire for further analysis. The collection consists of 68 teeth (molar [n = 34], premolar [n = 26], incisor [n = 6] , canine [n = 1]), sourced from 5 countries (The United Arab Emirates [n = 11], Oman [n = 11], Iraq [n = 10], Iran [n = 19] and Yemen [n = 15]), from 62 subjects (male [n = 33], female [n = 29], age 11-70). All teeth were collected from living donors with the exception of 4 Iraqi samples which were collected from deceased donors with permission from the next of kin. Donors were asked to provide details of their place of origin (Figure 5). Samples were provided to the Centre of Forensic Provenancing with sample codes relating to the location of origin but no personal information was provided so that donors remain anonymous. It has not been possible to discriminate between first second or third molars.

The Middle East (Figure 4) is a region of great global interest due to the political unrest that has affected a number of countries for over twenty years. The most obvious examples being the war on terror (2001 - ) and the war in Iraq (2003 -) which were catalysed by the 9/11 terrorist attack on the World Trade Centre. In 2011 a number of uprisings and protests occurred in a number of Arab states including Syria, Egypt and Yemen which resulted in a number of deaths and a many reports of missing people. There is interest in the US and UK and by the United Nations for any techniques that might facilitate the identification of terrorists from the Middle East, in particular the provenance of suicide bombers. However this is only one possible application of this research. The Centre of Forensic Provenancing worked in collaboration with the Forensic Science service of the United Arab Emirates in the identification of origin of unknown remains of a woman found in Abu Dhabi.

The problem of missing people and unidentified remains is not reserved for only the countries of the West. Most recent forensic isotopic and elemental studies of human tissues have been focused on the US [1, 39, 28] and Europe [23, 40]. The availability of this collection of teeth samples from the Middle East offers a unique opportunity to look at the previously unexplored isotopic and elemental variation of modern humans from the Middle East. The sample set contains teeth from individuals originating from 19 different

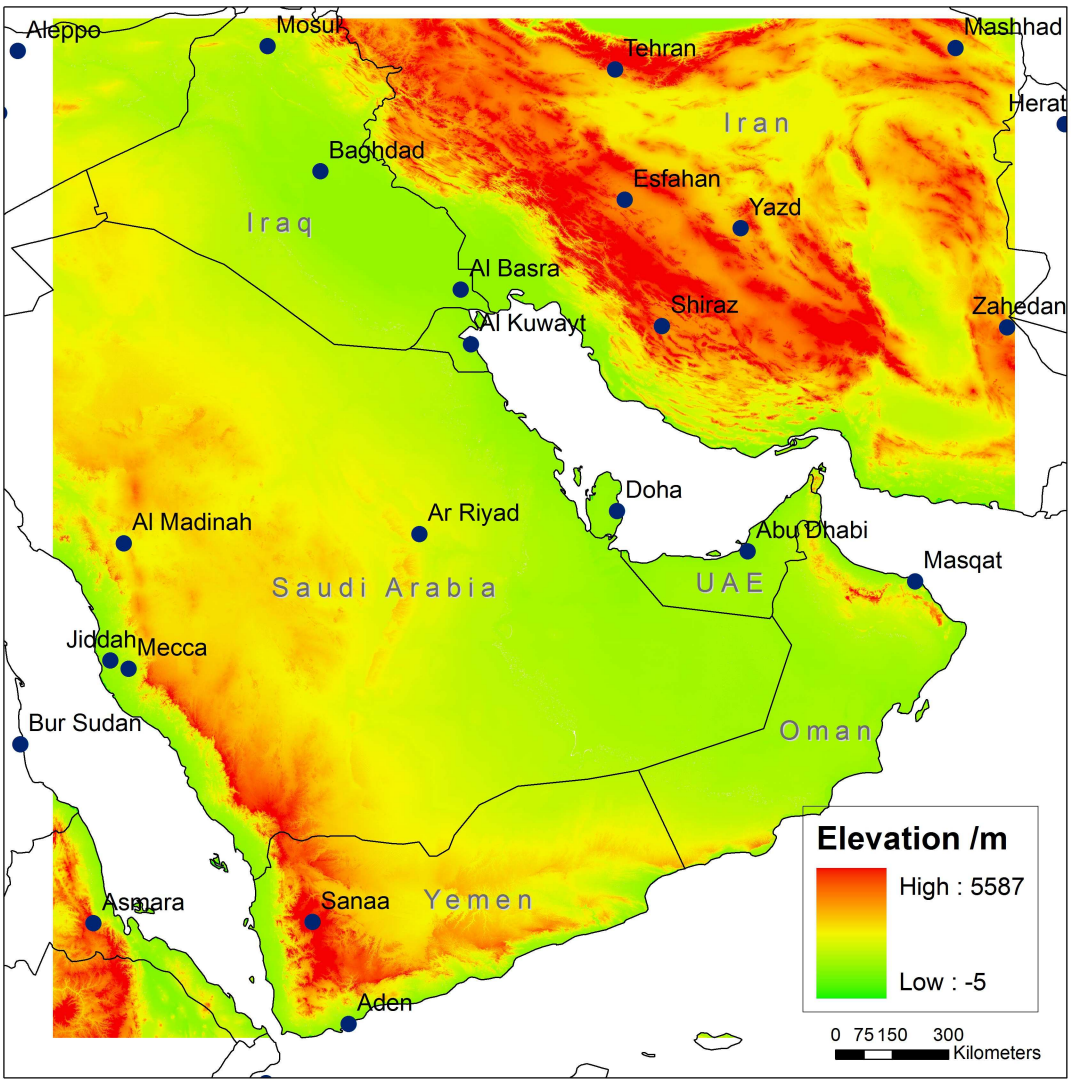


Figure 4: A reference map of the Middle East study region indicating the locations of countries and major cities. The background colour gradient represents elevation and is from the USGS 1km digital raster 'GTOPO30' [38].

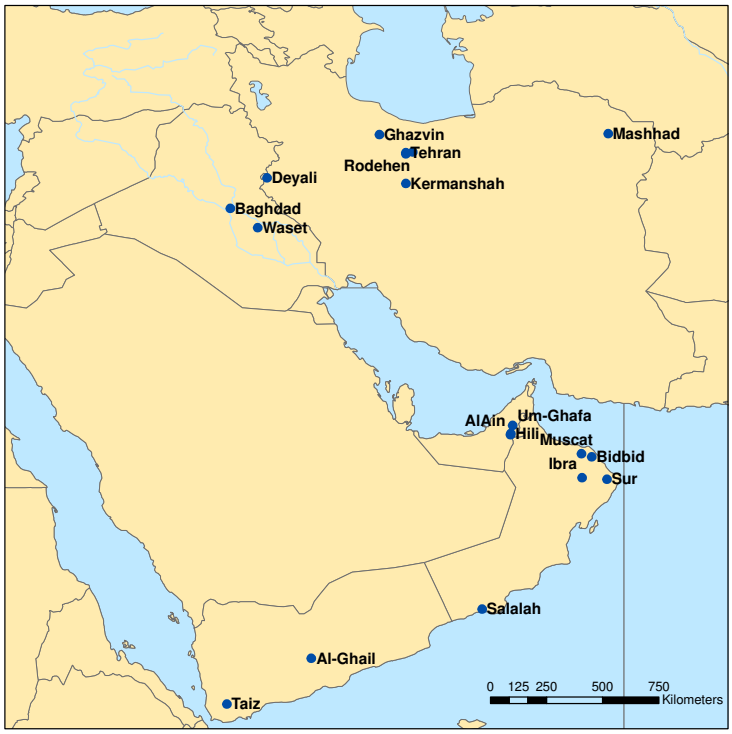


Figure 5: A map illustrating the sample distribution for the Middle East tooth collection.

cities from within 5 countries across the Arabian Peninsula and greater Middle East as shown by Figure 5 and Table 1. The sampling density is not fully representative of the Arabian peninsula, as can be see in Figure 5 the samples are biased to a transect from Baghdad in Iraq to Mashhad in Iran and to a handful of cities in the south and east of the peninsula. However this should offer sufficient information of the isotopic and elemental variation in the study region for this preliminary study. As has already been mentioned, obtaining suitable human tissue for this type of study is difficult. In the case that these preliminary samples show potential for the prediction of origin of individuals in the study region more samples can be obtained and measured to further refine the model in the future.

### 1.6.1 Economy and diet in the Middle East

The Middle East is best known for its production of oil, which accounts for the majority of the income in the region. However the countries within the Middle East do not benefit

equally from this natural resource. In this study, samples are available from Iran, Iraq, Oman, the United Arab Emirates and Yemen (See Figures 4 and 5) and these will be the focus of this thesis. Oman and the United Arab Emirates are high income countries [41] with GDP (Gross Domestic Product) per capita of $25,600 and $49,600 respectively [42]. Iran and Iraq are considered intermediate or middle income countries [41] with GDP per capita of $10,300 and $3,700 respectively [42]. Yemen is considered a low income country [41] with a GDP per capita of $2,700 [42]. The economical status of a country has a marked influence on the available dietary sources.

The traditional diet in the high income Gulf countries, Oman and the UAE, consists of dates, milk, fresh vegetables, fruit, whole wheat bread and a high proportion of fish and seafood, due to the successful fishing industry in these countries [41]. However, like many more developed and affluent countries around the world, this diet has become increasingly diversified due to the availability of imported international foods. There has been a massive increase in the intake of sugar and fat rich foods in Oman and UAE in the last decade which is thought to be due to availability and the shift in social classes [41].

Around half of the dietary intake in the intermediate income countries, Iran and Iraq, is from cereal crops such as wheat and rice [41] along with some fresh vegetables and meat. Chicken and lamb are popular meats in Iran [43]. The diet in Iraq is largely influenced by Iranian food. Like the high income countries, there has been a large increase in the amount of sugar and fatty foods consumed in Iran and Iraq, largely among the richer classes [41].

Around 60 - 80 % of the dietary intake of the low income countries such as Yemen is from cereal crops such as wheat or rice [41]. The proportion of meat in the diet is low for the general population although the higher social classes may have more access to meat, fish and speciality food similar to those found in the intermediate or high income countries [41].

Table 1: Middle East teeth samples used in this study. City of origin was provided by the sampled individuals. Coordinates were obtained from Google Earth. Teeth types are coded as follows: M = adult molar, PM = adult premolar, I = adult incisor, C = adult canine, m1 = deciduous molar.

| **Sample ID** | **Type** | **Origin** | **Country** | **Latitude (°)** | **Longitude (°)** |
|---|---|---|---|---|---|
| TE064 | M | Esfahan | Iran | 35.37 | 51.26 |
| TE065 | M | Tehran | Iran | 35.42 | 51.26 |
| TE066 | M | Kermanshah | Iran | 34.18 | 51.26 |
| TE067 | M | Tehran | Iran | 35.42 | 51.26 |
| TE068 | M | Tehran | Iran | 35.42 | 51.26 |
| TE069 | PM | Rodehen | Iran | 35.44 | 51.54 |
| TE070 | M | Ghazvin | Iran | 36.14 | 50.2 |
| TE071 | M | Ghazvin | Iran | 36.14 | 50.2 |
| TE072 | M | Sabzevar | Iran | 35.42 | 51.26 |
| TE073 | M | Sabzevar | Iran | 35.42 | 51.26 |
| TE074 | M | Tehran | Iran | 35.42 | 51.26 |
| TE075 | M | Mashhad | Iran | 36.17 | 59.36 |
| TE076 | M | Tehran | Iran | 35.42 | 51.26 |
| TE077 | M | Tehran | Iran | 35.42 | 51.26 |
| TE078 | M | Tehran | Iran | 35.42 | 51.26 |
| TE079 | M | Tehran | Iran | 35.42 | 51.26 |
| TE080 | M | Tehran | Iran | 35.42 | 51.26 |
| TE081 | M | Tehran | Iran | 35.42 | 51.26 |
| TE039 | PM | Waset | Iraq | 32.41 | 45.33 |
| TE040 | M | Waset | Iraq | 32.41 | 45.33 |
| TE041 | M | Baghdad | Iraq | 33.18 | 44.23 |

Continued on Next Page. . .

Table 1 – Continued

| Sample ID | Type | Origin | Country | Latitude (°) | Longitude (°) |
|---|---|---|---|---|---|
| TE042 | I | Baghdad | Iraq | 33.18 | 44.23 |
| TE043 | M | Baghdad | Iraq | 33.18 | 44.23 |
| TE044 | PM | Baghdad | Iraq | 33.18 | 44.23 |
| TE045 | C | Baghdad | Iraq | 33.18 | 44.23 |
| TE046 | PM | Baghdad | Iraq | 33.18 | 44.23 |
| TE047 | I | Deyali | Iraq | 34.4 | 45.7 |
| TE048 | I | Baghdad | Iraq | 33.18 | 44.23 |
| TE027 | I | Sur | Oman | 22.34 | 59.31 |
| TE028 | PM | Muscat | Oman | 23.37 | 58.29 |
| TE029 | I | Ibra | Oman | 22.41 | 58.32 |
| TE030 | M | Muscat | Oman | 23.37 | 58.29 |
| TE031 | M | Muscat | Oman | 33.18 | 44.23 |
| TE032 | PM | Sur | Oman | 22.34 | 59.31 |
| TE033 | PM | Sur | Oman | 22.34 | 59.31 |
| TE034 | PM | Salalah | Oman | 17 | 54.32 |
| TE035 | PM | Baloshistan | Oman | 28.8 | 65.33 |
| TE036 | PM | Bidbid | Oman | 23.24 | 58.7 |
| TE038 | PM | Muscat | Oman | 23.37 | 58.29 |
| TE016 | M | AlAin | UAE | 24.13 | 55.45 |
| TE017 | PM | AlAin | UAE | 24.13 | 55.45 |
| TE018 | PM | AlAin | UAE | 24.13 | 55.45 |
| TE019 | PM | AlAin | UAE | 24.13 | 55.45 |
| TE020 | PM | AlAin | UAE | 24.13 | 55.45 |
| TE021 | PM | AlAin | UAE | 24.13 | 55.45 |
| TE022 | PM | Hili | UAE | 24.17 | 55.46 |

Continued on Next Page. . .

Table 1 – Continued

| Sample ID | Type | Origin | Country | Latitude (°) | Longitude (°) |
|---|---|---|---|---|---|
| TE023 | PM | Um-Ghafa | UAE | 24.5 | 55.54 |
| TE024 | PM | UAE | UAE | 24.13 | 55.45 |
| TE025 | PM | Um-Ghafa | UAE | 24.5 | 55.54 |
| TE049 | I | Taiz | Yemen | 13.34 | 44.1 |
| TE050 | M | Al-Ghail | Yemen | 15.17 | 47.48 |
| TE051 | M | Al-Ghail | Yemen | 15.17 | 47.48 |
| TE052 | M | Al-Ghail | Yemen | 15.17 | 47.48 |
| TE053 | PM | Al-Ghail | Yemen | 15.17 | 47.48 |
| TE054 | M | Al-Ghail | Yemen | 15.17 | 47.48 |
| TE055 | PM | Al-Quada | Yemen | 15.17 | 47.48 |
| TE056 | M | Al-Ghail | Yemen | 15.17 | 47.48 |
| TE057 | PM | Al-Ghail | Yemen | 15.17 | 47.48 |
| TE058 | M | Al-Ghail | Yemen | 15.17 | 47.48 |
| TE059 | M | Habayer | Yemen | 15.17 | 47.48 |
| TE060 | PM | Al-Ghail | Yemen | 15.17 | 47.48 |
| TE061 | PM | Al-Ghail | Yemen | 15.17 | 47.48 |
| TE062 | m1 | Al-Ghail | Yemen | 15.17 | 47.48 |
| TE063 | M | Al-Oyon | Yemen | 15.17 | 47.48 |

## 1.7 Thesis outline

This thesis is concerned with the development and validation of oxygen and strontium isotope and trace element models for the prediction of human origin. The main focus of this study has been the Middle East due to the availability of samples from that region as described in section 1.6. Each chapter in this thesis is concerned with one aspect of the study. Each chapter includes an introductory section to the techniques being used followed by experimental, results, discussion and conclusions made.

Chapter 2 describes the oxygen isotope analysis of the tooth enamel carbonate from the Middle East tooth collection, development of a new drinking water isoscape for the Middle East based on measured samples and values from the literature and the development of a tooth enamel carbonate isoscape based on the measured teeth.

Chapter 3 describes the strontium isotope analysis of the tooth enamel from the Middle East tooth collection and the development of a strontium isoscape for the study region based on the underlying geological units.

Chapter 4 is concerned with the trace element analysis of the Middle East tooth collection by LA-ICP-MS and the differentiation of the samples based on their trace element 'fingerprint' by multivariate statistical methods.

In Chapter 5 the isoscapes produced in chapters 2 and 3 are used as the foundation for a new multi-isotope probability-scape for the Middle East. That is, an inverted isoscape which returns a probability of origin rather than a band of isotope space. In this chapter, two simulated and one real forensic case are described to highlight the potential of this new probabilistic approach to isotope mapping in forensics.

Chapter 6 provides some final conclusions and thoughts on the future of the use of isotope and trace element data for the identification of human remains.

# Chapter 2

# Stable isotope analysis

## 2.1 An introduction to the processes governing isotope fractionation in nature

Stable isotope analysis is a well established analytical tool that has been applied to a number of scientific disciplines during its 100 years of development [44]. In the last decade, the potential of stable isotope analysis has been recognised by the forensic science community resulting in a wide and rapidly growing body of literature on the subject. Examples of applications of stable isotope analysis in forensic research include; the determination of origin and authentification of food [45], wildlife forensics [46, 47], determination of origin of contraband substances [48, 49] and forensic human identification [25, 1, 50, 51].

Stable isotope analysis can be applied to forensics in two ways. The first approach is to produce an isotopic ‘fingerprint’ or ‘signature’ for an object of interest in order to compare it to samples in a database or to samples related to a particular case (for example, determining whether drugs found on a suspect are related to drugs seized in a raid). The second approach takes advantage of the systematic spatial variation of certain stable isotope systems in order to link a sample of interest to a source region. In the provocatively titled chapter ’Stable Isotope Fingerprinting - Chemical Element DNA’ [52], Meier-Augenstein

draws attention to the similarity between the specificity produced by a multi-isotope fingerprint of a sample of interest with that of human DNA. Although stable isotope analysis is unlikely to compete with DNA analysis as the main analytical tool for the identification of human remains, it can provide a large amount of information for a forensic investigation to complement other analytical techniques in order to draw a conclusion. Stable isotope analysis may prove particularly useful for aiding the identification of human remains where DNA identification is not possible.

This chapter provides an introduction to stable isotope analysis as an analytical tool and its application in forensics before describing how, in this study, stable isotope analysis of tooth enamel carbonate has been used to produce the first prediction model (isoscape) for the identification of origin of human remains in the Middle East.

### 2.1.1 An introduction to stable isotope fractionation and the processes that lead to isotope fractionation in nature

The majority of the 92 naturally occurring elements on the Earth exist as combinations of two or more isotopes. That is each elemental atom contains the same number of protons and electrons but may vary in the number of neutrons. Hence isotopes of an element have different atomic mass values. For example oxygen, the main element of interest in this chapter has three stable isotopes; $^{16}O$, $^{17}O$ and $^{18}O$. Stable isotopes are those that do not undergo radioactive decay. As the stable isotopes do not decay over time their average natural isotopic abundance is constant (see Table 2).

However, isotopologues of compounds containing the light stable elements (C, N, O, H, S, Li, B and Si) can undergo isotope fractionation due to mass dependent processes (and some mass independent processes which are outside the scope of this study) such as evaporation or metabolic reactions in a living organism, leading to large natural ranges in the isotopic composition of these compounds (see Section 2.1.1.1). Note that mass dependent fractionation processes also affects the isotopes of heavy elements (see Chapter

Table 2: Average relative abundance of the stable isotopes of commonly measured light stable elements

| Element | Stable Isotope | Average abundance, % |
|---|---|---|
| Hydrogen | $^{1}H$ | 99.985 |
| | $^{2}H$ | 0.015 |
| Carbon | $^{12}C$ | 98.9 |
| | $^{13}C$ | 1.1 |
| Nitrogen | $^{14}N$ | 99.63 |
| | $^{15}N$ | 0.37 |
| Oxygen | $^{16}O$ | 99.762 |
| | $^{17}O$ | 0.038 |
| | $^{18}O$ | 0.2 |

3) but these processes are more easily observed in the isotopes of light elements due to the large mass difference between isotopes.

Isotopic data for the light stable elements is measured as a ratio (R) of the heavy isotope abundance divided by the light isotope abundance of a given compound relative to the isotopic ratio of a standard reference material (R$_s td$) and is reported as a delta ($\delta$) value in 'per mil' (‰) units as given by Equation 1. Reporting isotopic compositions in this way has a number of advantages. Firstly, by dividing the isotopic ratio of the sample by that of the standard, noise and fluctuations in the signal during analysis are removed leading to improved precision. Furthermore, using internationally accepted standards means that measurements have been normalised to IAEA guidelines and are therefore comparable to data produced by other laboratories. Finally, delta values give a larger range of integer values compared to absolute ratios (R) making them easier to remember and more user friendly.

$$\delta R = \frac{R_s - R_{std}}{R_{std}}.1000 \tag{1}$$

Where $R_s$ is the isotopic ratio of the sample (e.g. $^{18}O/^{16}O$), $R_{std}$ is the isotopic ratio of the international reference standard and results are in ‰.

Examples of international reference materials include; Vienna standard mean ocean water

(VSMOW) ($\delta^{18}O$ and $\delta^{2}H$), Vienna Pee Dee Belemnite (VPDB) ($\delta^{13}C$ and $\delta^{18}O$) and atmospheric Air (AIR) ($\delta^{15}N$).

The variation in the isotopic composition of the light stable elements is an important tool for the understanding of natural processes as these elements are abundant within the Earths crust, the biosphere, the hydrosphere and the atmosphere. The isotopic composition of light element containing compounds can provide a wealth of information describing the environmental conditions of their formation where the fractionation processes are understood [53].

#### 2.1.1.1 Isotopic fractionation processes

The range in isotopic compositions observed for a given compound in nature are generally driven by mass dependent chemical reactions or physiochemical processes. In principle there are two types of isotope effect that lead to isotopic fractionation, kinetic fractionation caused by the mass dependence of the chemical reaction kinetics and thermodynamic fractionation caused by the mass dependence of phase changes [15].

The difference in mass between the common and rare isotopes ($\Delta m$) of a light element is proportionally very large when compared to **most** heavier elements. For example the oxygen isotope ratio is calculated from the $^{18}O$ and $^{16}O$ isotopic abundances and $\Delta m$ is 2 mass units or 12.5 % of the mass of the most abundant isotope. In comparison the heavier strontium isotope ratio ($^{87}Sr/^{86}Sr$) has a $\Delta m$ of 1 mass unit or 1.2 % of the mass of the common isotope. Hence for reactions where mass is a determining factor the change in isotopic composition is much more pronounced in the stable isotopes of the lighter elements.

**Mass dependence of bond strength (vibrational energy)** is ultimately responsible for the large range of isotopic compositions of a compound observed in natural and synthetic materials. As such it is useful to consider a few basic physical principles of a chemical

bond in order to understand why the heavier isotopologue of a compound reacts at a different rate to the lighter isotopologue.

The kinetic energy of a rigid body is defined by the moment of inertia $I$ and its angular velocity $\omega$ as given in Equation 2:

$$E_{vib} = \frac{1}{2} I \omega^2 \tag{2}$$

The moment of inertia $I$ for a system containing two masses (i.e. a diatomic molecule) is dependent on the reduced mass of the system $\mu$ and the bond length $r$ and is given by Equation 3:

$$I = \mu r^2 \tag{3}$$

where the reduced mass $\mu$ of a two atom system with masses $m_1$ and $m_2$ is given by Equation 4:

$$\mu = \frac{m_1 m_2}{m_1 + m_2} \tag{4}$$

Measuring the vibrational absorption (Equation 5 of a molecule using spectroscopy enables the calculation of $I$ and hence bond length $r$.

$$\Delta E = 2B = \frac{h}{4\pi^2 c I} \tag{5}$$

The bond length and hence bond strength has been shown to be related to the reduced mass of the system. Hence reaction rates for isotopologues of the same compound will also be dependent on the reduced mass of the system.

**Kinetic isotope fractionation** is the most significant isotope effect [15] and refers to the fractionation that occurs during reactions involving the formation or braking of a

chemical bond. As has been shown, bond strength is mass dependent and hence bonds to heavier isotopes of an element will be stronger than those to the lighter isotope and hence the lighter isotopologue will tend to react faster than the heavy isotopologue leading to a product that is isotopically lighter than the precursors.

**Isotopic fractionation during physiochemical processes** such as diffusion, evaporation and two-phase partitioning is the result of mass dependent differences in the kinetic energy (diffusion) or vibrational energy (phase change) of isotopologues of a given compound. Such isotope effects are commonly, incorrectly termed kinetic isotope effects. Meier-Augenstein [15] suggests that a more chemically accurate terminology is the **thermodynamic isotope effect**.

If one considers the reaction rate constant (k) of a reaction or phase change between a precursor and its products to actually be comprised of two subtly different reaction rate constants $k_L$ and $k_H$ for the light and heavy isotopologues respectively, the ratio of these two constants becomes the fractionation factor $\alpha$ as given by Equation 6.

$$\alpha = \frac{k_H}{k_L} \tag{6}$$

In the case where $k_L$ is larger than $k_H$, i.e. the reaction rate of the light isotopologue is faster than that of the heavier isotopologue then $\alpha$ will be $<1$ and the product of the reaction will have an isotopic composition that is lighter than the precursor compound. The fractionation factor $\alpha$ can be related to the equilibrium constant (K) and the number of atoms exchanged (n) by Equation 7 and to $\delta$ by Equation 8.

$$\alpha = K^{1/n} \tag{7}$$

$$\alpha_{AB} = \frac{\delta_A + 10^3}{\delta_B + 10^3} \tag{8}$$

### 2.1.2 Isotopic fraction of meteoric water

It was noted that the heavier isotopologues of meteoric water (HDO and $H_2{}^{18}O$) are precipitated preferentially due to their lower saturation vapour pressures causing them to concentrate in the liquid phase [54]. The controls that govern the fractionation between the heavy and light species are considerably more complex in nature than equilibrium processes described previously. Environmental processes are generally not closed systems and so the fractionation cannot entirely be described by equilibrium reactions. Craig and Gordon [54] describe a series of models considering increasingly complex systems of mass transfer between liquid water and water vapour in the atmosphere. In a closed system, fractionation between liquid water and water vapour is shown to be proportional to the kinetic transport effects at the boundary layer between liquid and vapour (condensation and escape, molecular diffusion through the laminar layer and turbulent diffusion in the turbulent section). The fractionation between liquid and vapour is also proportional to the relative humidity of the different layers and hence temperature and pressure. In an open system equilibrium is only achieved at the liquid - vapour boundary where relative humidity = 100 %. Water vapour can be removed from the system by air masses causing the liquid phase to become increasingly enriched in the heavier isotopic species. This process can be quantified by the Rayleigh fractionation equation (Equation 9).

$$R_t = R_0 f^{(1-\alpha)} \tag{9}$$

where $R_0$ is the initial isotope ratio of the phase of interest, $R_t$ is the isotope ratio at time t, $\alpha$ is the fractionation factor between the two species as given by Equation 7 and $f$ is the fraction of the phase of interest remaining at time t.

#### 2.1.2.1 Temperature dependence of fractionation

The relationship between the isotopic fractionation factor $\alpha$ and temperature for liquid water and water vapour at equilibrium was described by Majoube [2]. For oxygen isotope

fractionation the equation is:

$$\alpha_v^l(^{18}O) = 0.9845exp(0.7430/T) \tag{10}$$

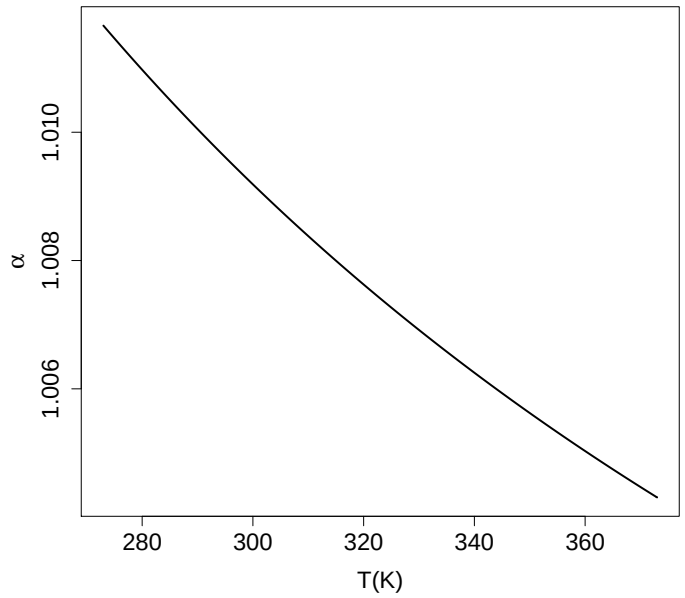


Figure 6: The temperature dependence of $\alpha_v^l(^{18}O)$ at equilibrium as given by Majoube[2], Equation 10

and the curve is shown in Figure 6. From this relationship it can be shown that under equilibrium conditions the fractionation factors for liquid water and water vapour at 0°C, 20°C and 40°C are 1.0116, 1.0098 and 1.0082 respectively. I.e. condensation/ evaporation reactions occurring at low temperatures lead to greater fractionation than those occurring at higher temperatures. However the difference in fractionation factors (3.6 ‰ between 0 °C and 40 °C) at equilibrium does not account for the large range in isotopic values that are observed in nature. This is due to the complex non-equilibrium conditions that determine the evaporation, transport and condensation of water in the real world. The driving factor for the large amount of fractionation is the Rayleigh distillation effect previously described in Equation 9, and the Clausius-Clapeyron law (Equation 11) which describes the relationship between temperature and the saturation vapour pressure [55].

$$p_v = Cexp(-D/T) \tag{11}$$

where C is a constant for water, D is L/G (L is the molar heat of evaporation (44.4x$10^3$ J/mole) and G is gas constant 8.3 J/Kmole) and T is the temperature in Kelvin.

Van der Veer *et al* determined an empirical relationship between the $\delta^1 8$O of global meteoric water and temperature based on observations from the GNIP data stations, Equation 12.

$$-5.9exp(-0.041T_{cq}) - 2.4 \tag{12}$$

where $T_{cq}$ is the mean temperature of the coldest quarter. Van der Veer clearly demonstrates that there is an exponential relationship between temperature an isotopic composition of precipitation and that the $\delta^{18}$O composition tends towards that of VSMOW (0 ‰) at high temperatures (Figure 7).

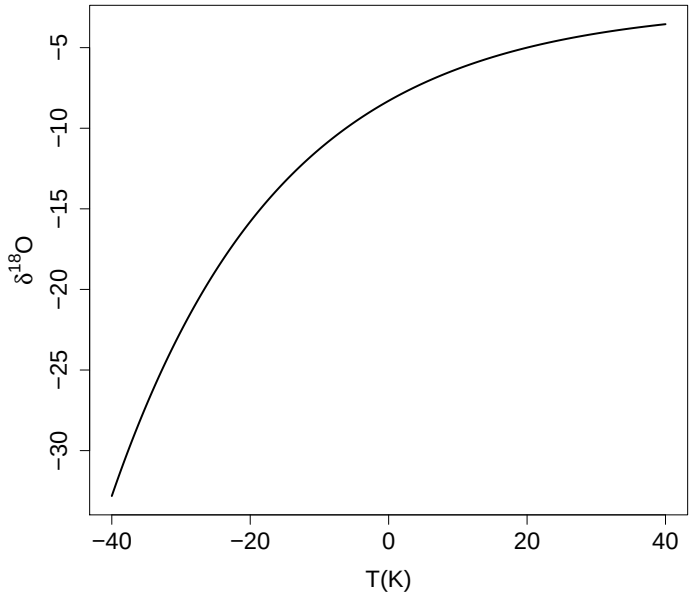


Figure 7: The temperature dependence of $\delta^{18}O$ of global meteoric waters from the GNIP database as determined by Van der Veer *et al* [3]

## 2.2 Literature review: How have stable isotopes been utilised in forensic research?

Over the past decade the use of stable isotope analysis for human identification has become more widely reported in forensic literature and has even made its way into the public eye through documentaries such as 'History: A cold case' [56] which demonstrated how stable isotope analysis might be used to help build a migrational profile of archaeological human remains. The majority of the literature focuses on individual cases [23, 16, 57] where the isotopic composition of the human tissue from a set of remains is compared to a database such as the Global Network of Isotopes in Precipitation (GNIP, see Section 2.2.1). Other than for human hair [1], there have been no validated prediction models for the identification of human geographical origin.

The creation of isotope based prediction models or 'isoscapes' [14] has been greatly advanced in recent years by studies covering a wide range of disciplines. One research objective of this study is to examine the spatial isotopic and elemental variation in tooth enamel samples from the Middle East (Section 1.2) and to model this spatial variation in isoscapes in order to investigate the hypothesis that 'the $\delta^{18}$O isotopic composition of human tooth enamel carbonate is directly related to the $\delta^{18}$O isotopic composition of local drinking water and therefore should prove a viable method for the prediction of origin of an individual'. The following sections provide a concise review of the literature relating to the use of stable isotope analysis in forensics before moving on to provide a more comprehensive review of the literature concerning the development and applications of stable isotope analysis of human tissue.

### 2.2.1 Understanding the mechanisms of oxygen isotopic fractionation in precipitation

In order to understand the isotope ratio variation in a matrix of interest it is necessary to first understand the isotope ratio variation of the inputs into that matrix. In the case of hydrogen and oxygen isotopes in most natural (plants, animals, etc.) and some man made systems (chemical synthesis), more often than not the main input is water. The fractionation of water in the hydrological cycle is well described by the Craig-Gordon model, mentioned previously (see Section 2.1.2), and a concise description of these fractionation processes is given by Dansgaard [58]. In 1961 the International Atomic Energy Agency (I.A.E.A.) and the World Meteorological Organisation (W.M.O.) initiated a world wide survey of oxygen and hydrogen isotopes in precipitation. The project was initially introduced to analyse the tritium content of precipitation after the testing of atomic weapons during the 1950s. Since then the Global Network of Isotopes in Precipitation (GNIP) has provided monthly and annual isotope data for over 500 collection stations around the world (Figure 25).

This database has been the basis for a number of **global** spatial precipitation models that have attempted to provide a tool for the estimation of oxygen and hydrogen isotope ratios of rain water anywhere in the world. Initial attempts by Yurtserver and Gat [60] to map the oxygen and hydrogen isotope ratios around the world used basic contouring between the GNIP stations; linking IAEA stations with similar isotope composition with contours. Birks *et al* [61] attempted to interpolate the point data using geospatial interpolation methods. Bowen and Wilkinson [62] first proposed modeling the oxygen and hydrogen isotope values of the IAEA collection stations against geographical variables (Latitude and Altitude, Equation 13) to take into account Rayleigh distillation of atmospheric vapour.

$$\delta^{18}O = -0.0051LAT^2 + 0.1805LAT - 0.002ALT - 5.247r^2 = 0.80 \qquad (13)$$

Where LAT is the absolute latitude and ALT is altitude in metres.

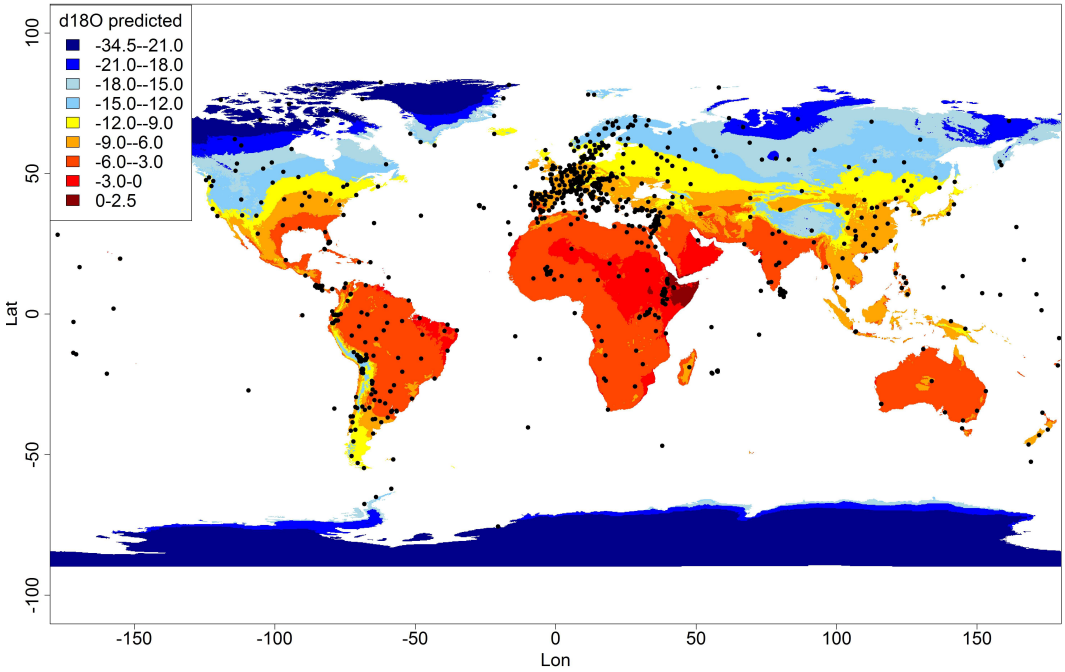


Figure 8: An isoscape of the global $\delta^{18}$O variation in precipitation based on Bowen *et al* 2003 [59]. The black circles represent the locations of the Global Network for Isotopes in Precipitation (GNIP) sampling stations upon which the model is based.

Bowen and Revenaugh [59] further improved on this model by applying a nonlinear least squares method and introducing a spatial correlation function to take into account the variability not described by latitude and altitude (Figure 25). A different model was published by van der Veer *et al* [3] who considered climatic factors such as temperature (WorldClim, [63]) as independent variables in the model. The model of Bowen and Revenaugh [59] has been used in subsequent papers to produce models of precipitation [64], tap water [65] and bottled water [66]. These models are commonly used in recent literature to predict the isotope composition of source waters of samples of interest. Little research has been done into the errors and uncertainty associated with these prediction models, nor into the deviation from the models at a local or regional scale. Blind application of these models, particularly in the field of forensic science could lead to repercussions in the future.

### 2.2.2 Stable isotope analysis as a forensic tool

IRMS started to make an appearance in the literature as a forensic tool towards the end of the 20th Century. In the past decade the number of publications and applications for the technique have increased as illustrated in the review paper by Benson [67]. Forensic science is concerned with the analysis of evidence in order to aid a legal dispute. IRMS is a useful tool to this end as it can be used both to compare the 'chemical fingerprint' of a piece of evidence found at a crime scene to that of corresponding evidence found with a suspect, or, where the chemical processes involved in the synthesis of the evidence material are understood, IRMS can be used to link the evidence to its source materials (for example drug production). The later case is the concern of the majority of the literature. In order to fully utilize IRMS, a better understanding of the isotope fractionation factors during chemical processes is required.

The application of IRMS in forensics has been wide ranging including examples of: the determination of authenticity and origin of food products [45, 68, 32, 69], the determination of origin of illicit drugs [49, 48], tracing explosive materials to the precursor materials [70], wildlife forensics [66, 46] and the identification of human remains [23, 71, 51]. A number of organisations have been founded to raise awareness of stable isotope analysis in the field of forensics and to produce recognised operating protocols to allow for comparison between laboratories. The Forensic Isotope Ratio Mass Spectrometry Network (FIRMS) was established in 2002 and has since held 6 inter laboratory comparisons and 4 international conferences, details of which, as well as the network mission statement and technical strategy are available on their website [72]. The Natural Isotopes and Trace Elements in Criminalistics and Environmental Forensics (NITECRIME) network was an EU funded project started in 2001 which aimed to develop techniques for trace element and isotopic analysis of forensic samples. The EU funded TRACE project [73] established in 2005 aimed to develop techniques including IRMS for the authentification and provenancing of food products.

### 2.2.3 Stable isotope analysis of human tissue

The analysis of stable isotopes in human tissue was initially developed for paleoclimate studies [74, 75, 76, 77] (See Section 2.2.3.1) due to the observed relationship between the $\delta^{18}O$ values of biogenic apatite in bones and teeth of mammals and those of local meteoric water (see Tables 3 and 5).

Human migration and identification studies can apply similar principles, although great care must be taken when working with modern samples as the assumption that the largest input of oxygen into the bone is local meteoric water needs to be validated. The 'globalisation' of food sources and modern supermarket culture means that a large proportion of human diet is not sourced locally and could act to reduce the degree of isotopic 'identity' of regional populations [25]. In fact it has been shown that as little as 27% of oxygen found in human hair from the US [1] is derived from local drinking water while this figure is slightly more (40 %) in Asia [34] where the diet is more locally sourced and 70 % for isolated indigenous populations [33] (see Section 1.5.1).

Stable isotope analysis has proved a useful tool for archaeological studies on migration and residential histories of ancient populations, where it is assumed that the proportion of 'imported' or non-local food and water would have been limited. A concise review of earlier archaeological studies implementing stable isotope analysis is provided by Schoeninger and Moore [78]. White *et al* [79] used oxygen isotope techniques to show statistical significance between populations of three archaeological sites in Mexico. Variation in the results for the site in Tiotihuacan (Mexico) was hypothesised to be caused by immigration of women and children from areas north of the city. The study also highlighted the importance of all possible water sources being considered, especially in a large city where much of the drinking water may have come from ground water wells as well as from precipitation.

Hoogewerff [16] and Muller [57] investigated the origin of Oetzi, a prehistoric 'iceman' found naturally mummified in the Hauslabjoch pass in the central Alps. Trace element

concentrations and oxygen, carbon and strontium isotope data from the iceman's bones and teeth were combined to reconstruct the migrational history of the iceman. It should be noted that Hoogewerff *et al* and Muller *et al* reached different conclusions concerning the migrational history of the iceman. This highlights the fact that conclusions from archaeological studies are often open to interpretation. In forensic studies there must not be scope for interpretation as this could mean the difference between conviction or freedom for an individual.

Buzon and Bowen [13] utilised carbon, oxygen and strontium isotope ratios to determine the proportion of immigrants within the population at Tombos on the river Nile. These cases highlight the importance of combining isotopic techniques for the understanding of human population movements.

Fraser et al [71] have made first steps towards combining global isotopic data (C, N, O and H) for modern humans, reporting a range from 9.2 - 19.0 ‰ for $\delta^{18}O$ of modern human hair allowing differentiation between regions, particularly Europe, Africa, America and Asia. By taking a longitudinal profile of hair or nail samples, natural variation in isotope signal over time was recorded and changes in geographical location were identified over the short term [71, **?**]. In conjunction with the other stable isotope data Fraser *et al* conclude that inter and intra- individual variation should be considered globally in order to determine the significance of the observed differentiation. They also state that more research is required at a national level to determine whether the geographical differentiation within a country is possible. Meier-Augenstein and Fraser [23] present the first successful study in which stable isotope analysis was applied to a modern day forensic case. Multiple isotopes of a deceased subjects hair and nails were measured (C, N, O, H) and the results compared to samples of a control subject. The information collected enabled the police to identify the victim and subsequently the murderers in the case. Ehleringer *et al* present the first validated isoscape model for the prediction of $\delta^{18}O$ and $\delta D$ values of modern human hair. The fractionation of oxygen and hydrogen that occurs in the formation of hair keratin was modeled based on series of fractionations assuming the inputs to be drinking

water (measured from tap waters across the US [80]) and dietary water (assumed to be homogeneous due to the 'continental supermarket'. The model explains $<$85 % of the variation observed. This is currently the only validated prediction model for human tissue in the literature.

#### 2.2.3.1 Methods for the $\delta^{18}O$ analysis of biogenic Phosphate

Oxygen isotope analysis of biogenic phosphate has seen significant advances in the past 50 years, due to its importance as an indicator of paleotemperatures and paleoenvironments. Tudge first isolated the $PO_4^3-$ anion as $BiPO_4$ in 1960 [81] by a series of quantitative precipitation reactions. The oxygen was released from the phosphate group by fluorination with $BrF_3$ and measured using a Nier type double collector IRMS instrument. Initially the technique was applied to the analysis of shells and skeletons of modern and fossilised marine species. The research of Urey *et al* in the 1950s [82, 83] concentrated on using oceanic calcium carbonate as a paleo-thermometer, making the assumption that calcium carbonate deposited by marine creatures is in thermal equilibrium with the surrounding water. This research was later complimented by the research group of A. Longinelli during the 1960s when they were able to establish a method, again using flourination, for the analysis of phosphate deposits from marine organisms [84, 85, 86].

Longinelli later proposed [86] that the analysis of phosphate from the bones of mammalian species could provide paleoclimate information based on the assumption that the oxygen in bone phosphate is precipitated from body water and that the isotopic composition of the body water should be in agreement with the local drinking water and hence an indicator of the isotopic composition of local meteoric water. An advantage of working with mammalian bones is that mammals are homeotherms and so fractionation caused by temperature should be constant and independent of environmental temperature. A pioneering paper in this field by Longinelli [74] was a catalyst for further investigation into the $\delta^{18}O$ values of human bone phosphate. Longinelli reported the $\delta^{18}O$ results for human body water (blood, n = 62, 7 regions) and human bone phosphate (n = 59, 10 regions)

compared with the local drinking water from each region yielding the relationships given in Equations 14 and 15.

$$\delta^{18}O_{BW} = 0.60(\pm 0.03) * \delta^{18}O_{MW} + 0.68 \;\; (r = 0.98) \tag{14}$$

$$\delta^{18}O_{BP} = 0.64(\pm 0.03) * \delta^{18}O_{MW} + 22.37 \;\; (r = 0.98) \tag{15}$$

where $\delta^{18}O_{BW}$, $\delta^{18}O_{MW}$ and $\delta^{18}O_{BP}$ are the $\delta^{18}O$ of the body water, local meteoric water and bone phosphate respectively. Subsequent papers [75, 87, 77] have published similar linear relationships between phosphate and drinking water, the linear regression from these papers are shown in Table 3.

Frike *et al* [88, 89] present two studies into the seasonal variation of $\delta^{18}O$ in herbivore mammalian tooth enamel. Stuart-Williams and Schwarcz [90] present a similar study. The longitudinal $\delta^{18}O$ signature of tooth enamel samples of modern beavers was compared to that of ancient Giant Beaver (Castoroides Ohioensis). Fluxes controlling the variation of the $\delta^{18}O$ signal were modeled. The study concluded that beavers were a good indication of seasonal variation of $\delta^{18}$O composition of precipitation due to their rapid tooth growth and high sensitivity to small isotopic changes in meteoric water. Samples were taken in a longitudinal pattern down the tooth sample where positions nearest to the crown represent the oldest material.

Table 3: Linear regression parameters for the relationship between $\delta^{18}$O of human bone phosphate and drinking water reported in the literature

| Reference | Gradient | Intercept | R |
|---|---|---|---|
| Longinelli (1984) [74] | 0.64($\pm$0.03) | +22.37 | 0.98 |
| Luz (1984) [75] | 0.78 | +22.7 | 0.97 |
| Levinson (1987) [87] | 0.46 | +19.4 | 0.93 |
| Daux (2008) [77] | 0.58 | +21.5 | 0.87 |

The biogenic fractionation from meteoric water to bone phosphate of $\sim$ +22.37 ‰ (humans) was not explained in the Longinelli paper [74]. A supporting paper by Luz *et al*

[75] attempted to quantify this fractionation in a number of mammalian species (including humans), by considering a flux model approach. This paper suggests that the oxygen isotope composition of body water is a function of the net inputs versus the net outputs. The inputs are drinking water, atmospheric oxygen (respiration) and oxygen ingested through food. The outputs to consider are urine, sweat, exhaled water vapour and $CO_2$ (respiration) (see Figure 9).

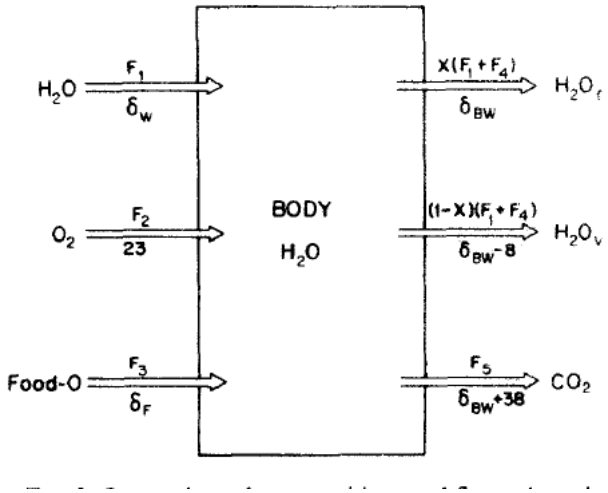


Figure 9: A box model (from Luz *et al* (1984), [75]) illustrating the fluxes of oxygen isotopes through a mammalian body. The inputs are water, atmospheric oxygen and food bound oxygen. Outputs are waste water (excretion), water vapour (breath) and carbon dioxide (respiration). F1-5 represent these fluxes.

The results from [75] suggest that the isotopic composition of body water of certain species are more reliant on drinking water than others. Animals with high water inputs and low metabolic activity would be more suited to a paleoclimatic study. Langlois et al [91] and Kohn et al [92] present concise studies into oxygen fluxes affecting the isotopic signal of bone and tooth enamel within mammals. Langlois presents a detailed box-model that has been compared with success to results from other published studies. Cerling *et al* [93] conducted a study to model isotope turnover rate in animals using the reaction progress variable ln(1-F), where F is the proportion of the input signal that has been transfered to the product (F=0 at t = 0 and F=1 at equilibrium), to determine the rate constants of the turnover. Cerling *et al* describe how mass change of the subject during

the measurement period has an effect on the rate constant. The fractionation of oxygen that occurs within the body is still mostly a black box. Studies such as those mentioned are slowly beginning to provide some understanding of the fractionation processes. Factors such as metabolism, health and age of the subject need to be considered when using isotope analysis on human samples as there will be a fractionation factor that is dependent on the individual.

Another focus of recent studies has been the development of the wet chemistry to produce improved reproducibility and to decrease the amount of tooth enamel of bone required. The $BiPO_4$ reduction by fluorination method is labour intensive due to the multi step precipitation reactions. This method also requires a large amount of apatite sample and is hazardous due to the hygroscopic nature of $BiPO_4$ [94]. In 1960, around the same time that Tudge [81] developed the $BiPO_4$ isolation method, two research groups were working on an alternative method for the isolation of phosphate as silver phosphate. Anbar *et al* [95] titrated a solution containing orthophosphate ions with silver perchlorate and sodium hydroxide to precipitate crystals of $Ag_3PO_4$, which was later pyrolysed at 1000 $^{\circ}C$ to produce a 10% yield of $O_2$ gas. Firsching [96] quantitively precipitated large silver phosphate crystals from solution by the volatization of ammonia (ammoniacal solution). The method of reducing the silver phosphate to $CO_2$ has progressed from the hazardous fluorination by $BrF_5$ method [94] to pyrolysis by graphite [97, 98]. This less hazardous method has opened the $\delta^{18}O$ analysis of phosphate to the wider scientific community [99] and provides comparable reproducability (Table 4).

#### 2.2.3.2 Isotopic composition of biogenic carbonate

Mammalian biogenic apatite contains oxygen bound as carbonate as well as phosphate (see Section 1.5). Analysing the carbonate rather than phosphate fraction of modern enamel or bone samples is attractive as sample size required is small (1-10 mg) and there is relatively little sample preparation required [100]. The modern method of apatite carbonate analysis is based on the method of analysing geological carbonate by the reaction

Table 4: Reproducibility for the $\delta^{18}O$ analysis of phosphates cited in the literature

| Sample | n | $\delta^{18}O \pm (1\sigma)$ | Method | Reference |
|---|---|---|---|---|
| NIST SRM 120c | 15 | 19.64±0.08 | Fluorination | [94] |
| | 5 | 21.8±0.34 | Graphite pyrolysis | [97] |
| | 13 | 21.36±0.18 | Fluorination | [100] |
| | | 21.8±0.2 | Graphite pyrolysis | [88] |
| | | 21.8±0.15 | Graphite pyrolysis | [89] |
| | | 21.74±0.37 | Graphite pyrolysis | [98] |
| | 3 | 22.58±0.09 | Fluorination | [101] |
| | 2 | 21.27±0.02 | Graphite pyrolysis | [101] |
| | 18 | 20.09±0.51 | TCEA | [101] |
| | 17 | 21.75±0.2 | Graphite pyrolysis | [76] |
| | 21 | 21.70±0.14 | Graphite pyrolysis | [77] |
| $Ag_3PO_4$ (Aldrich) | 11 | 19.64±0.08 | Fluorination | [94] |
| | 14 | 10.42±0.25 | Fluorination | [98] |
| NIST SRM 694 | 20 | 19.62±0.18 | Fluorination | [100] |

with >100% phosphoric acid to produce $CO_2$ as proposed by McCrea [102]. Originally this reaction would take place in sealed vessels at 25 °C until the reaction was considered complete. Subsequent studies have improved the efficiency and precision of the technique by using an automated online system with a common acid bath or acid dosing [103].

There are a number of limitations to the application of this technique to biogenic apatite carbonates that must be considered. Firstly there is a fractionation factor $\alpha_{SC-CO_2}$ associated with the conversion of the structural carbonate (SC) to carbon dioxide (Equation 16). The fractionation factor for geological materials such as calcite are well documented [102, 104, 105]. However it is not possible to measure the fractionation factor for biogenic apatite as it contains oxygen as phosphate and hydroxide moieties as well as carbonate which means that the total $\delta^{18}O_{SC}$ cannot be measured. It is therefore necessary to make the assumption that the fractionation of structural carbonate in the biogenic apatite is the same as in calcite and so samples are normalised to a calcite standard ($\alpha_{calcite-CO_2}$ (@90 $^{\circ}C$) = 1.00795 ± 0.00003 [105]).

$$\alpha_{SC-CO_2} = \frac{^{18}O/^{16}O_{SC}}{^{18}O/^{16}O_{CO_2}} \tag{16}$$

Bryant *et al* [100] have shown that the fractionation factor ($\alpha_{SC-P}$) between the structural carbonate and phosphate fractions of modern horse and wild boar apatite is 1.0086 $\pm$ 0.0007. Similar results were obtained from modern mammalian bone by Iacumin *et al* [21], $\alpha_{SC-P}$ = 1.0090. The $\delta^{18}O_{SC}$ values were compared to local meteoric water and showed a strong linear relationship ($r^2$ = 0.98). The regression equations from these studies are shown in table 5.

A second limitation that must be considered is that of diagenic alteration [21]. It is generally accepted that phosphate bound oxygen is stable after its formation and does not exchange with the surrounding environment and hence its diagenesis is negligible [75]. Carbonate however reacts rapidly with its surroundings, particularly in an aqueous environment. Diagenesis of carbonate can occur due to dissolution-reprecipitation reactions, ion exchange at the mineral surface or precipitation of secondary minerals in the apatite matrix [106]. Koch *et al* [107] suggest a method for the 'clean up' of diagenically altered hydroxy apatite and suggest that tooth enamel is more resistant than bone material due to the lower organic content. A later study by Zazzo *et al* [106] concluded that both phosphate and carbonate are susceptible to diagenesis under normal inorganic conditions (deionized water) although the exchange rate for carbonates is approximately 10 times that for phosphate. Under organic conditions (microbial environment) phosphate reacted at a faster rate than carbonate. Again enamel was found to be less susceptible to diagenesis than bone material. Iacumin et al [21] describe an elegant method for determining the extent of diagenesis by analysis of the correlation between bone phosphate and bone carbonate. The $\delta^{18}O$ of both carbonate and phosphate in bone is proven to be related to

Table 5: Linear regression parameters for the relationship between $\delta^{18}O$ values for mammalian bone and enamel structural carbonate ($\delta^{18}O_{SC}$), phosphate ($\delta^{18}O_P$) and meteoric water ($\delta^{18}O_{MW}$)

| Reference | Sample | n | Regression | $r^2$ |
|---|---|---|---|---|
| [100] | Modern horse | 42 | $\delta^{18}O_{SC}$ = 1.02$\delta^{18}O_P$ + 8.3 | 0.986 |
| [21] | Modern mammals | 31 | $\delta^{18}O_P$ = 0.98$\delta^{18}O_{SC}$ - 8.5 | 0.98 |
| [21] | Modern deer | 31 | $\delta^{18}O_{SC}$ = 0.998$\delta^{18}O_{MW}$ + 33.63 | 0.98 |
| [50] | Modern humans | 5 | $\delta^{18}O_{SC}$ = 0.350$\delta^{18}O_{MW}$ + 27.6 | 0.85 |

the $\delta^{18}O$ of body water (and hence drinking water) with good correlation (R = 0.98).

The small amount of sample preparation required and the high throughput of $\delta^{18}$O analysis of carbonates makes it an attractive method for the analysis of modern human tooth samples in forensics and will be the method used in this study.

### 2.2.4 Isoscapes: Modeling and mapping spatial stable isotope variation for forensic application

Spatial mapping of geochemical data is not a new concept. For decades chemical maps have been used as an important tool for geologists, prospectors and mining companies. In the last decade geochemical mapping has seen increasing application across the scientific community as online datasets have improved availability of spatial geochemical data [108, 109]. Jason West and Gabe Bowen recognised the interdisciplinary importance of spatial maps of isotopic fractionation and coined the term 'Isoscape' to describe the development of 'Isotope landscapes'; maps of the spatial isotope variation of a material of interest. Isoscapes can be based solely on the spatial interpolation of measured isotope values, however it is often more useful to relate measured isotopic composition at a given point to some environmental, physical or climatic variable. Isoscapes have already been applied to a wide range of applications including ecology [47, 110, 111, 112], paleoclimate [113] , forensic science [50, 1, 114] and hydrology [115, 62, 59, 116].

#### 2.2.4.1 Forensic isoscapes in the literature: Potentials and pitfalls

Forensic science investigation often involves determining the origin of a crime scene sample of interest, whether that be linking a DNA swab to a suspect, a drug sample to a certain drugs shipment or a soil sample from a suspects shoe to the crime scene. In Section 2.2.2 the use of stable isotope analysis for the determination of origin of a sample of interest was introduced. The next step forward for isotope forensics is to be able to determine the spatial location of origin of a sample based on its isotopic fingerprint. This has led

to a new field of research in the forensic community with groups working towards the understanding of spatial isotopic variation in forensic samples, particularly human tissue. Development of forensic isoscapes is at the cutting edge of stable isotope applications [50] and as understanding of the processes contributing to spatial isotopic variation improves and databases of measured samples grow the accuracy and precision of these isoscapes should be improved.

Spatial isotope variation of a matrix of interest can be determined by modeling the processes and mechanisms that determine fractionation. These may be based on climate and environmental variables. Alternatively the isotope variation may be determined by linear regression between the isotope signature of the matrix and a source material such as water. The precision of these prediction models is limited by the understanding of the processes involved. The isotopic composition of a material is determined by the isotopic composition of the source materials and the conditions and processes that are involved in the formation of the material. In the case of oxygen isotope variation, which is the main focus of this thesis, the main source material is generally environmental water.

As has been described in Section 2.2.1 a great deal of research has been carried out on the global $\delta^{18}$O and $\delta$D isotopic variation in precipitation, most of which are based on the GNIP database. Models that have been published based on this dataset ([62, 59, 3]) are very useful at a large inter-continental scale, explaining 76 - 79 % of the isotopic variation of the GNIP database [117]. However these models are limited at a smaller regional scale due to local climate conditions and limited sampling density in some areas. This limitation must be considered when using data from these models.

In the case of human tissue, oxygen and hydrogen isotope signature is mainly derived from drinking water which may not necessarily be the same as local precipitation. Dutton *et al* [64] present river water isoscapes for $\delta^{18}$O and $\delta$D for the conterminous USA. It was shown that in the western United States the isotopic difference between river water and precipitation is between -1 and -12 ‰ for oxygen. That is river water in the western United States has a lighter isotopic signature than would be expected if mean annual precipitation

was the source. This was attributed to a high input of isotopically lighter precipitation in river catchments at high elevation. Bowen *et al* [65] present a first Isoscape of tap water isotope ratios. Again it is shown that in the western United States tap water has a distinctly lighter isotopic signature than the modeled annual precipitation (-2 - -5.6 ‰). In Texas and the central US tap water is significantly heavier than that of local precipitation (2.6 - 10.5 ‰) [65]. The lighter tap water regions are attributed to altitude and seasonality effects as well as the effect of old, pre-Holocene groundwater. Heavier regions are attributed to post precipitation evaporation.

This thesis is concerned with the spatial oxygen isotopic variation observed in modern human tissue, in particular human tooth enamel. At present the number of validated isoscapes for human tissue is limited. Ehleringer *et al* [1] present the first example of a validated isoscape for the prediction of origin of human hair samples for the USA which was able to explain 85 % of the isotopic variation in the population. The remaining variation was attributed to local variation in diet. In a subsequent study Thompson *et al* [34] performed a similar study based on individuals from Asia, observing that there is a higher consumption of locally produced foods than was found for the USA resulting in a larger gradient for the relationship between the drinking water and human hair $\delta^{18}$O and $\delta^{2}$H isotopic composition (Section **??**). Ehleringer *et al* [50] present a first attempt to use tooth enamel carbonate forensically to identify the location of origin for modern humans. A tap water isoscape of the USA was calibrated to tooth enamel carbonate by linear regression ($\delta^{18}O_c$=0.350$\delta^{18}O_{dw}$ + 27.6 ‰, $r^2$ = 0.85). This was based on only 5 samples but indictates that tooth enamel carbonate is likely to be a useful matrix for forensic investigation of human origin.

When isoscape models are used to predict the origin of an unknown sample the result is a band of isotopic space from which the sample may have originated. If only one isotope is used and there is no supporting forensic intelligence for the investigation this may result in a band covering several thousand square kilometers over multiple continents. Single isoscapes are most useful where there is some *a priori* knowledge of the sample so that

questions such as: could this sample come from location X or did this sample come from location A or location B can be answered. It is hypothesised that by combining Isoscapes of multiple isotope systems the band of isotopic space from which the sample could have originated can be significantly reduced in cases where no *a priori* knowledge is available.

The most important consideration for these examples is that precision of Isoscape predictions is limited by the level of understanding of the processes that determine the spatial isotopic variation. If a box model approach is taken [1], all dietary and environmental inputs need to be understood to maximize the isotopic variation that can be described by the model. As well as this the fractionation between inputs and the matrix of interest (i.e. keratin) need to be understood. If a regression approach is to be used, a large sample size is required and multiple samples from the same location will enable the understanding of local variation. Ehleringer *et al* [50] highlight the fact that the same forces that shape the isotopic composition of water are likely to be reflected in the isotopic composition of both hair and tooth enamel.

## 2.3 Analytical methods

### 2.3.1 Isotope Ratio Mass Spectrometry: An introduction to IRMS instrumentation

Isotope Ratio Mass Spectrometry (IRMS) encompasses over 100 years of research and development [44]. The first description of an instrument that could be considered to be a mass spectrometer came in 1912 by J. Thomson [118]. In the study the mass spectrometer was used to obtain a mass spectrum of carbon dioxide. The introduction of the Nier mass spectrometer in 1947 [119] provided the basis for modern isotope ratio mass spectroscopy and was the first instrument described containing all the elements that are still present in IRMS today: a gas source, magnetic sector, multiple ion collectors and an inlet system for handling the sample and reference gas. The following sections provide a description of the elements of modern IRMS instrumentation. For the purpose of this study the following sections are concerned with the Dual Inlet - IRMS analysis of $\delta^{18}O$ of water samples, carbonate (from bioapatite) and phosphate (from bioapatite).

#### 2.3.1.1 Sample preparation

**Analysis of the isotopic composition of water and aqueous solutions** became established during World War II due to the large amount of heavy water being produced for the 'Manhattan Project', the US initiative to develop the first atomic bomb. Subsequent development has lead to the application of IRMS in a wide range of disciplines including chemistry, biology, geology, hydrology, forensic science and archeology (see Section 2.2).

In order to measure the $^{18}O$ isotopic composition of water samples they must be converted into a form that can be introduced into the mass spectrometer. Methods include the direct introduction of water, chemical conversion to $CO_2$ and the method that will be used in this study, the equilibration of water with carbon dioxide [120]. The equilibrium of water

with carbon dioxide is based on the research of Harold Urey [121].

A few mL of water are injected into an evacuated vessel, then $CO_2$ of known isotopic composition is introduced. The vessels are shaken for a period of $\geq$6 hours to facilitate the equilibrium reaction which is described by Equations 17, 18 and 19:

$$CO_{2(g)} \overset{K_e}{\rightleftharpoons} CO_{2(aq)} \tag{17}$$

$$CO_{2(aq)} + H_2O_{(l)} \overset{K_h}{\rightleftharpoons} H_2CO_3 \overset{K_l}{\rightleftharpoons} H^+ + HCO_3^- \tag{18}$$

$$C^{16}O_{2(g)} + H_2^{18}O_{(l)} \overset{K_{tot}}{\rightleftharpoons} C^{16}O^{18}O_{(g)} + H_2^{16}O_{(l)} \tag{19}$$

where $K_e$, $K_h$, and $K_l$ are the equilibrium constants for gas exchange, hydration and dissociation respectively. $K_{tot}$ is the equilibrium constant of the overall reaction. $K_{tot}$ can be substituted into Equation **??** to calculate the fractionation factor $\alpha$ ($\alpha_{H_2O}^{CO_2}$ = 1.0412 at 25 °C [120]). The equilibrated $CO_2$ can then be introduced into the mass spectrometer.

**Analysis of hydroxy apatite in human bones and teeth** can involve complex chemistry in order to transform the bound oxygen into a form that can be easily introduced into the mass spectrometer such as CO or $CO_2$ (see Sections 2.2.3.2 and 2.2.3.1). Analysis involves converting the isotope of interest into a gas phase for introduction into the mass spectrometer. Until recently the sample preparation was performed offline and the analytical precision was highly dependent on investigator error. Modern techniques utilise elemental analysers containing a reducing agent such as carbon or an autosampler connected to a common acid bath for reaction with >100 % phosphoric acid [15, 122].

#### 2.3.1.2 Sample inlet system

A system consisting of valves and capillaries is utilised to ensure that the gaseous sample is introduced into the mass spectrometer at a constant flow rate. Generally the system is constructed of stainless steel that is inert to the sample gas [123]. There are two types of inlet system for IRMS, continuous flow and duel-inlet. All measurements in this study were performed using duel-inlet IRMS. A Duel-Inlet IRMS works on the premise that the sample is measured alongside a reference standard gas by alternating between the two gases multiple times during the analysis. This is achieved by storing the gases in separate reservoirs and using a changeover valve which allows multiple alternative measurements of the sample and reference gas while maintaining equal pressure and flow parameters. The gases are transferred from the reservoirs to the changeover valve by capillary (0.1 mm i.d.) with crimps at the ends to produce the viscous gas flow. The use of capillaries and crimps prevents the direct effusion of the sample into the ion source which would lead to kinetic fractionation.

#### 2.3.1.3 Ion source

In order to separate the gas molecules by mass they must be ionised as in standard mass spectrometry. Ionisation is achieved by the bombardment of the gas molecule (M) with electrons ($e^-$) produced by a hot filament (Equation 20):

$$M + e^- \rightarrow M^+ \bullet + 2e^- \tag{20}$$

The efficiency of the ionisation reaction is determined by the ionisation cross section, the number of electrons produced in the ion source, the energy of the electrons and the number of molecules present. The more efficient the ionisation process the more sensitive the mass spectrometer will be [123]. Electrons are produced by a heated tungsten (W) filament which are accelerated across the ion box by an electrostatic potential (E = 50-150 eV) and collected at the other side by an electron trap. The path of the electrons is

controlled by a magnetic field. The generated ions are extracted from the ion box using a series of ion lenses at specified electric potentials.

#### 2.3.1.4 Magnetic sector

Ions, accelerated to velocity (v) at the exit of the ion source, enter into the magnetic sector of the instrument which consists of a permanent or electromagnet that deflects the path of the ions perpendicular to the initial path. The radius of the deflection is given by Equation 21.

$$r^2 = \frac{2V}{B} \times \frac{m}{z} \tag{21}$$

Where r is the radius of deflection, V is the accelerating voltage, B is the strength of the magnetic field, m is the fragment mass and z is its charge [15]. From this equation it is clear that heavier ions will have a larger radius while lighter ions will be deflected more and have a smaller radius providing they have the same ionic charge (most positive ions produced in the source are +1) and are subjected to the same electric and magnetic field.

#### 2.3.1.5 Ion detector

The ion detector consists of 2 or more Faraday cups, which collect the ion species of interest and turn the signal into an electrical impulse. The introduction of the dual detector by Nier (1947) [119] revolutionised isotope analysis as simultaneous analysis by separate amplifiers completely cancels fluctuations of the ion current due to temperature changes or electron beam instability [123]. Modern IRMS systems use three or more Faraday cups which minimise false detector currents and allows for each cup to be accurately tuned to measure one mass exclusively. When measuring the bulk isotopic composition of $CO_2$ the Faraday cups are tuned to collect the most abundant species , masses 44 ($C^{12}O^{16}O^{16}$), 45 ($C^{13}O^{16}O^{16}$, $C^{12}O^{17}O^{16}$) and 46 ($C^{12}O^{18}O^{16}$, $C^{13}O^{17}O16$).

### 2.3.2 Cavity ring down spectroscopy

Cavity Ring Down Spectroscopy (CRDS) is an optical technique that takes advantage of the mass dependency of molecular vibrations in order to determine the stable isotopic composition of a sample. Electromagnetic energy is absorbed by a molecule as described by the Beer-Lambert Law (Equation 22).

$$\frac{I}{I_\circ} = \exp^{-\sigma l} \tag{22}$$

where I and $I_\circ$ are the intensity of transmitted light and incident light respectively, $\sigma$ is the absorption cross section and l is the pathlength. Conventional infrared spectrometers have limited sensitivity at low concentrations of a trace gas. CRDS overcomes this limitation by utilizing a mirrored cell (see Figure 10) that increases the effective pathlength to many kilometers, hence improving absorption and sensitivity. Radiation is introduced to the cavity by single-frequency laser. Ring down is measured by switching off the laser source and observing the time taken for the signal to decay exponentially to zero. If the cell is empty the decay is only caused by radiation lost from the slightly transparent mirror. When a sample is present signal can also be lost by absorption of the energy by the molecules hence the decay is quicker. The decay signal can be converted into an isotopic composition by the instrument software. Currently instruments are commercially available for the analysis of liquid and vapourised water ($\delta^{18}O$ and $\delta^{2}$H), carbon dioxide ($\delta^{13}C$), methane ($\delta^{13}C$) and nitrous oxide ($\delta^{15}N$ and $\delta^{18}O$).

### 2.3.3 Analysis of drinking water from the Middle East by CRDS

Drinking water samples from the United Arab Emirates (n = 5) and Oman (n = 1) were collected by colleagues travelling in those areas. Water was collected in 50 mL HDPE bottles, ensuring that no headspace remained when the bottles were sealed. Bottles were further sealed with parafilm and were refrigerated until analysis. Time between collection

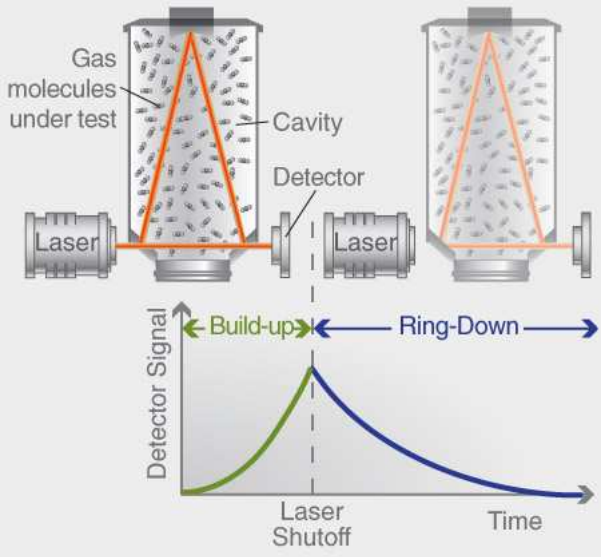


Figure 10: Schematic of a cavity ring down cell, illustrating the increased path length and the process of measuring the ring down signal. (Source: http://www.picarro.com)

and analysis was $<$ 1 week. The samples were pipetted into 2 mL chromatography vials (( 400 $\mu$L)) with PTFE septa and analysed by Picarro CRDS (see Section 2.3.2) [124]. Three calibrations standards with known isotopic compositions (VSMOW scale), USGS W64444 ($\delta^{18}O$ = -51.4 $\pm$ 0.03 ‰, $\delta D$ = -399.1 $\pm$ 0.4 ‰), GISP ($\delta^{18}O$ = -24.76 $\pm$ 0.09 ‰, $\delta D$ = -189.5 $\pm$ 1.2 ‰) and USGS W67400 ($\delta^{18}O$ = -1.97 $\pm$ 0.02 ‰, $\delta D$ = 1.25 $\pm$ 0.4 ‰) were run at the start and end of the analysis. Sample results were calibrated to these calibration standards by linear least squares regression. A laboratory standard NTW (Norwich Tap Water) was measured along with the standards to monitor reproducibility of the results. Each sample was measured 6 times and the first three measurements discarded to account for the memory effect [124].

### 2.3.4 Direct analysis of $\delta^{18}$O of human tooth enamel carbonate by IRMS

Tooth surface was cleaned with Milli-Q water. A small amount of enamel was removed from the crown of each tooth using a diamond cutting wheel taking care to do minimal damage to the tooth. 1.3 mg of the tooth enamel was weighed into stainless steel

reaction capsules which were then placed into a 47 position carousel and evacuated to high vacuum. The samples were reacted with >100% phosphoric acid (d = 1.92 g/cm$^3$) in a common acid bath. The evolved $CO_2$ was cryogenically purified and analysed by DI-IRMS (Europa-SIRA II DI-IRMS). Results were reported versus VPDB. An in-house carbonate reference material UEA-CMST ($\delta^{18}O_{VPDB}$ = -2.04 ‰) was measured alongside the samples (12 replicates per batch) to allow for correction due to matrix effects by single point calibration in accordance with the standard method applied by SIL. An in-house enamel reference material THCB-RP10 (-6.4 $\pm$ 0.2 ‰, n = 15) was prepared from enamel material removed from a number of human teeth collected for method development and homogenising by first powdering with a diamond cutting wheel followed by further grinding and mixing using a pestle and mortar. This reference was measured in triplicate along with each batch of case study teeth in order to observe the reproducibility of the analysis.

## 2.4 Results

### 2.4.1 Middle East drinking water analysis

5 drinking water samples collected from the United Arab Emirates and 1 from Oman were measured in triplicate using a Picarro $H_2O$ CRDS. Measurement precision of the triplicates was $< 0.1$ for $\delta^{18}$O and $< 0.3$ for $\delta^{2}$H. Results for each of the water samples are shown in Table 6. The range of isotopic compositions within the 7 samples was small which is to be expected as all of the samples originated from within a small geographical area. The $\delta^{18}O_{VSMOW}$ composition of the water samples range from -2.1 to - 2.4 ‰ and the $\delta^{2}H_{VSMOW}$ composition range from -12.6 to -15.3 ‰ with the exception of sample CFP-TW-014 (Masafi mineral water) which has a $\delta^{2}H_{VSMOW}$ composition of -4.9 ‰. This sample is significantly enriched in the heavier isotope of hydrogen than the other samples. This may be due to evaporation at the source or during purification and packaging. These results will be combined with published isotopic data from water within the study region to produce an improved water isoscape of the Middle East (Section 2.6).

Table 6: $\delta^{18}$O and $\delta^{2}$H isotopic composition of drinking water samples from the Middle East. Values are reported against VSMOW

| Sample | Source | Lat (°) | Long (°) | $\delta^{18}O \pm \sigma$ | $\delta D \pm \sigma$ |
|---|---|---|---|---|---|
| CFP-TW-009 | Oman tap water | 23.579 | 58.570 | -2.4 $\pm$ 0.0 | -13.5 $\pm$ 0.3 |
| CFP-TW-013 | Abu Dhabi tap water | 24.462 | 54.371 | -2.3 $\pm$ 0.0 | -15.3 $\pm$ 0.1 |
| CFP-TW-014 | Abu Dhabi 'masafi' mineral water | 24.462 | 54.371 | -2.2 $\pm$ 0.0 | -4.9 $\pm$ 0.2 |
| CFP-TW-015 | Abu Dhabi 'hilton' mineral water | 24.462 | 54.371 | -2.3 $\pm$ 0.1 | -14.2 $\pm$ 0.1 |
| CFP-TW-017 | Abu Dhabi tap water | 24.462 | 54.371 | -2.1 $\pm$ 0.1 | -12.9 $\pm$ 0.3 |
| CFP-TW-018 | Al Ain Mineral water | 24.206 | 55.749 | -2.2 $\pm$ 0.1 | -12.6 $\pm$ 0.3 |

### 2.4.2 Middle East tooth enamel carbonate analysis

Samples of enamel extracted from the collection of Middle East Teeth (Section 1.6, Figure 5) were measured using Dual Inlet IRMS. Instrument precision was monitored by repeated analysis of an in house carbonate standard and was generally $<$0.2 ‰ ($1\sigma$) for $\delta^{18}$O (4 replicates of the standard were run at the beginning and end of each batch). Enough

tooth enamel was collected from 26 samples to perform replicate analysis, which resulted in an average precision of $\pm$ 0.3 ‰ for $\delta^{18}O$. Reproducibility was monitored by the triplicate analysis of a homogenised tooth enamel powder (THCB-RP10) used as a laboratory standard with each batch. Precision of the triplicates was 0.1 ‰ ($1\sigma$) for $\delta^{18}O$ for each batch (with the exception of the first batch which had a precision of 0.2 ‰). Over the course of the 5 batches the mean $\delta^{18}O_{VPDB}$ of the THCB-RP10 lab standard was -6.4 $\pm$ 0.2 ‰ ($1\sigma$). Of the 68 samples, results were obtained for 58. The remaining 10 samples were either considered too decayed for measurement, or were lost during analysis due to low $CO_2$ yield. $\delta^{18}O_{VSMOW}$ for the tooth enamel carbonate was calculated from the relationship; $\delta^{18}O_{VSMOW}$ = 1.03092*$\delta^{18}O_{VPDB}$ + 30.92 ‰ as given by Sharp *et al* [125]. $\delta^{18}O_{VSMOW}$ for the Middle East Teeth range from 21.8 ‰ to 29.2 ‰ (mean($\pm1\sigma$) = 25.0 ($\pm$1.8) ‰).

## 2.5 Discussion

In order to test whether $\delta^{18}O_{VSMOW}$ can be used to differentiate between locations in the Middle East, summary statistics for each of the 19 locations of origin were calculated and are reported in Table 8. A boxplot (Figure 11) was produced to visualise the population statistics for each of the cities of origin. From the boxplot it can be seen that two main groups can be differentiated. The cities from the south of the Arabian peninsula (Taiz - Um-Ghafa) are enriched in $^{18}O$ compared to most of the cities from the north of the study region (Waset - Mashhad). Deyali in Iraq and Kermanshah in Iran are enriched in $^{18}O$ compared to the other northern cities. This could be due to consumption of desalinated water or due to dietary inputs. However n = 1 for each of these locations so they could represent outliers from the general population. More samples are required to test this. The sample from Ibra is the most enriched in $^{18}O$. The four cities with n $>$ 5 samples can be used to get an impression of the expected local isotopic variation in human populations from the Middle East. Local variation is likely due to a combination of dietary

sources available at a location, sex and fitness of the individuals, number of drinking water sources. More samples are required to further understand the local variation within human populations but this data can be considered a preliminary estimatation. Tehran, Iran (n = 12), has a range of 2.3 ‰ ($\mu$ = 23.2, $\sigma$ = 0.7 ‰). Al-Ghail, Yemen (n = 8), has a larger local range of 3.3 ‰ ($\mu$ = 26.7, $\sigma$ = 1.1 ‰). Al Ain, UAE (n=7), has a local range of 3.3 ‰ ($\mu$ = 26.6, $\sigma$ = 1.1 ‰). Baghdad, Iraq (n=7) has a much smaller local range of 1.2 ‰ ($\mu$ = 22.9, $\sigma$ = 0.4 ‰). This may be an artifact of the small sample size but it may represent a more averaged diet and water intake of the population which would be expected in a developed capital city such as Baghdad.

Analysis of variance was performed between the sample origins. ANOVA confirms the observations from the boxplot, there is significant difference between the different locations at the 95 % confidence level (F value = 15.2, F Crit = 1.9, P(>F) = 2.2E-12). Tukey's honestly significant difference test compares the mean on each location to every other location. Of the 171 comparisons, only 30 were significantly different at the 95 % confidence level. As was observed in the boxplot (Figure 11) these differences were between cities in the southern Arabian Peninsula compared to the cities in the north of the study region. The comparisons that were significantly different are listed in Table 9.

Table 7: Measured $\delta^{18}O_{VPDB}$ values of the Middle East tooth enamel samples. The childhood origin of the teeth is presented along with coordinates and altitude for each location. Replicates were measured for samples with sufficient material available, for these samples the mean and standard deviation ($1\sigma$) are reported along with the number of replicates measured (n).

| **Sample ID** | **Origin** | **Country** | **Latitude (°)** | **Longitude (°)** | **Altitude (m)** | $\delta^{18}O_{VPDB}$ | **1$\sigma$** | **n** |
|---|---|---|---|---|---|---|---|---|
| TE064 | Esfahan | Iran | 35.37 | 51.26 | 933 | -6.4 | | |
| TE065 | Tehran | Iran | 35.42 | 51.26 | 967 | -7.6 | | |
| TE066 | Kermanshah | Iran | 34.18 | 51.26 | 900 | -5.0 | 0.3 | 3 |
| TE067 | Tehran | Iran | 35.42 | 51.26 | 967 | -7.1 | | |
| TE068 | Tehran | Iran | 35.42 | 51.26 | 967 | -6.8 | | |
| TE069 | Rodehen | Iran | 35.44 | 51.54 | 926 | -6.6 | 0.4 | 2 |
| TE070 | Ghazvin | Iran | 36.14 | 50.20 | 1221 | -7.0 | | |
| TE071 | Ghazvin | Iran | 36.14 | 50.20 | 1221 | -7.0 | | |
| TE072 | Sabzevar | Iran | 35.42 | 51.26 | 967 | -7.9 | | |

Continued on Next Page...

Table 7 – Continued

| Sample ID | Origin | Country | Latitude (°) | Longitude (°) | Altitude (m) | $\delta^{18}O_{VPDB}$ | 1$\sigma$ | n |
|---|---|---|---|---|---|---|---|---|
| TE073 | Sabzevar | Iran | 35.42 | 51.26 | 967 | -8.8 | 0.7 | 3 |
| TE074 | Tehran | Iran | 35.42 | 51.26 | 967 | -7.6 | | |
| TE075 | Mashhad | Iran | 36.17 | 59.36 | 1777 | -6.7 | | |
| TE076 | Tehran | Iran | 35.42 | 51.26 | 967 | -6.7 | | |
| TE077 | Tehran | Iran | 35.42 | 51.26 | 967 | -6.6 | | |
| TE078 | Tehran | Iran | 35.42 | 51.26 | 967 | -7.7 | | |
| TE079 | Tehran | Iran | 35.42 | 51.26 | 967 | -7.9 | | |
| TE080 | Tehran | Iran | 35.42 | 51.26 | 967 | -7.8 | | |
| TE081 | Tehran | Iran | 35.42 | 51.26 | 967 | -7.7 | | |
| TE082 | Afghanistan | Afghanistan | 36.42 | 67.60 | 1321 | -7.5 | | |
| TE039 | Waset | Iraq | 32.41 | 45.33 | 15 | -6.2 | | |
| TE040 | Waset | Iraq | 32.41 | 45.33 | 15 | -5.6 | | |
| TE041 | Baghdad | Iraq | 33.18 | 44.23 | 31 | -7.8 | | |
| TE042 | Baghdad | Iraq | 33.18 | 44.23 | 31 | -7.1 | | |

Continued on Next Page...

Table 7 – Continued

| Sample ID | Origin | Country | Latitude (°) | Longitude (°) | Altitude (m) | $\delta^{18}O_{VPDB}$ | 1$\sigma$ | n |
|---|---|---|---|---|---|---|---|---|
| TE043 | Baghdad | Iraq | 33.18 | 44.23 | 31 | -8.2 | 0.0 | 3 |
| TE044 | Baghdad | Iraq | 33.18 | 44.23 | 31 | -7.8 | | |
| TE045 | Baghdad | Iraq | 33.18 | 44.23 | 31 | -8.0 | | |
| TE046 | Baghdad | Iraq | 33.18 | 44.23 | 31 | -7.6 | | |
| TE047 | Deyali | Iraq | 34.40 | 45.70 | 513 | -4.9 | | |
| TE048 | Baghdad | Iraq | 33.18 | 44.23 | 31 | -7.7 | | |
| TE027 | Sur | Oman | 22.34 | 59.31 | 209 | -4.7 | | |
| TE028 | Muscat | Oman | 23.37 | 58.29 | 1268 | -5.3 | | |
| TE029 | Ibra | Oman | 22.41 | 58.32 | 346 | -1.7 | | |
| TE030 | Muscat | Oman | 23.37 | 58.29 | 1268 | -4.1 | 0.3 | 2 |
| TE031 | Muscat | Oman | 33.18 | 44.23 | 31 | -5.3 | | |
| TE032 | Sur | Oman | 22.34 | 59.31 | 209 | -4.2 | 0.2 | 2 |
| TE034 | Salalah | Oman | 17.00 | 54.32 | 17 | -2.8 | 0.2 | 2 |
| TE035 | Baloshistan | Oman | 28.80 | 65.33 | 970 | -4.2 | | |

Continued on Next Page...

Table 7 – Continued

| Sample ID | Origin | Country | Latitude (°) | Longitude (°) | Altitude (m) | $\delta^{18}O_{VPDB}$ | 1$\sigma$ | n |
|---|---|---|---|---|---|---|---|---|
| TE036 | Bidbid | Oman | 23.24 | 58.70 | 340 | -4.6 | 0.4 | 3 |
| TE038 | Muscat | Oman | 23.37 | 58.29 | 1268 | -5.3 | | |
| TE016 | AlAin | UAE | 24.13 | 55.45 | 175 | -5.4 | 0.2 | 2 |
| TE017 | AlAin | UAE | 24.13 | 55.45 | 175 | -4.3 | | |
| TE018 | AlAin | UAE | 24.13 | 55.45 | 175 | -4.4 | 0.2 | 2 |
| TE019 | AlAin | UAE | 24.13 | 55.45 | 175 | -3.6 | | |
| TE020 | AlAin | UAE | 24.13 | 55.45 | 175 | -2.3 | | |
| TE021 | AlAin | UAE | 24.13 | 55.45 | 175 | -3.8 | | |
| TE022 | Hili | UAE | 24.17 | 55.46 | 216 | -4.8 | | |
| TE023 | Um-Ghafa | UAE | 24.50 | 55.54 | 240 | -4.1 | | |
| TE024 | UAE | UAE | 24.13 | 55.45 | 175 | -4.1 | 0.7 | 3 |
| TE025 | Um-Ghafa | UAE | 24.50 | 55.54 | 240 | -4.4 | | |
| TE049 | Taiz | Yemen | 13.34 | 44.10 | 1651 | -5.2 | | |
| TE050 | Al-Ghail | Yemen | 15.17 | 47.48 | 1524 | -4.7 | | |

Continued on Next Page...

Table 7 – Continued

| Sample ID | Origin | Country | Latitude (°) | Longitude (°) | Altitude (m) | $\delta^{18}O_{VPDB}$ | 1$\sigma$ | n |
|---|---|---|---|---|---|---|---|---|
| TE052 | Al-Ghail | Yemen | 15.17 | 47.48 | 1524 | -5.1 | 0.1 | 3 |
| TE054 | Al-Ghail | Yemen | 15.17 | 47.48 | 1524 | -3.5 | | |
| TE055 | Al-Quada | Yemen | 15.17 | 47.48 | 1524 | -2.1 | | |
| TE056 | Al-Ghail | Yemen | 15.17 | 47.48 | 1524 | -3.5 | 0.2 | 3 |
| TE057 | Al-Ghail | Yemen | 15.17 | 47.48 | 1524 | -3.6 | | |
| TE059 | Habayer | Yemen | 15.17 | 47.48 | 1524 | -5.2 | | |
| TE063 | Al-Oyon | Yemen | 15.17 | 47.48 | 1524 | -4.9 | | |

Table 8: Summary statistics for each of the sample locations for the Middle East tooth enamel carbonate $\delta^{18}$O measurements (n = 58). Results are reported against the VSMOW standard.

| Origin | Mean $\delta^{18}O_{VSMOW}$ | $\sigma$ | n |
|---|---|---|---|
| Al-Ghail | 26.7 | 1.1 | 8 |
| AlAin | 26.6 | 1.1 | 7 |
| Baghdad | 22.9 | 0.4 | 7 |
| Bidbid | 26.2 | | 1 |
| Deyali | 25.9 | | 1 |
| Esfahan | 24.3 | | 1 |
| Ghazvin | 23.7 | 0.0 | 2 |
| Hili | 27.0 | | 1 |
| Ibra | 29.2 | | 1 |
| Kermanshah | 25.7 | | 1 |
| Mashhad | 24.0 | | 1 |
| Muscat | 25.8 | 0.6 | 4 |
| Rodehen | 24.1 | | 1 |
| Salalah | 28.0 | | 1 |
| Sur | 26.4 | 0.3 | 3 |
| Taiz | 25.5 | | 1 |
| Tehran | 23.2 | 0.7 | 12 |
| Um-Ghafa | 26.4 | 0.4 | 3 |
| Waset | 24.8 | 0.4 | 2 |

### 2.5.1 The effect of tooth type on $\delta^{18}$O composition of tooth enamel

As was mentioned in Section 1.5.2.1 only 66 % of the teeth used in this study are second or third molars and earlier erupting teeth (incisors, canines and premolars) are not considered as reliable for forensic purposes [15]. For that reason it is important to ascertain whether the results from the non molars are still useful for retaining isotopic identity. Figure 12 shows boxplots comparing the $\delta^{18}$O isotopic composition of tooth enamel for the different tooth types for A) the whole population, B) Yemen, C) Oman and D) Iraq. The collection from Iran contains all molars except for one premolar and the collection from UAE contains only premolars and therefore these collections could not be used to compare tooth type.

From the figure it can be seen that if we compare tooth type over all locations there is significant overlap between the populations but the median values for incisors and premolars

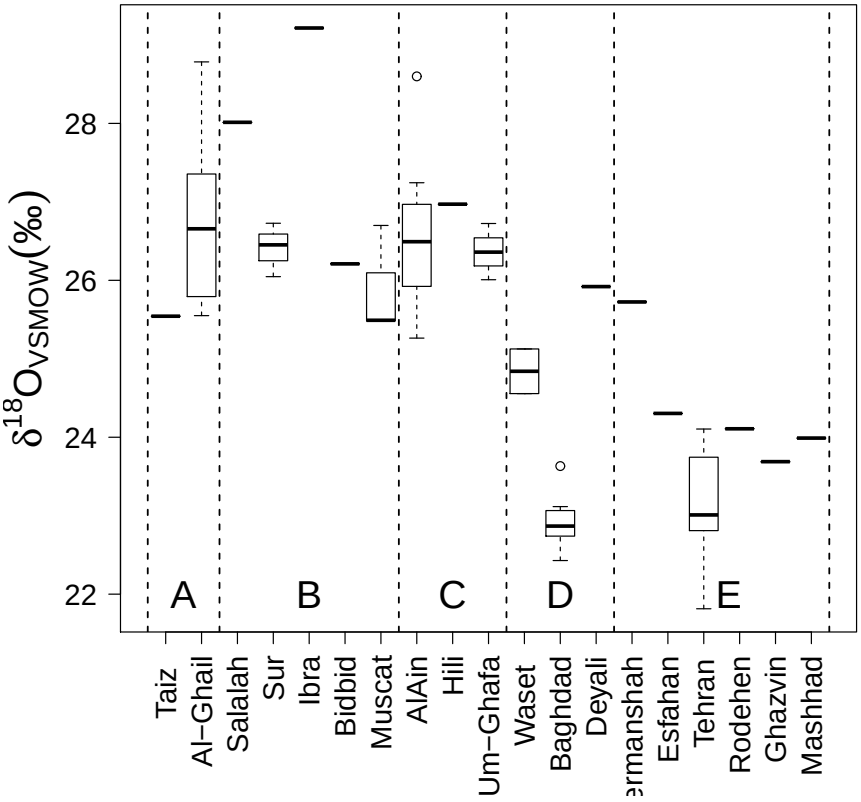


Figure 11: A box plot of the $\delta^{18}O_{VSMOW}$ composition of the Middle East teeth (n=58) based on location of origin. The city of origin of the tooth samples is shown on the X axis. The cities are ordered according to country where A = Yemen, B = Oman, C = UAE, D = Iraq and E = Iran. For each of the 'boxes' the thick black line represents the median (or the sole value where n = 1), the box represents the inter-quartile range and the whiskers show the range. Open circles are possible outliers.

Table 9: Locations of origin for tooth enamel that can be differentiated using $\delta^{18}$O composition at the 95 % significance level by Tukey's HSD test.

| Location A | Location B | P |
|---|---|---|
| Al Ghail | Baghdad | <0.001 |
| Al Ghail | Ghazvin | 0.002 |
| Al Ghail | Tehran | <0.001 |
| Al Ain | Baghdad | <0.001 |
| Al Ain | Ghazvin | 0.004 |
| Al Ain | Tehran | <0.001 |
| Baghdad | Bidbid | 0.03 |
| Baghdad | Hili | 0.002 |
| Baghdad | Ibra | <0.001 |
| Baghdad | Muscat | <0.001 |
| Baghdad | Salalah | <0.001 |
| Baghdad | Sur | <0.001 |
| Baghdad | Um-Ghafa | <0.001 |
| Bidbid | Tehran | 0.047 |
| Esfahan | Ibra | 0.008 |
| Ghazvin | Ibra | <0.001 |
| Ghazvin | Salalah | 0.006 |
| Ghazvin | Sur | 0.042 |
| Ghazvin | Um-Ghafa | 0.049 |
| Hili | Tehran | 0.004 |
| Ibra | Mashhad | 0.003 |
| Ibra | Muscat | 0.032 |
| Ibra | Rodehen | 0.005 |
| Ibra | Tehran | <0.001 |
| Ibra | Waset | 0.005 |
| Muscat | Tehran | <0.001 |
| Salalah | Tehran | <0.001 |
| Sur | Tehran | <0.001 |
| Tehran | Um-Ghafa | <0.001 |

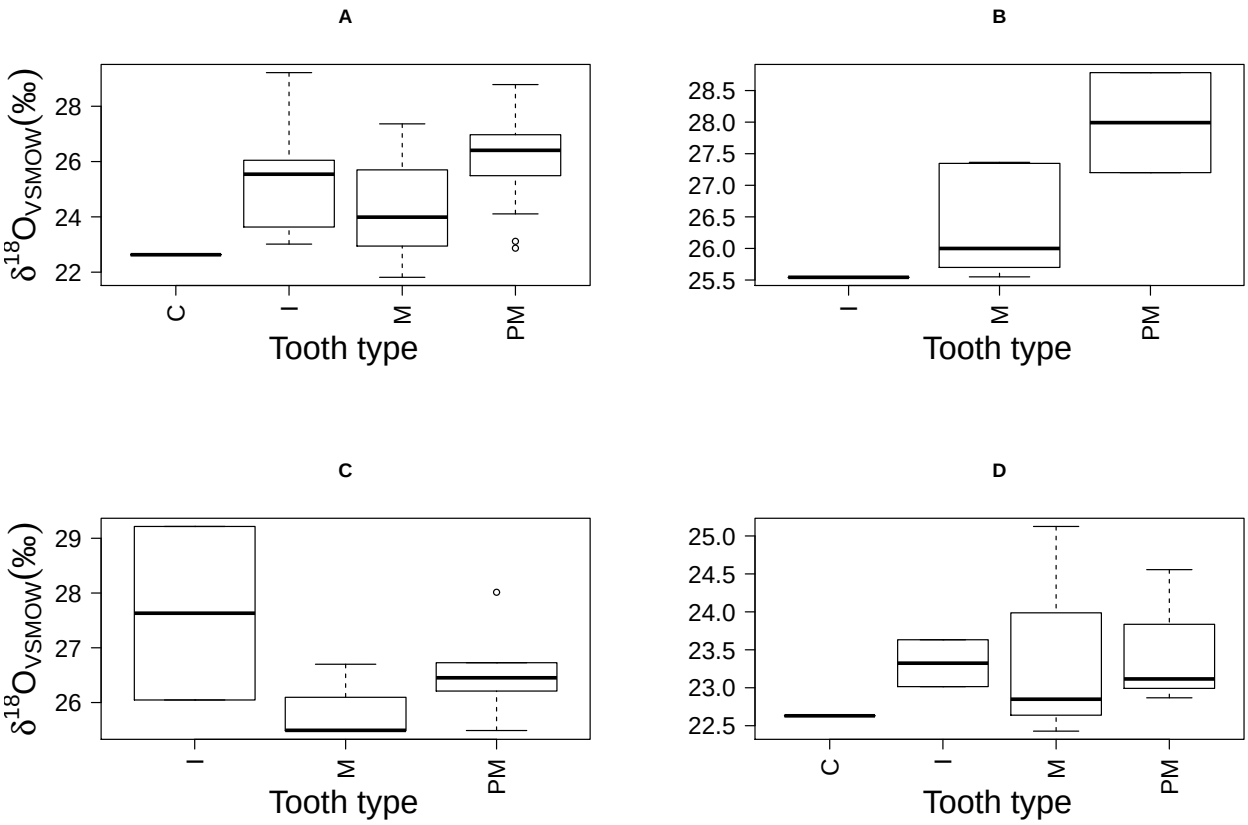


Figure 12: A box plot of the $\delta^{18}O_{VSMOW}$ composition of the Middle East teeth comparing tooth type. A) All teeth, B) Yemen, C) Oman and D) Iraq. For each of the 'boxes' the thick black line represents the median (or the sole value where n = 1), the box represents the inter-quartile range and the whiskers show the range. Open circles are possible outliers.

is slightly elevated compared to that of molars and ANOVA on the data set confirms that there is indeed significant difference between the tooth types for the whole population. The elevated values for incisors and premolars could be expected due to the enriched nature of mothers milk during weaning. However the number of teeth of each type from each region is not equal, hence this statistical significance is inconclusive and may be due solely to the small number of samples and the fact that the sample set is not representative of the whole population. If one observes the boxplots for the individual locations it becomes clear that there is no systematic pattern in the isotopic compositions of the different teeth types and there is overlap in all three of the locations. All the data lies well within a range of 3 ‰ which is the range observed for individual locations in previous studies in the US [31] and the UK [126]. Therefore, for the case of this study one can conclude that the non-molar teeth are representative of the local isotopic composition in the Middle East cities and all results shall be used in the following sections.

It has been shown that the $\delta^{18}$O composition of tooth enamel carbonate can be used to differentiate between populations in the Middle East study region. However with this small database it is only possible to look at differences between the 19 cities for which there are samples (and multiple samples are available for only 9 of these sites). It is therefore necessary to use the measured data to study the relationship between the $\delta^{18}$O composition of tooth enamel and the $\delta^{18}$O composition of drinking water so that a spatial model can be produced to model the expected $\delta^{18}$O composition of tooth enamel over the entire study region. The following sections describe efforts to produce a new isoscape for the prediction of tooth enamel carbonate $\delta^{18}$O composition.

## 2.6 Development of a new drinking water isoscape for the Middle East

It is hypothesised that the ability of currently available global precipitation isoscapes to describe the $\delta^{18}$O variation in the Middle East is limited, due to the low number of GNIP sampling sites in the region, combined with a complex local climate. In an attempt to elucidate the spatial isotopic variation of the Middle Eastern study region, isotopic data for water samples from a number of published sources and 7 unpublished samples measured in lab have been compiled into a small database. The relationship between the collected water data and a number of climate variables has been considered in order to develop a spatial isotope model that explains the highest amount of variation. The following section describes in detail the processes involved in the development of the new drinking water isoscape of the Middle East.

### 2.6.1 Water and climate data from the study region

#### 2.6.1.1 Climate and geographical data for the Middle East

High resolution global climate data is now readily available to the scientific community thanks to online sources [127]. In this study, climate data from the WorldClim BIO database [63] ('bio_5m_esri.zip', [128]) was used. This database includes spatially interpolated climate layers for 19 variables, created from between 14,900 and 24,500 stations. The resolution of the raster data is 5 arc minutes (approximately 100 km$^2$). Elevation data were acquired from the USGS 1-km digital raster ('GTOPO30', usgsdem).

#### 2.6.1.2 Isotopic data for water samples from the Middle East

There is relatively little isotopic information from water in the literature covering the Middle Eastern peninsula compared with other areas in the world. The majority of the data

that is available comes from hydrological studies concerned with aquifer recharging in this arid environment. For this study $\delta^{18}$O and $\delta$D data for water from 8 publications have been chosen due to spatial data being included. The water in these publications is from various sources within the hydrological cycle, long term average precipitation [129, 130], spring water [131, 132, 133], ground water from wells or bore holes [132, 134] and bottled mineral water [80]. Also included were; long term mean precipitation values for the three GNIP stations on the Arabian Peninsula that have recorded sufficient data (Tehran, Tehran East and Bahrain, [135]); unpublished data from 5 tap water samples collected and a mineral water sample collected by the Centre of Forensic Provenancing and measured in house and a tap water sample measured at the University of Dundee. It is suggested that the isotopic composition of these long term averaged sources is more representative of local water supply which mainly comes from deep aquifers. There are a number of values in the literature for individual precipitation events which have been excluded as they are not representative of the water consumed by human populations in the study region. In total the database contains data from 31 locations across the study region (Figure 13). The database is shown in Table 10. For the purpose of this study it is assumed that the water sources in the database are representative of drinking water in the region. The Middle East is an arid region and as the human population increases there is ever increasing demand for water. Some of the water has to be supplied by desalination of sea water which may have an impact on the local isotopic signal in some areas. However the main source of water in the Middle East are deep aquifers. Therefore the groundwater and spring water compiled in this database should be representative of water being pumped for human consumption.

### 2.6.2 Comparison of published water data to existing global isotope models

In order to test the hypothesis that existing global isoscapes [3, 59] of $\delta^{18}$O composition in precipitation have limited predictive power in regions with low sampling density such

Table 10: Isotopic composition of water samples from the Middle East. $\delta^{18}$O and $\delta$D have been reported as per mille values against VSMOW. Standard deviations have been reported where multiple samples from the sample location were measured. Water samples are from a number of long term averaged sources: A) Long term mean precipitation, B) Spring water, C) Groundwater, D) Bottled mineral water, E) Tap water. Data was compiled from a number of sources as described in section 2.6.1.

| Location | Type | Lat (°) | Long (°) | $\delta^{18}$O ($\pm\sigma$) | $\delta$D ($\pm\sigma$) | n | Reference |
|---|---|---|---|---|---|---|---|
| Bahrain | A | 26.27 | 50.62 | -0.4 | 5 | 1 | [135] |
| Tehran | A | 35.68 | 51.32 | -5.3 | -36 | 1 | [135] |
| Tehran East | A | 35.74 | 51.58 | -4.3 | -50 | 1 | [135] |
| Shiraz | B | 28.79 | 51.45 | -4.6 | -18 | 1 | [133] |
| Isfahan | A | 35.37 | 51.26 | -7.0 | -39 | 1 | [130] |
| Shiraz | C | 29.58 | 52.62 | -6.5 | -36 | 1 | [132] |
| Shiraz | B | 29.63 | 52.55 | -6.7 | -33 | 1 | [132] |
| Shiraz | C | 29.29 | 53.31 | -7.3 | -39 | 1 | [132] |
| Baghdad | D | 33.32 | 44.39 | -6.6 ($\pm$4.2) | -43($\pm$29) | 7 | [80] |
| Raudhatain | C | 26.99 | 47.65 | -3.5($\pm$0.3) | -11($\pm$2) | 11 | [134] |
| Umm Al Aish | C | 26.77 | 47.77 | -2.9($\pm$0.4) | -10($\pm$4) | 3 | [134] |
| Muscat | E | 23.58 | 58.57 | -2.4 | -14 | 1 | CFP |
| Batinah | C | 23.64 | 57.88 | -3.4($\pm$0.1) | -15($\pm$1) | 3 | [136] |
| Salalah | A | 17.04 | 54.09 | -0.8 | 5 | 1 | [129] |
| Qairoon Hairitti | A | 17.25 | 54.08 | -0.6 | 7 | 1 | [129] |
| Saiq | A | 23.10 | 57.70 | 0.1 | 10 | 1 | [129] |
| Khayber | B | 25.83 | 39.29 | -2.8($\pm$0.2) | -11($\pm$2) | 3 | [131] |
| Madinah | B | 24.45 | 39.64 | -2.0($\pm$0.1) | -3($\pm$2) | 3 | [131] |
| Jeddah | B | 21.50 | 39.20 | -1.1($\pm$0.9) | -4($\pm$4) | 2 | [131] |
| Makkah | B | 21.44 | 39.82 | -2.0($\pm$0.4) | -5($\pm$2) | 3 | [131] |
| AL-Lith | B | 20.15 | 40.27 | -4.2($\pm$0.3) | -23($\pm$1) | 3 | [131] |
| Jizah | B | 16.89 | 42.57 | -3.3($\pm$0.3) | -14($\pm$1) | 2 | [131] |
| Al-Quatif | B | 26.67 | 49.96 | -3.7($\pm$0.3) | -27($\pm$2) | 6 | [131] |
| Al-Gharra | B | 31.06 | 37.62 | -4.1 | -30 | 1 | [131] |
| Al-Hasa | B | 25.33 | 49.63 | -5.0($\pm$0.1) | -37($\pm$1) | 7 | [131] |
| Jizan | D | 16.88 | 42.57 | -1.9 | -13 | 1 | [80] |
| Dammam | E | 26.28 | 50.20 | -5.2 | -34 | 1 | Dundee |
| Abu Dhabi | D | 24.46 | 54.37 | -1.9 | -13 | 1 | [80] |
| Abu Dhabi | E | 24.46 | 54.37 | -2.2($\pm$0.1) | -12($\pm$5) | 4 | CFP |
| Al Ain | D | 24.21 | 55.75 | -2.2 | -13 | 1 | CFP |
| Sana'a | A | 15.48 | 44.22 | -1.5 | -2 | 1 | [129] |

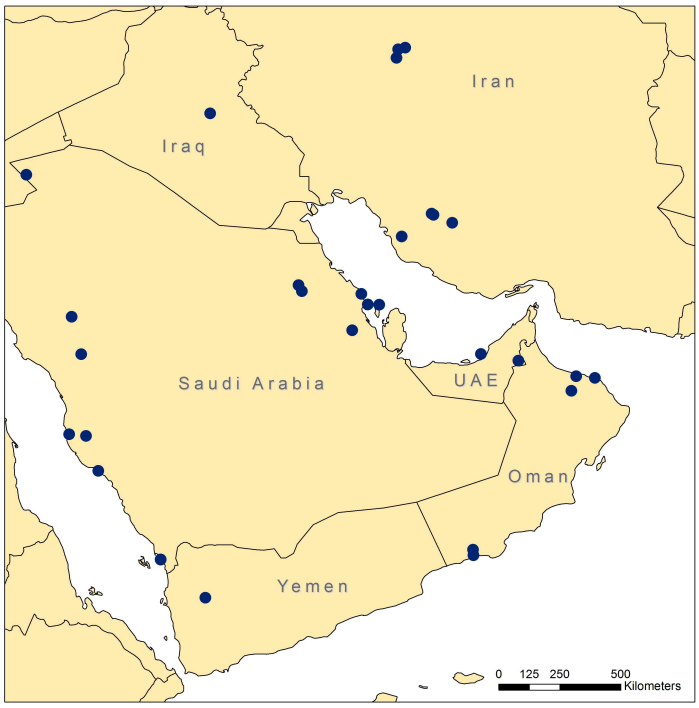


Figure 13: A map showing the origin of the water samples used to create the Middle East drinking water isoscape. Blue circles represent the location of sampling.

as the Middle East, measured data must be compared to the modeled values. The most commonly used precipitation isoscape is the Online Isotopes in Precipitation Calculator (OIPC) [137] which is based on the model of Bowen and Wilson [62] and refined by Bowen and colleagues in [59] and [114] and is described in Section 2.2.1. This model describes approximately 76% of the isotopic variation in the GNIP database. OIPC predictions were obtained from the public website for each of the geographical locations from the Middle East water database described previously. A second model that was proposed more recently is the temperature based approach of Van Der Veer *et al* [3]. This model is not available online so values have been predicted for each spatial location from the Middle East water database using Equation 23:

$$\delta^{18}O_{precip} = -5.9exp^{(-0.041*T)} - 2.4 \tag{23}$$

where T is the temperature of the coldest quarter which was the climate variable that

explained the most (79 %) of the isotopic variation of the GNIP dataset.

#### 2.6.2.1 Statistical comparison of the measured and modeled $\delta^{18}$O data

The mean measured $\delta^{18}$O isotopic composition of the water samples was -3.4 $\pm$ (2.1, 1$\sigma$) ‰ with a minimum and maximum of -7.3 and 0.1 ‰ respectively. The population statistics for the OIPC predicted values is comparable with a mean of -3.3 $\pm$ (2.0, 1$\sigma$) ‰ with a minimum and maximum of -7.6 and -0.7 respectively. The Van Der Veer temperature model seems to be biased towards lighter isotopic composition with a mean of -5.3 $\pm$ (1.0, 1$\sigma$) ‰ and minimum and maximum of -7.6 and -4.4 ‰ respectively. Figure 14 shows histograms of the residuals between measured and modeled values of $\delta^{18}$O for each of the models. For the OIPC model the mean difference -0.12 ‰ ($\bar{d}$) is not significantly different from zero. However |d|>1 ‰ for 55 % of the population and |d|>3 ‰ for 13 % of the population. The histogram for the Van Der Veer temperature model clearly shows that the modeled values are significantly lighter than measured values with a mean difference ($\bar{d}$) of 2.22 ‰. This is due to the fact that the variation in the model is much larger at high temperature (See [3]) and due to the nature of an exponential model the rate of isotopic change with temperature rapidly decreases at high temperature (>30 °C) so predicted values at high temperature are considerably lighter than found in nature. |d|>1 ‰ for 74 % of the population and |d|>3 ‰ for 29 % of the population.

Two paired T tests were performed using Equations 24 and 25. The first T test between the measured and OIPC values suggested that there was no significant difference at the 95 % confidence level (t = 0.35, p = 0.74). The second T test between the measured and the Van Der Veer modeled values suggested that there was significant difference between the measured and modeled values at the 95 % confidence level (t = 7.38, p = 0.00).

$$d = \delta^{18}O_{measured} - \delta^{18}O_{modeled} \tag{24}$$

where $d$ is the difference between paired samples.

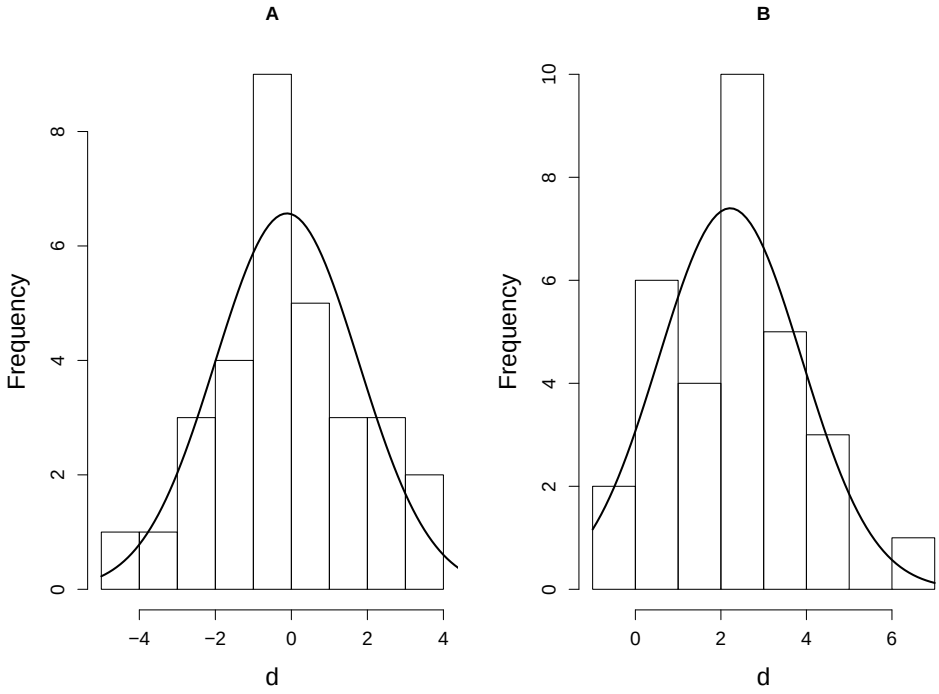


Figure 14: Histograms showing the residuals (d ‰) between A) the OIPC model and B) the Van Der Veer (2009) temperature model $\delta^{18}$O predictions and measured $\delta^{18}$O values of water samples (n = 31) from the Middle East. The curves represents the expected normal distribution of the data.

$$t = \bar{d}\sqrt{n}/s_d \tag{25}$$

where $\bar{d}$ is the mean difference between paired samples and $s_d$ is the standard deviation of d.

Sum of squares of the response variable (SSY, Equation 26) and the sum of squares of error (SSE, Equation 27) were calculated for each of the models and these were used to calculate $r^2$ values (Equation 28) for each of the models. The OIPC explains only 17% of the isotopic variation observed in the Middle East samples ($r^2$ = 0.17) while the Van Der Veer temperature model explains none of the variation ($r^2$ = -0.83).

$$SSY = \sum (y - \bar{y})^2 \tag{26}$$

where $y$ is the measured $\delta^{18}$O composition of the water samples and $\bar{y}$ is the mean of y.

$$SSE = \sum (y - y*)^2 \tag{27}$$

where $y*$ is the modeled $\delta^{18}$O composition of the water samples.

$$r^2 = \frac{SSY - SEE}{SSY} \tag{28}$$

It has been shown that, within the Middle East, the OIPC model produces values that are not significantly different to the measured values at the 95 % confidence level. However the model residuals are high with over half of the predictions differing from the measured values by $>$ 1 ‰ and the model explains only 17 % of the isotopic variation in the study region. The Van der Veer temperature model produces predictions that are significantly different to the measured values at the 95% confidence level with almost 75% of the predictions differing from the measured values by $>$ 1 ‰. Of the two models the OIPC explains the isotopic variation of the Middle East more accurately but for the purpose of this study a better model is required in order to reduce the error of final predictions.

### 2.6.3 Derivation of a new water isoscape based on geographical and climatic variables

It is the aim of this study to link the $\delta^{18}$O composition of human tooth enamel to drinking water in order to be able to predict the spatial origin of an unknown tooth enamel sample. In order to achieve this it is necessary to first accurately predict the isotopic composition of drinking water. As described in Section 2.1.1.1 both evaporation and condensation fractionation events are temperature dependent according to Rayleigh processes [58]. It has been shown that the global temperature based model [3] is inadequate for describing the isotopic variation of the study region. The study region has an arid climate characterised by low annual rainfall and high temperatures (Figure 16). Consideration of local climate variables may lead to improved understanding of the isotopic variation in the region.

#### 2.6.3.1 Climate of the study region

The study region covers the Arabian Peninsula, Iraq and Iran and is an area characterised by extreme climatic and geographical conditions. The majority of the region is classified as arid or semi arid. Annual rainfall is variable and typically less than 150 mm on the Arabian Peninsula and less than 50 mm in the Rub' Al Khali (Empty Quarter) [138]. The Zagros Mountains in Western Iran and Eastern Iraq, the Al Hajar Mountains in Oman and the elevated region in Western Yemen may receive significantly more precipitation a year (150 - 1200 mm) although again this is highly variable (Figure 16). There are two major sources of precipitation. The first consists of winter cyclones, which carry water from the Eastern Mediterranean and are funneled down the Arabian Peninsula by northwesterly winds known as the 'Shamal' [138]. The second source is from the summer Indian Monsoon system carried by southeasterly winds, which may contribute a small amount of rainfall to the UAE and the southern coast of Oman and Yemen (see Figure 15).

Temperatures in the study region are extreme, with summer temperatures in the central

Arabian Peninsula reaching above 48 °C and dropping below freezing in the winter. At high altitude in the Zagros Mountains temperatures in winter may drop to -20 °C while areas along the southern coastline of Yemen and Oman rarely experience temperatures below 10 °C. The annual temperature range is highest in Iran and Iraq ($T_{MAX} - T_{MIN}$ = 35-45 °C) and decreases towards the south of the Arabian Peninsula, with lowest temperature range occurring on the Yemen and Oman coastline ($T_{MAX} - T_{MIN}$ = 10-15 °C) (Figure 16. Annual mean temperature in the study region varies from around 0 °C at the peaks of the Zagros mountains to $>$30 °C in The Rub' Al Khali desert in Saudi Arabia, Oman and the UAE (based on values from the WorldClim database [63] (Figure 16).

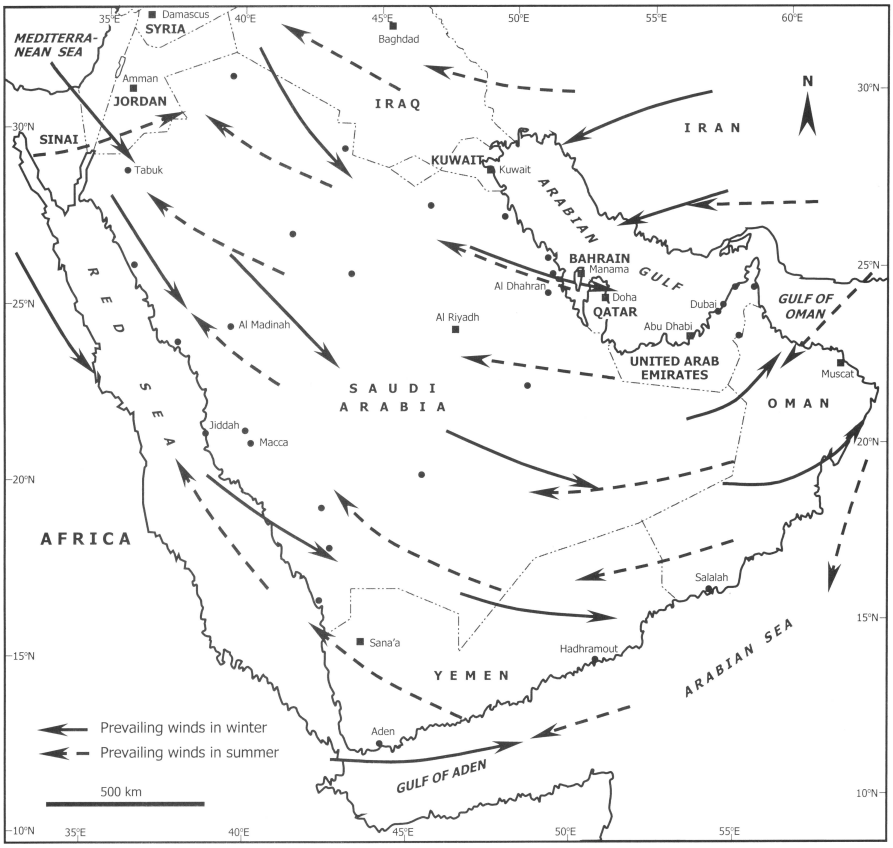


Figure 15: Seasonal prevailing wind direction in the Arabian Peninsula. From 'Hydrology of and Arid Region' [138].

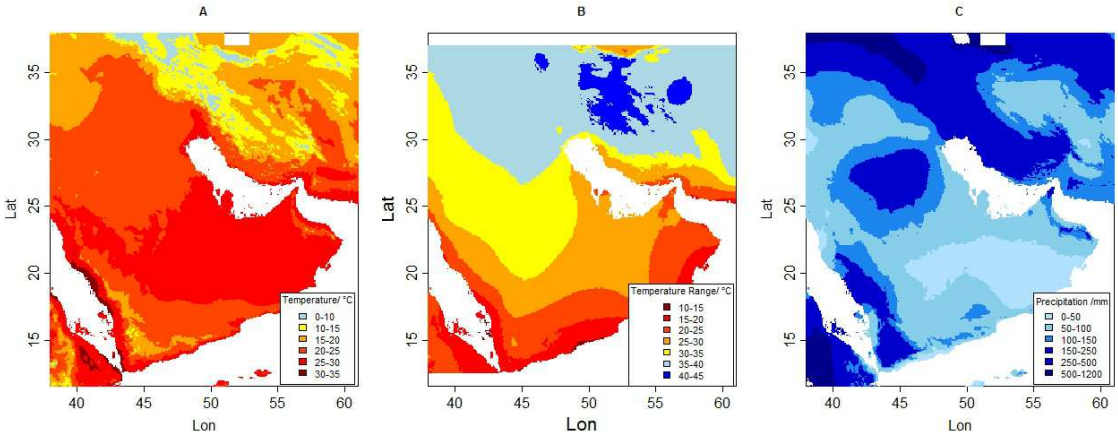


Figure 16: A) Annual mean temperature (°C), B) Annual temperature range (°C and C) Annual Precipitation (mm) of the Middle East. Data is from the WorldClim Bio database [63].

#### 2.6.3.2 A new Local Meteoric Water Line (LMWL) for the study region

A new Local Meteoric Water Line (LMWL) has been prepared from the collated water data from the Middle East study. Least squares linear regression was used to define the LMWL for the region (Figure 17). The gradient of the LMWL, 7.1 ($\pm$ 0.6) is significantly shallower than that of the Global Meteoric Water Line, 7.96 ($\pm$ 0.02) [139] which is characteristic of a non-equilibrium evaporative environment [58]. This is to be expected in the dry, hot and arid climate of the study region and suggests that the isotopic variation of the region may be more complex than that of areas effected by only equilibrium processes. The Deuterium Excess of the study region is 6.2 ($\pm$ 2.4) and $r^2$ for the regression is 0.83.

### 2.6.4 The relationship between $\delta^{18}$O of water and geographical and climatic variables in the study region

As has been shown in Section 2.6.2, existing global models of $\delta^{18}$O in precipitation are unsuitable for the study region. This is likely due to the complex climate creating local fractionation conditions that deviate from equilibrium. It is therefore necessary to create a local water $\delta^{18}$O model based on the local conditions. Considering the climate of the

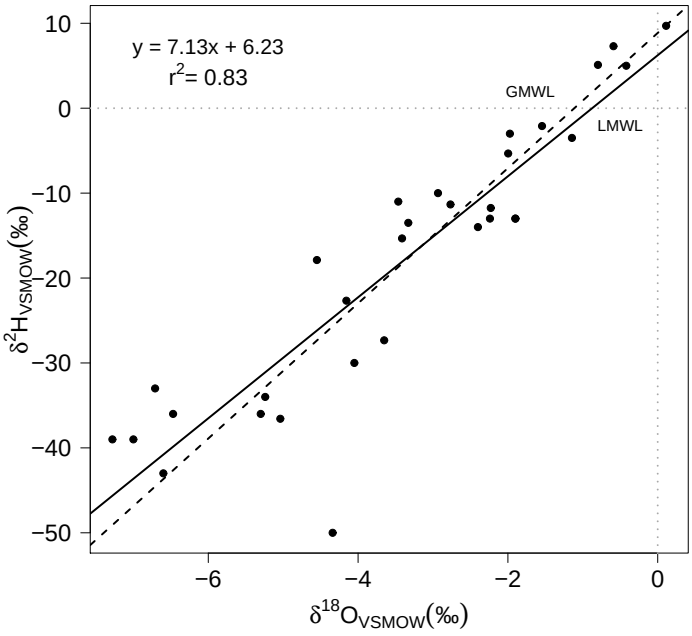


Figure 17: The Local Meteoric Water Line (LMWL, solid line) of the study region, calculated by least squares regression of the available Middle East water data (n=31) is given by the equation in the figure. The Global Meteoric Water Line (GMWL, dashed line), y = 7.96x + 8.89 [139] is included for reference.

study region it is clear that the $\delta^{18}$O composition of drinking water will be a mixture of two signals. The first is winter precipitation originating from the Mediterranean which provides the majority of the regions water [138]. The second, summer precipitation originating from the Indian ocean will provide a small fraction to the final drinking water but is be expected to be considerably enriched in the heavier isotope due to higher temperatures (temperature effect) and lower volume (amount effect) compared to the winter precipitation [138]. It is hypothesised that the isotopic variation in the study region can be explained mainly by the temperature effect due to the extreme temperatures observed but the amount effect must also be considered due to the arid environment. There may also be a distance effect as the majority of rainfall originates in the Mediterranean and this will also be considered in the modeling approach. In order to test these hypotheses and to create a new local $\delta^{18}$O drinking water isoscape for the study region, climate variables from the WorldClim database [127] and a number of geographical variables (Latitude, Altitude, distance from source) will be tested as model variables.

#### 2.6.4.1 Geographical variables

Least squares linear regression was used to determine the relationship between the $\delta^{18}$O composition of the Middle East waters (n = 31) and four geographical variables. **Altitude** and **latitude** were chosen according to the OIPC method [62]. As can be seen in Figure 16 the annual mean temperature increases from north to south, while precipitation increases south to north, hence latitude may be a good proxy for the temperature and amount effects that lead to the isotopic fractionation in the region. Previous studies have shown that the global trend in oxygen isotope fractionation can be described by a polynomial relationship with latitude [62, 59, 114]. Linear regression was chosen in this study as the study region is small enough that curvature in the isotopic data is negligible. A number of studies have also shown that there is a significant linear 'altitude effect' on isotopic composition in high altitude regions [62, 59, 114]. **Distance from the Mediterranean** and **distance from the coast** (calculated using ArcGIS - Near tool) were also chosen in order to test whether

Table 11: An overview of the model coefficients for the relationship between the $\delta^{18}$O composition of meteoric water (n = 31) and local climate variables in the Middle East. Exponential models fitted are in the form y = A - B*exp(-C*x). In all cases A was not significantly different to 0. Linear models are in the form y = A*x + B. Where there was no clear relationship between the dependent and independent variable, no model was fitted. A number of the more significant correlations are shown in Figures 18, 19 and 20.

| Model Variable | Model Fitted | A | B | C | $r^2$ |
|---|---|---|---|---|---|
| Annual Temp.range | Exponential | 0 | 0.45 | -0.07 | 0.59 |
| Temp. seasonality | Exponential | 0 | 0.82 | -0.0002 | 0.54 |
| Mean Temp. wettest quarter | Exponential | 0 | 1.19 | 0.01 | 0.49 |
| Latitude | Linear | -0.26 | 3.16 | - | 0.48 |
| Precip. Coldest quarter | Linear | -0.3 | -1.65 | - | 0.47 |
| Min. Temp. coldest month | Exponential | 0 | 5.01 | 0.05 | 0.37 |
| Mean Temp. coldest quarter | Exponential | 0 | 7.19 | 0.05 | 0.37 |
| Distance from coast | Linear | -0.65 | -2.53 | - | 0.31 |
| Precip. wettest quarter | Linear | -0.02 | 1.81 | - | 0.24 |
| Mean Diurnal Range | Linear | -0.03 | 0.85 | - | 0.22 |
| Annual Precip. | Linear | -0.01 | -1.88 | - | 0.21 |
| Mean Annual Temp. | Exponential | 0 | 10.91 | 0.05 | 0.2 |
| Precip. wettest month | Linear | -0.04 | -2.14 | - | 0.16 |
| Isothermality | Exponential | 0 | 9.91 | 0.03 | 0.14 |
| Precip. Warmest quarter | Linear | 0.03 | -3.71 | - | 0.13 |
| Distance from Med | Linear | 0.11 | -5.28 | - | 0.09 |
| Precip. driest quarter | Linear | 0.1 | -3.76 | - | 0.08 |
| Altitude | Linear | -0.0006 | -3.04 | - | 0.04 |
| Max. Temp. warmest month | None | - | - | - | - |
| Precip. Seasonality | None | - | - | - | - |
| Mean Temp. driest quarter | None | - | - | - | - |
| Mean Temp. warmest quarter | None | - | - | - | - |
| Precip. driest month | None | - | - | - | - |

the distance from these two points influences the isotopic composition of precipitation in the region. Figure 18 confirms that there is a weak negative correlation between $\delta^{18}$O composition and latitude, explaining around 48% of the isotopic variation ($r^2$ = 0.48). There is no correlation observed for altitude or distance from the Mediterranean and only a very weak negative corrlation ($r^2$ = 0.31) with distance from the coast. Fitted coefficients and $r^2$ values for all the models are reported in table 11.

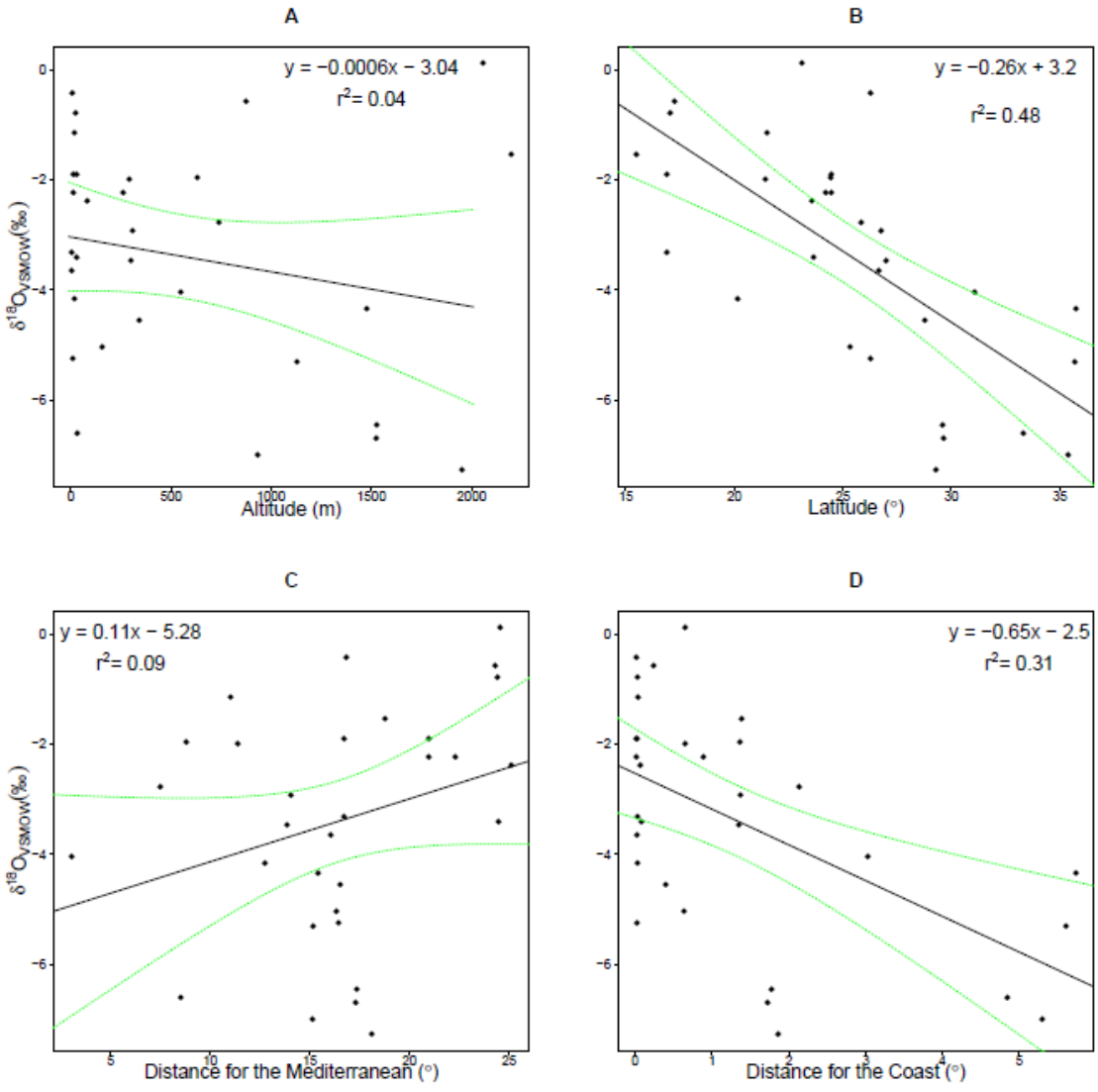


Figure 18: Scatter plots showing the relationship between the $\delta^{18}$O composition of meteoric water (n = 31, Table 10) and geographic variables: A) Altitude (m), B) Latitude (°), C) Distance from the Mediterranean (°) and D) Distance from the coast. Least squares linear regression lines are shown (black lines) along with the model 95 % confidence intervals (green lines).

#### 2.6.4.2 Temperature effect

Non linear exponential regression in the form $\delta^{18}$O = A + B*exp(CT) (where T is the temperature variable), was used to fit models between the $\delta^{18}$O composition and temperature variables from the BIOclim database. An exponential model was chosen due to the predicted relationship between temperature and isotopic composition as described in Section 2.1.1. Figure 19 shows the correlation between four temperature variables and $\delta^{18}$O composition (**Mean annual temperature**, **maximum temperature**, **minimum temperature** and **temperature range**). Fitted coefficients and $r^2$ values for all 10 temperature variables are reported in Table 11. The asymptotic coefficient (A) was not significantly different from 0 ($P > 0.05$) for all of the temperature variables.

The temperature variables measured in summer (**Mean Temp. warmest quarter**, **Mean Temp. driest quarter** and **Max Temp. warmest month**) showed no correlation with the $\delta^{18}$O composition of drinking water so no models were fit for these variables. This suggests that the small amount of summer precipitation does not have a significant effect on the overall isotopic composition.

There was an acceptable correlation for mean temperature of the wettest quarter ($r^2$ = 0.49) confirming the suggestion that the bulk drinking water signal will be dominated by the seasonal winter rainfall.

The best correlation of the temperature variables was given by **annual temperature range** which explained almost 60% of the variation in the study region. This was also the variable that explained the most variation out of all of the variables tested. There is a negative relationship between temperature range and $\delta^{18}$O. Areas with a small range in temperature tending to have isotopically heavier water while areas with large temperature range tend to have isotopically lighter water. This can be explained by the fact that areas with the largest range in temperatures have cold winters ($< 0$ °C), hot summers ($> 30$ °C) and receive the higest rainfall. Areas with small temperature range are hot ($> 30$ °C) all year round and receive little rainfall. Using temperature range to model the isotopic

variation in the study region takes into account temperature, seasonality and to a small degree, amount effect.

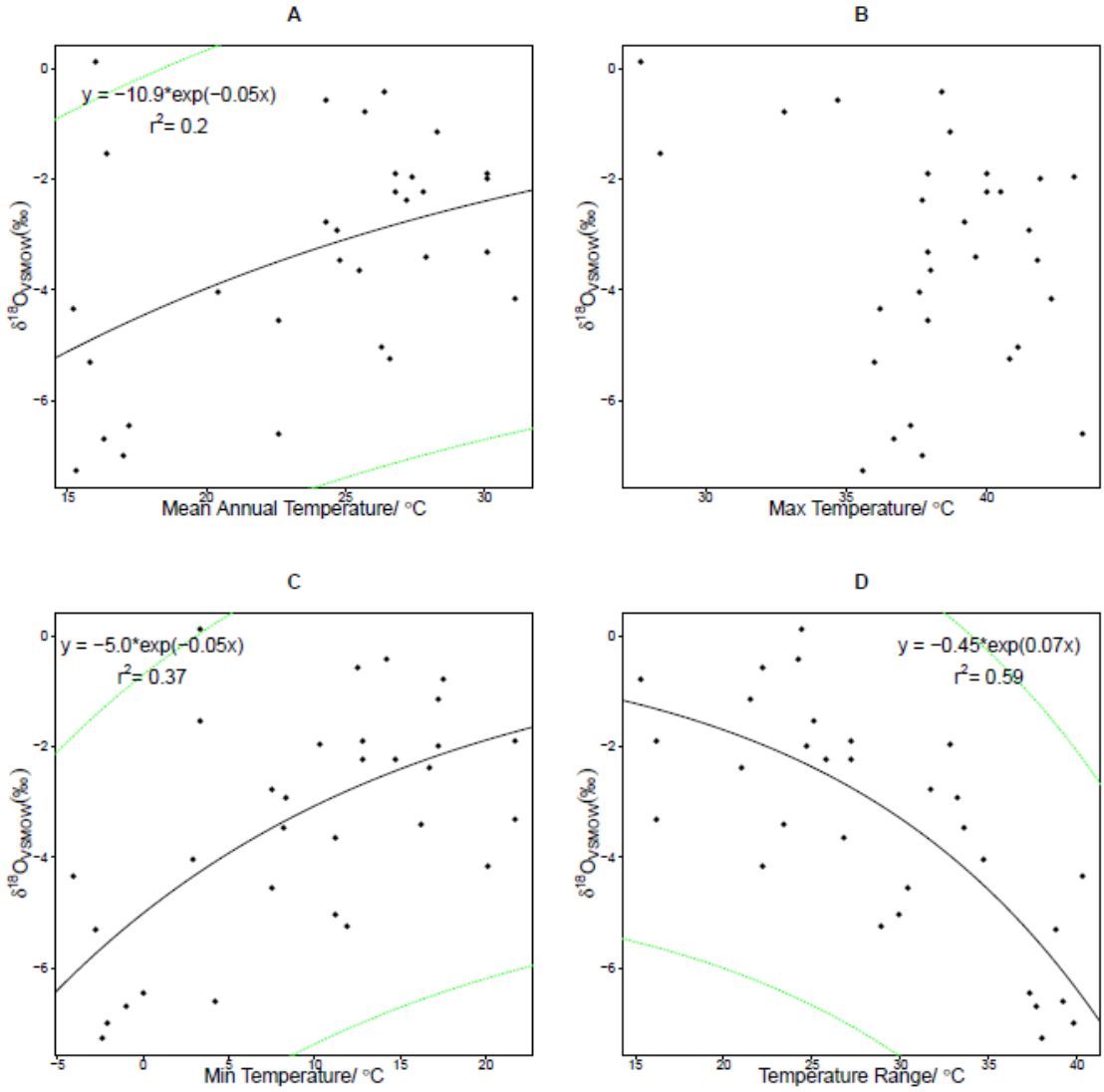


Figure 19: Scatter plots showing the relationship between the $\delta^{18}$O composition of meteoric water (n = 31, Table 10) and temperature variables: A) Mean annual temperature (°C), B) Maximum temperature of the warmest month (°C), C) Minimum temperature of the coldest month (°C) and D) Annual temperature range. Non linear exponential regression lines are shown (black lines) along with the model 95 % confidence intervals (green lines) except for B which had no clear correlation.

#### 2.6.4.3 Precipitation effect

Least squares linear regression was used to fit models between the $\delta^{18}$O composition of drinking water and the precipitation variables from the BIOclim database (Figure 20, Table 11). The precipitation variables measured in summer (**Precip. driest month**, **Precip. driest quarter** and **Precip. warmest quarter**) again showed little or no correlation suggesting that the small amount of precipitation that falls in the summer has little effect on the bulk isotopic composition of drinking water. There is a reasonable correlation for **precipitation in the coldest quarter** ($r^2$ = 0.47) suggesting that the isotopic composition of the drinking water may be affected by an amount effect as well as by temperature.

#### 2.6.4.4 Multiple regression approach

From Table 11 it is clear that temperature range explains the most variation in the isotopic composition of drinking water for the study region. There is however a significant correlation for precipitation in the coldest quarter suggesting that it may be possible to improve the temperature model by addition of an amount effect variable. A histogram of the residuals of the temperature range model is shown in Figure 22. Precipitation in the coldest quarter was plotted against the temperature model residuals (Figure 21). A linear model with intercept set to 0 was fitted through the data. There is a very weak negative correlation observed ($r^2$= 0.04). However the gradient is not significantly different from 0 (P $>$0.05) so it was concluded that there is no relationship between the residuals and precipitation. Temperature range is accepted as the best variable for the explanation of isotopic composition of drinking water in the study region. The $\delta^{18}$O drinking water model (referred to from here as the DW_mod) that will be used to create the isoscapes in the following sections is given by equation 29, where $\beta_1$ = -0.45 and $\beta_2$ = 0.07 :

$$\delta^{18}O_{dw} = \beta_1 * exp(\beta_2 * T_{range}) \tag{29}$$

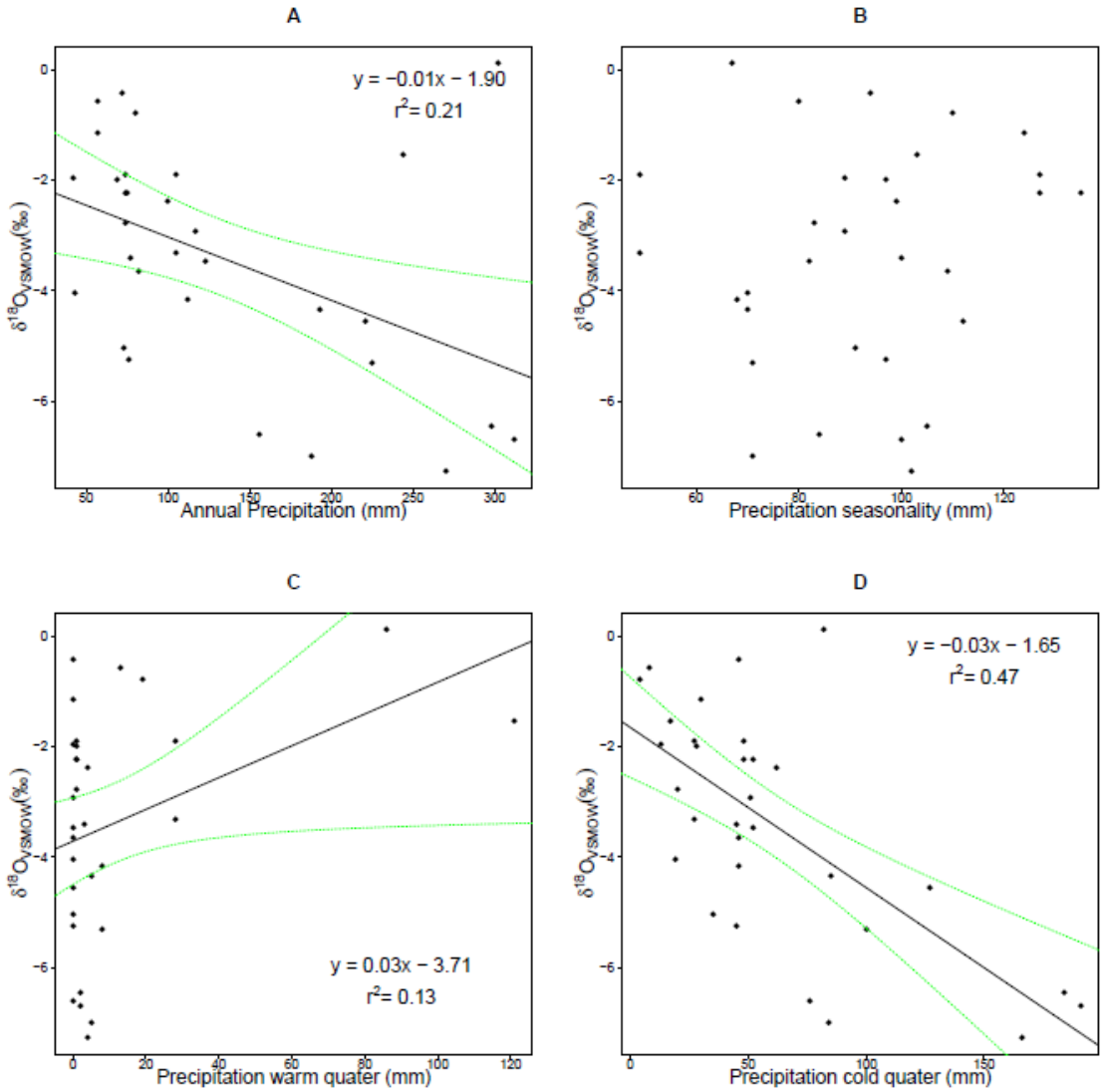


Figure 20: Scatter plots showing the relationship between the $\delta^{18}$O composition of meteoric water (n = 31, Table 10) and amount effect variables: A) Total annual precipitation (mm), B) Precipitation seasonality ($\sigma$ * 100), C) Precipitation in the warmest quarter (mm) and D) Precipitation in the coldest quarter. Least squares linear regression lines are shown (black lines) along with the model 95 % confidence intervals (green lines) except for C which had no clear correlation.

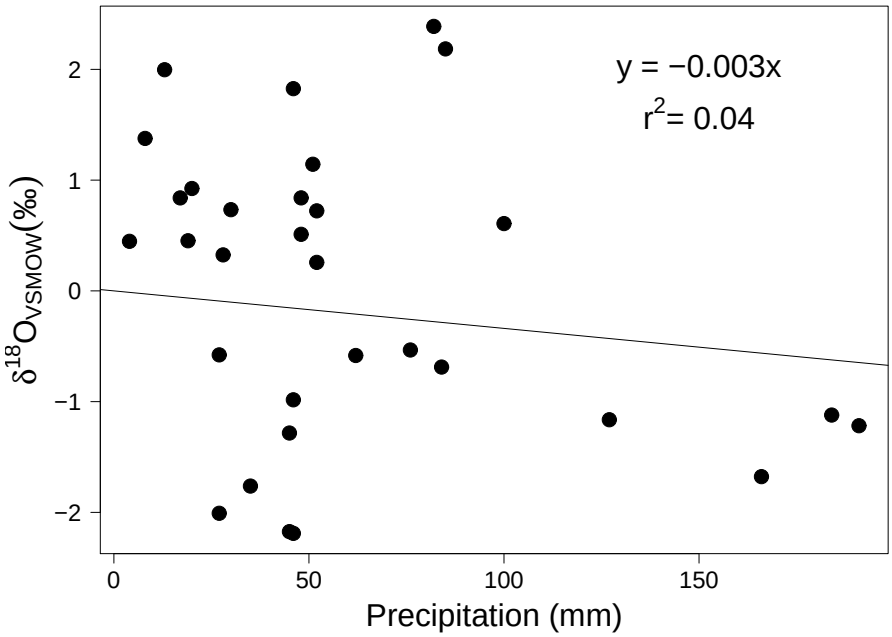


Figure 21: Scatter plot showing the relationship between the residual variance from the temperature range model and precipitation in the coldest quarter.

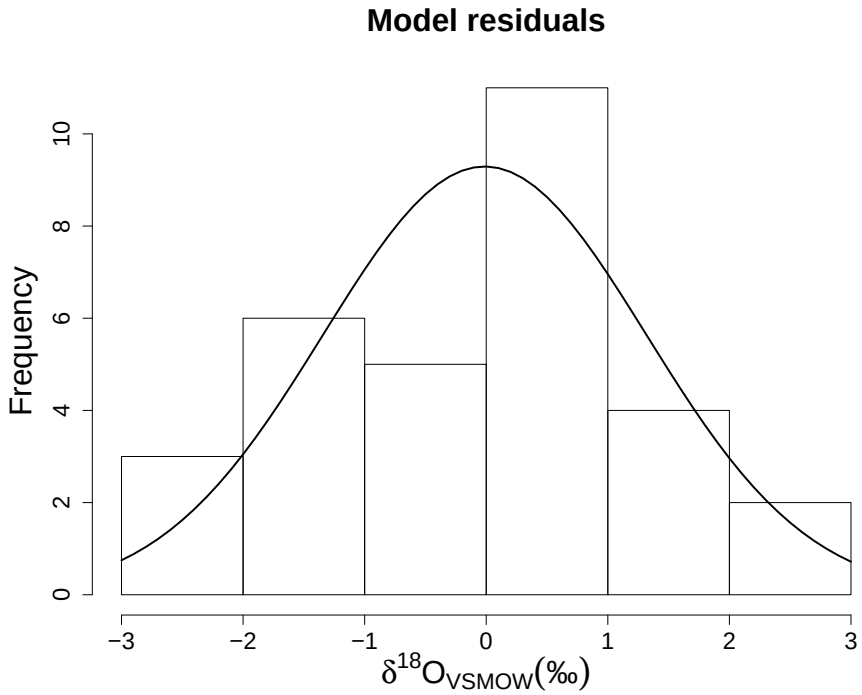


Figure 22: Histogram showing the residuals between the exponential temperature range model $\delta^{18}$O predictions and measured $\delta^{18}$O values of water samples (n = 31) from the Middle East. The curves represents the expected normal distribution of the data.

### 2.6.5 Spatial interpolation of the drinking water model

Previous studies involving the creation of precipitation isoscapes ([62, 3]) have taken into account the spatial variance of the residuals by using simple kriging. Kriging is a spatial interpolation algorithm that estimates a value for a given point based on a weighted average of the surrounding points. The distance weightings used in kriging are assigned by using measured data to create an experimental variogram. The residuals ($\hat{\epsilon}$) from the DW_mod (Figure 22) were calculated using Equation 30:

$$\hat{\epsilon} = Y_i - \bar{Y} \tag{30}$$

where $Y_i$ is the measured $\delta^{18}\mathrm{O}_v smow$ value of the water samples and $\bar{Y}$ is the modeled value. The residuals were used to generate an experimental variogram which is defined by Equation 31:

$$\gamma(\hat{h}_j) = \frac{1}{2N_h}\sum_{i=1}^{N_h}(Z(s_i) - Z(s_i + h))^2 \tag{31}$$

where $Z(s_i)$ is a value at location $s_i$ and $Z(s_i + h)$ is a value at a distance of h from the initial point. $N_h$ is the number of data pairs at distance $h$. The semivariogram for the residuals of DW_mod is shown in Figure 23. There is no clear spatial correlation in the data and this is largely due to the low number of samples and the uneven coverage of the Middle East water data. Using the gstat package in R (statistical software) a nugget semivariogram was calculated (nug = 1.91, Figure 23) and the kriged residuals were added to the water model. However this did not improve the DW_mod and it was decided that as there was no spatial correlation in the data the original non linear exponential DW_mod would be used. In order to improve on this model more samples and better spatial coverage is required in order to observe the spatial variation in the study region. However, with the data available, Occam's razor will be observed - the simplest available model is the best.

An isoscape of the modeled $\delta^{18}$O composition of drinking water was created by applying the model from equation 29 to the Worldclim BIO annual temperature range grid and is shown in Figure 24. The expected range in the $\delta^{18}$O composition of drinking water in the study region is 7.2 ‰(-8.5 - -1.1). The isotopically lightest drinking water is predicted in the north of the study region in highlands of Iran and Iraq. The isotopically heaviest drinking water is expected along the southern coast of the Arabian Peninsula. It was the aim of this section of the study to create a new drinking water isoscape for the Middle East that improved on the existing global models. It has been shown in Section 2.6.2.1 that the Van der Veer model [3] was unsuitable for predicting drinking water $\delta^{18}$O composition for the Middle East study region. The OIPC model [62] explained 17% of the variance in the isotopic compostion of drinking water in the study region and the residuals from the model ranged from -4.03 ‰ to 3.29 ‰ (mean = -0.12 ‰, $\sigma$ = 1.88 ‰). The newly developed isoscape presented here explains 59 % of the isotopic variation of drinking water in the study region. The residuals from the new model range from -2.19 ‰ to 2.39 ‰ (mean = -0.01 ‰, $\sigma$ = 0.59 ‰). The new model could be further improved by more rigorous sample collection and improved sampling density which would allow for the spatial variation to be considered.

#### 2.6.5.1 Model variance

In order for the newly produced isoscape to be useful for forensic application the error associated with the model predictions must be considered. In previously mentioned examples ([3, 59]) spatial kriging of the residuals was applied which allows for an estimation of the spatial variance in the model. In this example a simple non linear exponential regression is applied without kriging of the residuals as no spatial correlation was observed. Therefore it is assumed that the variance in the model is uniform for all locations. As such the variance in the model is described by the population of the residuals from the model predictions given by Equation 32:

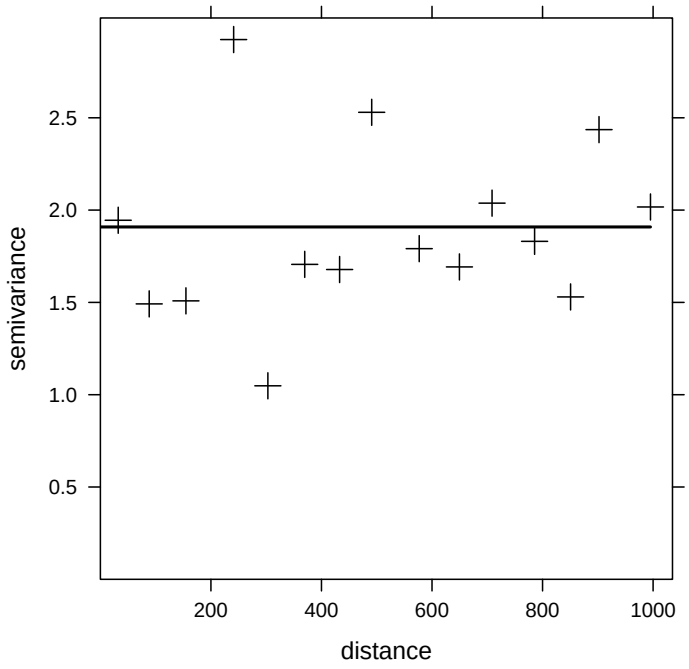


Figure 23: A semivariogram of the Middle East water model residual values. The points show no spatial correlation and only a nugget value of 1.91 has been applied (black line).

$$s_{dw}^2 = \frac{\sum (\hat{\epsilon} - \bar{\epsilon}))^2}{n-1} \tag{32}$$

where $\hat{\epsilon}$ is the residual value between the modeled and measured value of $\delta^{18}$O as given by Equation 30 and $\bar{\epsilon}$ is the mean value of the residuals from the model ($\bar{\epsilon}$ = -0.01 ‰). The exponential model variance $s_{dw}^2$ = 0.35 ‰. From this the 95 % confidence intervals of the model predictions can be calculated based on Equation 33:

$$C.I.(95\%) = \pm 2.04\sqrt{s_{dw}^2} \tag{33}$$

where 2.04 is the critical t value at the 95 % confidence level. The 95 % confidence interval for the model predictions is $\pm$ 1.2 ‰.

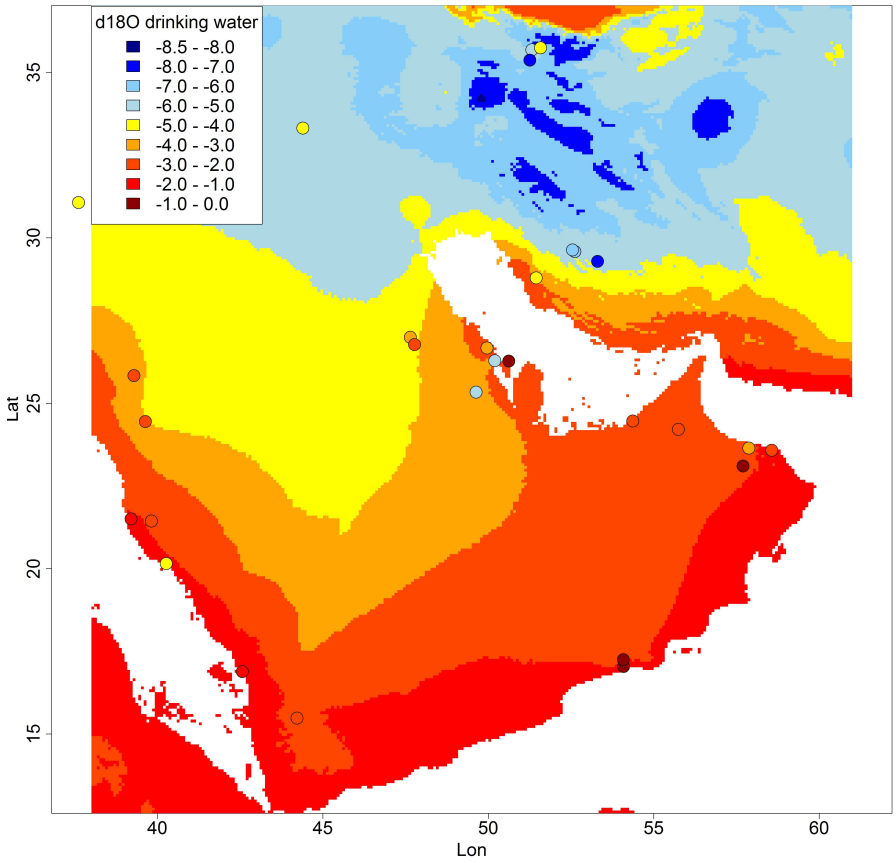


Figure 24: An isoscape showing the spatial variation in $\delta^{18}$O composition of drinking water in the Middle East. Values are reported in ‰ relative to VSMOW. Filled circles represent the sample locations used to create the model and the colours (see key) are representative of the mean $\delta^{18}O_{VSMOW}$ composition of the water samples.

## 2.7 Calibration of the isotope model for tooth enamel carbonate

In order to be a useful tool for forensic provenancing, the $\delta^{18}$O in drinking water isoscape must be calibrated to the matrix of interest. In this case the matrix of interest is human tooth enamel. In this section, the method presented by Wunder ([19]) has been used to calibrate the drinking water model to tooth enamel carbonate $\delta^{18}$O.

### 2.7.1 Model assumptions

A number of assumptions have been made in the development of the calibrated isoscape. As was shown in Section 2.2.3 the overall $\delta^{18}$O isotopic composition of human tissue is determined by oxygen from drinking water, food water and oxygen from the atmosphere. For the purpose of this model it is assumed that the largest and most significant input to the system is drinking water.

Secondly it is assumed that drinking water is sourced locally. According to Alsharhan *et al* [138] this is not unreasonable as precipitation recharged groundwater provides around 60-70 % of the water needs in the Arabian Peninsula. However there is depletion in the Arabian aquifers and desalination plants are used to reach the requirements of the human population. Desalinated water is produced by distillation or reverse osmosis of seawater. Where desalinated water is the main source of drinking water the $\delta^{18}$O composition of human tissue may be significantly enriched in $^{18}$O ($\delta^{18}O_{VSMOW}$ seawater $\approx$ 0 ‰).

Thirdly it is assumed that the origin of the teeth used to calibrate the drinking water model were recorded accurately and the individuals did not travel significantly during the first 14 years of their lifetime [25] so that the isotopic composition of the tooth enamel is representative of the local isotopic inputs. While this is a rather large assumption it is necessary as children who traveled a significant distance during childhood would be likely to have an isotopic composition that is altered from that expected for the town of origin.

In the case of individuals from the Middle East it is probably a fairly safe assumption due to the relative geographic isolation of the populated regions in these countries caused by the arid environment and the relatively low income of individuals in these countries making travel a luxury for these populations. In the case that an individual has moved significantly during their early years of life one would expect the isotopic composition to be an outlier in that local population and will be treated as such.

Finally it is assumed that any local difference in fractionation between drinking water and tooth enamel caused by individual metabolism, health or sex is negligible compared to the overall isotopic variation. Further study is required into these variables.

### 2.7.2 The relationship between isotopes of water and tooth carbonate

The $\delta^{18}$O composition of tooth enamel can be related to that of drinking water by the calibration $y_{ij} = f(x_j) + \epsilon_{ij}$, where $y_{ij}$ is the measured $\delta^{18}$O of tooth enamel carbonate from sample $i$ which originated from location $j$, $f(x_j)$ is a function that relates the measured value $y_{ij}$ to the drinking water isoscape value $x$ at location $j$ and $\epsilon_{ij}$ is the residual value from the calibration. Drinking water values of $\delta^{18}O$ were estimated from the new Middle East drinking water isoscape (Equation 29). The fractionation factor between tooth enamel carbonate and drinking water ($\alpha_{DW}^{TEC}$) for the measured tooth enamel samples was calculated using Equation 8: $\alpha_{DW}^{TEC}$ = 1.029 ($\pm$ 0.001, 1$\sigma$). This is in agreement with the $\alpha_{DW}^{TEC}$ of 1.030 reported by Iacumin *et al* [21]. As shown by Figure 26, the relationship between $\delta^{18}$O of drinking water and tooth carbonate ($f(x_j)$) can be defined by a simple least squares linear regression in the form:

$$y_{ij} = \beta*_0 + \beta*_1 x_j + \hat{\epsilon} \tag{34}$$

where $\beta*_0$ and $\beta*_1$ are the carbonate model coefficients ($\beta*_0$ = 28.1, $\beta*_1$ = 0.77). $x_j$ is the $\delta^{18}$O composition of the drinking water at location $j$ which was predicted from the drinking water model. $\hat{\epsilon}$ is the model residual.

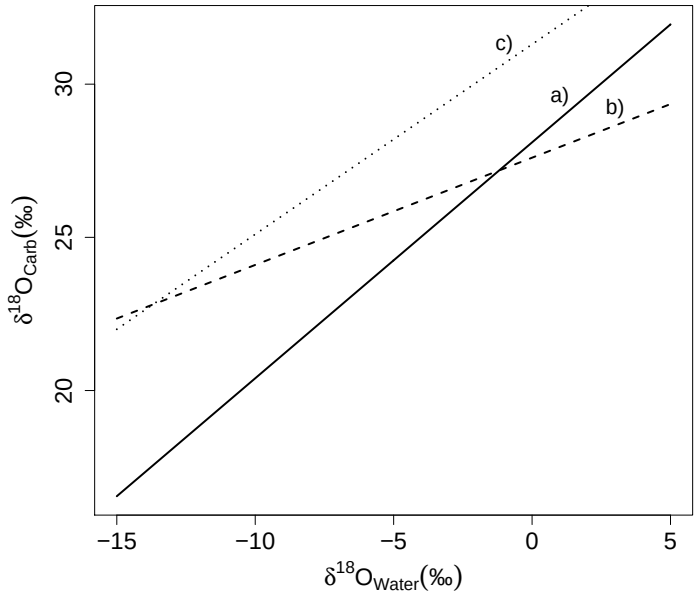


Figure 25: Comparison of the measured regression between tooth enamel carbonate and drinking water $\delta^{18}$O and that of previously publish data. a) The measured regression for the Middle East tooth collection, $\delta^{18}O_{Carb}$ = 0.77$\delta^{18}O_dw$ + 28.1, b) USA [50], $\delta^{18}O_{Carb}$ = 0.35$\delta^{18}O_dw$ + 27.6 and c) Europe [74], $\delta^{18}O_{Carb}$ = 0.62$\delta^{18}O_{dw}$ + 31.3

If the regression model for the Middle East teeth collection is compared to the preliminary data presented by Ehleringer *et al* [50] for the US ut is clear that the gradient is significantly higher (0.77 vs. 0.35). This is likely due to a larger input of local drinking water in the Middle East diet compared to the 'Continental supermarket' diet of the US that was discussed in Section 1.5.1. A first-order interpretation of these results is that only 35 % of the oxygen in tooth enamel was derived from local drinking water in the US compared to 77 % in the Middle East confirming the assumption that the majority of the water consumed in the study region is sourced locally despite the arid conditions. The slope of the US model is almost identical to that of the model for oxygen in hair keratin described in an earlier study by Ehleringer *et al* [1] further confirming that only around 35 % of oxygen in the US diet is from local sources. A third model derived from the study of Longinelli [74] for individuals from early 20th Century Europe has a slope of 0.62 suggesting a fairly localised diet (62 %) but the values are significantly enriched in the heavier isotope compared to the Middle East model. One can postulate that this shift may be due to differences in physiology between the European caucasian population and the Middle Eastern Arabic population. While many of the proccess base models in the published literature include consideration of water fluxes and metabolic activity [50, 75] there have been no studies actively comparing populations with different ethnic backgrounds. This preliminary comparison of the carbonate models clearly shows that individuals from different populations around the world cannot be predicted by one global model but should be considered seperately in order to improve the effectiveness of these models.

The new tooth enamel carbonate (TEC) model (equation 34) describes 70 % of the overall isotopic variation in human tooth enamel from the study area. The remaining variation is likely due to differing diets or physiology of the individuals from whom the teeth came. In order to improve the model it would be useful to study the isotopic composition of local diets from the Middle East study region and to determine the proportion of the diet that is produced locally. It has also been observed that individuals from a more wealthy

background are more likely to have access to internationally sourced delicacies where as the more impoverished proportion of the population may be forced to source cheaper, locally produced foods, hence social status may need to be considered when using these prediction models for forensic purpose.

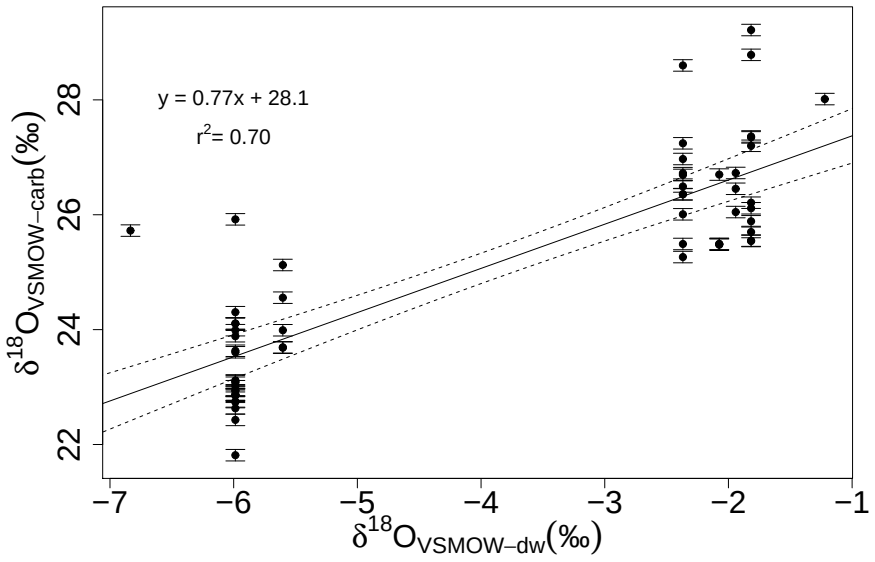


Figure 26: Scatter plot showing the least squares linear regression correlation (black line) between the $\delta^{18}$O composition of human tooth enamel carbonate from the Middle East (n =58) and the locally available drinking water. the 95 % confidence intervals of the regression are shown (dotted black lines). Isotope compositions are reported as per mille (‰) values against VSMOW.

The TEC model (Equation 34) was used to calibrate the Middle East drinking water isoscape (Figure 24) resulting in the tooth enamel carbonate $\delta^{18}$O isoscape, Figure 27. The expected range of $\delta^{18}$O composition in tooth enamel carbonate across the study region is approximately 6 ‰ (21.7 - 27.3 ‰). The lightest tooth enamel isotopic compositions are expected in the north of the study region in the highland areas of Iraq and Iran, with the highest composition expected along the south coast of the Arabian peninsula (Yemen and Oman) as well as along the southern Iranian coast. Isotopic composition of tooth enamel is expected to increase as one moves south east through the Arabian penin-

sula. The coloured circles in Figure 27 represent the mean $\delta^{18}O_{carb}$ of the measured tooth samples at those locations. The residuals between the measured and modeled isotopic composition for these samples are shown in figure 28.

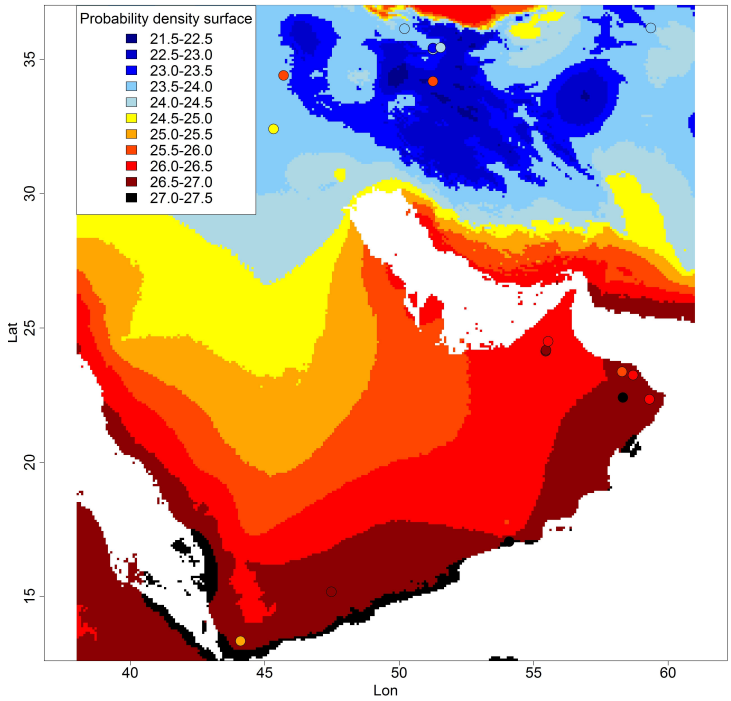


Figure 27: An isoscape showing the spatial variation in $\delta^{18}O$ composition of human tooth enamel carbonate in the Middle East. Values are reported in ‰ relative to VSMOW. Filled circles represent the sample locations used to create the model and the colours (see key) are representative of the mean $\delta^{18}O_V SMOW$ composition of the tooth enamel samples.

#### 2.7.2.1 Model variance

The variance in the carbonate model ($s^2_{cb}$) was calculated from the residuals between the measured and modeled values as in the drinking water isoscape using Equation 32. The carbonate model variance ($s^2_{cb}$) was 1.0 ‰. The 95 % confidence interval of the model predictions is $\pm$ 1.96 ‰.

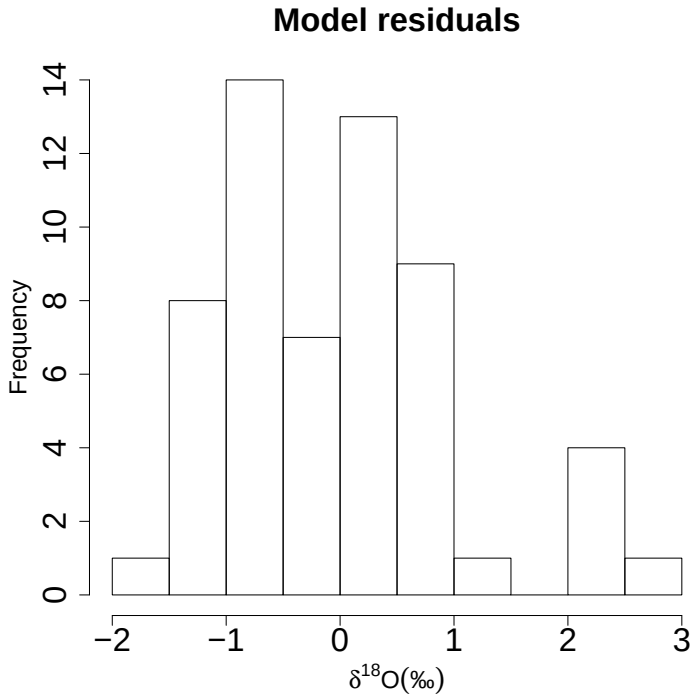


Figure 28: Histogram showing the residuals between the tooth enamel carbonate $\delta^{18}$O predictions and the measured $\delta^{18}$O values of the teeth (n = 58) from the Middle East.

### 2.7.3 Application of the $\delta^{18}O_{carb}$ isoscape

In this section, the newly developed tooth carbonate $\delta^{18}$O isoscape shall be applied to three case studies to illustrate how the isoscape may be applied in a forensic case and also to highlight some of the limitations of such models. The first and second case studies are based on samples selected from the Middle East tooth collection as hypothetical examples. The third case study is taken from an actual forensic case involving the remains of an unidentified female found in Abu Dhabi (UAE).

#### 2.7.3.1 Case study 1

Sample X3 is taken from an official forensic case from the Abu Dhabi police Forensic Services. The remains of an unidentified female were found in Abu Dhabi (UAE). It was hypothesised that the woman may have originated in India based on anthropological features. $\delta^{18}O_{VSMOW}$ composition of the tooth enamel carbonate was carried out at

the University of Dundee and the results compared to the OIPC [59] and van Der Veer [3] precipitation models. Here the results are compared to the new Middle East model to determine whether it is likely that the woman could have originated from the United Arab Emirates. The $\delta^{18}O_{VSMOW}$ composition of the tooth enamel carbonate was 28.7 ‰ ($\pm$ 0.6, 1$\sigma$). Figure 29 shows the possible regions of origin in the Middle East. The $\delta^{18}O_{VSMOW}$ composition of the tooth is not consistent with any location within the Middle East although the 95 % confidence limit does cover the south coast of the Arabian peninsula. It is unlikely that the woman originated in the United Arab Emirates.

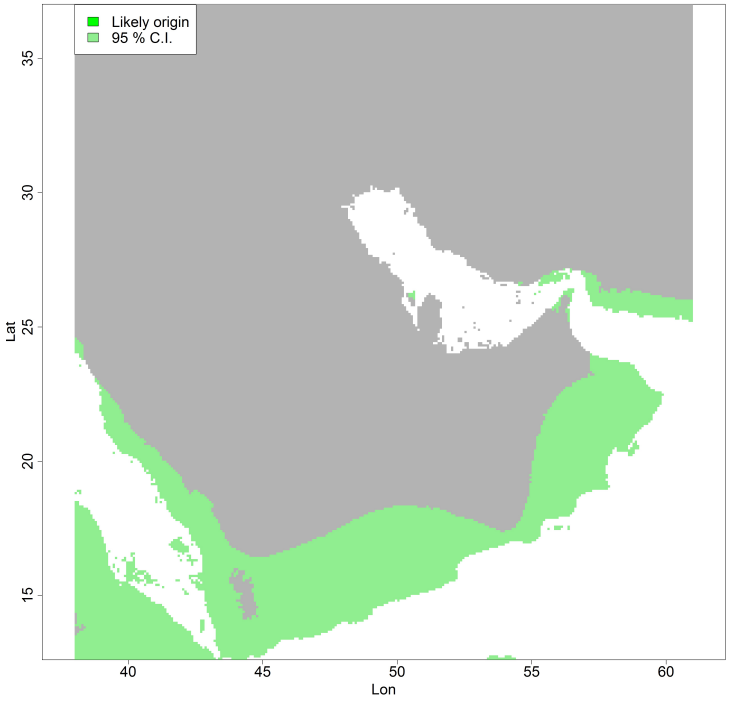


Figure 29: An isoscape showing the likely origin of an unidentified tooth sample (X3) based on $\delta^{18}O$ composition (28.7 ‰).

### 2.7.3.2 Case study 2

Sample X1 is taken from the Middle East teeth collection and is known to have originated from Muscat, Oman. In this hypothetical example it shall be assumed that the tooth is from unidentified remains with no information about likely origin. The $\delta^{18}O_{VSMOW}$ composition of the tooth enamel carbonate was 26.7 ‰ ($\pm$ 0.3, 1$\sigma$). Figure 30 illustrates

the band of likely origin based on this isotopic composition (dark green). The light green area illustrates the 95 % confidence interval of the model. It can be seen that the sample is likely to have originated from the south of the Arabian peninsula in Oman or Yemen but it is also possible that it could have originated from UAE or Saudi Arabia. Without further information, the conclusions that can be drawn from this isoscape are limited.

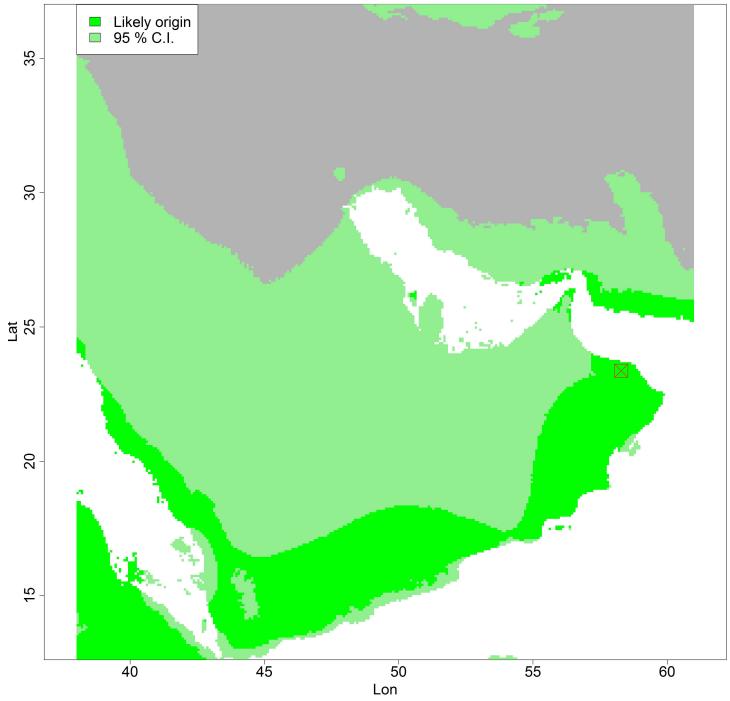


Figure 30: An isoscape showing the likely origin of tooth sample (X1) based on $\delta^{18}$O composition (26.7 ‰). The red box shows the known origin (Muscat, Oman) of the tooth sample.

#### 2.7.3.3 Case study 3

Sample X2 is taken from the Middle East teeth collection and is known to have originated from Tehran, Iran. In this hypothetical example it is assumed that tooth is from unidentified remains and that the individual is thought to have been from Tehran, Iran. The $\delta^{18}O_{VSMOW}$ composition of the tooth enamel carbonate was 24.0 ‰ ($\pm$ 0.3, 1$\sigma$). Figure 31 illustrates the band of likely origin based on this isotopic composition (dark green). As in the previous example, the light green area illustrates the 95 % confidence interval

of the model. The $\delta^{18}O_{carb}$ composition of the tooth is consistent with that expected in Tehran. However the band also covers a large area of the rest of Iran and Iraq. The band representing the 95 % confidence limits of the model predictions cover the majority of the study region. It can be said that the sample could not be differentiated from Tehran based on the isotopic composition but the same could be said about a large portion of the study region. In Chapter 5 a new probabilistic approach to isoscape modelling will be introduced from which a likelihood of the tooth originating in Tehran can be calculated.

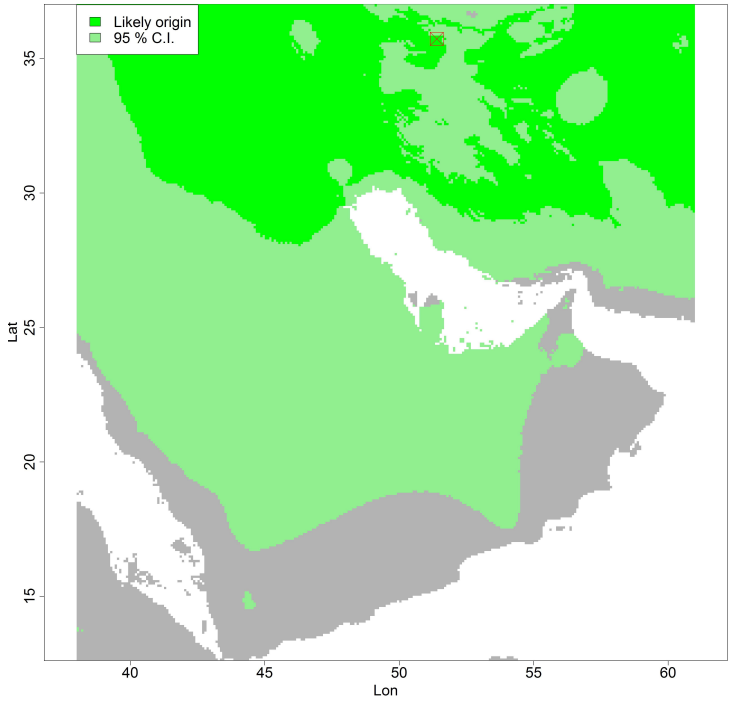


Figure 31: An isoscape showing the likely origin of tooth sample (X2) based on $\delta^{18}O$ composition (24.0 ‰). The red box shows the known origin (Tehran, Iran) of the tooth sample.

## 2.8 Conclusions

In order to use $\delta^{18}$O composition to determine the origin of a sample of forensic interest, the spatial isotopic variation of that sample must be understood. This often means calibrating the $\delta^{18}$O composition of that sample to its source materials which in the case of biological samples is generally water. The availability of online $\delta^{18}$O information from the GNIP database and isoscapes such as the Online Isotopes in Precipitation Calculator [59] has lead to an increase in spatial isotopic studies. Due to the relative ease of generating spatial data from these models, it is easy to continue blindly and overlook the limitations in the generated data. The global models based on the GNIP database are limited in some areas of the world due to complex climates that cause the isotopic composition of precipitation to deviate from global patterns. These areas are often further limited by low sampling density. The Middle East is one such region.

The $\delta^{18}$O composition of measured water samples from within the Middle East have been compiled into a small database. This data was used to test currently available global $\delta^{18}$O in precipitation models and to create a new model that better explains the spatial $\delta^{18}$O variation of water within the study region. The new $\delta^{18}$O model was based upon an exponential relationship with the annual temperature range (BIOclim [127]) in the study region. The factors controlling the isotopic composition of precipitation in the region are complex, and the new model is inevitably over simplified. By collecting more samples and including further climate variables (such as relative humidity) it may be possible to further improve upon the model. This may be an area of interest for future study. The new model has been shown to explain 59 % of the isotopic variation, an improvement of 42 % on the OIPC model.

Following on from this the new drinking water $\delta^{18}$O isoscape was calibrated to 68 tooth enamel carbonate samples from known origin within the study region to produce a human tooth enamel carbonate $\delta^{18}$O isoscape that explains 70 % of the isotopic variation within the tooth samples. The correlation between these variables suggests that the assumption

that the main source of hydration and therefore $\delta^{18}$O composition of individuals is local drinking water is valid. The unexplained variation is due to oxygen input through diet, non local water and the natural variation in drinking water isotopic composition in the study region. The carbonate model could be improved by collecting food from the study region and including a dietary variable in the model and also by collecting further tooth samples so that the intra-population variation can be further understood. This is the first example of a tooth enamel carbonate isoscape for the prediction of human origin in the Middle East. This is a preliminary model with more research required to improve both the drinking water $\delta^{18}$O predictions and the calibration to human tooth enamel carbonate. However, the initial findings show great potential, already explaining 70 % of the isotopic variation in the study region and showing a clear ability to differentiate between samples from within the study region, particularly between samples from the southern Arabian Peninsula and Iraq and Iran in the north. In Chapter 5 these isoscapes will be used as the foundations for a new probabilistic approach for the presentation of spatial isotopic data that it is hoped will improve on the differentiating power of the models.

# Chapter 3

# Strontium isotope analysis

## 3.1 Introduction

It has been suggested in the literature that by measuring the strontium isotope composition ($^{87}Sr/^{86}Sr$) of a biological material such as human bioapatite, it is possible to infer the geological environment from which the sample originated, due to food chain transfer. This chapter will examine the research hypothesis, 'the $^{87}$Sr/$^{86}$Sr isotopic composition of human tooth enamel is directly related to the $^{87}$Sr/$^{86}$Sr composition of an individuals diet which in turn is related to the $^{87}$Sr/$^{86}$Sr composition of the source region based on underlying soil and geology. Hence $^{87}$Sr/$^{86}$Sr composition of an individuals tooth enamel should offer an indication of their origin assuming that the majority of their diet was sourced locally' (Section 1.4). Strontium isotope analysis of human bone has been discussed for over 30 years in the archaeological literature and it is hoped that it is a useful variable to include in a multi-isotope approach to prediction modeling. This chapter will present a concise introduction to strontium isotope fractionation and the transfer of that signal from bedrock to humans, before describing how, in this study, strontium isotope composition of tooth enamel samples has been used to produce the first strontium isoscape for the provenancing of human remains from the Middle East.

### 3.1.1 Strontium isotope fractionation

Most rocks contain detectable amounts of strontium and rubidium at trace levels. Rb is a Group IA alkali metal with two naturally occurring isotopes: $^{85}Rb$ and $^{87}Rb$ with natural abundances 72.17 % and 27.83 % respectively. Rubidium is never concentrated enough to form its own minerals. However the rubidium ion ($Rb^{+}$, ionic radius = 1.48 Å) can substitute in all the main potassium ($K^{+}$, ionic radius = 1.33 Å) containing minerals due to its similar ionic radius . Rubidium concentration is highest in the igneous mica and potassium feldspar minerals but low in plagioclase feldspar due to the smaller sodium ($Na^{+}$, ionic radius = 0.95 Å) coordination site. Strontium is a group IIA alkaline earth metal with four stable isotopes: $^{88}Sr$, $^{87}Sr$, $^{86}Sr$ and $^{84}Sr$. The isotopic composition of strontium is not constant and is dependent on the initial Rb/Sr and $^{87}$Sr/$^{86}Sr$ ratio of the target sample. Nier [140] reported abundance ratios for pure strontium metal to be: $^{87}Sr/^{86}Sr$ = 0.7119, $^{86}Sr/^{88}Sr$ = 0.1194, $^{84}Sr/^{88}Sr$ = 0.0068. In modern strontium isotope analysis Nier's value for $^{86}Sr/^{88}Sr$ is still used to correct for mass dependant fractionation of samples. Strontium ions ($Sr^{2+}$, ionic radius = 1.13 Å) are commonly concentrated in calcium containing minerals and potassium feldspars where they can substitute for $Ca^{2+}$ (0.99 Å) and $K^{+}$ (1.33 Å) respectively. Strontium favours 8-fold coordination sites where as calcium can form 8 and 6 fold coordination sites, hence, unlike rubidium, strontium can become concentrated in the liquid phase and form its own minerals (i.e. strontianite) [141].

The importance of rubidium concentration in relation to strontium isotope ratios is due to the radioactive decay of $^{87}$Rb, one of the naturally occurring isotopes of rubidium, to $^{87}Sr$ by the mechanism (Equation 35):

$$^{87}Rb \rightarrow ^{87}\ Sr + \beta^{-} + \upsilon + Q \tag{35}$$

Where $\beta^{-}$ is a beta particle with negative charge, $\upsilon$ is a neutrino and Q is the decay energy (Q $^{87}$Rb = 0.275 Mev). This means that the level of $^{87}Sr$ within Rb containing rock is

constantly increasing. The half life of $^{87}Rb$ is generally considered to be 5.0 ($\pm$ 0.2) *$10^{10}$ years [142]. The relationship between time and $^{87}Sr$ concentration is given by Equation 36:

$$\frac{^{87}Sr}{^{86}Sr} = \frac{^{87}Sr}{^{86}Sr_0} + \frac{^{87}Rb}{^{86}Sr} * (\exp^{\lambda t} - 1) \tag{36}$$

Where $^{87}Sr/^{86}Sr$ is the ratio of the isotopes at the time of analysis, $^{87}Sr/^{86}Sr_0$ is the ratio of the isotopes at the time of mineral formation, $^{87}Rb/^{86}Sr$ is the ratio of the isotopes at the time of analysis, $\lambda$ is the decay constant (1.39 *$10^{-11}$ yrs$^{-1}$, [142]) and t is time in years since the mineral formation event. From this equation it can be observed that the $^{87}Sr/^{86}Sr$ ratio of a given sample is proportional to the $^{87}Sr/^{86}Sr$ at the time of formation, the initial concentration of $^{87}Rb$ in the original mineral and the age of the mineral. Due to the differentiation of these three contributing factors in global geology it is expected that different geological units, formed under different chemical conditions and at different periods in time will exhibit differing $^{87}Sr/^{86}Sr$ isotope ratios and hence $^{87}Sr/^{86}Sr$ may be a useful indicator for spatial origin.

It is useful to express the abundance of $^{87}Sr$ as a ratio against $^{86}Sr$ as it is easier to accurately measure a ratio in the laboratory. When considering a geological sample the $^{88}Sr$, $^{86}Sr$ and $^{84}Sr$ abundance in the rock are constant as these isotopes are stable. Hence variation occurs only due to the radiogenic decay of $^{87}Rb$. When considering biological samples it is important to consider mass-dependent fractionation effects that occur during transfer up trophic levels.

Strontium is a high mass element and therefore fractionation effects are small and their effects are removed during measurement by normalisation to the stable $^{86}Sr/^{88}Sr$ ratio (0.1194, Nier (1938) [140]). This means that only fractionation effects caused by the radiogenic decay of $^{87}Rb$ and hence those caused by geological and temporal effects are considered.

Using Equation 36 with initial values; ($^{87}$Sr/$^{86}$Sr)$_0$ = 0.701, Rb/Sr = 0.18 and t = 2.5 billion years the average $^{87}Sr/^{86}Sr$ of the Earths' crust can be estimated to be 0.719 [141]. This ratio is highly variable, depending on the Rb and Sr content and the age of the rock, hence different geologies yield different strontium isotope ratios. As previously mentioned strontium and rubidium substitute selectively into certain minerals and hence the initial rubidium and strontium concentration of a rock unit depends on the mineral content. The rocks of the continental crust are enriched in silicates, alumina and alkali metals compared to the upper mantle which is enriched in silica, iron and magnesium. Therefore the rocks of the continental crust (granites) contain a higher Rb/Sr ratio than those formed from the upper mantle (basalts). From equation 36 it can be predicted that the strontium isotope ratios of basalts will be lower than those of granites. Research has confirmed this prediction with $^{87}Sr/^{86}Sr$ values of basalts ranging from 0.702-0.706 and a proposed estimate for continental crust of 0.719 based on measurement of surface water [141].

Sedimentary rocks are composed of minerals and rocks that originate from weathering of pre-existing rock formations. The $^{87}Sr/^{86}Sr$ ratios of sedimentary rocks are therefore dependent on the composition of the source material and the time at which they were deposited. A high proportion of marine sediments are composed mainly of calcium carbonate derived from biological processes. As such the initial $^{87}Sr/^{86}Sr$ ratio of marine limestone or marine clays should be close to that of the ocean at the time of deposition. Faure *et al* [143] demonstrated that the $^{87}Sr/^{86}Sr$ ratio of the ocean is $0.7093 \pm 0.0005$ and is essentially homogeneous. They also suggest that the strontium isotopic composition of the ocean is dependent on contributions from weathering of old silicate continental crust, weathering of volcanic rocks and weathering of carbonate and sulfate rocks. The contribution of each factor was modeled and it was concluded that up to 80 % of the strontium in the oceans is contributed from a carbonate source. Strontium isotope ratios in different geological units are well documented in the literature over the past 50 years and it is beyond the scope of this study to provide a detailed review of strontium isotope

ratios in global geology.

The geology and expected strontium isotope ratios of the case study region is described in section 3.1.4. Faure and Powell [141] compiled a useful guide to the strontium ratios of different rock types with citations to major studies which will be useful when considering the expected Sr ratios for the areas of my study.

### 3.1.2 Transfer of strontium isotope ratios from geology to the biosphere

Strontium input into the local biosphere is from a combination of local surface mineralogy (which is determined by underlying geology unless there has been significant movement of surface deposits), water (precipitation, surface water, ground waters and seawater in marine systems), anthropogenic sources, atmospheric dust deposition and in coastal regions - sea spray. Weathering of bedrock allows strontium to be transferred into surface deposits, soils and the ground water which can then be taken up by plants and eventually animals [144].

The $^{87}Sr/^{86}Sr$ of the local surface mineralogy is determined by the geology on which it was formed according to the relationship given in Equation 36. Strontium ratios of many geological units have been reported in the literature and those that have not may be inferred from areas with similar mineral deposits formed at similar times. Modeling of strontium ratios from geological information available will be discussed in the literature review.

The $^{87}Sr/^{86}Sr$ ratio of ground water is determined by the strontium isotope ratio of soluble minerals from the surrounding soil and bedrock that are able to exchange with the water of the local geology. Voerkelius *et al* [145] determined the range of $^{87}Sr/^{86}Sr$ isotope ratios of European mineral waters to be from 0.7035 for areas containing young basaltic rocks to 0.7777 for areas rich in old Lower-Paleozoic rock. The $^{87}Sr/^{86}Sr$ ratio of precipitation is approximately equal to that of the oceans which is generally agreed

to be homogeneous with a value of 0.7093 ($\pm$ 0.0005) [146]. It has however been observed that aerosols derived from the sea, terrestrial dust or anthropogenic sources can significantly alter this ratio.

Strontium from soil and water is transferred to plants and animals through the food chain. The concentration of strontium tends to decrease with increasing trophic level due to the increased elemental selectivity of animals compared to plants. This is a characteristic that has been used in the study of paleodiets as the Sr/Ca ratio measured in ancient populations can help to determine the proportion of meat and vegetables in diet [144]. However the $^{87}Sr/^{86}Sr$ composition is not significantly changed as strontium is transferred through the food chain and as mentioned previously , mass dependent fractionation is corrected for by normalising to the stable $^{86}Sr/^{88}Sr$ ratio (0.1194, [140]). Hence the $^{87}Sr/^{86}Sr$ composition of the soil and water is maintained up the food chain into plants and animals.

The range of $^{87}Sr/^{86}Sr$ composition within bedrock is large. Even within one geological unit the minerals that comprise it may show significantly different Sr signals. As mentioned by Price [147] there is significantly less differentiation in strontium isotopic composition within a region as you move up the food chain which is due to an averaging effect caused by the larger feeding ranges of animals further up the food chain.

Dahl [148] presents a concise paper outlining the biochemical processes that lead to the Sr deposition within human bones. Bone and teeth are composed mainly of hydroxy apatite mineral ($Ca_{10}(PO_4)_6(OH)_2$) and similar substituted calcium carbonate minerals. As mentioned previously (Section 3.1.1) $Sr^{2+}$ can substitute for $Ca^{2+}$ in rock minerals due to the steric and ionic similarities between the ions. Strontium can substitute for the $Ca^{2+}$ ions in the hydroxy apatite matrix of human bones and teeth by a similar process. Studies involving the administration of known concentrations of strontium into the diet of mice and rats observed two mechanisms for the uptake of strontium into the bone. The first being a rapid process of ionic exchange between $Ca^{2+}$ and $Sr^{2+}$, the second being a slower process of $Sr^{2+}$ incorporation into the mineral matrix [148]. Rate of incorporation

of strontium into bone was shown to be dependent on the dose level of strontium and also on the sex of the subject. It should not be assumed that subjects from the same population consuming the same diet will contain the same concentration of strontium within their bones or teeth as it is dependent on individual metabolism. However, strontium isotope ratios are not dependent on the concentration ingested and therefore should represent the average strontium isotope ratio of ingested strontium. Difficulty will arise when considering a modern population with multiple dietary sources of strontium as it cannot be assumed that every subject in the population can be described by the same mixing model. However it may be possible to capture the populations isotopic variation either by measurement of human samples or by determining the range in local bio-available strontium.

The strontium isotope composition of human bone material is determined by the 'concentration-weight average of the Sr that was ingested' [28]. If it is assumed that the dietary input of a subject was produced locally then it can be inferred that the strontium isotope ratio of the subject will be reflected by the range in local bio-available strontium. The alternative hypothesis is that, assuming that the diet of modern humans is not locally sourced (modern supermarket culture), the $^{87}Sr/^{86}Sr$ ratio of human bones and teeth will take on a more global average and therefore not be proportional to the local geology.

### 3.1.3 Literature review: Strontium isotope analysis as a tool for forensic human identification

Strontium isotope ratios have been used by geologists to age rocks and minerals for over 50 years and by archaeologists to understand ancient population migrations for the past 30 years. However the use of strontium isotope analysis for forensic applications has been much more recent. Despite its infancy, strontium isotope forensics has shown great potential as a tool for the determination of origin of a number of forensically interesting samples. Aggarwal *et al* [149] and more recently Oulhote *et al* [150] have published re-

view papers outlining the potential applications of strontium isotope analysis. Aggarwal et al [149] suggest that the technique has only recently been applied in forensics due to expensive instrumentation, difficulty of measurement and the complex sample preparation.

Strontium isotope analysis has been successfully applied to a number of forensic applications as highlighted by the aforementioned review papers [149, 150]. In particular, strontium isotope analysis has proven a useful tool for the authentification and provenancing of a number of food products [45]. Food authentication has become an important area of forensic research due to the multi-billion dollar food adulteration and food fraud industry [68]. Strontium isotope analysis has been applied to a wide variety of food products including; wine [151, 152], cheese [153], butter [154], meat [155] and milk [156]. These examples are preliminary studies based on relatively small sample sets but they highlight the potential of the technique where suitable databases are collected [45]. An alternative to the database approach is to anchor measured values into an isoscape model. Voerkelius *et al* (2009) present a mineral water strontium isoscape based on samples collected as part of the EU funded TRACE project [145].

In a pilot study by West *et al* [157] it has also been shown that strontium isotope analysis may also been used for the determination of provenance of the illicit substance, marijuana. In this example the strontium isotope composition of marijuana was shown to correlate with underlying bedrock, although the age only based model of Beard and Johnson (2000) [28] consistently predicted lower ratios than those measured. Strontium isotope analysis has also been used for the determination of origin of archaeological artifacts [158], wildlife samples e.g. ivory [159, 160] and human remains [40, 28, 16].

#### 3.1.3.1 Determination of local bioavailable $^{87}Sr/^{86}Sr$ signal for human provenance studies

The affinity of the $Sr^{2+}$ ion for calcium containing minerals is well documented due to the relationship between Ca/Sr ratios in bone material and trophic level, which has been used to provide an insight into paleodiets [144]. The use of strontium isotopes as an indicator of migration of human populations was first suggested by Ericson [161]. In this concise study Ericson suggested that the strontium isotope ratios measured in bone material could be linked to diet and hence to a geological region. It was also suggested that tooth enamel might be a good indicator of 'premarital' residence (4 - 12 years old) where as the turnover rate of bone material of approximately 6 years makes it a good indicator for recent migration history. The study also highlighted some important limitations to the technique that are still very relevant, especially for modern human populations: Geological variation between catchments, catchment distance (particularly a problem for modern 'supermarket' cultures), characterisation of bioavailable strontium for the catchment, biogenic contamination of exterior tooth enamel, diagenic contamination of ancient samples. Ericson used published values for the underlying geology of the study region as an estimate for bioavailable strontium. Ericson also made the observation that coastal populations with a large dietary input from marine sources ($^{87}Sr/^{86}Sr \sim 0.7091$) will be difficult to differentiate between, although this may be a useful characteristic to allow the differentiation between coastal and inland populations. Subsequent archaeological studies have applied strontium isotope analysis to determine the migration history of human populations or to identify migrants within a population. Price and colleagues [162, 26, 11, 147] used strontium isotope ratios to describe the dynamics of a 13th Century human population from Grasshopper Pueblo, Arizona, US.

Price [147] suggests that using small mammals or insects would be the best method for spatial prediction of strontium ratios within unknown human bones. A number of studies have utilised small mammals as an indicator of the local strontium signals, particularly in archaeological studies [163, 11]. Surface water may be used to get an estimate of the

$^{87}Sr/^{86}Sr$ signal for an area. Sillen [164] reported values for field mice that were indistinguishable from that of the local water source.

Evans *et al* [165] measured plant and water samples (n = 319) from most of the major lithologies across the UK. The results for each lithology were averaged and the resulting values applied to a geological map of Great Britain to create the first published Isoscape map for the UK. The authors highlight that the model is a preliminary attempt to model the complex system of $^{87}Sr/^{86}Sr$ across the UK and it is expected to become a more powerful tool as more data is added. The main limitation of these examples is that in order to define the strontium isotope variation at a large (international/ global) scale, hundreds of biological samples are required. On the smaller scale areas of interest in archaeological studies [163, 11, 164, 166], proxies such as small mammals have been successful in predicting resident and migrant populations at archaeological sites. In modern forensics however, it would be much more useful to understand strontium variation at a much larger scale due to the increased mobility of the modern human population. Evans *et al* [165] was the first study example to demonstrate how multiple samples might be used to produce a spatial model at a national scale but it was a preliminary study and many more samples are required to improve the spatial coverage and further resolve the isotopic variation of each geological unit.

Hoogewerff *et al* [16] applied stable isotope (C, O) and strontium isotope ratios to determine the migrational history of Ötzi, a prehistoric male found mummified in the Central Alps. The strontium isotope ratios of the subjects rib (0.718636 $\pm$ 6) and femur (0.717970 $\pm$ 6) were measured as a proxy for the last 5-10 years of the iceman's life. The local bioavailable strontium was determined by measurement of a collection of archaeological skulls from the limestone region in the south (0.7088 - 0.7098) and the central crystalline Alps (0.7120 - 0.7320). It was concluded from the strontium isotope data that the Iceman had his domicile in the crystalline region of the Alps. Müller *et al* present a follow up study of the iceman's remains [57]. In this study the strontium isotopes in the iceman's teeth (0.7203 - 0.7206) and femur (0.7175 - 0.7181) were measured. The femur values are

in agreement with those measured by Hoogewerff. However this study concluded that the Iceman had lived in a region south to that suggested by Hoogewerff. The local bioavailable strontium in this study was predicted from soil leachates from the various lithologies. This does not take into account strontium input from precipitation but is a rough indicator of the local variation. Bentley [24] and Aggarwal *et al* [149] provide detailed reviews of the use of strontium isotope ratios for human archaeological studies. More recent studies highlight difficulties in resolving populations that originate from areas with similar bioavailable strontium isotope ratios. Montgomery *et al* [167] considered mixing models for regional populations based on two end members: precipitation (0.7092 for coastal regions but varying inland where there are terrestrial aerosol sources) and food (dependent on the underlying geology). However there are a number of issues with this method that make it undesirable for forensic studies. Firstly the model is concentration weighted. This assumes that if the population eats the same diet then strontium will be deposited in skeletal tissue in similar concentrations. This is known not to be the case. Secondly there is the possibility that the mixing lines are due to post-mortem diagenesis. Comparison of enamel to dentin measurements suggests that diagenesis has not altered the enamel. Diagenesis is a problem that must be considered when dealing with archaeological remains. Budd *et al* [168] present a study of diagenesis effect on tooth material, concluding that diagenesis of the strontium isotopic ratio in tooth dentin is common and variable so could not be modeled. Tooth enamel remains the material of choice for archaeological studies due to its greater mineral content making it resilient to diagenesis.

In what has become one of the most influential papers on Strontium isotopes in human skeletal material, Beard and Johnson [28] presented the first large scale (Continental USA) 'isoscape' map of strontium isotope ratios. The model is based on Equation 36 and assumes that the $^{87}Sr/^{86}Sr_0$ is 0.705 for all geologies and hence only takes into account the age of the rock. From the model the range of strontium isotope ratios across the USA is 0.70485 for young Quaternary rocks to 0.73198 for ancient Archean rocks. The paper highlights the problem of internationally sourced food consumed by humans in the last

30 years making it difficult to link modern remains to a local signal. They also suggest that the best way to determine local strontium signal is to compile a database from like samples (i.e. tooth enamel). It is also suggested that strontium isotopes are more useful if the forensic questions are general such as 'Was the person born in place A or place B?' rather than open questions such as 'Where does this person come from?'.

The literature review has shown that strontium isotope measurements are widely accepted for the determination of origin of archaeological human remains and that a number of studies have tried to characterize regions of interest by measuring sources of bioavailable strontium such as water, vegetation, small mammals, soil leeches or skeletal material of known origin. This seems to be the most reasonable method of mapping $^{87}Sr/^{86}Sr$, however it relies on the availability of a large number of biological samples from the region of study. To the knowledge of the author, no studies have been undertaken to determine the bioavailable $^{87}Sr/^{86}Sr$ of the Middle East study region which is the area of interest for this study.

### 3.1.4 Geology and strontium chemistry of the Middle East

The Middle East can be separated into two geologically distinct areas. The first is a stable platform of Archean rock overlaid by marine sedimentary deposits in the south which includes most of the Arabian Peninsula. The second is a much younger, highly disturbed folded region in the north (including Iran and northern Iraq) that has been greatly affected by the movement of the Asian tectonic plate [169]. Geological maps of Iran and the Arabian Peninsula are available in digital format from the USGS and are based on open file reports OFR-97-470-B and OFR-97-470-G [170, 171]. The geological layers were joined using ArcToolbox functionality in ArcMap 9.2 (ESRI) to create the geological map of the study region (Figure 32). The Arabian Peninsula consists of two distinct geomorphological areas. The Arabian shield to the west of the Peninsula is bound by the Red Sea and extends approximately half the distance across the peninsula and include

the majority of Saudi Arabia and Western Yemen. The Arabian Shield is an exposure of Precambrian crystalline rock that is visible across the Arabian desert and in areas of the Yemeni Highlands. The east of the peninsula consists mostly of younger Cenozoic to Paleozoic sedimentary deposits including limestone, sandstone and shale. This region is rich with petroleum deposits which formed between the sedimentary layers. The majority of the study region is formed from sedimentary rock (mainly sandstone and shale) with only a small region of intrusive volcanic material, the Yemen trap series in the Yemeni highlands. The geological layer in Figure 32 was simplified into geological Era in order to facilitate the analysis of the strontium isotope data from the tooth enamel samples. The resulting 'simplified' geological map of the study region is shown in Figure 33.

In order to interpret the tooth enamel strontium isotope data it may be useful to compare the measured data with data available in the literature from previous studies in the Middle East. To the knowledge of the author there have been no previous studies of $^{87}Sr/^{86}Sr$ composition of modern human samples of known origin in the Middle East but there have been a number of geological studies that can give some indication of the expected strontium isotopic composition in the underlying geology. The Omani Jabal Akhdar mountains and Batinah coastal plain in Oman were studied by Weyhenmeyer *et al* [172] as part of a hydrological investigation. They report $^{87}Sr/^{86}Sr$ composition of 0.7200 for Pre-Permian sediments found in the mountains and 0.7067 - 0.7080 for the younger Mesozoic limestones. The $^{87}Sr/^{86}Sr$ composition of groundwater found on the Batinah coastal plain ranged from 0.7120 at the foothills of the Jabal Akhdar mountains to 0.7095 further onto the coastal plain. Chiesa *et al* (1989) [173] report strontium isotope ratios for the Yemeni trap series between 0.7036 and 0.7062.

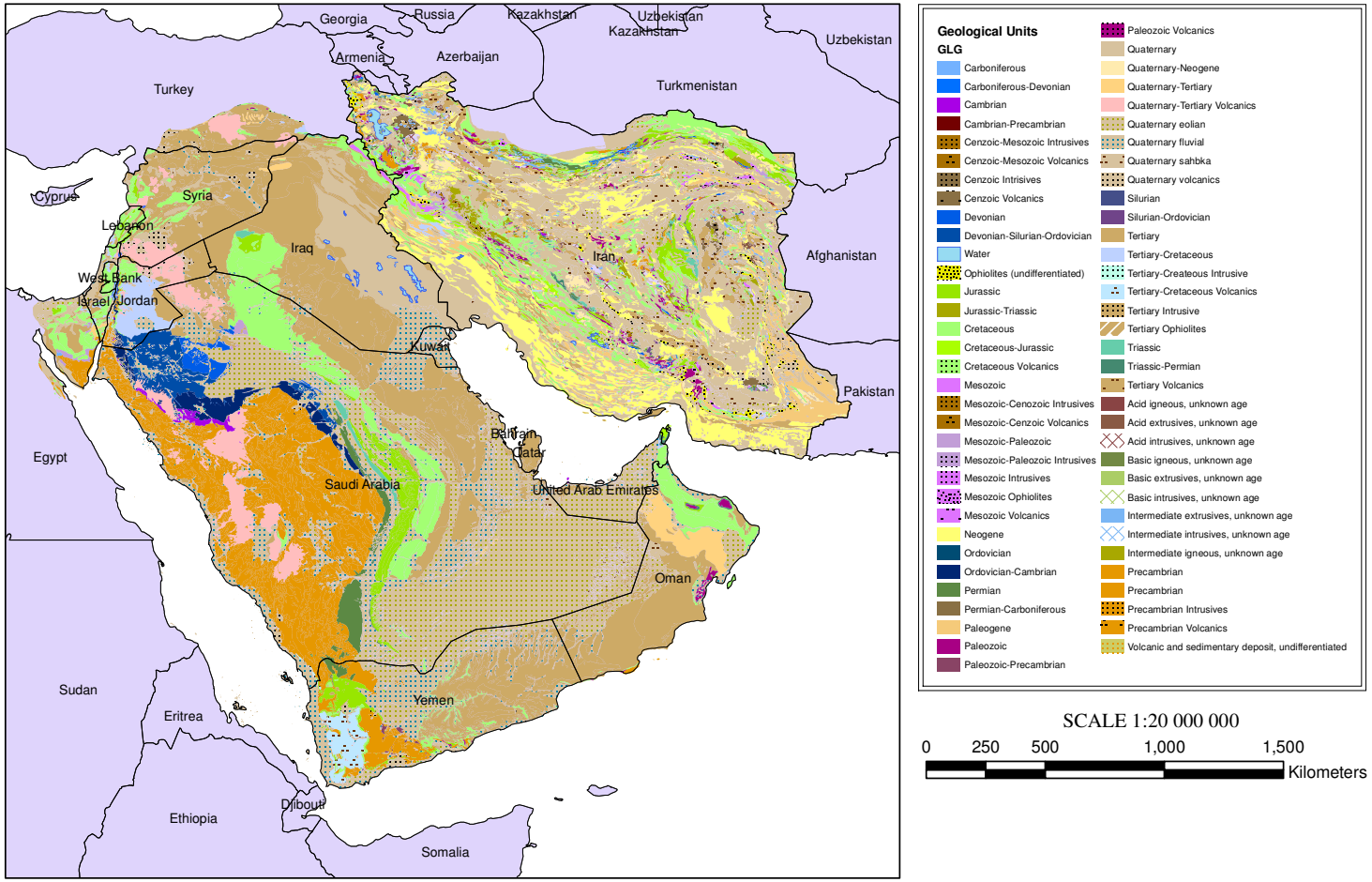


Figure 32: Map showing the geology of the Arabian Peninsula and Iran. The map is projected to the WGS-1984 datum. Geological layers were created by the United States Geological Survey as described in open file reports 97-470G and 97-470B and are available online for public access. The layers were compiled into this image using ArcMAP 9.2 by ESRI.

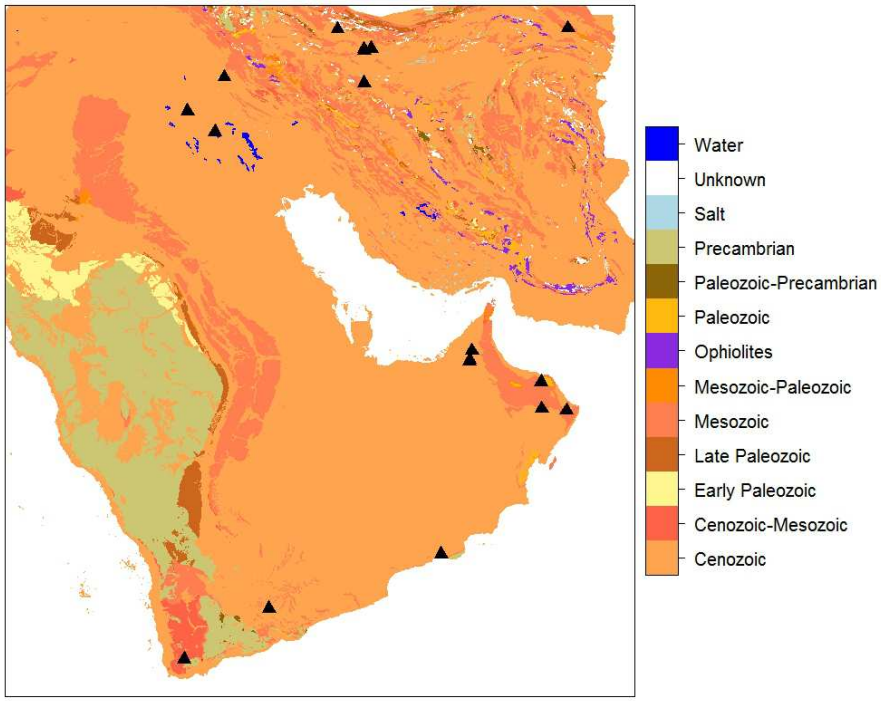


Figure 33: A simplified map of Middle Eastern geology (Modified from USGS geological layers). Origins of the Middle Eastern teeth samples (n = 53) are marked (filled triangles).

## 3.2 Analytical methods

### 3.2.1 Multi Collector - Inductively Coupled Plasma - Mass Spectroscopy (MC-ICP-MS) instrumentation

MC-ICP-MS is a relatively new mass spectrometry technique; the first instrument being produced by VG Elemental in 1990 and developed further over the last 2 decades. This technique was initially developed in order to determine the isotopic composition of elements with high ionisation potentials (i.e. Lu, Hf and W isotope systems) that were difficult to determine by the traditional thermal ionisation method (TIMS). MC-ICP-MS combines an Inductively Coupled Plasma (ICP) ionisation source with a magnetic sector mass spectrometer equipped with multiple Faraday collection cups (see Figure 34. The coupling of the plasma source to the magnetic sector is not a trivial task as will be discussed in detail in Section 3.2.1.3. MC-ICP-MS has been shown to rival TIMS for accuracy and precision for the measurement of isotopic composition of elements such as Sr and Nd and surpass TIMS for measurement of high ionisation potential elements. It also greatly surpasses the limited precision of quadrupole ICP-MS instruments [174].

#### 3.2.1.1 Sample inlet

Samples are introduced into the ICP by injection via an auto sampler. The sample volume introduced into the plasma must be carefully controlled as excess sample would extinguish the plasma. Control is achieved by passing the sample (either by self-aspiration or by peristaltic pump) through a nebuliser which produces an Ar aerosol containing sample droplets of various size [175]. Droplets of an intermediate size ($\leq$10 $\mu$m, approximately 1-2 % of the sample injected) are able to form a vapour which is then passed into the ICP. It is important to acheive a uniform aerosol with constant flow rate in order to maintain short-term signal stability.

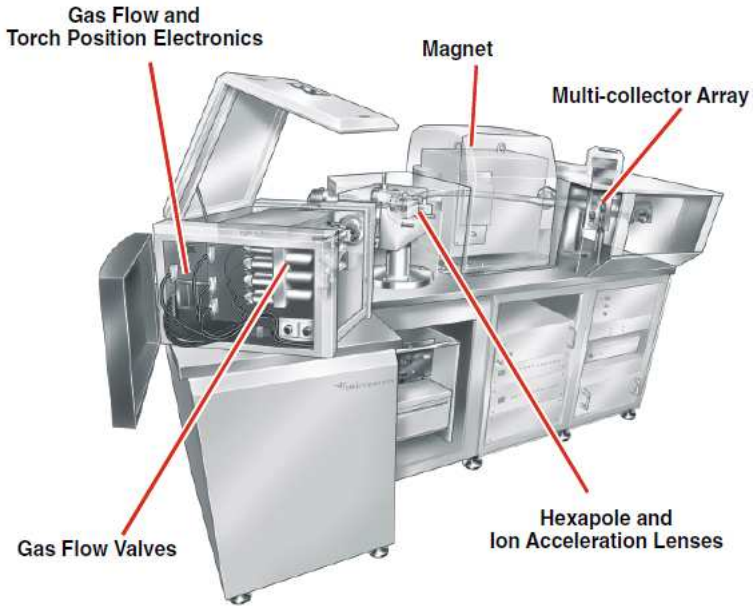


Figure 34: IsoProbe: Multi Collector - Inductively Coupled Plasma - Mass Spectrometer (Source : Micromass, Isoprobe User's guide [175])

#### 3.2.1.2 Generation of an argon inductively coupled plasma

Inductively Coupled Plasma (ICP) is generated by argon gas that is passed through a series of concentric quartz tubes in the plasma torch. The gas emerges at the tip passing through an induction coil, supplied with an AC current (Frequency = 27MHz, Power = 2kW) by a radio frequency generator. The current passing through the coil creates a stabilising magnetic field according to Flemming's rules (Figure 35). The plasma is ignited by the introduction of free electrons from a high-voltage spark. The electrons are accelerated by the magnetic field and collide with argon molecules with high energy producing Argon cations and free electrons which are also accelerated by the magnetic field causing further ionisation events releasing thermal energy which results in a plasma at temperatures of 6000 - 10000K [175]. The sample aerosol is introduced from the spray chamber into the base of the plasma where it undergoes four changes of state: desolvation from aerosol to a dry particle, vaporisation from particles to individual molecules, dissociation from molecules into individual atoms and finally ionisation from atoms to positively charged cations. The ionisation energy required to remove the first electron of an atom varies

between elements but the high energy of the ICP is sufficient to ionise 80 % of elements. The first ionization potential of Strontium is $\sim$ 5.7 eV and the ICP is able ionise almost 100% of the strontium sample [175].

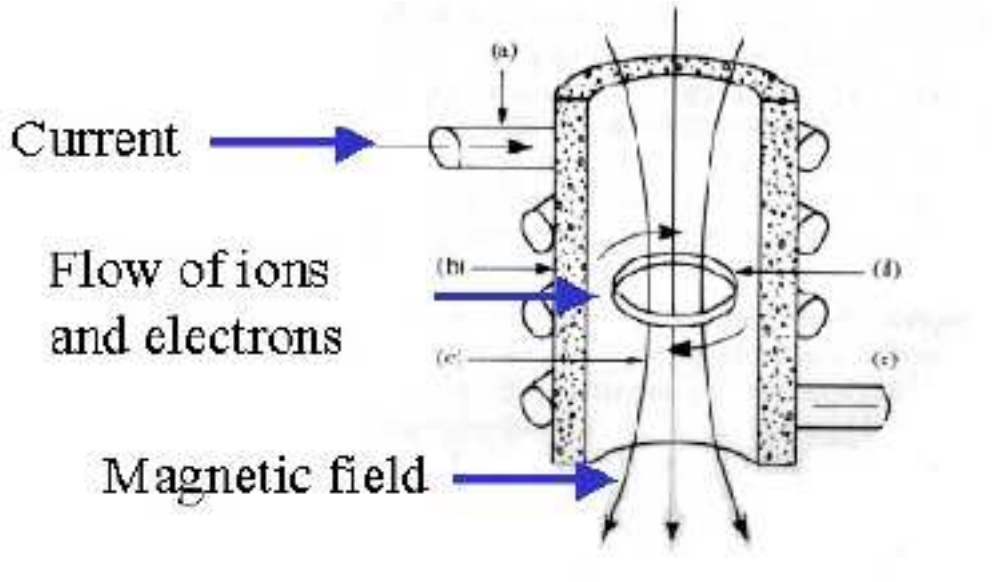


Figure 35: Generation of an argon ICP (Source : Micromass, Isoprobe User's guide [175])

#### 3.2.1.3 Plasma - MS interface

The interface section of the Isoprobe links the ICP to the magnetic sector of the instrument and is vital for the efficient transfer of ionised sample. Ionised sample from the plasma is passed through a primary 'sampler' cone (orifice diameter = 1.1 mm) into a partially evacuated expansion chamber and then through a second 'skimmer' cone (orifice diameter = 0.7 mm) before being accelerated into the hexapole by a 'collimator' cone [175] (Figure 36). The skimmer cone selectively samples the ions, atoms and photons in the sample removing any larger molecules increasing analytical precision of the instrument. Sensitivity can be optimised by changing the distance between the plasma and sample cone to allow the most efficient transfer of sample, also by ensuring that the sample and skimmer cones are free from sample residue that may cause blockages.

The RF hexapole has two functions. Removal of neutral atoms, electrons and photons allowing only the positively charged ions in the sample to pass through into the magnetic

sector of the instrument and to reduce the energy spread of the ions by collision with neutral helium collision gas. The sample jet that is passed into the hexapole collision cell is scattered by inelastic collisions between sample and collision gas. Non charged particles are lost and the positively charged ions are directed into the centre of the axis of the hexapole where they undergo further collisions, reducing the energy spread of the ions from $\sim$ 15 V to $<$1 V in a process known as thermalisation. This is important as the magnetic sector separates ions by mass and velocity so a large spread in the kinetic energy of the ions results in blurring of the mass peaks [174]. The ions are accelerated and focused by a lens stack to an energy of 6 kV before entering the magnetic sector of the instrument.

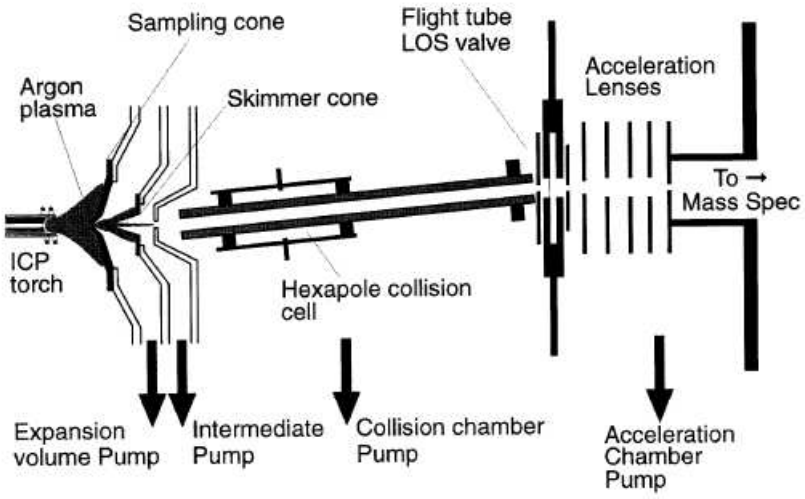


Figure 36: A schematic of the plasma interface and hexapole collision cell of the IsoProbe MC-ICP-MS (Source : Rehkämper (2001) [174])

#### 3.2.1.4 Magnetic sector

The magnetic sector of the instrument is capable of the large mass dispersion required for isotopic analysis [174]. The wide flight tube allows for the simultaneous collection of isotopes with up to 17 % mass dispersion (i.e. 17 amu at mass 100). The magnet separates the the ions according to their momentum which is proportional to the energy and mass to charge ratio of the ion. As shown in figure 37 the fast, laminated magnet of the IsoProbe

uses $90°$ extended geometry ion optics [175] which allows for ion separation and reduces ion beam reflection. The nominal radius of the magnet is 270 mm. The magnetic field required for separation is expressed by equation 37 [175].

$$B = 143.95(mV)/r \tag{37}$$

Where B is the magnetic field (Gauss), m is the atomic mass of the ion, V is voltage and r is the radius (cm).

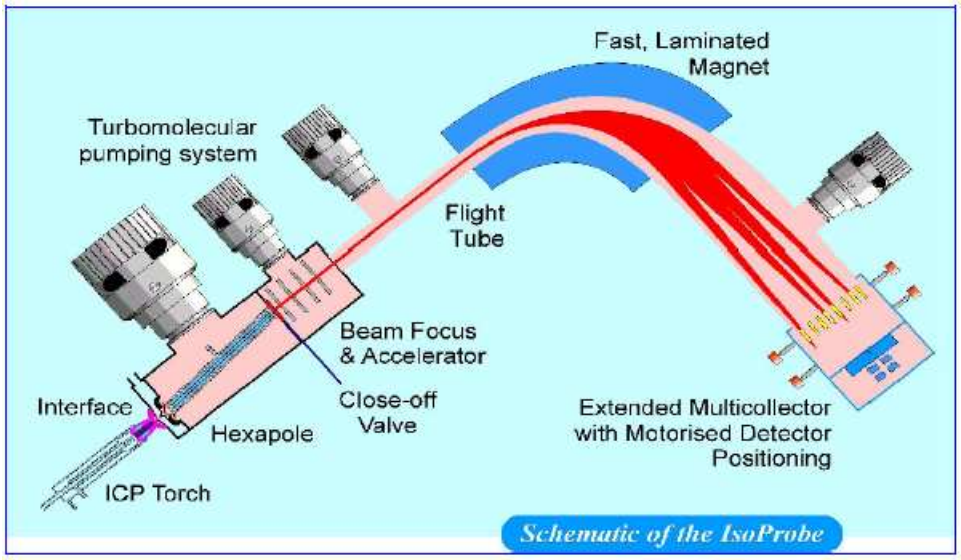


Figure 37: A schematic illustrating the sample introduction, focusing and mass separation within the IsoProbe MC-ICP-MS (Source : Micromass, Isoprobe User's guide [175])

#### 3.2.1.5 The multi collector array

Using a detector array with multiple Faraday cups permits the simultaneous collection of the separated isotopes [174]. Flat top peaks are generated due to the low energy spread of the separated focused ion beams. This enables minor fluctuations in the magnetic field, ion focusing or plasma stability to be canceled an allows accurate measurement of isotope ratios. The IsoProbe instrument used in this study is fitted with nine Faraday collectors. The Faraday collectors can be positioned and tuned separately to allow a wide range of elemental isotope signatures to be measured. The collector configuration used

for strontium analysis in this study is shown in Table 12. The sensitivity of the Faraday cups is sufficient for measurement of ppm to ppt concentrations of analyte.

Table 12: IsoProbe Faraday cup configuration for strontium isotope collection

| Faraday Cup | Isotope collected |
|---|---|
| H5 | $^{88}$Sr |
| H4 | $^{87}$Sr |
| H3 | $^{86}$Sr |
| H2 | $^{85}$Rb |
| H1 | $^{84}$Sr |
| Axial | $^{82}$Kr |

#### 3.2.1.6 Mass bias

Due to the preferential transport of heavy isotopes from the ICP into the mass analyser, isotopic ratio measurements deviate from true values. This process is known as mass bias and is more prominent during the measurement of low mass elements (Figure 38). Mass bias is expressed as the deviation of a measured isotope ratio ($R_{meas}$) compared to the known isotope ratio ($R_{true}$), normalised to a mass difference ($\Delta M$) of 1 amu as shown in Equation 38:

$$Massbias = ((R_{meas}/R_{true}) - 1)/\Delta M \tag{38}$$

Mass bias in measurements of radiogenic isotope compositions (e.g. $^{87}$Sr/$^{86}$Sr) can be corrected for by normalising to to a known constant isotope ratio of the same element [176]. The $^{86}$Sr/$^{88}$Sr ratio found in nature is constant and so can be used to correct for mass bias in the $^{87}$Sr/$^{86}$Sr ratio. The difference between the measured and reference $^{86}$Sr/$^{88}$Sr ratio of the reference standard (NIST SRM 987 = 0.1194) can be calculated using Equation 38 and the measured $^{87}$Sr/$^{86}$Sr can then be corrected accordingly [177].

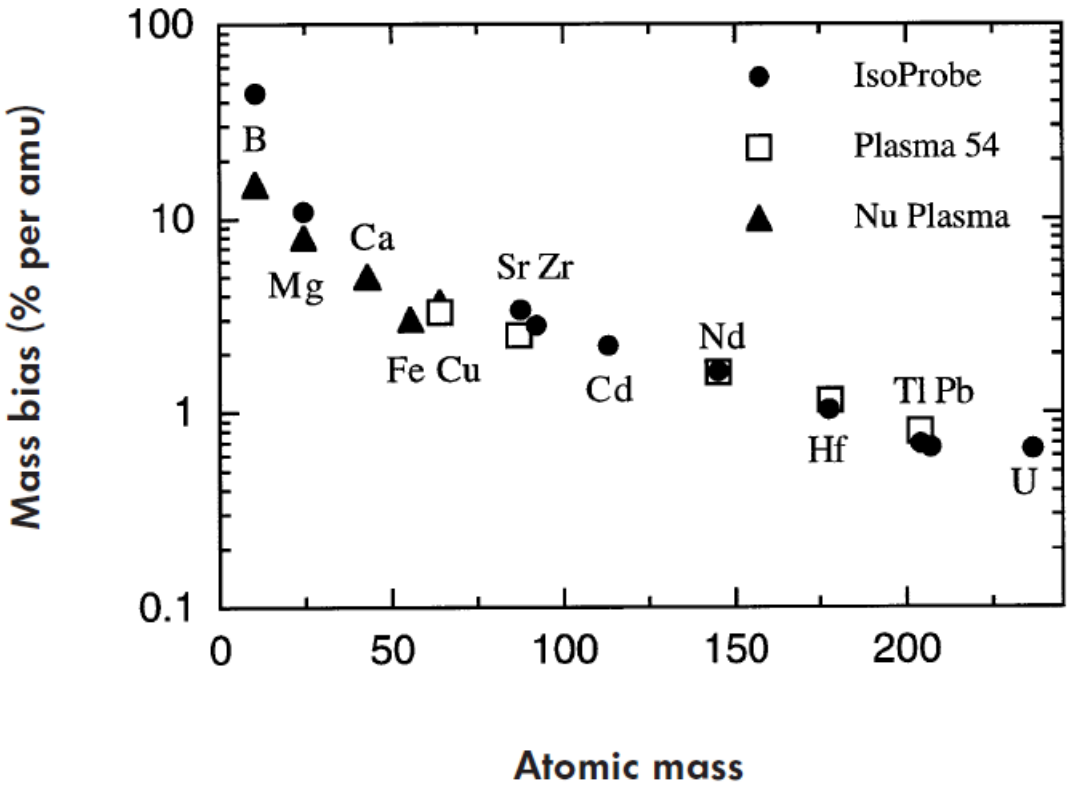


Figure 38: Mass bias per amu (%) of elements commonly measured using MC-ICP-MS. Source: [176]

## 3.2.2 Strontium isotope analysis of human tooth enamel

### 3.2.2.1 Sample preparation

53 teeth from the 'Middle East' case study (as described in Section 1.6) were analyzed for their $^{87}Sr/^{86}Sr$ isotope ratios. 8 aliquots of NIST SRM 1400a bone ash standards (40 mg, NIST, Gaithersburg, MD, USA), were prepared alongside the samples as a reference standard. The teeth were pre cleaned by sonication (15 minutes) in Milli-Q water, dried overnight in a drying oven and a small amount of surface enamel powder ($\sim$ 200 mg) was then removed using a Dremel® diamond cutting wheel. The tooth enamel ($\sim$ 40 mg) was digested (>12 hrs) in Savillex vials (5 mL) by the addition of concentrated, laboratory distilled, nitric acid (1 mL) and concentrated, ultra-pure, hydrogen peroxide

(0.5 mL). The digested samples were dried on a hotplate and the residue resuspended in 8 M $HNO_3$ (0.5 mL).

#### 3.2.2.2 Strontium and lead extraction by Eichrom ion exchange resin

Both strontium and lead were extracted from the digested tooth enamel in separate fractions using the method described here. Note that lead isotopes were collected for a separate study and will not be included in this thesis. Strontium and lead were both extracted using Pb.Spec™ ion exchange resin supplied by Eichrom Technologies (Darien, IL) [178]. The method for dual extraction using the lead resin was developed in lab by A. Hoogerwerff-Gergellj (unpublished) by taking advantage of the ion retention of the lead resin at different acid concentrations as reported by Horwitz *et al* [178]. IEC columns were prepared using nitric acid cleaned syringes (1 mL) into which a thin layer of glass wool was inserted followed by Pb.Spec™ resin ($\sim$ 450 $\mu$L) and a final layer of glass wool. The column was washed with 0.1 M $HNO_3$ (5 mL) to remove contamination and conditioned using 8 M $HNO_3$ (5 mL). The samples were then loaded onto the prepared columns and the eluent discarded. Rubidium and other contaminants were eluted from the columns with 8 M $HNO_3$ (8 mL) and the eluent discarded. Strontium was eluted from the columns with 1 M $HNO_3$ (8 mL) and the eluent collected in acid cleaned Savillex vials (15 mL) for analysis. Lead was eluted from the columns with 0.05 M ammonium oxalate (8 mL) and the eluent collected in acid cleaned Savillex vials (15 mL) for analysis. The collected Sr and Pb eluents were dried on a hotplate and resuspended in 2 % $HNO_3$ (3 mL).

#### 3.2.2.3 Strontium isotope ratio analysis by MC-ICP-MS

**Determination of Strontium concentration in the extracted eluent.** The samples (0.5 mL) were diluted with 2 % $HNO_3$ containing a 10 ppb internal standard (Rh, Ge and Pt). Merck KGaA (Darmstadt, Germany), multi element standard solution VI (110580) was

used to prepare a set of 6 calibration standards (100x - 20000x dilutions in 2 % $HNO_3$ plus internal standard). 5 aliquots of NIST SRM 1640 standard reference water (NIST, Gaithersburg, MD, USA), was measured as a reference material. The strontium and lead concentrations were determine by Agilent 7500CS ICP-MS (see Section 4.2.1). Strontium concentrations for the teeth sample strontium extracts ranged from 12.6 ppm to 75.5 ppb.

**Analysis by MC-ICP-MS** Strontium and lead isotope ratios of the samples were measured in 6 batches over 3 days using an Isoprobe Multi Collector - Inductively Coupled Plasma - Mass Spectrometer (MC-ICP-MS). Samples with strontium concentration of $>$ 200 ppb were diluted to 200 ppb and run in 5 batches and were fractionation corrected using a 200 ppb NIST SRM 987 $SrCO_3$ standard, (NIST, Gaithersburg, MD, USA). 12 samples had strontium concentrations of $<$ 200 ppb. These were diluted to 100 ppb (n = 10) and 50 ppb (n = 2) and measured in one batch with 100 ppb and 50 ppb NIST SRM 987 fractionation correction standards.

## 3.3 Results

### 3.3.1 Middle East tooth enamel $^{87}$Sr/$^{86}$Sr

The teeth from the 'Middle East' collection (n = 53) were analysed for their strontium isotope composition by MC-ICP-MS. Samples were measured in 6 batches over 3 days. Instrument precision was determined by repeated analysis of a NIST 987 standard ( $1\sigma$ = 0.000021). Reproducibility ($1\sigma$ = 0.000056) was determined by triplicate analysis of 8 samples. The $^{87}Sr/^{86}Sr$ ratios of the enamel samples ranged from 0.70770 to 0.71120 with a median of 0.70895. The data is presented in Table 13. Latitude and longitude were obtained using Google Earth based on the city of origin. The stratigraphy and rock type for the Middle East samples was obtained from the USGS geological maps described in the open-file reports 97-470B [170] and 97-470G [171].

### 3.3.2 Discussion

By plotting the $^{87}Sr/^{86}Sr$ isotopic composition of the Middle East tooth samples against strontium concentration (measured by LA-ICP-MS, see Chapter 4.1) the teeth can be visibly separated into three regions of strontium elemental space. The first region is defined by higher strontium isotope ratios of approximately 0.7095 - 0.7110 and strontium concentration between 70 - 320 ppm. This region contains 5 samples, 4 of which were from Muscat, Oman and the fifth sample from Sur in Oman. The second region, containing the majority of the samples (n = 40), is defined by strontium isotope ratios of between 0.7075 and 0.7092 and strontium concentrations of 70 - 320 ppm. The samples in this region are mainly from Iran, Iraq and the UAE with two samples from Oman. The final region is characterised by strontium isotope ratios of between 0.7080 - 0.7086 and strontium concentrations of 320 - 890 ppm. The samples that fall inside this region all originated from cities in Yemen. The most interesting observation from this plot is that the third region can clearly be distinguished from the other regions based on strontium

concentration. Strontium concentration in human tooth enamel is determined mainly by diet and is an indicator of trophic level as concentration tends to decrease up the food chain. Hence the higher concentrations observed in the Yemeni samples may be due to a higher percentage of vegetables and lower percentage of meat in the diet. All of the samples in this region originated from Al-Ghail in Yemen except for one sample originating in Taiz. The large spread in strontium concentrations may be indicative of a large range of diets being consumed in the region.

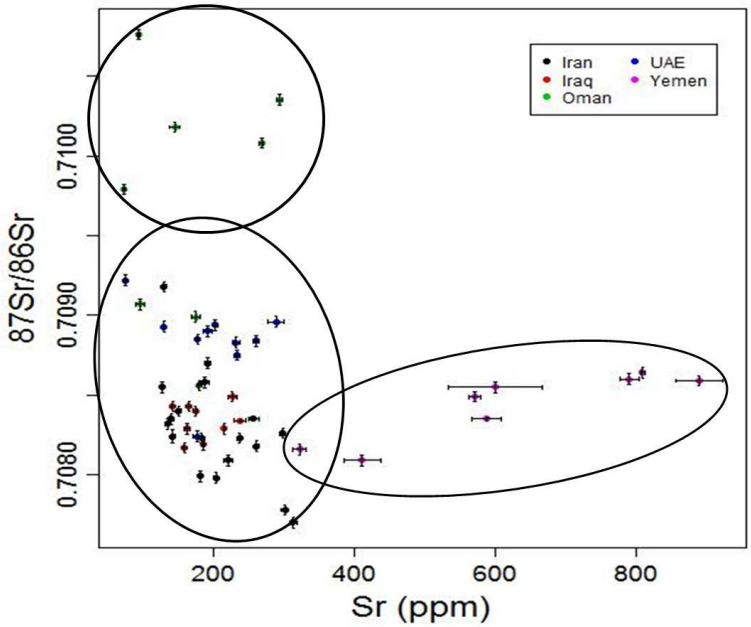


Figure 39: A scatter plot of $^{87}Sr/^{86}Sr$ composition and strontium concentration for human tooth enamel samples from the Middle East. Error bars show 1 standard deviation of the replicate measurements. The points are coloured according to the country of origin (Legend). Three areas of elemental space have been highlighted by free hand ellipses to highlight the different signatures observed in the study region.

If each of the 18 cities for which there are teeth samples is considered to be a population with its own dietary sources, strontium isotope ratios may be useful for distinguishing between those locations. Summary statistics were calculated for each of the 18 locations of known origin (Table 14). The summary data for each of the locations has been visualised as a box plot in Figure 40. From the box plot it is clear that the majority of the locations

have a strontium isotope ratio of between 0.708 and 0.709.

Great care must be taken when interpreting the data in this region of the box plot as the majority of the locations are only defined by one sample. It is common in provenance studies based on small sample sizes to conclude that there is a significant difference between two regions when in reality the sample size is too small to take into account the total variance in the population. If the sample size is increased it becomes clear that the regions cannot be differentiated by $^{87}Sr/^{86}Sr$ alone. From the summary table (Table 14) it can be observed that the locations from which larger sample sizes have been measured (n $>$ 5), the populations have a standard deviation of between 0.0001 and 0.0003. Baghdad has the smallest population variance (0.00011) which is consistent with the $\delta^{18}$O measurements in the previous chapter suggesting that the population in Baghdad consume a fairly average diet which may be expected in a developed capital city where the majority of people consume a diet bought from the supermarket. If it is assumed that each of the locations has a variance of 0.0001 - 0.0003 there is likely to be significant overlap between almost all of the locations. Sur and Muscat are the only exceptions with strontium isotope ratios of $>$ 0.709.

Analysis of variance was performed with origin as the grouping variable. ANOVA shows that there is significant difference between locations at the 95 % confidence interval (F value = 11.3, F crit = 1.9, P($>$F) = 1.4E-09). Tukey's HSD was performed, of the 153 comparisons only 22 showed significant difference at the 95 % confidence level. Of these 21 were between Muscat, Sur and the rest of the locations as suggested by the box plot (Figure 40). There is also significant difference between Tehran (Iran) and Al Ain (UAE). Clearly the differentiating power of $^{87}Sr/^{86}Sr$ on its own is limited in the Middle East study region. However it has been shown that there are significant differences between Muscat and Sur in Oman and the rest of the study region. It has also been shown that when combined with strontium concentration (Figure 39) the samples from Yemen can also be differentiated from the rest of the study region. From a forensic perspective this may prove very useful. Particularly in the case of a closed question such as was sample

X from location A or location B.

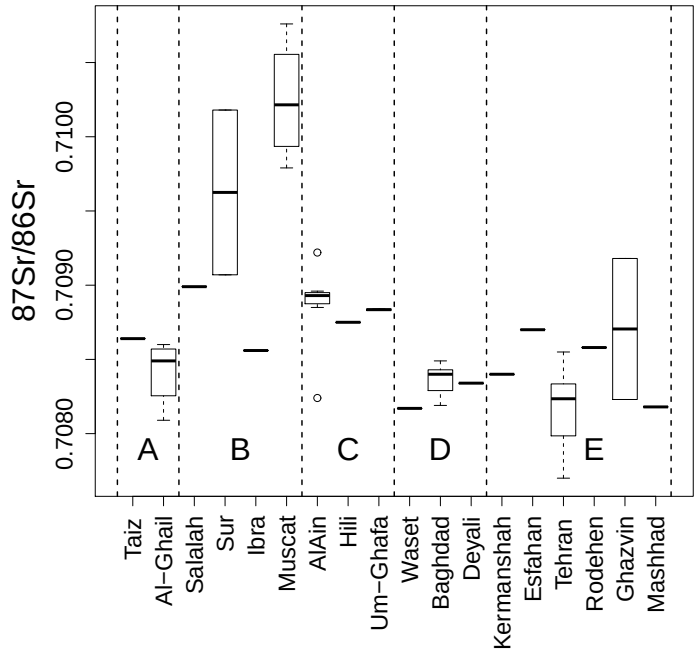


Figure 40: A box plot comparing the measured $^{87}$Sr/$^{86}$Sr composition of human tooth enamel based on the city of origin. The thick central line represents the median value, the box represents the interquartile range and the whiskers represent the extreme values. The box plot has been split into 5 sections by country, A = Yemen, B = Oman, C = UAE, D = Iraq and E = Iran

The strontium isotope composition of tooth enamel observed at each location is directly related to the strontium isotope composition of the diet that is consumed in that region. If it is assumed that the majority of food and water is sourced locally to the location in question it can be hypothesised that the strontium isotope composition observed in the local diet and hence, human tissue will be directly related to the underlying geology. The underlying geology for each sample location was assigned from the simplified geological map of the study region (Figure 33) as described in Section 3.1.4.

Of the 53 samples measured from the study region, 45 originate from locations overlying Cenozoic sedimentary rock. The mean $^{87}Sr/^{86}Sr$ composition of this group of samples was 0.70851 ($\pm$ 0.00044, 1$\sigma$). 4 samples originating from Mashhad (Iran), Ibra (Oman), Taiz (Yemen) and Kermanshah (Iran) overlay Mesozoic sedimentary rock and

have a mean $^{87}Sr/^{86}Sr$ composition of 0.70845 ($\pm$ 0.00020, 1$\sigma$). 4 samples from Muscat (Oman) overlay Paleozoic-Mesozoic sedimentary rock and have a mean $^{87}Sr/^{86}Sr$ composition of 0.71025 ($\pm$ 0.00041, 1$\sigma$).

The box plot of the strontium isotopic composition compared to underlying geology is shown in Figure 41. From the figure it is clear that there is no significant difference between the $^{87}Sr/^{86}Sr$ composition of tooth enamel from the locations overlying Cenozoic and Mesozoic bedrock. However, the samples from Muscat which overlay older Paleozoic-Mesozoic bedrock have considerably higher $^{87}Sr/^{86}Sr$ isotopic composition. One outlier in the Cenozoic group has a higher $^{87}Sr/^{86}Sr$ composition which is more comparable with the samples overlying Paleozoic-Mesozoic bedrock. The outlier is from Sur on the Eastern Omani coast approximately 150 Km from Muscat. It is possible that the food sources for Sur are similar to those from Muscat which would explain the similar isotopic composition. However, with only one sample from Sur it is impossible to tell if this outlying value is representative of the population of Sur or if it is indeed an outlier.

Analysis of variance and Tukey's HSD were performed to confirm the observations from Figure 41. ANOVA confirmed that there is significant difference between the simple geologies (F value = 30.6, F Crit = 1.9, P($>$F) = 2.1E-9). Tukeys HSD confirmed that there is no significant difference between the Mesozoic and Cenozoic populations at the 95 % confidence level (P = 0.89) and there is significant difference between samples from the Paleozoic-Mesozoic bedrock with both Cenozoic (P $<$0.001) and Mesozoic (P $<$0.001) geologies.

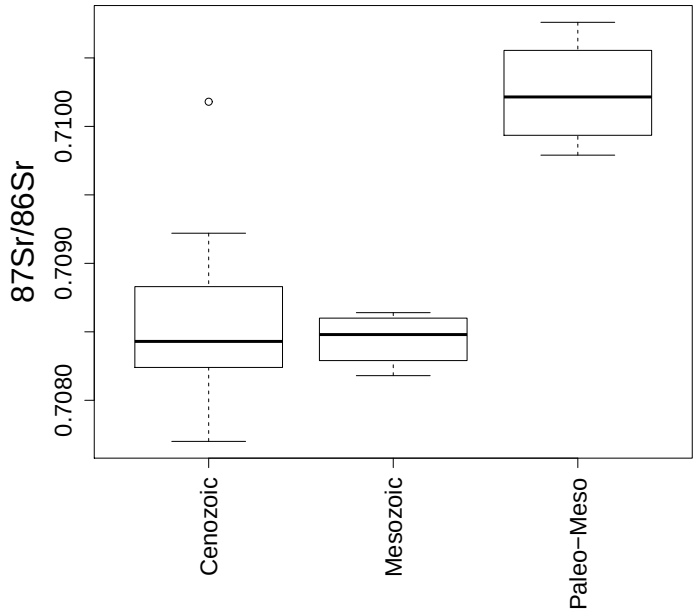


Figure 41: A box plot comparing the measured $^{87}Sr/^{86}Sr$ composition of human tooth enamel based on underlying geology of the sample location. The thick central line represents the median value, the box represents the interquartile range and the whiskers represent the extreme values.

Table 13: The $^{87}$Sr/$^{86}$Sr composition of the Middle East tooth enamel samples. The childhood origin of the teeth is presented along with coordinates and for each location. Stratigraphy and rock type were extracted from the simplified geological layer (Figure 33). Replicates were measured for samples with sufficient material available, for these samples the mean and standard deviation ($1\sigma$) are reported along with the number of replicates measured (n).

| **Sample ID** | **Origin** | **Country** | **Lat (°)** | **Long (°)** | **Stratigraphy** | **Rock type** | $^{87}Sr/^{86}Sr$ | **1$\sigma$** | **n** |
|---|---|---|---|---|---|---|---|---|---|
| TE016 | AlAin | UAE | 24.13 | 55.45 | Cenozoic | Sedimentary | 0.70922 | | |
| TE017 | AlAin | UAE | 24.13 | 55.45 | Cenozoic | Sedimentary | 0.70893 | | |
| TE018 | AlAin | UAE | 24.13 | 55.45 | Cenozoic | Sedimentary | 0.70896 | | |
| TE019 | AlAin | UAE | 24.13 | 55.45 | Cenozoic | Sedimentary | 0.70890 | | |
| TE020 | AlAin | UAE | 24.13 | 55.45 | Cenozoic | Sedimentary | 0.70824 | | |
| TE021 | AlAin | UAE | 24.13 | 55.45 | Cenozoic | Sedimentary | 0.70885 | | |
| TE022 | Hili | UAE | 24.17 | 55.46 | Cenozoic | Sedimentary | 0.70875 | | |
| TE023 | Um-Ghafa | UAE | 24.5 | 55.54 | Cenozoic | Sedimentary | 0.70884 | | |

Continued on Next Page...

Table 13 – Continued

| Sample ID | Origin | Country | Lat (°) | Long (°) | Stratigraphy | Rock type | $^{87}Sr/^{86}Sr$ | $1\sigma$ | n |
|---|---|---|---|---|---|---|---|---|---|
| TE024 | UAE | UAE | 24.13 | 55.45 | Cenozoic | Sedimentary | 0.70894 | | |
| TE025 | Um-Ghafa | UAE | 24.5 | 55.54 | Cenozoic | Sedimentary | 0.70883 | | |
| TE027 | Sur | Oman | 22.34 | 59.31 | Cenozoic | Sedimentary | 0.71018 | | |
| TE028 | Muscat | Oman | 23.37 | 58.29 | Paleozoic-Mesozoic | Sedimentary | 0.71035 | | |
| TE029 | Ibra | Oman | 22.41 | 58.32 | Mesozoic | Sedimentary | 0.70856 | | |
| TE030 | Muscat | Oman | 23.37 | 58.29 | Paleozoic-Mesozoic | Sedimentary | 0.71008 | | |
| TE031 | Muscat | Oman | 23.37 | 58.29 | Paleozoic-Mesozoic | Sedimentary | 0.70979 | | |
| TE032 | Sur | Oman | 22.34 | 59.31 | Cenozoic | Sedimentary | 0.70907 | | |
| TE034 | Salalah | Oman | 17.15 | 54.32 | Cenozoic | Sedimentary | 0.70895 | | |
| TE038 | Muscat | Oman | 23.37 | 58.29 | Paleozoic-Mesozoic | Sedimentary | 0.71076 | | |
| TE040 | Waset | Iraq | 32.41 | 45.33 | Cenozoic | Sedimentary | 0.70817 | | |
| TE041 | Baghdad | Iraq | 33.18 | 44.23 | Cenozoic | Sedimentary | 0.70849 | | |
| TE042 | Baghdad | Iraq | 33.18 | 44.23 | Cenozoic | Sedimentary | 0.70819 | | |
| TE043 | Baghdad | Iraq | 33.18 | 44.23 | Cenozoic | Sedimentary | 0.70829 | | |

Continued on Next Page...

Table 13 – Continued

| Sample ID | Origin | Country | Lat (°) | Long (°) | Stratigraphy | Rock type | $^{87}Sr/^{86}Sr$ | $1\sigma$ | n |
|---|---|---|---|---|---|---|---|---|---|
| TE044 | Baghdad | Iraq | 33.18 | 44.23 | Cenozoic | Sedimentary | 0.70843 | | |
| TE045 | Baghdad | Iraq | 33.18 | 44.23 | Cenozoic | Sedimentary | 0.70840 | | |
| TE046 | Baghdad | Iraq | 33.18 | 44.23 | Cenozoic | Sedimentary | 0.70843 | | |
| TE047 | Deyali | Iraq | 34.4 | 45.7 | Cenozoic | Sedimentary | 0.70834 | 0.00001 | 4 |
| TE048 | Baghdad | Iraq | 33.18 | 44.23 | Cenozoic | Sedimentary | 0.70829 | | |
| TE049 | Taiz | Yemen | 13.34 | 44.1 | Mesozoic | Extrusive volcanics | 0.70864 | | |
| TE052 | Al-Ghail | Yemen | 15.17 | 47.48 | Cenozoic | Sedimentary | 0.70860 | | |
| TE054 | Al-Ghail | Yemen | 15.17 | 47.48 | Cenozoic | Sedimentary | 0.70835 | 0.00001 | 2 |
| TE055 | Al-Quada | Yemen | 15.17 | 47.48 | Cenozoic | Sedimentary | 0.70809 | | |
| TE056 | Al-Ghail | Yemen | 15.17 | 47.48 | Cenozoic | Sedimentary | 0.70816 | | |
| TE057 | Al-Ghail | Yemen | 15.17 | 47.48 | Cenozoic | Sedimentary | 0.70859 | | |
| TE059 | Habayer | Yemen | 15.17 | 47.48 | Cenozoic | Sedimentary | 0.70849 | | |
| TE063 | Al-Oyon | Yemen | 15.17 | 47.48 | Cenozoic | Sedimentary | 0.70855 | | |
| TE064 | Esfahan | Iran | 35.37 | 51.26 | Cenozoic | Sedimentary | 0.70870 | | |

Continued on Next Page...

Table 13 – Continued

| **Sample ID** | **Origin** | **Country** | **Lat (°)** | **Long (°)** | **Stratigraphy** | **Rock type** | $^{87}Sr/^{86}Sr$ | **1**$\sigma$ | **n** |
|---|---|---|---|---|---|---|---|---|---|
| TE065 | Tehran | Iran | 35.42 | 51.26 | Cenozoic | Sedimentary | 0.70824 | 0.00001 | 2 |
| TE066 | Kermanshah | Iran | 34.18 | 51.26 | Mesozoic | Sedimentary | 0.70840 | | |
| TE067 | Tehran | Iran | 35.42 | 51.26 | Cenozoic | Sedimentary | 0.70832 | | |
| TE068 | Tehran | Iran | 35.42 | 51.26 | Cenozoic | Sedimentary | 0.70835 | | |
| TE069 | Rodehen | Iran | 35.44 | 51.54 | Cenozoic | Sedimentary | 0.70858 | | |
| TE070 | Ghazvin | Iran | 36.14 | 50.2 | Cenozoic | Extrusive volcanics | 0.70918 | | |
| TE071 | Ghazvin | Iran | 36.14 | 50.2 | Cenozoic | Extrusive volcanics | 0.70823 | | |
| TE072 | Tehran | Iran | 35.42 | 51.26 | Cenozoic | Sedimentary | 0.70778 | | |
| TE073 | Tehran | Iran | 35.42 | 51.26 | Cenozoic | Sedimentary | 0.70770 | | |
| TE074 | Tehran | Iran | 35.42 | 51.26 | Cenozoic | Sedimentary | 0.70855 | | |
| TE075 | Mashhad | Iran | 36.17 | 59.36 | Mesozoic | Sedimentary | 0.70818 | | |
| TE076 | Tehran | Iran | 35.42 | 51.26 | Cenozoic | Sedimentary | 0.70826 | | |
| TE077 | Tehran | Iran | 35.42 | 51.26 | Cenozoic | Sedimentary | 0.70823 | | |
| TE078 | Tehran | Iran | 35.42 | 51.26 | Cenozoic | Sedimentary | 0.70799 | | |

Continued on Next Page...

Table 13 – Continued

| **Sample ID** | **Origin** | **Country** | **Lat (°)** | **Long (°)** | **Stratigraphy** | **Rock type** | $^{87}Sr/^{86}Sr$ | **1**$\sigma$ | **n** |
|---|---|---|---|---|---|---|---|---|---|
| TE079 | Tehran | Iran | 35.42 | 51.26 | Cenozoic | Sedimentary | 0.70798 | | |
| TE080 | Tehran | Iran | 35.42 | 51.26 | Cenozoic | Sedimentary | 0.70809 | | |
| TE081 | Tehran | Iran | 35.42 | 51.26 | Cenozoic | Sedimentary | 0.70835 | 0.00001 | 2 |
| TE082 | Afghanistan | Afghanistan | - | - | - | - | 0.70904 | | |
| TE083 | - | Oman | - | - | - | - | 0.70931 | | |
| TE084 | - | Oman | - | - | - | - | 0.71120 | | |
| TE085 | - | Yemen | - | - | - | - | 0.70862 | | |

Table 14: Summary statistics for each of the sample locations of the Middle East tooth enamel strontium $^{87}Sr/^{86}Sr$ measurements (n = 53).

| Origin | Mean $^{87}Sr/^{86}Sr$ | $\sigma$ | n |
|---|---|---|---|
| Al-Ghail | 0.70840 | 0.00021 | 7 |
| AlAin | 0.70886 | 0.00030 | 7 |
| Baghdad | 0.70836 | 0.00011 | 7 |
| Deyali | 0.70834 | NA | 1 |
| Esfahan | 0.70870 | NA | 1 |
| Ghazvin | 0.70871 | 0.00067 | 2 |
| Hili | 0.70875 | NA | 1 |
| Ibra | 0.70856 | NA | 1 |
| Kermanshah | 0.70840 | NA | 1 |
| Mashhad | 0.70818 | NA | 1 |
| Muscat | 0.71025 | 0.00041 | 4 |
| Rodehen | 0.70858 | NA | 1 |
| Salalah | 0.70899 | NA | 1 |
| Sur | 0.70963 | 0.00078 | 2 |
| Taiz | 0.70864 | NA | 1 |
| Tehran | 0.70815 | 0.00025 | 12 |
| Um-Ghafa | 0.70884 | 0.00001 | 2 |
| Waset | 0.70817 | NA | 1 |

## 3.4 Development of a tooth enamel strontium isoscape for the Middle East

At present there are no published isoscape models of bioavailable strontium ($^{87}$Sr/$^{86}$Sr) for the Middle East. In Section 3.3.2 it was shown that the $^{87}$Sr/$^{86}$Sr isotopic composition of tooth enamel from 53 samples of known origin in the Middle East study region could be partially differentiated based on the underlying geology. In this section a new isoscape of strontium isotope ratios in human tissue is produce based on the population data from the Middle East teeth. This shall be compared to modeled values based on the Beard and Johnson age model [28] in order to determine whether using a simple age based model is suitable for the large scale (international and global) prediction of $^{87}$Sr/$^{86}$Sr composition in human samples. The aim of the new isoscape is to complement the $\delta^{18}$O TEC isoscape for application in modern forensic human identification studies in the Middle East.

Table 15: Locations of origin for tooth enamel that can be differentiated using $^{87}Sr/^{86}Sr$ composition at the 95 % significance level by Tukey's HSD test.

| Location A | Location B | P |
|---|---|---|
| A-Ghail | Muscat | <0.001 |
| A-Ghail | Sur | 0.001 |
| AlAin | Muscat | <0.001 |
| AlAin | Tehran | 0.002 |
| Baghdad | Muscat | <0.001 |
| Baghdad | Sur | <0.001 |
| Deyali | Muscat | <0.001 |
| Esfahan | Muscat | 0.005 |
| Ghazvin | Muscat | <0.001 |
| Hili | Muscat | 0.008 |
| Ibra | Muscat | 0.002 |
| Kermanshah | Muscat | <0.001 |
| Mashhad | Muscat | <0.001 |
| Mashhad | Sur | 0.032 |
| Muscat | Rodehen | 0.002 |
| Muscat | Salalah | 0.051 |
| Muscat | Taiz | 0.003 |
| Muscat | Tehran | <0.001 |
| Muscat | Um-Ghafa | <0.001 |
| Muscat | Waset | <0.001 |
| Sur | Tehran | <0.001 |
| Sur | Waset | 0.03 |

### 3.4.1 Prediction of $^{87}Sr/^{87}Sr$ isotope composition based on the age of underlying geology

As has been described in Section 3.1.1 strontium isotopic composition within the food chain is determined by weathering of strontium containing minerals in the Earth's geology. The strontium isotopic composition of a mineral in a geological unit is determined by the initial concentration of $^{87}$Rb and the age of the rock unit as given by Equation 39:

$$\frac{^{87}Sr}{^{86}Sr} = \frac{^{87}Sr}{^{86}Sr_0} + \frac{^{87}Rb}{^{86}Sr} * (\exp^{\lambda t} - 1) \tag{39}$$

The geology of the Middle East study region is shown in Figure 33 and is described in Section 3.1.4. Underlying geology for each of the tooth sample points of origin was extracted from this geological map. As can be seen in the geological map (Figure 33), the underlying geology of the majority of the Arabian peninsula, Iraq and Iran is young, Cenozoic rock (Age = 0.01 - 65 Ma) and is mainly sedimentary in character. 47 of the 53 samples originate from areas with underlying Cenozoic geology. 2 samples originate from the Omani mountains which are composed of mesozoic rock (Age = 65 - 251 Ma). The remaining 4 samples originate from Muscat in Oman which is characterised by undifferentiated Paleozoic-Mesozoic bedrock (Age = 200 - 416 Ma).

The most basic model available for the prediction of strontium isotope ratios is based on the age of the geology as used by Beard and Johnson (2000) [28]. The Beard and Johnson (2000) model was applied using an initial $^{87}Sr/^{86}Sr_0$ of 0.705 ([28]) and an initial $^{87}Rb/^{86}Sr$ 0f 0.677 (calculated from values in [141]). As can be seen in Figure 42 the Beard and Johnson model predicts significantly lighter isotopic compositions than those of the measured tooth enamel samples. It is notoriously difficult to predict the strontium isotopic composition of sedimentary rock as the initial $^{87}Sr/^{86}Sr_0$ is determined by the weathered material from which that the sediment has derived and the model value 0.705 may be significantly lower than the actual starting value. In order to accurately predict the strontium composition more information is required on the source of the sedimentary

material and individual model coefficients ($^{87}Sr/^{86}Sr_0$ and Rb/Sr) should be used for each geological unit rather than a bulk earth estimate. This is outside the scope of this thesis but will be considered in future publications.

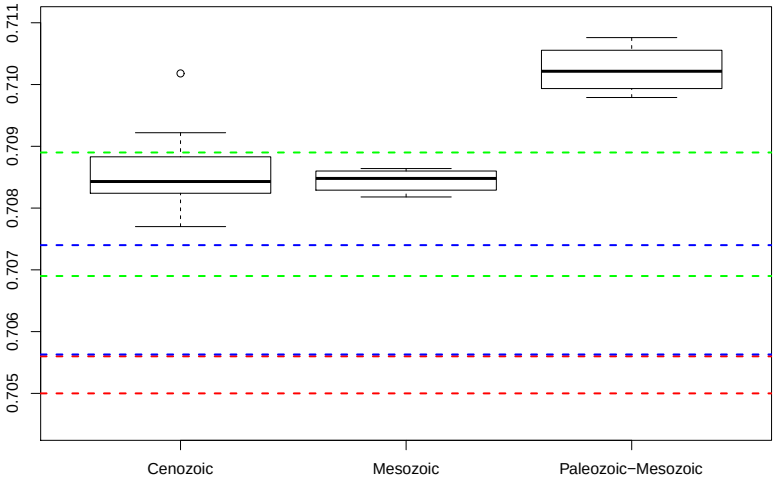


Figure 42: A box plot comparing the measured $^{87}$Sr/$^{86}$Sr composition of human tooth enamel based on the local geology (ME). The thick central line represents the median value, the box represents the interquartile range and the whiskers represent the extreme values. The 'Beard and Johnson' modeled range of $^{87}$Sr/$^{87}$Sr values based on geological age are included for each geology ( Red lines = Cenozoic limits, blue lines = Mesozoic limits, green lines = Paleozoic-Mesozoic limits).

#### 3.4.1.1 Prediction of $^{87}$Sr/$^{87}$Sr isotope composition based on European soil samples from similar geological units

Other than the teeth samples, there are no biological or geological samples from the Middle East available to this study for the estimation of the locally available strontium. An extensive database of soil samples was compiled by the Geochemical Mapping of Agricultural and grazing land Soil project (GEMAS) [179]. Strontium isotope measurements were performed by the Centre of Forensic Provenancing (Hoogewerff 2011 *in prep*).

$^{87}Sr/^{86}Sr$ isotope values from geological regions with closest similarity to those found in the Middle East were compared to the measured values for the tooth enamel samples from the Middle East (Figure 43). From the box plot it can be seen that the tooth enamel strontium isotope composition falls well within the range of the soil values. The range in values is much smaller for the teeth ($\sim$0.0015) than for the soils ($\sim$0.011). This is due to the strontium isotopic signal being averaged out as it moves up the food chain as suggested by Price *et al* [147]. The mean of the soil samples were compared to the mean of the tooth enamel samples by two sample t test for each geological unit. Statistically the mean $^{87}Sr/^{86}Sr$ isotopic composition for the soils from Cenozoic and Mesozoic geologies are significantly different to that of the teeth t = 5.63 ($P<0.05$) and t = 3.54 ($P<0.05$) respectively. The soil and teeth values for the Paleozoic-Mesozoic units (t = 1.47, P = 0.15) cannot be differentiated.

Despite statistical difference between the means of the soil and teeth populations for Cenozoic and Mesozoic sedimentary geologies the European measured soil values are clearly a better proxy for bioavailable strontium than the age model predictions described previously. Due to lack of suitable samples from the study region, for the purpose of this study geological units for which there are no measured tooth enamel, $^{87}Sr/^{86}Sr$ composition shall be approximated using the corresponding GEMAS soil samples. The range in values has been shown to be much higher (approximately 5 - 10 times) in the soil samples than in the tooth enamel samples due to food chain averaging. To account for this in the prediction model the assigned standard deviation of the $^{87}Sr/^{86}Sr$ population for each geological unit shall be one third of the standard deviation of the soil samples.

### 3.4.2 Construction of a new strontium isoscape

A new strontium isoscape was produced for the prediction of origin of tooth enamel samples from the Middle East study region based on underlying geology. Sufficient tooth enamel samples (n = 45) are available for the prediction of mean and range ($\sigma$) of tooth

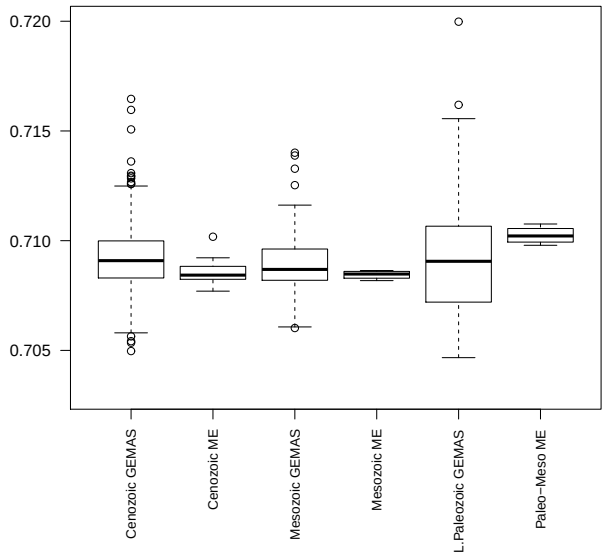


Figure 43: A box plot comparing the $^{87}Sr/^{86}Sr$ composition of human tooth enamel based on the local geology (ME). $^{87}Sr/^{86}Sr$ isotope composition of European soil samples from similar geological units are included for comparison (GEMAS).

enamel composition of individuals originating on Cenozoic bedrock. This makes up the majority of the study area. It has been shown in the previous section that the measured $^{87}Sr/^{86}Sr$ values for samples from Mesozoic (n = 4) and Early Paleozoic (n = 4) units fall within the range of those of the GEMAS soils from corresponding bedrock units in Europe. The mean $^{87}Sr/^{86}Sr$ composition of these geologies shall be given by the measured teeth samples but due to the small sample size for these geological units, the variance ($\sigma$) has been estimated as one third of the standard deviation of the GEMAS soil samples from the corresponding geological unit. The $^{87}Sr/^{86}Sr$ composition of the GEMAS soils for each of the geological units in the Middle East isoscape are shown in Figure 44. The assigned mean and standard deviation for each of the geological units in the new isoscape are shown in Table 16. The new strontium isoscape for the Middle East study region is shown in Figure 45. The standard deviation for the predicted values is shown in Figure 46.

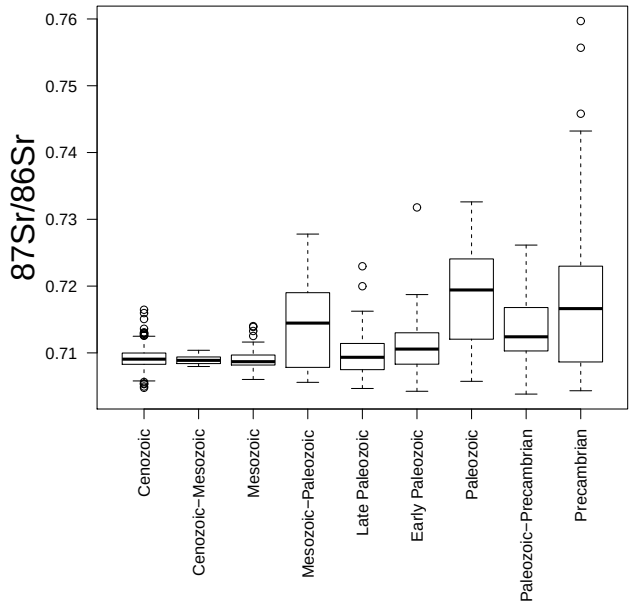


Figure 44: A box plot comparing the $^{87}Sr/^{86}Sr$ composition of the GEMAS soils based on the local geology (ME).

Table 16: Expected $^{87}Sr/^{86}Sr$ composition of tooth enamel samples from the Middle East based on underlying geology. $^{*}$ Values that are based on measured tooth enamel samples. The remaining values are predicted from the GEMAS soils as described.

| Geology | $^{87}Sr/^{86}Sr$ | $\sigma$ |
|---|---|---|
| Cenozoic | 0.7085$^{*}$ | 0.0004 |
| Cenozoic-Mesozoic | 0.7090 | 0.0003 |
| Mesozoic | 0.7084$^{*}$ | 0.0004 |
| Mesozoic-Paleozoic | 0.7105 | 0.0016 |
| Paleozoic | 0.7188 | 0.0029 |
| Late Paleozoic | 0.7099 | 0.0012 |
| Early Paleozoic | 0.7111$^{*}$ | 0.0048 |
| Paleozoic-Precambrian | 0.7129 | 0.0019 |
| Precambrian | 0.7179 | 0.0038 |

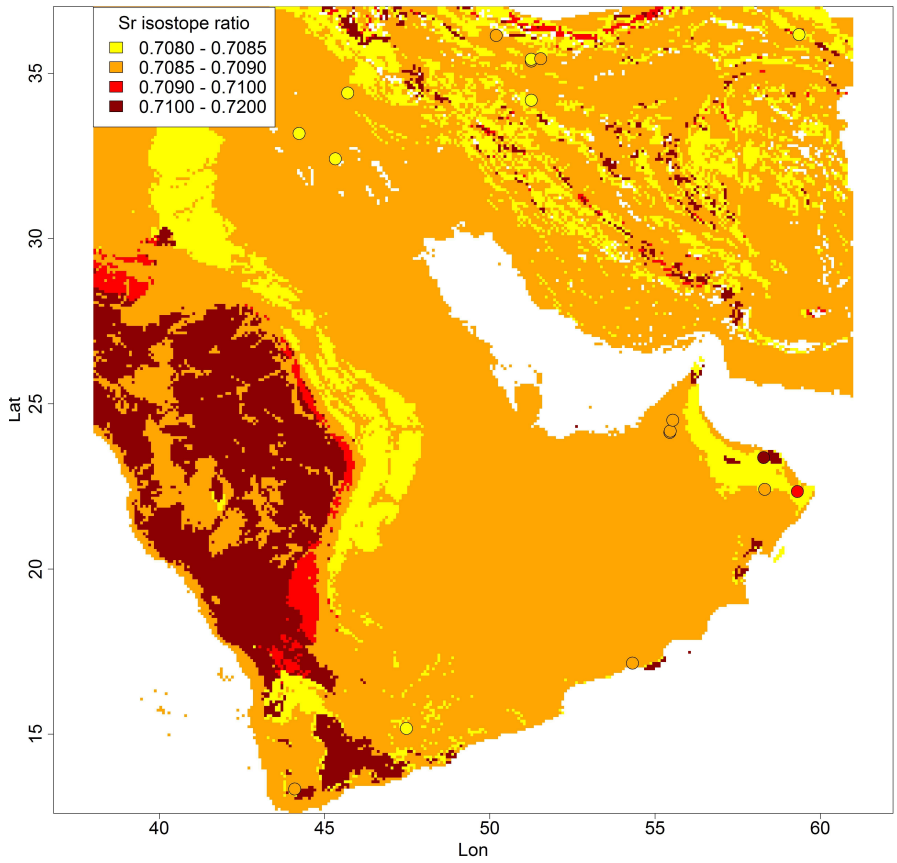


Figure 45: An isoscape of the expected $^{87}Sr/^{86}Sr$ isotopic composition of human tooth enamel in the Middle East.

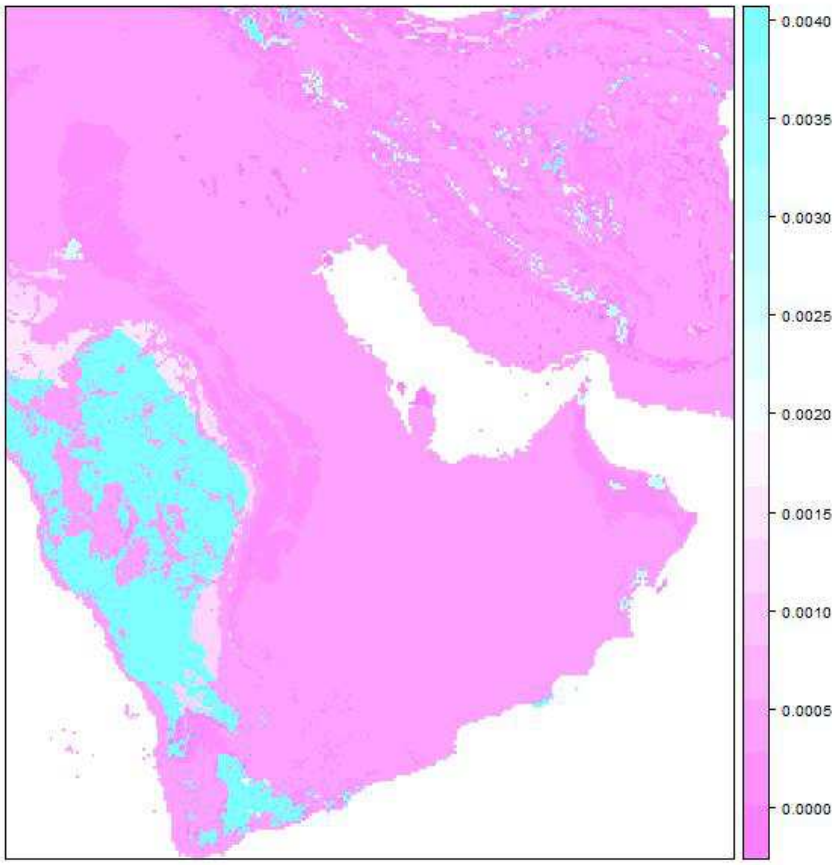


Figure 46: Expected standard deviation $^{87}Sr/^{86}Sr$ isotopic composition of human tooth enamel in the Middle East for each geology.

## 3.5 Conclusion

The geology of the Middle East is largely dominated by young Cenozoic sedimentary rocks. The majority of the samples measured in this study originated from areas overlying this rock type and could not be differentiated based on strontium isotope composition. However it has been shown that five samples originating from areas overlying older Mesozoic-Paleozoic sediment in Oman contained significantly higher strontium isotopic compositions and could therefore be differentiated from the rest of the Middle East population.

This observation suggests that a significant proportion of the diet originated from locally produced food. It is known that the region of Oman overlying the older Mesozoic-Paleozoic rock is one of the main growing regions for dates, limes and other fruit in Oman [41]. As strontium is highly concentrated in plants it is likely that these fruit sources may provide a large proportion of the dietary input of strontium in the region. This observation may also be useful for forensic cases in Oman as it has been shown that individuals from the region around Muscat have a local strontium signal that can be differentiated from the rest of the Middle East and therefore might be useful for determining whether unidentified remains from Muscat are from a local or an immigrant.

A new isoscape describing the isotopic composition of bioavailable strontium has been produced based on the measured samples and underlying bedrock units. Where no human samples were available values have been predicted based on the isotopic composition of soil samples collected from similar geological regions in Europe. It has been shown that strontium isotopic composition is useful for identification of individuals from the Muscat region of Oman. It is also likely that individuals from the old Precambrian Arabian shield in Saudi Arabia would exhibit higher isotopic compositions. However no samples were available to confirm this hypothesis. This is the first isoscape that has been produced describing the isotopic composition of bioavailable strontium in the Middle East and should be treated as a preliminary model due to the limited sampling density of the

study. However as more samples become available it is hope that the model will become more refined.

# Chapter 4

# Trace element analysis

## 4.1 Introduction

Due to the spatial variation of trace elements in nature, it may be possible to determine the source region of a sample of interest by measuring its trace element 'fingerprint'. The occurance of this spatial trace element variation has been exploited for decades in the fields of geology and mineral prospecting and much more recently for the provenancing of samples in forensic casework. This Chapter will examine the research hypothesis, 'trace element concentrations of human tooth enamel may vary significantly between regions due to differences in diet', by examining the measured trace elemental concentrations tooth enamel from individuals from across the Middle East. This section will briefly discuss the distribution of trace elements in the earths crust and the processes that lead to spatial elemental fingerprints in the biosphere, before looking in more detail at the forensic applications of trace element fingerprinting and the challenges of measuring trace element concentrations in human tissue, particularly tooth enamel.

### 4.1.1 An introduction to the factors leading to the trace element distribution observed in the Biosphere

Trace elements are those other than the eight principal rock forming elements of the Earth (Fe, O, Si, Mg, S, Ni, Ca and Al), occurring in minute quantities (ppm - ppb) within geological and organic materials. Despite the low abundance of the trace elements, many are vital for the continuation of life on the planet. For example 14 trace elements are known to be essential for the growth of all plants (B, Br, Cl, Co, Cu, F, I, Mn, Mo, Ni, Rb, Ti, V and Zn) [180], while 10 trace elements are essential for the optimal function of the human body (Mn, Co, Cu, Zn, Mo, I, F, Se, Cr and V) [181]. The deposition of trace elements within the Earth's crust is not uniform and has been determined by the culmination of over 4 billion years of complex geochemical and environmental processes.

#### 4.1.1.1 Chemical differentiation of the Earth

The trace elements became differentiated early in the formation of the Earth by separation into shells of different chemical composition (Figure 47). The large differences in temperature and pressure between the Earths centre and surface led to the separation of elements and minerals within the Earth. The lithosphere is defined as the rigid outer portion of the Earth consisting of the crust and the uppermost portion of the upper mantle [53]. The upper mantle is found approximately 40 km below the continents at the Mohorovicic discontinuity and stretches down about 400km. The upper mantle is heterogeneous because of the formation of magma from the continental crust at subduction zones found at destructive plate boundaries and has been found to be composed mainly of olivine, pyroxene and garnet. The Continental crust mainly consists of igneous and metamorphic rock (95 %) and sedimentary rock (5 %) [53]. 98 % of the mass of the continental crust consists of just 8 principal rock forming elements (Fe, O, Si, Mg, S, Ni, Ca and Al) [182]. Most elements are found as minerals, combinations of two or more elements [53]. Rocks comprise of a mixture of these minerals. Trace elements are able to substitute for the ions

in some minerals, hence the rock type is an important factor in the distribution of trace elements within the crust.

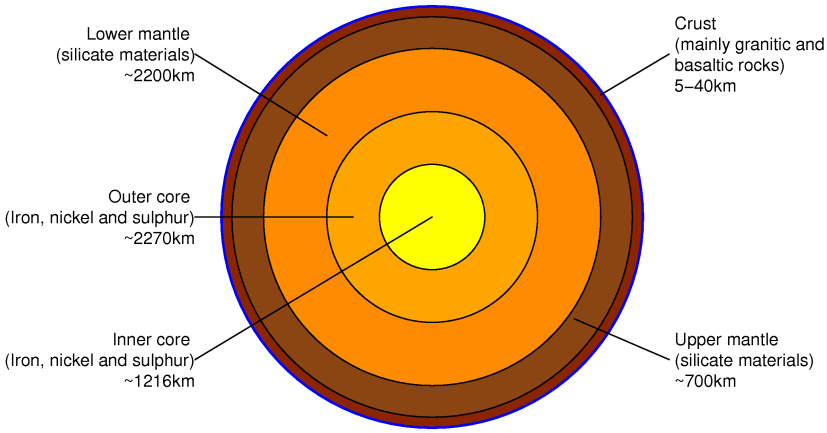


Figure 47: Cross section of the Earth, illustrating the different layers present and the basic properties of those layers.

Comparison of the abundance of the trace elements in the Earths crust to their abundance in the solar system indicates that significant differentiation has occurred and led to enrichment of some elements in the Earths Crust, particularly the Rare Earth Elements (REEs), and depletion of others [183] (Figure 48. The difference in elemental abundance between the Earths crust and the solar system can be illustrated by calculation of the enrichment factor (Equation 40). The natural abundances of the trace elements found on Earth can be attributed to their geochemical properties described by the Goldschmidt classification of elements [184]. By illustrating the enrichment factors of the elements in the crust it can be observed that the Earth's crust is enriched in most lithophile (silicate liquid) elements (e.g. the REEs), but depleted in most siderophile (iron liquid) and chalcophile (sulphide liquid) elements.

$$\text{Enrichment Factor} = \frac{\text{Abundance in the Earth's crust}}{\text{Abundance in the solar system}} \tag{40}$$

The enrichment of certain elements in the Earths crust can be used as an important tool for geochemical provenancing, as abundances of individual elements change depending on

the type of bedrock. This can be attributed to the geochemical properties of the elements and the physical conditions present during the formation of the bedrock. Igneous rocks for example are greatly differentiated due to the differences in geochemical properties such as pressure and temperature present during their formation and also, as the chemical composition of igneous rock is greatly dependent on the magma from which it forms. The composition of the magma in turn is dependent on the source rock and the extent of melting. The chemical compositions of igneous rocks have been widely studied and the data produced is very useful for determining which elements to expect in abundance in different types of bedrock. For example, ultramafic (low Si content) igneous rocks tend to be concentrated with Fe, Co, Ni Cr and Pt group elements, basaltic and intermediate rocks (∼25 % Si content) are enriched in Cu, Zn, Ag, Cd, Ti, Mn, Mo and Re, and low-Ca granites (high Si content) are abundant in REEs, Li, Be, Ta, W, Th, U, Sn and Hg. Sedimentary rocks are also highly differentiated due to physical conditions and transport steps during their formation [184].

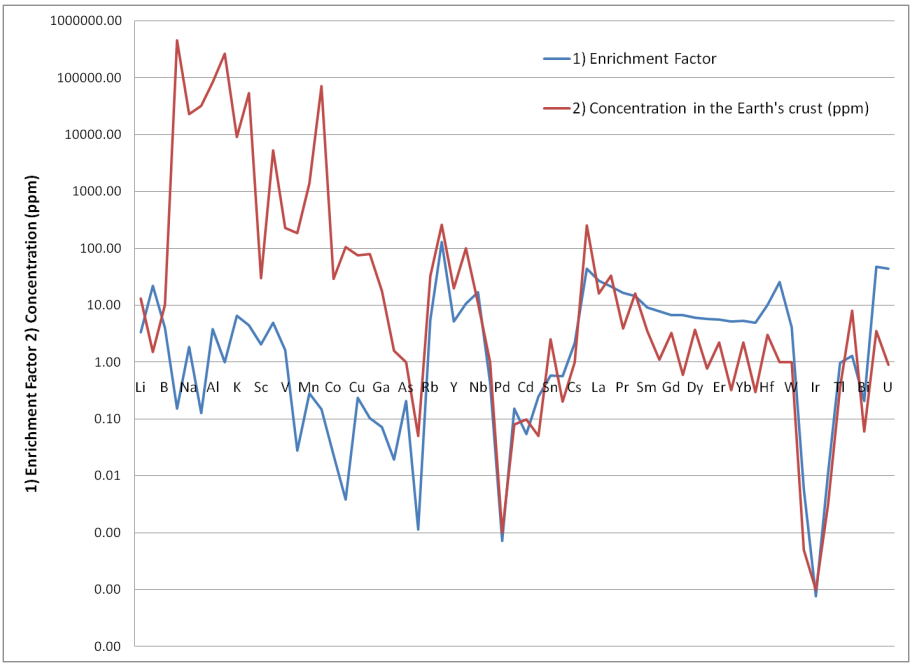


Figure 48: Line graph showing 1) The enrichment of elements in the Earth's crust in comparison to the solar system and 2) The concentration of elements in the Earths crust (ppm).

#### 4.1.1.2 Chemical differentiation of the Earth: From rock to biosphere

Soil is the interface between the lithosphere and the biosphere [184]. Approximately 99 % of the worlds soil is derived from mineral parent material that was formed by the weathering of bedrock, hence the trace element composition of a surface deposit is dependent on the trace element composition of its parent material. However, a combination of external factors have a strong influence on the final composition of the soil [185] and therefore the trace element composition.

Transport processes such as glacial or fluvial transport can lead to a soil composition that is not directly related to the underlying bedrock [184].

Anthropogenic sources also have a large impact on the final trace element composition of soils. Up to 1984 an estimated 0.5, 20, 240, 250 and 310 million tonnes of Cd, Ni, Pb, Zn and Cu had been mined and ultimately deposited into the biosphere [186]. Since then it is likely that these values have increased significantly [180]. Anthropogenic sources of trace elements that impact the biosphere include fertilisers, pesticides, sewage sludge, fossil fuel residue, general waste and pollution from mining and smelting. It is suggested that in urban and agricultural environments, anthropogenic sources are likely to outweigh natural sources of trace elements in the biosphere. Hence trace element concentration of modern soils can be significantly altered from the source bedrock material [186].

'Soil is the ultimate and most important sink of trace elements in the terrestrial environment' [186]. A soil's capacity for trace elements is determined by its ability to store trace elements in each of the following forms: 1) dissolved in soil solution, 2) attached to exchange sites in organic or inorganic constituents, 3) fixed into soil minerals (from bedrock), 4) precipitated with other compounds in the soil, and 5) incorporated into biological material (i.e. bacteria) [186]. Of these trace element 'stores', only trace elements in soil solution and attached to exchange sites are mobile and available for transfer into the food chain. Trace elements from these stores are known as bioavailable sources. The remaining stores may become mobile with time.

Bioavailability of trace elements in soils is determined by the pH and cation exchange capacity (CEC). Soils' affinity for trace elements is generally increased with increasing pH and hence bioavailability of trace elements is higher in acidic soils compared to neutral or basic soils [186]. The cation exchange capacity is determined by the number of cation binding sites within a soil. Soils with high organic and clay content tend to have higher CEC and therefore contain higher concentrations of bioavailable trace elements. Excess of trace element availability in soils can lead to phytotoxicity in plants. Hence a great deal of research has been conducted into producing the optimum soil growing conditions for plants [186].

#### 4.1.1.3 Chemical differentiation of the Earth: Trace elements in plants

Plants can be considered an intermediate reservoir of the trace elements between primary sources and the food chain [186]. Plants absorb trace elements from the soil, groundwater or atmosphere (Figure 49) by: 1) diffusion from the soil, 2) cation exchange from the surface of clay deposits occurring at the roots due to the respiration processes, and 3) foliar absorption from the air [180]. As previously mentioned, 14 trace elements are known to be essential for the growth of all plants (B, Br, Cl, Co, Cu, F, I, Mn, Mo, Ni, Rb, Ti, V and Zn) [180]. Deficiency in these essential elements can lead to abnormal growth, failure of life cycle and death [186]. It is also true that an excess in these essential elements can also lead to phytotoxicity [180]. A number of non essential and potentially toxic trace elements may also be absorbed by plants under the right conditions including Cd, Pb, Hg, and Sb.

Plant capacity for trace elements depends on a number of factors. Trace element absorption, selectivity and sensitivity varies greatly between plant species. Grasses and corn for example are very tolerant of toxic trace elements and can continue to grow even in soils with very high Cd concentration ($>$ 100ppm) [186]. Leafy vegetables such as lettuce and spinach are much less tolerant. Different genetic strains of these crops have shown different reactivity to harsh environments, a characteristic that has been taken advantage of in

agriculture.

Trace element concentration in plants is not homogeneous but varies between tissue types. The general trend of for trace element concentration in the tissue of trees and shrubs is, roots > foliage > branch. In grasses and cereal crops the trend is leaf > stem > husk > seeds, [186]. In general seeds tend to have the lowest concentration of trace elements in plant material. The distribution of trace elements within the different tissues of a plant is influenced by xylem transfer and the concentration in a specific tissue is related to the evapotranspirational loss of water from that tissue [186].

Soil conditions and climate also play a large role in the concentration of trace elements in plants. Deficiencies in trace elements may occur where bioavailability is reduced by abnormal climate conditions. Cold wet soils and hot dry soils result in reduced ionic mobility and hence lower bioavailability which can lead to low yields.

#### 4.1.1.4 Chemical differentiation of the Earth: Trace elements in animals

Trace elements are transferred from plants into the animal kingdom by ingestion. Animals may also ingest trace elements to a lesser extent through ingested water or inhaled from the atmosphere (see Figure 49). A significant proportion of the trace elements ingested by grazing animals comes directly from intake of soil, which can account for up to 14 % by weight of an animals diet [186]. Therefore the trace element concentrations found in farmed animals such as cows, sheep and pigs are likely to be significantly affected by anthropogenic sources of trace elements that have been added to the soil such as fertilisers. Farms close to urban areas may also be affected by trace elements common in fossil fuel pollution such as lead.

Like plants, a number of trace elements are essential for healthy growth and development of animals which include: Mg, K, V, Cr, Mn, Fe, Cu, Zn, Se, Sr and Mo [187]. Essential elements for animal development are defined as elements that lead to a significant growth response when the element is supplemented, and the animal shows signs of deficiency

when the element is excluded [186]. The physiological functions of the essential elements are well defined and are generally associated with the activation of specific enzymes or as a component of a vitamin or hormone [188].

Animals can also absorb non essential elements from their diet and as many species of animal have no homeostatic control over the non essential elements, they may become accumulated in animal tissue over time. For toxic elements such as Cd, Pb, Hg and As, accumulation of high concentrations may lead to health problems [188]. This is a concern in agriculture as accumulation of toxic elements in meat for human consumption can lead to health problems in the human population.

Despite a number of elements being essential for all animal species, a wide variety of elemental concentrations are observed within different species of the animal kingdom. For example Cu concentration in meat commonly consumed by humans ranges from 644 ppm in sheep to 270 ppm in cattle and only 22 ppm in swine (dry weight liver [188]). The large variety of elemental compositions observed across the animal kingdom is largely determined by the type, quality and amount of vegetation ingested as well as the composition of any meat that may also be consumed by animals higher in the food chain.

Like plants, the concentrations of trace elements in an animal is not homogeneous but varies greatly depending on the tissue. When considering sources of trace elements in a human diet this may be important, as the concentration of non essential and toxic elements tends to be higher in the liver of commonly consumed animals compared to the muscle flesh [188]. Calcified tissue such as bone and tooth has a high affinity for the alkali and alkali earth metals as these can substitute into the mineral lattice [189]. Lead is also accumulated in calcified tissue. Sharma and Shupe present lead concentrations from liver and bone tissue from rock squirrels which ranged from 1.3 - 26.7 ppm and 45.5 - 195.0 ppm respectively [190].

Clearly the trace element inter-relationships between soil, plants and animals are complex. Sharma and Shupe conducted a study on heavy metal concentrations in rock squir-

rels. They show that there is a good correlation between the concentrations of cadmium and arsenic found in soil and plants, but only a moderate to weak correlation for lead. There was little correlation between the elemental concentration found in plants and that of the squirrels other than for cadmium which showed a moderate relationship. [190]. This is a simple ecosystem, isolated from anthropogenic inputs (as far as possible), where the animal in question has a limited diet and small home range. For larger animals and humans the number of factors that control the concentration of trace elements is significantly larger due to the range in diet, larger home range and a large input from anthropogenic sources (Figure 49).

### 4.1.2 Trace elements in the human body

As in all animals, trace elements are essential for the optimal performance of the human body [181] performing vital functions such as controlling enzymatic activity, hormone activity and the development of teeth and bones. Trace elements shall be used in this thesis in an attempt to link unidentified human remains to a geographical region. However, as has been shown by Sharma and Shupe [190], trace elements in animal tissue are not necessarily correlated to the trace element concentration of the local available diet. This difficulty is amplified in humans due to the complex transport steps involved between bedrock and humans as illustrated by Figure 49.

#### 4.1.2.1 Sources of trace elements in the human body

Diet is the main source of trace elements in the human body (Figure 49). Modern humans (generally) consume both plants and animals (terrestrial and marine). As discussed in Sections 4.1.1.3 and 4.1.1.4, the trace element concentrations observed in plants and animals are dependent on multiple factors including species, tissue, environment and availability. The diet of modern humans, particularly in developed countries, is diverse due to the availability of multiple species of plants and animals, much of which will have been trans-

Table 17: Ranges of trace element concentrations observed in soil, plants, animals an humans. Concentrations observed in soil are from multiple references as cited in [186]. The range in concentrations observed in plants from [180] and [190] and represent measurements from a variety of plant species and tissues. The range in concentrations observed in animals are from cattle, sheep and swine (liver and muscle tissue) samples [188] and rock squirrels [190] (liver and bone tissue). The range in concentrations observed in humans are from [17], [191] and [181] and represent measurements of tooth enamel, liver, hair and blood samples.

| Trace Element | Soil ($\mu$g g$^{-1}$) | Plants ($\mu$g g$^{-1}$) | Animals ($\mu$g g$^{-1}$) | Humans ($\mu$g g$^{-1}$) |
|---|---|---|---|---|
| Ag | 0.01 - 8 | | | |
| As | <0.1 - 97 | 0.6 - 654.6 | <0.01 - 9.4 | <0.01 - 0.3 |
| B | 2 - 300 | 0.9 - 24 | | 0.7 |
| Ba | 10 - 5000 | | | 0.07 - 6.2 |
| Bi | 0.01 - 40 | | | |
| Cd | 0.01 - 2 | 0.4 - 9.9 | <0.1 - 26.7 | 0.3 - 4.1 |
| Co | 0.05 - 80 | 0.1 - 0.9 | | 0.02 - 41. |
| Cr | 1 - 3000 | 0.3 - 4.8 | | 0.02 - 4.1 |
| Cs | 0.3 - 20 | | | |
| Cu | <1 - 700 | 1.2 - 35 | 1.4 - 1151 | 0.024 - 1 |
| F | <10 - 3700 | | | 3.2 - 39 |
| Fe | Major | 5 - 7171 | 44.6 - 105.5 | 0.03 - 88 |
| Hg | <0.01 - 4.6 | | 0.01 - 1 | 0.03 - 12.2 |
| Mg | Major | | | 1811 - 9945 |
| Mn | <2 - 10000 | 50 -740 | <0.1 - 12.8 | 0.2 - 4.4 |
| Mo | 0.1 - 40 | | | 0.1 - 0.8 |
| Ni | 2 - 800 | 0.3 - 6 | | <0.01 -1.25 |
| Pb | 2 - 700 | 0.1 - 282.6 | 0.2 - 195 | 0.11 - 2.2 |
| Rb | | | | 0.074 - 4.6 |
| Sb | 0.2 - 8.8 | | | 0.1 |
| Se | 0.01 - 12 | | 0.01 - 7.71 | 0.19 - 1.4 |
| Sn | <0.1 - 200 | | | 0.2 |
| Sr | 4 - 3000 | | | 4.6 - 82 |
| Ti | 70 - 25000 | 1 - 46 | | 0.1 |
| Tl | 0.1 - 0.8 | | | |
| V | 3 - 500 | 0.5 - 2.8 | | 0.3 |
| W | 0.5 - 83 | | | |
| Zn | 1 - 2900 | 59 - 180 | 0.05 - 243 | 3.23 - 320 |

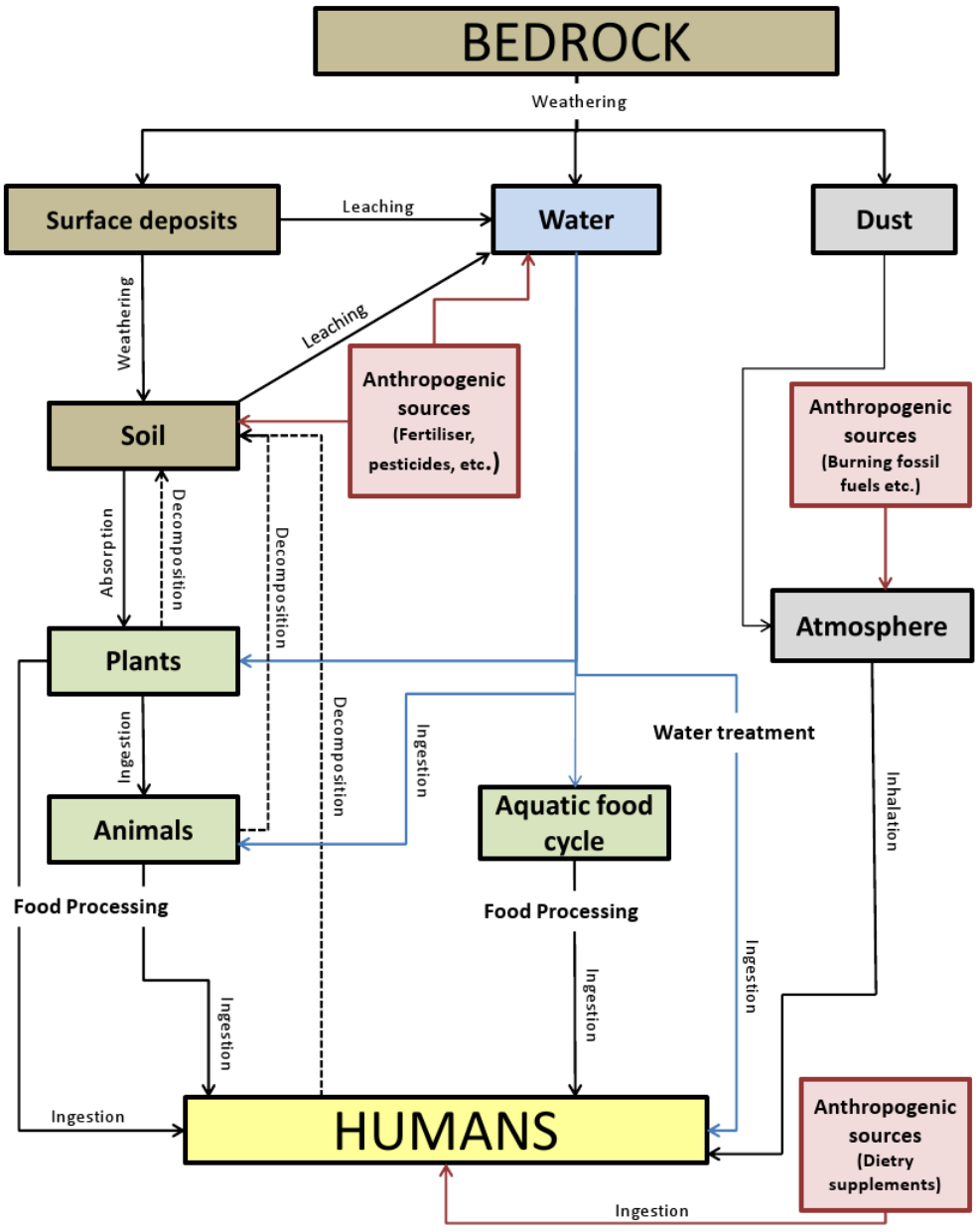


Figure 49: Trace element transport pathways from bedrock to humans

ported for hundreds of kilometers from its growing region thanks to improved packing, and preservation methods.

The trace element signature in plants and animals farmed for human consumption are likely to have little to no correlation with the natural trace element signature of the growing region due to the input of anthropogenic sources such as fertilisers, pesticides, man made animal feed and nutritional supplements. This signal may be further complicated during the manufacturing process by the addition of preservatives, colours and contaminants from processing machinery.

A further difficulty, particularly in the US and the developed western world, is the availability of dietary supplements. In the increasingly health conscious modern human population in the west, people are becoming more aware of the necessity of vitamins and minerals in a balanced diet. In a survey completed in 2000 [192], it was shown that approximately $ 1.7 billion was spent on vitamin and mineral supplements by the US public. Between 24 % (2 - 11 year old) to 55 % (70 years +) of the American population use daily supplements.

Trace elements may also be inhaled from the atmosphere. Lead in particular is associated with airborne environmental pollutants such as fossil fuel and industrial processes. Both cadmium and lead can be inhaled from tobacco smoke [193]. High concentrations of these elements in human tissue may be indicative of proximity to polluted industrial or urban areas which may be useful in forensic provenance studies of human remains.

#### 4.1.2.2 Essential elements in the human body

**Fluorine** is predominantly deposited in bones and teeth (98.9 % of total body content) [181]. Fluorine is necessary for increased resistance of tooth enamel and possibly bones [194, 187]. Deficiency can result in caries and a higher risk of osteoporosis.

**Magnesium** is one of the most common elements in the body accounting for approximately 0.05 % of the total body mass. Around 50 % of magnesium is found as a mineral constituent of bones or teeth. It is important for the activation of enzymes involved in metabolism as well as nerve activity. Deficiency can lead to muscle cramps, anorexia and depression [187].

**Potassium** is one of the most common elements in the body accounting for approximately 0.2 % of the total body mass. It is important for energy production and membrane excitability and transport [187].

**Vanadium** is predominantly deposited in fat (>90 %) [181]. Although its function in the human body is not well understood it is likely that it may have a role in the control of cholesterol [181].

**Chromium** is distributed throughout the body but is most concentrated in the skin (37 %) [181]. It is responsible for the activity of insulin and increases uptake of amino acids into the heart and liver [187]. Deficiency results in impared glucose tolerance and elevated cholesterol [181, 187].

**Manganese** is mainly concentrated in the bones and teeth (43.4 %) [181] and is an essential element in a number of biochemical processes within the human body including glucose and lipid metabolism and amino acids breakdown [187].

**Iron** is mainly present in the hemoglobin complex in blood (70.5 %) [181] and is vital for oxygen transport. Iron is also required for the activity of the Cytochrome complex that is an essential component of the electron transport chain. Deficiency can lead to anemia [194].

**Cobalt** is found predominantly in bone marrow (18.6 %) [181] although it is the least concentrated element in the human body. It is vital for the activity of vitamin $B_{12}$ [181].

**Copper** is concentrated predominately in muscle tissue (34.7 %) [181]. It is mainly responsible for the activity of oxidative enzymes and deficiency can result in anemia [194].

**Zinc** is concentrated predominantly in muscle tissue (65.2 %) [181]. Zinc is important for the activity of a number of enzymes involved in metabolism, cell growth and protein synthesis [187]. Deficiency can result in growth depression and reduced immune system response [194].

**Selenium** is found predominantly in muscle tissue (38.3 %) [181]. Selenium acts as an antioxidant and is involved in regulating the immune system. Deficiency can lead to heart failure (Keshan disease) and increased risk of cancer [187].

**Strontium** follows the physiological pathway of calcium and therefore is found almost exclusively in bone and teeth (99 %) [181]. Strontium hardens bones and teeth.

**Molybdenum** is concentrated predominantly in the liver (19 %) [181] and is responsible for the breakdown of toxic chemicals and drugs as well as the activity of enzymes involved in metabolism.

**Iodine** is mainly concentrated in the thyroid (87.4 %) [181]. It is involved in the synthesis of thyroid hormones [187]. Deficiency in pregnant women leads to an increased chance of still born or infant death after birth. Deficiency in the general population can result in goiter and hypothyroidism.

#### 4.1.2.3 Non-essential elements in the human body

A number of elements are found in human tissue but either have no essential function or their function have yet to be deduced. As mentioned previously lead and cadmium can be inhaled when present as environmental pollutants or as tobacco smoke. Lead has a strong affinity for bone and tooth apatite with 91.6 % of the total lead content being found in these tissues [181]. Cadmium is predominantly deposited in the kidneys and liver (27.8 %) [181]. Arsenic may be an essential element at low concentrations in the human body although this has yet to be confirmed. The major source of arsenic in humans is through food although proximity to industry or mining or smelting operations may cause elevated levels [181]. All of these elements are potentially toxic as they can accumulate in tissue over time to reach toxic levels [181].

### 4.1.3 Literature review: Trace element analysis for forensic provenancing

The idea that geological material might be used to link an individual to a crime scene was first introduced in the late 19th century by the most famous of criminal investigators, Sherlock Holmes in the writings of Sir Arthur Conan Doyle. The first recorded case of geological evidence being used to solve a criminal case came in 1908. By examining the macroscopic properties (colour, shape, and mineralogy) of a soil found on a suspected poachers shoes, Georg Popp was able to successfully link the individual to the crime scene. Since then the armory of geochemical forensic techniques has evolved and developed, incorporating many techniques from the earth sciences such as particle size analysis [195], scanning electron microscopy [196], isotope ratio analysis (IRMS) [52, 23, 25], and trace element analysis [197, 25, 198]. Trace element analysis in particular has seen an increase in interest over the last decade (Figure 50). This is largely due to improvements in instrumentation, allowing simultaneous analysis of around 50 trace elements per sample with greater accuracy and precision and requiring less sample [198].

Where sample size is not a limitation X Ray Fluorescence (XRF) may be used although it has become more common to utilise ICP spectrometry (ICP-AES and ICP-MS).

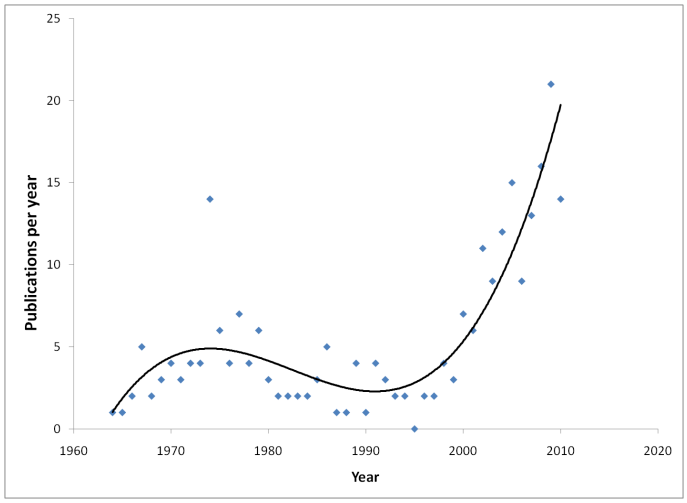


Figure 50: Number of publications per year for trace element analysis in forensics (Based on Scopus.com search with keywords **trace element** and **forensics**)

As described in Section 4.1.1 trace element concentrations in geological material vary spatially due to the physical and chemical conditions under which the material was formed. Hence rock, soil and sediment samples that may be visually indistinguishable may now be differentiated at a chemical level [198]. Pye *et al* [199], produced a study of soil samples from two small sample sites in the UK separated by approximately 10km. The main objectives of the study were to provide an indication of the intra and inter-site variation of soil samples based on a number of techniques including: ICP-AES and ICP-MS trace element analysis. Relatively little consideration has been given to the small scale spatial variability of soils which limits the extent to which it can be used in forensic investigation. It was shown that there was significant difference between the 2 sites for 41 of the 49 measured elements with 4 elements below detection limits and 4 elements, Zr, Hf, Tl and Pb showing no significant difference. Using PCA the two sample populations were clearly separated. The intra-site variation was significantly different at the two sites for a number of the measured elements. This highlights the fact that trace element concentrations in geological samples are the result of complex processes that makes it difficult to model. Even within a 1 $m^2$ area there may be a difference of between 0 - $>$50 % RSD.

Hence in studies utilising trace element analysis to differentiate between samples of interest it is important to have a database of reference samples that is sufficient to describe the inter and intra-site variation. Concheri *et al* [200], present a very recent case where soil particles found in a suspects car could be linked to the scene of a murder by trace element analysis. The results of the analysis were used as key evidence in the judicial court (Italy). Again the case highlights the necessity of compiling a suitable database with which to compare the suspect samples. It also clearly shows that if measured and reported correctly, trace element analsis can prove a useful forensic tool that is applicable in a court of law.

Trace elements from the lithosphere can be transfered to the biosphere and hydrosphere by biological and environmental processes as described briefly in Section 4.1.1. This means that not only can forensic trace element analysis be applied to geological samples but also to plants, animals and many man-made products that have natural starting materials. One of the main applications of forensic trace element analysis in the literature in recent years has been for the provenancing and authentification of high cost and specialist foodstuff such as wine [201, 202], tea [202, 203], olive oil [204], coffee [202] and cheese [153]. As with soils, the trace element distribution within foodstuff if determined by multiple variables including: geochemical environment at the location of growth, climate, health of the plant/ animal and anthropogenic contamination during growth and processing. Modeling the complex system would be nearly impossible so again it is important to compile databases of sufficient sample size to describe the intra and inter-population variation of the sample of interest for areas of interest. The EU funded TRACE project (www.trace.eu.org) is one organisation working to compile a European database of trace element and isotope information of food products as a forensic reference tool to combat food fraud. In the future it would be useful to produce a similar database for human tissue. It is often difficult to obtain reference samples of human tissue at a large enough scale to take into account the full variation in the population of the areas of interest. By compiling a global database in collaboration with other research groups around the world

the potential of trace element analysis for forensic human identification would be greatly increased. As well as food products trace element analysis has also been applied to the identification of origin of document paper [205], glass [206], bullet lead [207] and human tissue [16, 17, 25].

#### 4.1.3.1 Trace element analysis of human tissue in forensic investigation

As discussed previously (Section 4.1.2), trace elements become incorporated into human tissue through diet and the atmosphere. However absorption of trace elements into the various tissues of the human body is a complex process controlled by multiple variables which means that interpretation of trace element data in human tissue is not straight forward [208, 209]. In the last decade a number of archaeological studies have shown the value of trace element analysis for determining geographic origins of human populations, where suitable reference samples are available [210, 208, 189, 16]. Hoogewerff *et al* [16], illustrated the potential of trace elements (in support of isotopic measurements) for the identification of origin of an unknown sample. Again in this example, the trace element composition of the Iceman's bone tissue was compared to a database of human remains from the region. Until recently trace element analysis for the provenancing of human material was restricted to archaeological cases. There have been relatively few examples of trace elements being used to determine the migrational history of modern humans in the forensic literature [17, 25]. In a recent paper Castro *et al* use LA-ICP-MS to determine the trace element composition of modern human bone (n=12) and teeth samples (n=14). 75 % of the individuals could be differentiated by trace element composition of femur bones while principal component analysis of the tooth enamel samples enabled the successful identification of a simulated unknown sample.

The main limitation of trace element composition for provenance studies is clearly the almost unpredictable fractionation of trace elements in the human body [208]. In order to successfully utilise trace elements in forensic investigation a representative population of reference samples is required that describe the majority of the inter and intra site varia-

tion. It is likely that trace elements will be most useful in the confirmation or disproving of forensic intelligence suggesting a particular location of origin. Compilation of large global empirical datasets is probably the most useful approach for trace element forensics in the future. However compilation, management and quality control for such a dataset is likely to be expensive and time consuming. In this study a collection of 63 teeth of known geographic origin within the Middle East is available. These teeth shall form the foundations of a forensic database for the identification of individuals within the Middle East. It is hypothesised that trace element analysis shall compliment stable and radiogenic isotope information and provide an extra layer of information for the determination of origin of unknown samples.

### 4.1.4 Trace element analysis by LA-ICP-MS

Due to the unique nature of this teeth collection (see Section 1.6), analysis must be carried out with minimal damage to the teeth themselves. Laser ablation ICP-MS is a visually non-destructive technique in that the damage the laser causes to the tooth during the ablation is at a micrometer scale and is practically invisible to the naked eye [210]. LA-ICP-MS requires minimal sample preparation, reducing the risk of contamination and the need for sample dilution and allows for a high throughput of samples [211]. The common technique for sample preparation found in the literature involves preparing a thin section of the tooth by cutting with a diamond saw followed by ablation of the inner section of the enamel as laser ablation is ideally performed on a perfectly smooth surface to avoid coupling issues between the laser and the surface of the tooth that may result in loss of precision and poor reproducibility [210, 212, 213, 214]. This method is unsuitable for the current study due to the destructive nature of the sample preparation. Instead it is proposed that a surface profile is measured after pretreatment to remove any surface contamination. As the teeth in the Middle East collection are modern samples and have never been buried they should not have undergone any diagenesis hence surface contamination should be minimal. By thoroughly cleaning the surface with water followed by preab-

lation of the tooth surface before analysis any contamination should be removed. Most studies utilise a raster ablation pattern for analysis but in this case it may be more suitable to use a sequence of point ablations because the surface will not be perfectly flat.

One of the main issues affecting the application of LA-ICP-MS for quantitative analysis of forensic samples is the lack of suitable 'matrix matched' calibration and reference standards [210, 215]. Laser ablation standards need to be compositionally similar to the material to be analysed as physical properties significantly influence the ablation profile [216]. There are no available tooth enamel or hydroxy apatite standards available currently. As this technique advances this problem will need to be addressed and a small number of groups have begun working on solutions to this problem. Castro [17] uses a calibration method proposed by the NITE-CRIME (Natural Isotopes and Trace Elements in Criminalistics and Environmental Forensics) project. This involves preparation of calibration 'pellets' of NIST-1400 (bone ash) and NIST-1486 (bone meal) (National Institute of Standards and Technology, Gaithersburg, MD, USA). These are matrix matched to the samples in the study as the teeth were also ground and prepared as pellets. The samples were also analysed against the NIST-612 glass standard. Due to the destructive nature of the sample preparation, this method is not suitable in the current study. A number of papers report the elemental composition of tooth enamel as a semi-quantitative concentration relative to the NIST 610 and 612 glass standards (NIST, Gaithersburg, MD, USA), normalised to $^{43}Ca$ which is predominating in hydroxy apatite samples [210]. Due to a lack of a more quantitative alternative, this is the method that will be applied in this study.

## 4.2 Instrumental

### 4.2.1 Laser Ablation - Inductively Coupled Plasma - Mass Spectroscopy (LA-ICP-MS)

Inductively Coupled Plasma - Mass Spectroscopy (ICP-MS) was first made commercially available in 1983 [217, 218] and has since been used to determine the trace element concentration of a plethora of samples from across a multitude of disciplines. The main attractions of ICP-MS as an analytical tool are: its ability to measure concentrations of almost all the elements, low detection limits (sub ppt) due to high sensitivity and low background and fast analysis times of around 4 minutes for a measurement of all elements [218]. By coupling the micrometer scale resolution of Laser Ablation (LA) with the sensitivity of the ICP-MS technique it is possible to quickly generate a large amount of trace element data from a sample with little sample preparation required and virtually no damage to the sample (visually nondestructive) [219]. This makes it an attractive technique for the analysis of the teeth samples in this study as discussed in Section 4.1.4. LA-ICP-MS works on the same principal as MC-ICP-MS described in Section 3.2.1 where and high energy plasma is used to atomise and ionise the sample. However the electrostatic quadrupole and detector of the LA-ICP-MS are designed to scan a range of mass units in order to generate multi-element data. In this section the components of the LA-ICP-MS instrument will be described.

#### 4.2.1.1 Laser Ablation

Laser Ablation (LA) is a 'visually nondestructive' method of transferring a microscopic amount of a material from a sample into the ICP-MS for trace element analysis. The width and depth of the ablation crater is dependent on the intensity and beam width used during analysis and the ablation pattern required. For sensitive samples these settings can be optimised to produce minimal ($\mu$m scale) damage to the sample. The sample is placed in

the LA cell, sealed and purged with argon gas. The sample surface is then irradiated with a pulsed UV frequency laser, in this case a New Wave 213nm Nd:YAG laser (neodymium doped yttrium aluminum garnet crystal) [219]. The high energy photons from the laser remove material from the sample as a fine aerosol. The yield of ejected particles is dependent upon the intensity and beam width of the laser [220]. Ablated sample is then transfered in to the ICP via argon carrier gas.

#### 4.2.1.2 Generation of an Argon Inductively Coupled Plasma and the Plasma-MS interface

Generation of the ICP and the transfer of the ablated sample into the magnetic sector is similar to the processes described in Section 3.2.1. Further information for the quadrupole ICP-MS can be found in 4.2.1.

#### 4.2.1.3 The mass analyser

The mass analyser in a ICP-MS is used to separate ions according to their mass to charge ratio (m/z). In the case of the instrument used in this study the mass analyser is a quadrupole mass filter. This is the most common type of mass analyser, used in approximately 90 % of all ICP-MS instruments [218]. The quadrupole mass filter consists of four parallel metal rods arranged in a square, on axis with the ion beam. Ideally the rods have a hyperbolic cross section as this is the most efficient shape for generating the hyperbolic fields required for mass seperation [218].

In order to achieve mass separation of the ions, a dynamic hyperbolic electric field is generated by applying a direct current (DC) voltage and alternating current (AC) voltage to the rods. The AC voltage is the same for all the rods (2 MHz - 3 MHz [218]) but is out of phase between the two pairs of rods. The DC voltage is positive on one pair of rods and negative on the other. The electric field produced acts as a filter, allowing only the set mass unit to pass through. Ions of lighter or heavier mass will have unstable trajectories

through the field and is lost from the ion beam [218]. The DC and AC current can be varied very quickly so that all mass units (2 - 260 amu) can be measured in around 4 minutes.

#### 4.2.1.4 Ion detection: Electron multiplier

One of the main reasons for the high sensitivity of ICP-MS analysis is the use of an electron multiplier detector as this allows the signal from just one ion to be multiplied into a measurable signal against the background. The important characteristics of a detector in such a system are high sensitivity, a wide linear dynamic range and a low random background (determined by the plasma and ion lens system) [218]. The principle behind an electron multiplier involves the positive ion that has passed through the quadrupole striking the negatively charged dynode in the detector. The impact carries enough energy to release two or more electrons from the dynode which then impact with the second dynode. This releases more electrons. A detector generally contains 12 to 24 dynodes [218] and can multiply a signal by $10^8$ times. The signal is then given as an output in counts per second that can be converted into ppm using standard calibration methods.

### 4.2.2 Trace element analysis of human tooth enamel by LA-ICP-MS

The collection of 63 human teeth from the middle east study were analysed for trace element concentration using Laser Ablation - Inductively Coupled Plasma - Mass Spectrometry. Samples were first sonicated in Milli-Q water (15 minutes) and dried to remove any surface contamination. A New Wave UP-213 nm laser ablation system (ESI®, Portland, OR, USA) was used for the ablation of the samples. The sample cell was purged with argon prior to ablation. A line was ablated (60 %, 8 hz, 250 $\mu$m) on the surface of each tooth to further remove surface contaminaion. 5 spots were ablated (60 %, 8 hz, 100 $\mu$m, 60 seconds ablation period) within the pre-ablated trench and the trace element concentrations of 15 elements (Mg, K, Ti, V, Cr, Mn, Fe, Ni, Cu, Zn, Se, Sr, Mo, Cd, Ce and Pb)

were measured using a Thermo ICP-MS. The raw data were calibrated semi-quantitatively to NIST SRM 612 and NIST SRM 610 glass standards (NIST, Gaithersburg, MD, USA) and $Ca^{43}$ used as an internal standard to normalise the data as in [210]. Precision and accuracy were monitored by repeated measurement (n=21) of the NIST SRM 610 glass standard for quality assurance (Table 18). The perecentage error from the NIST certified values was less than 1 % for all elements with the exception of Ca (4.15 %).

Table 18: Measured and certified trace element concentrations (ppm) of the NIST610 glass reference standard

| Element | Measured value | Certified value | Error (%) |
|---|---|---|---|
| Mg | 467±8 | 465 | 0.44% |
| K | 486±10 | 486 | 0.06% |
| Ca | 85228±5687 | 81833 | 4.15% |
| Ti | 435±14 | 434 | 0.33% |
| V | 441±9 | 442 | 0.07% |
| Cr | 405±8 | 405 | 0.02% |
| Mn | 433±8 | 433 | 0.05% |
| Fe | 459±12 | 457 | 0.33% |
| Co | 405±8 | 405 | 0.07% |
| Ni | 443±9 | 444 | 0.16% |
| Cu | 429±9 | 430 | 0.20% |
| Zn | 456±9 | 456 | 0.17% |
| Se | 109±21 | 109 | 0.00% |
| Sr | 498±8 | 497 | 0.12% |
| Mo | 377±6 | 377 | 0.01% |
| Cd | 259±4 | 259 | 0.20% |
| Pb | 413±8 | 413 | 0.18% |

## 4.3 Results and discussion

Mean elemental concentrations of 14 trace elements measured in 63 Middle Eastern teeth of known origin are presented in Tables 25 - 27. Each tooth was ablated in 5 locations in order to take into account the inhomogeneity in human tooth enamel. Values reported are the mean of the 5 ablation measurements. The standard deviation of the replicates is presented in Tables 25 - 27. The population distributions of the 63 samples for each element are shown by the histograms in Figure 51. Eleven of the elements are log normally distributed (Mg, K, V, Cr, Mn, Fe, Cu, Se, Sr, Mo and Pb) so in order to calculate summary statistics for these elements the values have been log transformed prior to calculation and the results then transformed back into ppm by inverse log transform.

Summary statistics for the total population are shown in Table 19. The elements present at highest concentration were Mg (638 - 7713 $\mu$g g$^{-1}$), K (75 - 551 $\mu$g g$^{-1}$), Zn (201 - 1274 $\mu$g g$^{-1}$) and Sr (73 - 1273 $\mu$g g$^{-1}$) . This is to be expected as Mg, K and Zn are amongst the most highly concentrated elements in the human body. Mg, K and Sr all have a high affinity for the hydroxy apatite mineral in human bone and teeth as they are able to easily substitute into the $Ca^{2}+$ position in the mineral matrix [181]. The remaining elements were present at mean concentrations of $<$10 $\mu$g g$^{-1}$. The majority of the mean trace element concentrations observed in this dataset are comparable with values previously cited in the literature (Table 17). However it is observed that for a number of samples, Ni, Cu, Se, Sr and Pb appear at higher concentrations in these samples than has been observed previously. This may be an effect environmental or anthropogenic sources specific to regions in the Middle East. This may prove useful for differentiating between populations and will be discussed further in Section 4.3.1. Results that were below detection limit were substituted with half the detection limit.

Table 19: Summary statistics (Concentration median ($\mu$g g$^{-1}$) (Min - Max)) for the 15 trace element concentrations measured by LA-ICP-MS based on the population of 63 human teeth from the Middle East

| Element | Concentration(Min - Max) | Element | Concentration(Min - Max) |
|---|---|---|---|
| Mg | 1036(638 - 7713) | Cu | 2.46(0.01 - 65.80) |
| K | 194(75 - 551) | Zn | 819(201 - 1274) |
| V | 0.21(0.00 - 2.81) | Se | 11.4(0.11 - 33.66) |
| Cr | 0.64(0.03 - 2.27) | Sr | 215(73 - 1273) |
| Mn | 2.80(0.62 - 94.43) | Mo | 0.35(0.02 - 1.61) |
| Fe | 3.28(0.05 - 31.27) | Cd | 0.73(0.04 - 1.67) |
| Ni | 3.14(0.02 - 6.29) | Pb | 7.65(0.57 - 45.98) |

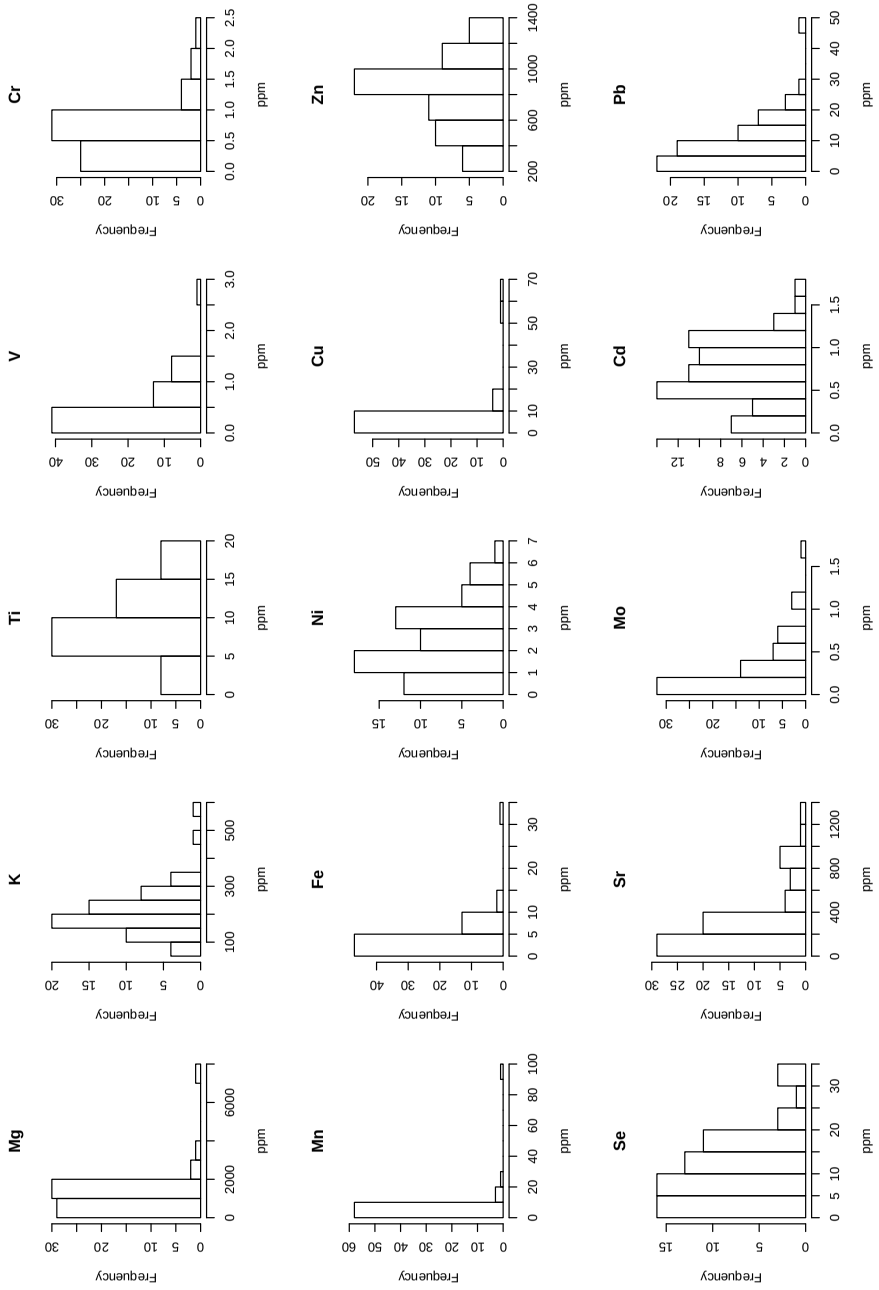


Figure 51: Histograms showing the population distribution of 15 elemental concentrations for a collection of modern human teeth originating in the Middle East (n = 63). Concentrations are in ppm.

### 4.3.1 Differentiation between geographical locations in the Middle East based on trace element concentration

It is the aim of this section to determine whether the tooth trace element concentrations are useful for the differentiation of origin of individuals from the Middle East. The samples were divided into 19 subsets representing the 19 locations from which the tooth samples originated (Table 20). This study is based on a small sample size (n = 63) and as such many of the locations are represented by very few samples. 15 locations are represented by $<5$ samples and 10 of these have only 1 sample. It is the nature of studies involving human tissue to be based on a small number of samples due to the difficultly of obtaining suitable samples of know origin. It must be recognised that the following statistical models presented in this chapter are limited by the small sample size and should be considered preliminary data. Models can be improved in the future as more samples become available. It would be beneficial for data measured by individual research groups to be compiled into a central database for public access and this is something that can be addressed in future research.

In order to determine which of the measured trace elements are useful for differentiating between the human populations from the Middle East, summary statistics have been calculated for each element for each of the 19 locations and are reported in Tables 20-23. The summary data is visualised in the spider plot (Figure 52) and box plots (Figure 53 - 56) to facilitate interpretation of the data. Analysis of variance (ANOVA) was performed on the dataset to determine which of the elements showed significant difference between the populations. The results for each of the measured elements is discussed in this section.

Table 20: Mean, standard deviation and range of trace element concentrations of the Middle East teeth for each of the sampling locations

| Origin code | Origin | n | Mg | K |
|---|---|---|---|---|
| A | Esfahan (Iran) | 1 | 988 | 214 |
| B | Tehran (Iran) | 12 | 1022±4(638 - 3896) | 138±1(75 - 255) |
| C | Kermanshah (Iran) | 1 | 719 | 182 |
| D | Rodehen (Iran) | 1 | 1033 | 225 |
| E | Ghazavin (Iran) | 2 | 716±164(709 - 723) | 146±2(89 - 240) |
| F | Mashhad (Iran) | 1 | 969 | 111 |
| G | Waset (Iraq) | 2 | 1356±1(1160 - 1584) | 129±1(119 - 139) |
| H | Baghdad (Iraq) | 7 | 1006±2(861 - 1123) | 186±1(94 - 277) |
| I | Deyali (Iraq) | 1 | 1103 | 234 |
| J | Sur (Oman) | 3 | 934±2(801 - 1069) | 138±1(126 - 160) |
| K | Muscat (Oman) | 4 | 926±1(888 - 975) | 179±1(157 - 204) |
| L | Ibra (Oman) | 1 | 2154 | 459 |
| M | Salalah (Oman) | 1 | 898 | 140 |
| N | Bidbid (Oman) | 1 | 983 | 157 |
| O | AlAin (UAE) | 7 | 1313±1(841 - 7713) | 216±1(177 - 274) |
| P | Hili (UAE) | 1 | 1408 | 323 |
| Q | Um Ghafa (UAE) | 2 | 974±1(957 - 991) | 231±1(208 - 255) |
| R | Taiz (Yemen) | 1 | 1392 | 271 |
| S | Al Ghail (Yemen) | 14 | 1567±3(1242 - 2064) | 250±1(156 - 551) |

Table 21: Mean, standard deviation and range of trace element concentrations of the Middle East teeth for each of the sampling locations ctnd.....

| Group.1 | V | Cr | Mn | Fe | Ni |
|---|---|---|---|---|---|
| A | 0.14 | 0.62 | 4.76 | 2.81 | 1.07 |
| B | 0.07±3.70(0.01 - 0.33) | 0.47±1.54(0.23 - 0.82) | 2.86±1.93(1.36 - 10.37) | 1.89±3.18(0.14 - 5.93) | 1.05±0.75(0.04 - 2.38) |
| C | 0.26 | 0.41 | 1.30 | 4.44 | 1.36 |
| D | 0.20 | 0.41 | 2.80 | 2.90 | 1.43 |
| E | 0.00±1.6(0.00 - 0.17) | 0.38±1.02(0.37 - 0.39) | 5.16±6.08(1.44 - 18.51) | 5.29±1.15(4.79 - 5.85) | 1.37±0.55(0.98 - 1.75) |
| F | 0.09 | 0.57 | 1.20 | 4.27 | 1.07 |
| G | 0.38±1.35(0.31 - 0.48) | 0.83±1.14(0.76 - 0.92) | 5.56±1.03(5.45 - 5.67) | 5.67±1.41(4.45 - 7.22) | 3.43±0.68(2.95 - 3.91) |
| H | 0.31±1.93(0.13 - 1.17) | 0.58±1.50(0.34 - 0.96) | 4.48±1.86(1.80 - 8.71) | 6.92±2.57(2.49 - 31.27) | 4.06±1.21(2.28 - 5.83) |
| I | 0.09 | 1.09 | 94.43 | 3.54 | 4.32 |
| J | 1.33±1.93(0.83 - 2.81) | 0.65±1.50(0.41 - 0.86) | 3.08±5.46(0.97 - 21.65) | 2.91±2.73(1.01 - 7.46) | 3.46±1.04(2.50 - 4.56) |
| K | 0.75±1.41(0.46 - 1.01) | 0.69±2.07(0.32 - 1.65) | 2.41±1.44(1.80 - 4.03) | 1.77±4.57(0.23 - 7.56) | 3.86±1.53(2.19 - 5.81) |
| L | 0.90 | 0.81 | 1.12 | 2.42 | 2.27 |
| M | 1.09 | 0.94 | 2.42 | 5.86 | 3.06 |
| N | 1.16 | 0.19 | 4.66 | 5.38 | 5.41 |
| O | 0.90±1.34(0.59 - 1.40) | 0.87±2.14(0.24 - 2.27) | 2.40±2.17(1.03 - 10.19) | 3.76±1.70(1.38 - 6.80) | 3.09±1.75(0.88 - 6.29) |
| P | 0.76 | 1.72 | 0.90 | 0.50 | 2.32 |
| Q | 0.70±1.15(0.64 - 0.77) | 1.03±1.63(0.73 - 1.46) | 1.20±2.51(0.62 - 2.30) | 1.59±1.89(1.01 - 2.49) | 1.74±1.50(0.68 - 2.81) |
| R | 0.05 | 0.33 | 1.86 | 2.87 | 3.31 |
| S | 0.12±3.13(0.01 - 0.73) | 0.45±2.44 (0.03 - 0.93) | 3.58±1.80(0.99 - 9.14) | 1.93±3.87 (0.05 - 7.28) | 1.72±1.19(0.02 - 3.94) |

Table 22: Mean, standard deviation and range of trace element concentrations of the Middle East teeth for each of the sampling locations ctnd..

| Group.1 | Cu | Zn | Se | Sr | Mo |
|---|---|---|---|---|---|
| A | 2.51 | 1011 | 7.84 | 192 | 0.07 |
| B | 0.83±2.98(0.18 - 2.84) | 1026±207(665 - 1274) | 10.19±1.54(4.21 - 17.72) | 198±1(126 - 313) | 0.10±2.10(0.02 - 0.32) |
| C | 2.14 | 1069 | 10.74 | 150 | 0.07 |
| D | 2.20 | 602 | 8.34 | 187 | 0.31 |
| E | 2.42±1.02(2.38 - 2.46) | 1191±14(1181 - 1201) | 6.91±2.06(4.14 - 11.53) | 175±2(129 - 236) | 0.07±2.05(0.04 - 0.12) |
| F | 2.39 | 704 | 8.09 | 261 | 0.05 |
| G | 0.21±3.51(0.09 - 0.51) | 681±236(514 - 848) | 14.90±1.47(11.32 - 19.62) | 142±1(126 - 159) | 0.54±1.05 (0.52 0.56) |
| H | 0.12±6.45(0.01 - 1.06) | 924±171(713 - 1206) | 18.40±1.58(8.85 - 33.66) | 179±1(142 - 226) | 0.59±1.51(0.35 - 1.01) |
| I | 0.25 | 593 | 26.17 | 238 | 0.42 |
| J | 8.74±2.06(5.20 - 19.96) | 851±134(735 - 997) | 1.80±2.57(0.69 - 4.58) | 106±1(86 - 144) | 0.12±1.84(0.07 - 0.23) |
| K | 8.07±5.52(1.70 - 65.80) | 910±66(847 - 981) | 6.01±2.75(1.51 - 17.10) | 152±2(73 - 294) | 0.09±2.38(0.03 - 0.17) |
| L | 2.49 | 265 | 22.39 | 179 | 0.11 |
| M | 3.11 | 809 | 1.44 | 174 | 0.08 |
| N | 11.03 | 905 | 8.13 | 226 | 0.06 |
| O | 5.11±3.66(1.29 - 53.11) | 865±205(653 - 1240) | 3.97±6.10(0.12 - 30.11) | 165±2(74 - 289) | 0.19±2.65(0.05 - 0.63) |
| P | 3.59 | 945 | 5.16 | 233 | 0.25 |
| Q | 4.12±1.52(3.06 - 5.54) | 870±31(848 - 891) | 8.86±1.68(6.14 - 12.79) | 245±1(231 - 260) | 0.51±5.07(0.16 - 1.61) |
| R | 0.09 | 473 | 22.77 | 809 | 1.06 |
| S | 0.65±5.45(0.03 - 3.19) | 434±128(201 - 626) | 5.99±4.35(0.11 - 21.41) | 711±1(322 - 1273) | 0.31±2.18(0.07 - 1.07) |

Table 23: Mean, standard deviation and range of trace element concentrations of the Middle East teeth for each of the sampling locations ctnd..

| Group.1 | Cd | Pb |
|---|---|---|
| A | 0.87 | 4.97 |
| B | 0.56±0.53(0.04 - 1.26) | 7.21±1.56(2.71 - 13.06) |
| C | 0.97 | 4.62 |
| D | 0.98 | 4.64 |
| E | 1.00±0.10(0.93 - 1.08) | 3.26±1.04(3.17 - 3.36) |
| F | 0.95 | 10.62 |
| G | 0.54±0.38(0.26 - 0.81) | 7.58±3.49(3.13 - 18.36) |
| H | 0.86±0.23(0.69 - 1.29) | 11.92±1.61(5.33 - 21.21) |
| I | 0.85 | 45.98 |
| J | 0.48±0.09(0.39 - 0.57) | 5.44±2.05(2.57 - 10.80) |
| K | 0.52±0.02(0.50 - 0.54) | 12.80±3.00(2.54 - 29.35) |
| L | 0.38 | 0.57 |
| M | 0.43 | 15.20 |
| N | 0.56 | 19.95 |
| O | 0.67±0.53(0.14 - 1.67) | 6.64±1.88(3.05 - 17.59) |
| P | 0.63 | 1.01 |
| Q | 0.44±0.05(0.40 - 0.47) | 4.63±1.07(4.42 - 4.85) |
| R | 0.68 | 3.35 |
| S | 0.90±0.30(0.43 - 1.45) | 5.87±2.65(1.12 - 24.14) |

#### 4.3.1.1 Magnesium

Magnesium was the most concentrated element measured in the Middle East tooth enamel samples. The lowest mean concentration (719 $\mu$g g$^{-1}$) was observed in the sample from Kermanshah (C) with the highest (2154 $mu$g g$^{-1}$) being observed in Ibra (L). The spider plot (Figure 52) shows little differentiation between the populations. The boxplot (Figure 53) shows that there is considerable overlap between most of the populations with concentrations of close to 1000 $\mu$g g$^{-1}$. Five of the locations (G, L, P R and S) show slightly elevated magnesium concentrations of $>$1300 $\mu$g g$^{-1}$ and two outliers exceed 3000 $\mu$g g$^{-1}$ (3896 and 7713 $\mu$g g$^{-1}$). ANOVA suggests that there **is not** a significant difference in the magnesium concentrations of teeth within the study region at the 95 % confidence level (Table 24).

Magnesium is an essential element that is one of the most abundant in the human body and is readily available in human diet which may explain why there is no significant difference observed for this element. Wheat is a particularly good source of magnesium [187] and the slightly elevated magnesium concentrations observed at locations G, L, P, R and S may be indicative of a higher percentage of wheat in the diet.

#### 4.3.1.2 Potassium

The lowest mean concentration of potassium (111 $\mu$g g$^{-1}$) was observed in Mashhad (F) with the highest (459 $\mu$g g$^{-1}$) in Ibra (L). The spider plot (Figure 52) shows little differentiation between most the populations although it can be seen that Ibra (L) is separated from the other locations. The boxplot (Figure 53) confirms this observation. Some differentiation may be possible (i.e. J and O) but there is significant overlap between most of the locations. ANOVA suggests that there **is** significant difference in the potassium concentration of teeth within the study region at the 95 % confidence level (Table 24.

Potassium is an essential element and is readily available in the human diet. Good sources include: fish, seeds, dried fruits, chocolates and dates. These commodities are more

available in the wealthy countries of the Middle East including Oman and the UAE [41]. The high potassium concentration observed in Ibra, Oman (L) and Hili, UAE (P) may be indicative of a wealthier diet.

#### 4.3.1.3 Vanadium

Observed mean vanadium concentrations were highest at Bidbid (N) (1.2 $\mu$g g$^{-1}$) and lowest in Tehran (B) (0.1 $\mu$g g$^{-1}$). The spider plot (Figure 52) shows clear differentiation between the locations. From the boxplot (Figure 53) it is clear that the locations are split into two groups. The populations from Iran (A-F), Iraq (G-I) and Yemen (R-S) exhibit significantly lower vanadium concentrations than those from Oman (J-N) and UAE (O-Q). ANOVA confirms that there is significant difference in the vanadium concentration of teeth within the study region at the 95 % confidence level (Table 24.

The clear distinction in vanadium concentration between Oman and UAE with Iran, Iraq and Yemen is likely due to a higher consumption of vanadium rich seafood in Oman and UAE.

#### 4.3.1.4 Chromium

The lowest mean concentration of chromium (0.2 $\mu$g g$^{-1}$) was observed in Bidbid (N) with the highest (1.7 $\mu$g g$^{-1}$) in Hili (P). There is little visible differentiation between locations in the spider plot (Figure 52). The boxplot (Figure 53) shows that there is overlap between most of the locations. The population from Al Ain (O) has a large range of values describing almost all of the variation of the study region. ANOVA suggests that there **is not** a significant difference in the Chromium concentrations of teeth within the study region at the 95 % confidence level (Table 24).

#### 4.3.1.5 Manganese

Manganese is significantly higher in Deyali, Iraq (I, 94 $\mu$g g$^{-1}$) than any other location in the study region ($<$10 $\mu$g g$^{-1}$) and over 20 times higher than anything previously published. Only one sample is available originating from Deyali so it is not possible to conclude whether this is a characteristic of a localised diet or simply an outlier in the data. Manganese acts as a co enzyme in the human body. It is fairly common in food, occurring in most fruit, vegetables, eggs and fish. It is unlikely that the dietary intake of individuals at this location would be almost 10 times greater than that of the rest of the Middle East. It is possible that this individual was consuming a high manganese diet or manganese supplement for health reasons resulting in the observed concentration. However without more samples it is uncertain if this sample is representative of the Deyali human population. Performing ANOVA on the dataset , excluding the possible outlier suggests that there **is not** a significant difference in the manganese concentrations of teeth within the study region at the 95 % confidence level (Table 24).

#### 4.3.1.6 Iron

There is over a factor of 10 difference between the minimum and maximum concentration of iron for the locations. Hili (P) in the UAE has the lowest observed iron concentration (0.5 $\mu$g g$^{-1}$) while Baghdad had the highest (6.92 $\mu$g g$^{-1}$). The spider plot (Figure 52) clearly shows this differentiation. From the boxplot (Figure 54) however it is clear that the range in iron concentrations for all locations represented by more than one sample are similarly large causing overlap between all locations. ANOVA confirms that there **is not** a significant difference in the iron concentrations of teeth within the study region at the 95 % confidence level (Table 24).

#### 4.3.1.7 Nickel

The lowest mean concentration of nickel (1.1 $\mu$g g$^{-1}$) was observed in Tehran (B) with the highest (5.41 $\mu$g g$^{-1}$) in Bidbid (N). The highest reported value for nickel concentration found in the literature was 1.25 $\mu$g g$^{-1}$ (Table 17) so clearly nickel intake is high in the Middle East. The spider plot (Figure 52) shows some differentiation between most the populations. The boxplot (Figure 54) clearly shows that the nickel concentration observed in Iran (A-F) is significantly lower than those observed in Iraq (G-I) and Oman (J-N). The range of nickel concentration in UAE and Yemen overlap with both groups. ANOVA confirms that there **is** a significant difference in the nickel concentrations of teeth within the study region at the 95 % confidence level (Table 24).

Nickel concentration is highest in soy beans, chocolate, oats, whole wheat and is generally higher in vegetables than in meat [221]. The lower nickel concentration of Iran compared to the other countries may be due to limited access to these food sources. Nickel can also be inhaled from the atmosphere and is a common environmental pollutant. However it is unlikely that the nickel content of the air in Iran is significantly lower that the rest of the study region.

#### 4.3.1.8 Copper

Taiz (R) and Baghdad (H) are characterised by the lowest copper concentration (0.1 $\mu$g g$^{-1}$), while Sur, Muscat and Bidbid in Oman contain the highest concentrations of copper (8.7, 8.1 and 11.0 $\mu$g g$^{-1}$ respectively). The spider plot (Figure 52) shows clear differentiation between the locations. The boxplot (Figure 54) clearly shows that the copper concentration observed in Iraq (G-I), Yemen (R-S) and Tehran (B) is lower than those observed in Oman (J-N) and UAE (O-Q) although there is some overlap between these populations. ANOVA confirms that there **is** a significant difference in the copper concentrations of teeth within the study region at the 95 % confidence level (Table 24).

The lower copper concentration found in the samples from B, G-I and R-S is consistent

with previously published values (Table 17). The higher values observed in Oman and UAE suggest a high copper dietary source or an anthropogenic source. Cu is found in high concentration in shellfish [187]. As the vanadium concentration in these samples was also high, a high percentage of seafood in the diet is probably the most likely cause.

#### 4.3.1.9 Zinc

The lowest mean concentration of zinc (265 $\mu$g g$^{-1}$) was observed in Ibra (L) with the highest (1191 $\mu$g g$^{-1}$) in Ghazavin (E). The spider plot (Figure 52) shows some differentiation between the locations with Ibra being much lower than the other groups. The boxplot (Figure 55) shows differentiation between a number of the locations. Taiz (R) and Al Ghail (S) in Yemen and Ibra (L) in Oman exhibit significantly lower zinc concentrations than the rest of the study region. Esfahan (A), Tehran (B), Kermanshah (C) and Ghazavin (E) in Iran have slightly elevated zinc concentrations compared to the rest of the study region. ANOVA confirms that there **is** a significant difference in the zinc concentrations of teeth within the study region at the 95 % confidence level (Table 24).

Zinc is an essential element and is one of the most abundant in the human body. Zinc is found in the highest concentration in red meat. Populations R and S from Yemen and L from Ibra may have low zinc concentrations due to a low percentage of meat in the diet.

#### 4.3.1.10 Selenium

The lowest mean concentration of selenium (1.4 $\mu$g g$^{-1}$) was observed in Salalah (M) with the highest (26.2 $\mu$g g$^{-1}$) in Deyali (I). Concentrations observed in the Middle East teeth were generally higher than values previously reported in the literature (Table 17). However the values reported were for soft tissue and to the authors knowledge, selenium in tooth enamel has not previously been reported. The spider plot (Figure 52) shows some differentiation between locations with a reasonable range of mean concentrations. The boxplot (Figure 55) shows that there is significant overlap between the locations although

the median concentrations of Waset (G) Baghdad (H) and Deyali (I) in Iraq were higher than the rest of the populations. ANOVA suggests that there **is not** a significant difference in the Selenium concentrations of teeth within the study region at the 95 % confidence level (Table 24).

#### 4.3.1.11 Strontium

Taiz (R) and Al Ghail (S) in Yemen contained significantly higher levels of strontium than the rest of the study region (809 and 711 $\mu$g g$^{-1}$ respectively). The lowest observed strontium concentration (106 $\mu$g g$^{-1}$) was in Sur (J). The spider plot (Figure 52) and boxplot (Figure 55) both show differentiation between R and S and the remainder of the populations. Locations A-Q show significant overlap in strontium concentrations. ANOVA confirms that there **is** a significant difference in the strontium concentrations of teeth within the study region at the 95 % confidence level (Table 24).

Strontium is an indicator of trophic level as it tends to decrease in concentration as trophic level increases [222]. Previous studies have reported strontium concentrations in teeth up to 82 $\mu$g g$^{-1}$ (Table 17). The majority of the Middle East teeth measured in this study contained a higher concentrations with most exhibiting a concentration of between 73 - 300 $\mu$g g$^{-1}$. This may indicate a higher proportion of vegetables and cereals in the diet of individuals from the Middle East. The teeth from Yemen had significantly higher concentrations of strontium. Yemen is the poorest of the countries in the study region and the majority of diet is expected to come from cereals [41] which could explain this observation.

#### 4.3.1.12 Molybdenum

The lowest mean concentration of molybdenum (0.1 $\mu$g g$^{-1}$) was observed in Mashhad (F) with the highest (1.1 $\mu$g g$^{-1}$) in Taiz (R). The spider plot (Figure 52) shows clear differentiation between the locations. The boxplot (Figure 55) shows that generally

the median molybdenum concentrations in Iran (A-F) and Oman (J-N) were lower than those for Iraq (G-I), UAE (O-Q) and Yemen (R-S) although there is some overlap in the populations. ANOVA suggests that there **is** a significant difference in the molybdenum concentrations of teeth within the study region at the 95 % confidence level (Table 24).

#### 4.3.1.13 Cadmium

The lowest mean concentration of Cadmium (0.4 $\mu$g g$^{-1}$) was observed in Ibra (L) with the highest (1.0 $\mu$g g$^{-1}$) in Rodehen (D). The spider plot (Figure 52) shows little differentiation between the locations. The boxplot (Figure 56) confirms that there is little differentiation with the majority of the locations overlapping in a range from 0.1 - 1.5 $\mu$g g$^{-1}$. ANOVA suggests that there **is not** a significant difference in the Cadmium concentrations of teeth within the study region at the 95 % confidence level (Table 24).

Cadmium is introduced into the human body mainly as an atmospheric pollutant from anthropogenic sources. One sample from Al Ain was an outlier, being higher than the remainder of the samples (1.7 $\mu$g g$^{-1}$). This could be indicative of a heavy smoker or someone who works at or near an industrial area .

#### 4.3.1.14 Lead

The lowest mean concentration of lead (0.6 $\mu$g g$^{-1}$) was observed in Ibra (L) with the highest (46.0 $\mu$g g$^{-1}$) in Deyali (I). The spider plot (Figure 52) shows significant differentiation between the locations. The boxplot (Figure 56) shows that the main difference in concentrations is between the extremes Ibra (L) and Deyali(I) while the remainder of the locations show significant overlap. ANOVA suggests that there **is** a significant difference in the lead concentrations of teeth within the study region at the 95 % confidence level (Table 24).

Lead is introduced into the human body mainly through inhalation from pollution (Figure 49) and has a high affinity for bone and tooth tissue. The significantly higher lead concen-

tration observed in the individual from Deyali may indicate daily exposure to high levels of pollution, possibly a job in a factory or similar. Both cadmium and lead were lowest in Ibra suggesting that there is low pollution in this city. Ibra is an ancient city with little industry and a main income from tourism.

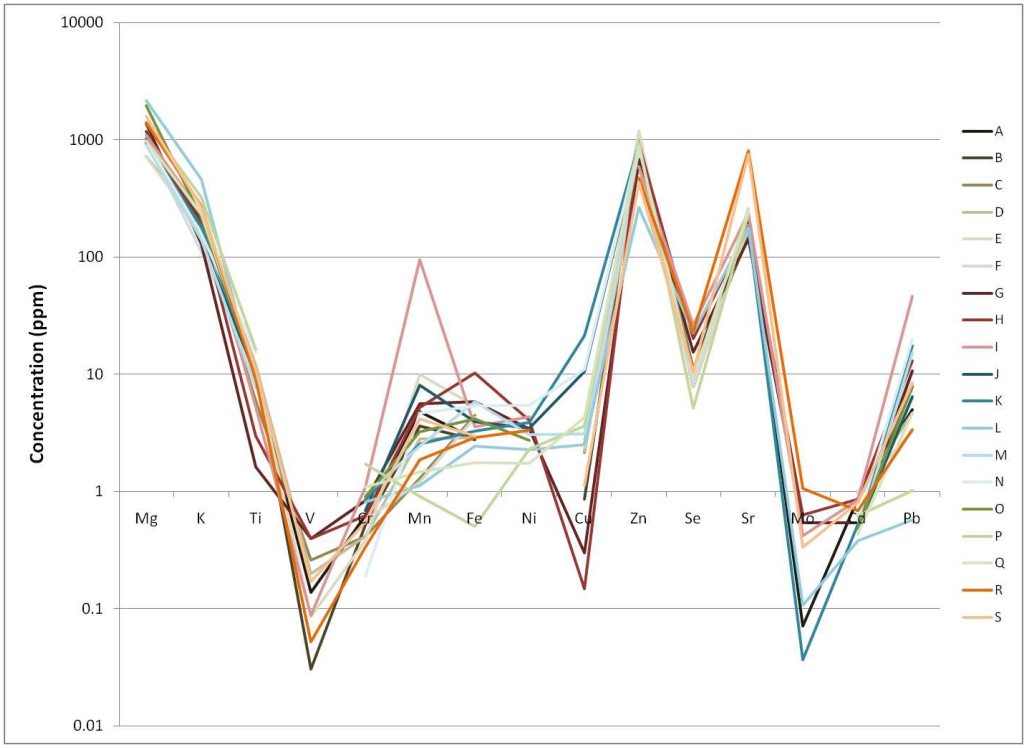


Figure 52: Spider diagram showing the average concentration (ppm, log scale) of 15 elements found in the tooth enamel of individuals (n = 63) from 19 locations within 5 countries of the Middle East. Grey scale lines (A - F) represent locations within Iran, red lines (G - I) Iraq, blue lines (J - N) Oman, green lines (O - Q) the United Arab Emirates and the orange lines (R - S) Yemen.

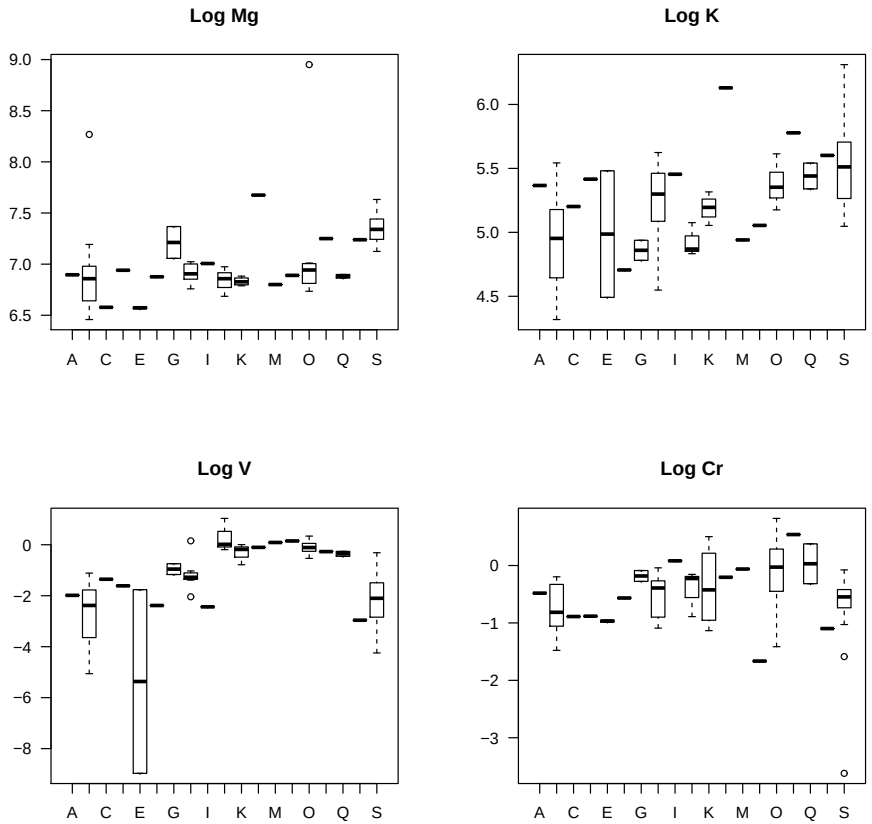


Figure 53: Box plots showing the elemental concentrations of Mg, K, V and Cr for a collection of modern human teeth from the Middle East. Each box plot has been split into the locations of origin (A-S) so that differences in concentration can be observed between locations. The central thick black line of each box represents the median concentration for that population, the box represents the inter-quartile range and the whiskers show the maximum and minimum concentrations. Locations where only 1 tooth was available are shown by a single black line. Elements are plotted as log concentrations (log $\mu$g g$^{-1}$) due to the log normal distribution of those elements.

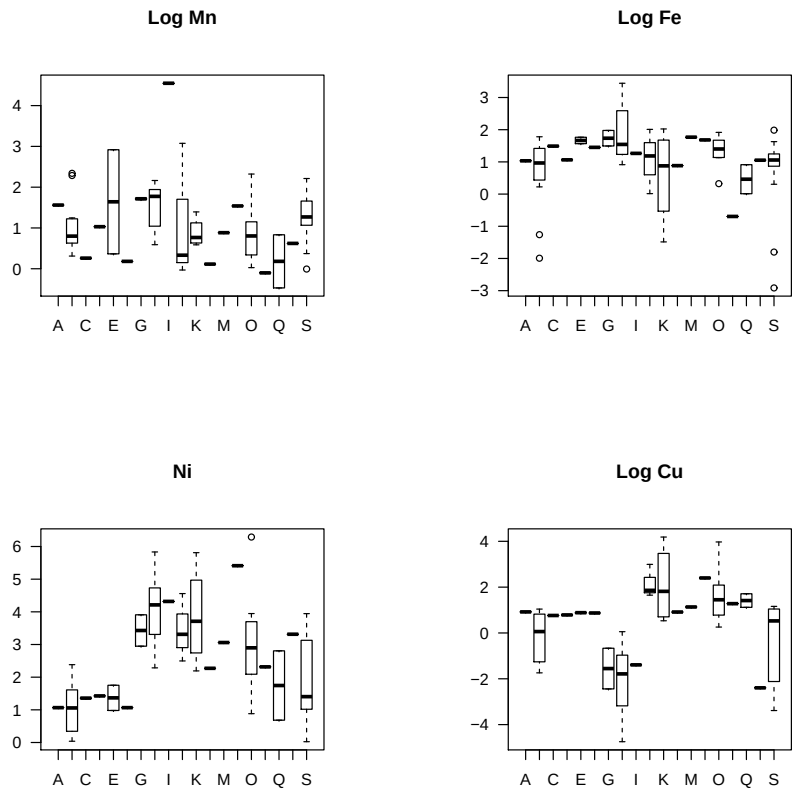


Figure 54: Box plots showing the elemental concentrations of Mn, Fe, Ni and Cu for a collection of modern human teeth from the Middle East. Each box plot has been split into the locations of origin (A-S) so that differences in concentration can be observed between locations. The central thick black line of each box represents the median concentration for that population, the box represents the inter-quartile range and the whiskers show the maximum and minimum concentrations. Locations where only 1 tooth was available are shown by a single black line. Ni is plotted in $\mu$g g$^{-1}$ while the remaining elements are plotted as log concentrations (log $\mu$g g$^{-1}$) due to the log normal distribution of those elements.

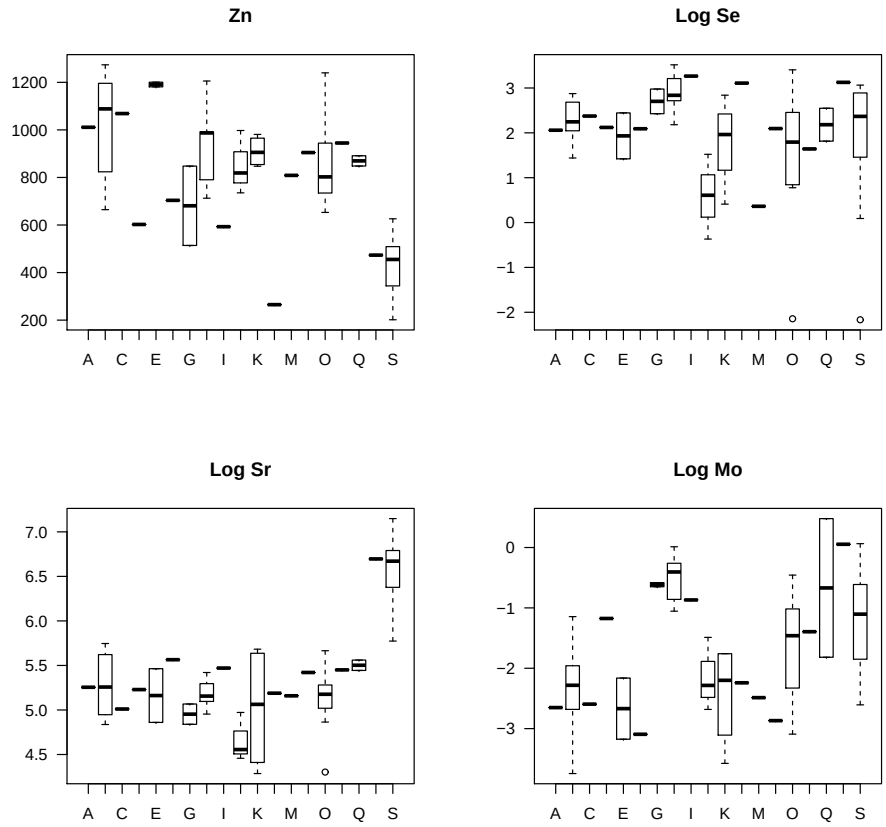


Figure 55: Box plots showing the elemental concentrations of Zn, Se, Sr and Mo for a collection of modern human teeth from the Middle East. Each box plot has been split into the locations of origin (A-S) so that differences in concentration can be observed between locations. The central thick black line of each box represents the median concentration for that population, the box represents the inter-quartile range and the whiskers show the maximum and minimum concentrations. Locations where only 1 tooth was available are shown by a single black line. Zn is plotted in $\mu$g g$^{-1}$ while the remaining elements are plotted as log concentrations (log $\mu$g g$^{-1}$) due to the log normal distribution of those elements.

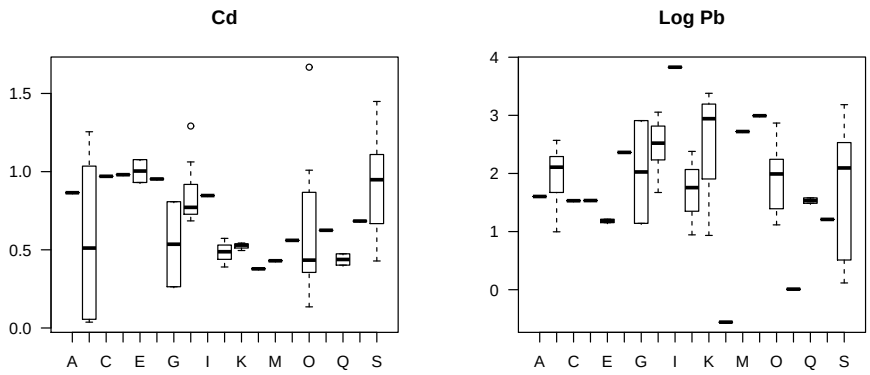


Figure 56: Box plots showing the elemental concentrations of Cd and Pb for a collection of modern human teeth from the Middle East. Each box plot has been split into the locations of origin (A-S) so that differences in concentration can be observed between locations. The central thick black line of each box represents the median concentration for that population, the box represents the inter-quartile range and the whiskers show the maximum and minimum concentrations. Locations where only 1 tooth was available are shown by a single black line. Cd is plotted in $\mu$g g$^{-1}$ and Pb is plotted as log concentration (log $\mu$g g$^{-1}$) due to the log normal distribution.

### 4.3.2 Principal component analysis of the trace element data

Principal component analysis (PCA) is a multi variate statistic technique used to determine a small number of linear combinations from many variables in order to differentiate between groups. Here PCA is used to distinguish between the Middle Eastern populations A-S. The 'princomp' function in R [223] was used to calculate the weightings for the principal components and to visualise the data. The 8 elements determined by ANOVA to show significant differences between groups (K, V, Ni, Cu, Zn, Sr, Mo and Pb) were assigned as the variables for the multivariate model. Figure 57 illustrates the proportion of the variance in the data represented by each of the principal components. The first two components describe 50 % of the variance (Figure 58) and the third component represents a further 16 % of the variance (Figure 59). The remaining 5 components describe the final 34 % of the variance.

Figure 58 is a bi-plot of the first two principal components. Sample points are shown as a letter referring to the location of origin (A-S) of the sample as defined in Table 20. Red arrows show the loadings of each element on the principal components. Strontium and potassium show strongest negative loadings on PC1 while zinc, nickel, copper and vanadium have the strongest positive loadings on PC1. Lead and zinc have strongest positive loadings on PC2 and copper, nickel, vanadium and potassium have the strongest negative loading on PC2.

The direction of the elemental loadings can be described by considering dietary sources of these elements. To the left hand side of the plot strontium and potassium have the biggest loadings with molybdenum also in that direction. These three elements represent a high cereal or vegetable and low meat diet which might be expected in the poorer Middle Eastern countries. Samples originating from Taiz and Al Ghail in Yemen (R and S) lie in this area of the bi-plot which is expected as Yemen is the poorest of the countries from the study. The sample from Ibra in Oman also falls to the left had side of the which might suggest a vegetarian or low meat diet for that individual.

The right hand side of the plot can be split into two groups. The top right group has a strong zinc loading which is indicative of a diet rich in red meat. Samples originating from Esfahan (A), Tehran (B), Kermanshah (C), Ghazavin (E)and Mashhad (F) in Iran fall into this area of the plot along with an individual from Baghdad (H) and one from Al Ain (O). The bottom right group has strong copper, nickel and vanadium loadings which are nearly identical. These elements are indicative of a high seafood diet and are found in high concentrations in more expensive foods such as chocolate and dates. Samples from Sur (J), Muscat (K), Salalah (M) and Bidbid (N) in Oman and Al Ain (O) and Hili (P) in the UAE fall into this area of the plot. UAE and Oman are the richest of the Middle Eastern countries and are have a large trade in seafood and dates [41].

Lead has a small loading compared to the other elements, suggesting that the dietary elements describe most of the variation in the study region.

Figure 59 is a three dimensional plot of the first three principal components. The points have been colour coded by country of origin as national/ cultural identity is most likely to be the best predictor of dietary traditions. The plot clearly shows that the individuals from the different countries form clusters although there is some overlap between these clusters. Yemen (light blue) is clearly differentiated from the rest of the study region.

Figure 60 is an ellipse plot of the two major principal components. Ellipses show the extent of the 95 % confidence intervals for each country. Ellipses were plotted using the VEGAN package available in R [223]. From this plot the groupings of samples can be clearly seen. There is significant overlap of the ellipses towards the centre of the plot (0,0), but there is more possibility of differentiation towards the edges. The ellipse defined by the samples from Yemen is seperated from the remainder of the samples with very small areas of overlap with the ellipsis for Iran, Iraq and UAE. The ellipses representing Iran, Iraq, UAE and Oman all show considerable overlap. However apart from Iraq which completely overlaps with the other contries, the ellipses do have regions that could be differentiated.

Table 24: The results of analysis of variance on 15 trace element concentrations between sampling locations (Fcrit=2.07)

| Element | F value | Pr(>F) | Element | F value | Pr(>F) |
|---|---|---|---|---|---|
| Mg | 1.29 | 0.24 | Cu | 2.98 | <0.01 |
| K | 2.81 | <0.01 | Zn | 7.35 | <0.01 |
| V | 3.66 | <0.01 | Se | 1.06 | 0.42 |
| Cr | 0.99 | 0.5 | Sr | 9.58 | <0.01 |
| Mn | 0.99 | 0.5 | Mo | 3.38 | <0.01 |
| Fe | 0.79 | 0.7 | Cd | 0.79 | 0.7 |
| Ni | 3.35 | <0.01 | Pb | 2.19 | 0.02 |

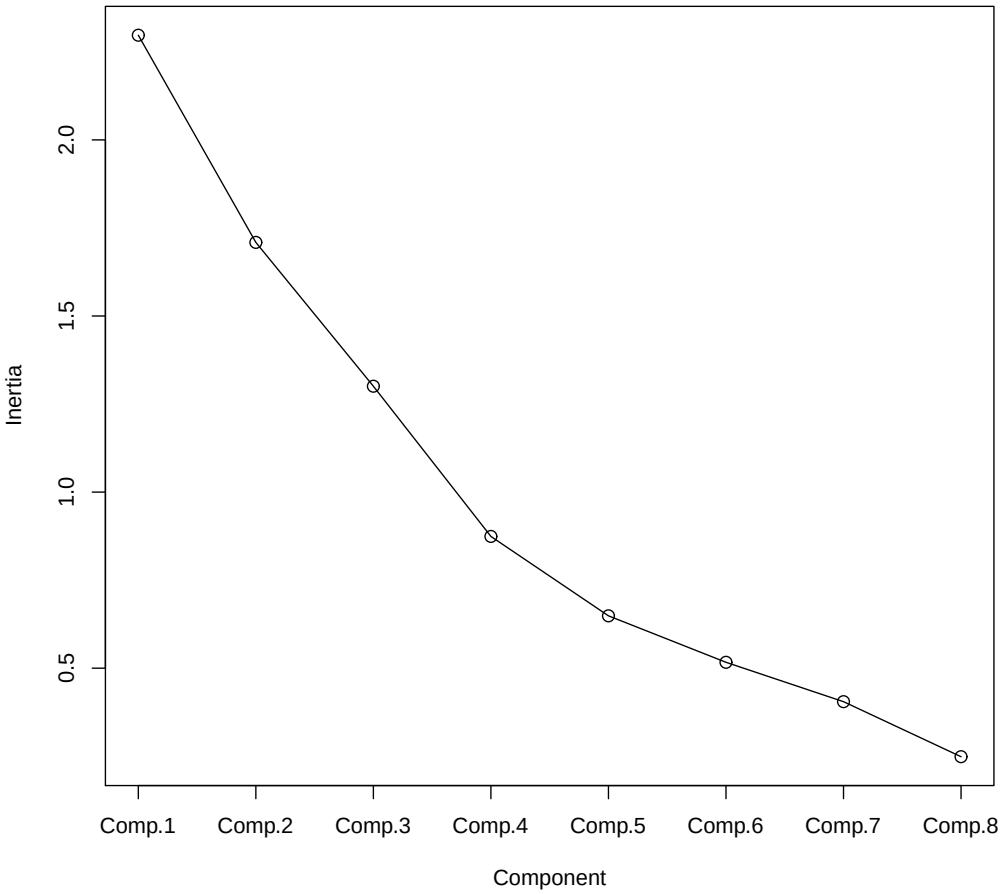


Figure 57: Scree plots showing the proportion of variance represented by the individual principal components of the Middle East human tooth samples.

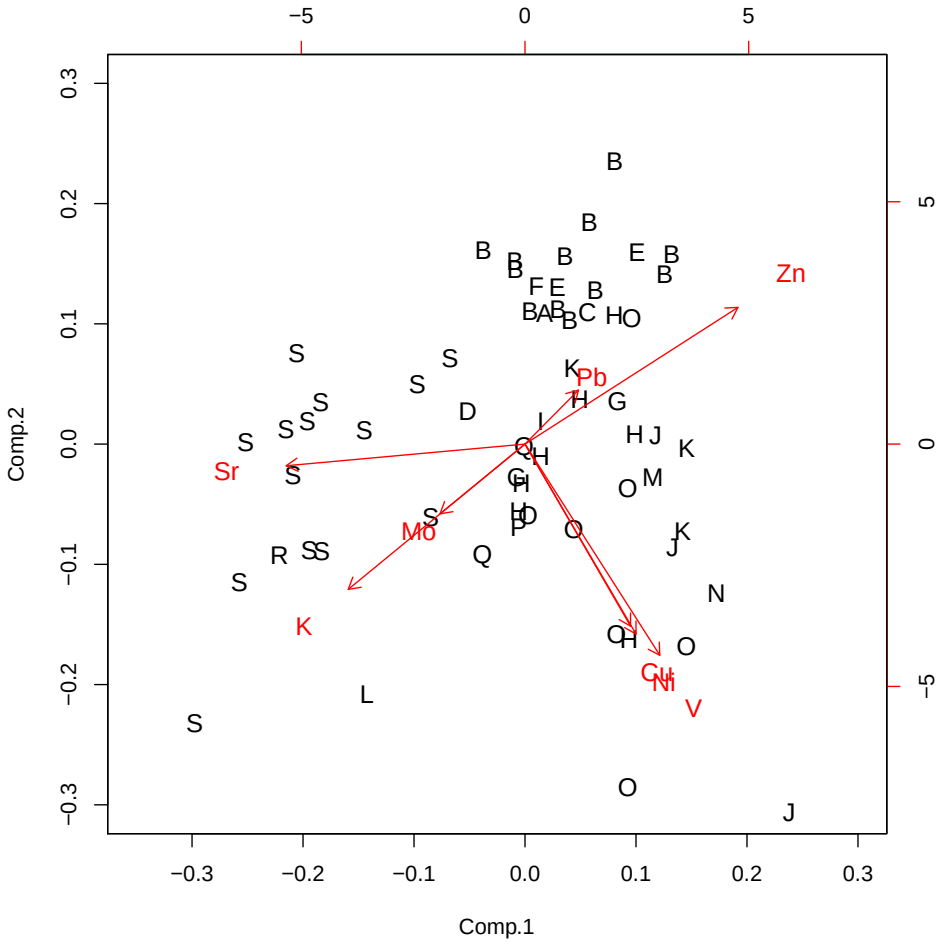


Figure 58: Bi plot of the principal components of the Middle East human tooth samples calculated using Principle Component Analysis (PCA). Sample points are shown as letters A-S representing the 19 locations of origin of the teeth. Red arrows represent the direction and magnitude of the loadings of each trace element concentration.

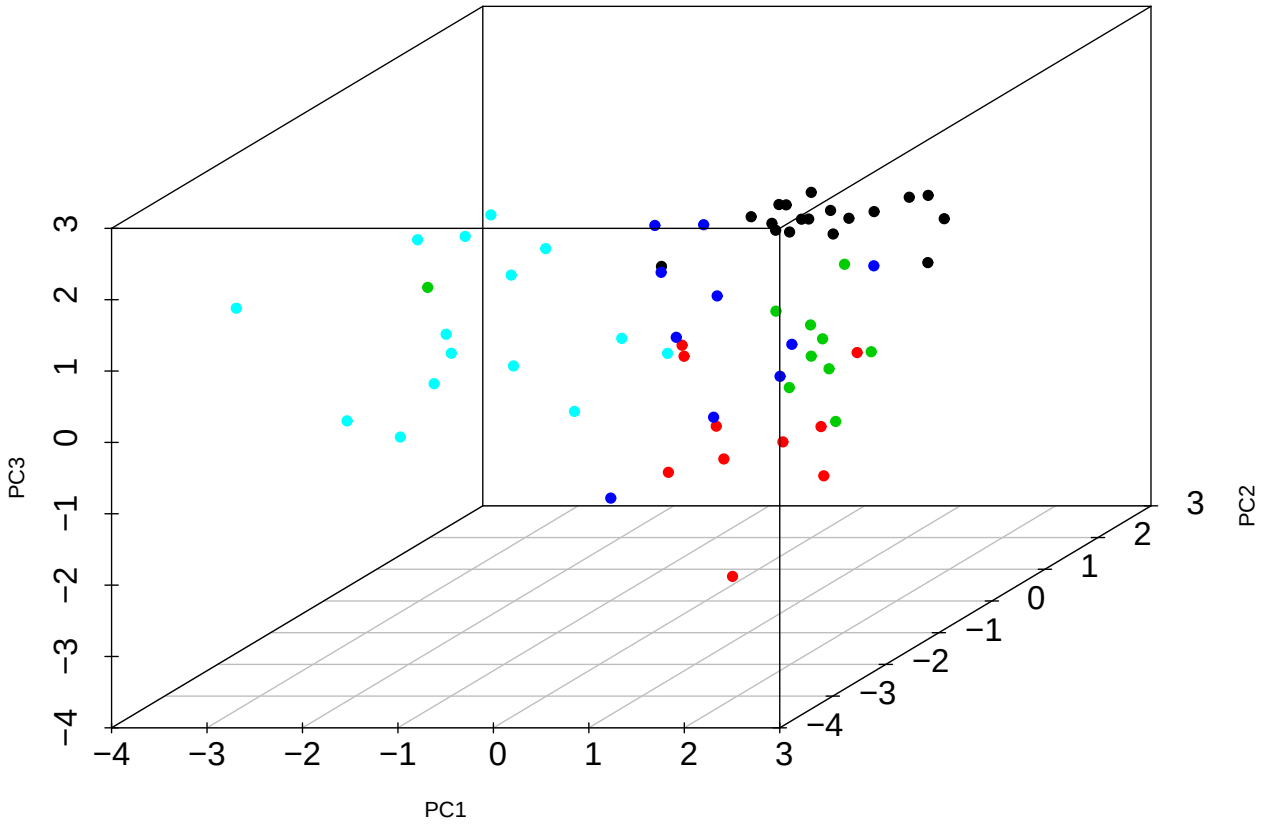


Figure 59: 3D scatter plot of the three principal components of the Middle East human tooth samples calculated using Principle Component Analysis (PCA). The points are coloured to indicate country of origin where: black = Iran, red = Iraq, green = Oman, Blue = UAE and light blue = Yemen.

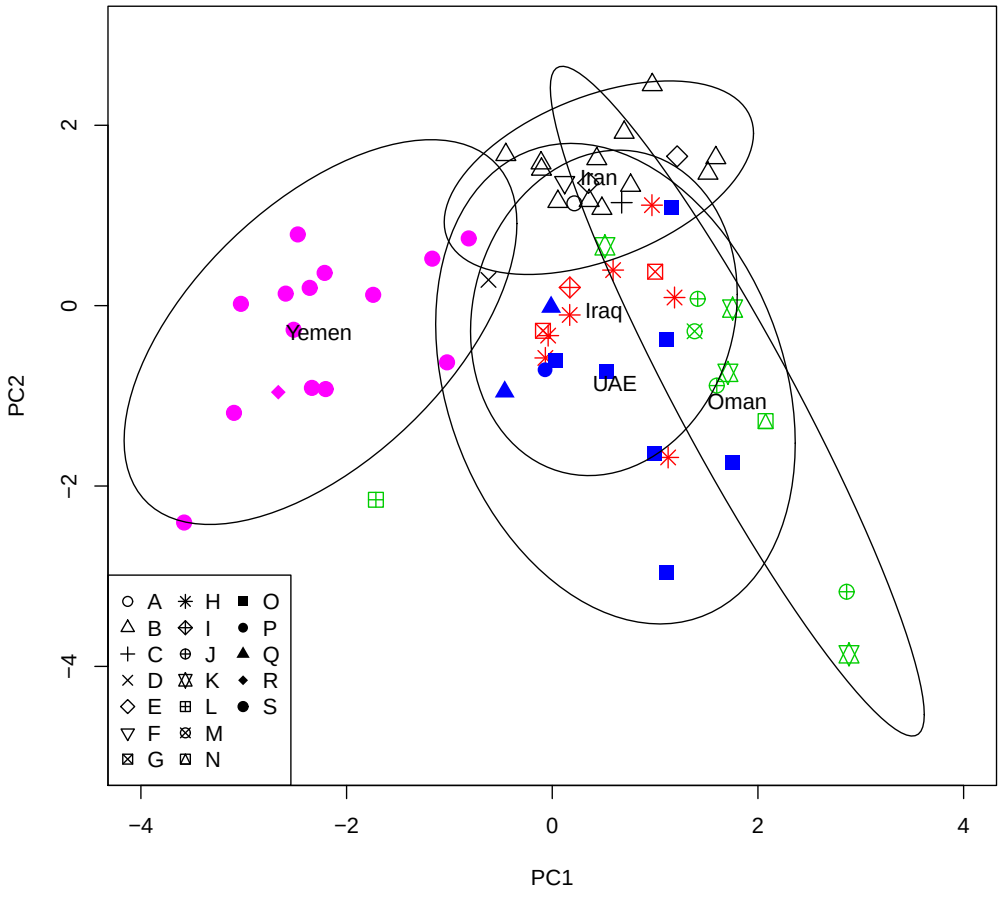


Figure 60: Ellipsoid plot of the principal components of the Middle East human tooth samples. Ellipsoids show the 95 % confidence extent for each of the locations of origin where n >1 and were calculated using the ordiellipse functionality in the VEGAN package for R. Points are coloured so that the country of origin can be clearly seen, black = Iran, red = Iraq, blue = UAE, green = Oman and grey = Yemen.

### 4.3.3 Using trace element concentrations to determine the origin of an unknown sample

Three samples from the Middle East tooth collection were chosen to be treated as questioned samples in order to test the suitability of trace element analysis for the differentiation of human samples from the Middle East. Sample X1 is known to have originated in Tehran, Iran, sample X2 from Muscat, Oman and sample X3 from Al Ghail, Yemen. The principal components calculated previously were used to transform the questioned samples and these were added to the ellipse plot for interpretation (yellow circles, Figure 61).

Sample X1 can be seen to fall within the ellipse for Iran although it is close to falling outside of the 95 % confidence limit. Refering to the bi plot 58 this region of the plot is defined by high red meat consumption and the questioned individual may have consumed more than average for the region.

Sample X2 can be seen to fall within the ellipses of Oman and UAE. It is also close to the Iraqi ellipse although it is outside of the 95 % confidence limit it can be concluded that it is unlikely to have originated from within Iraq. As has been discussed, UAE and Oman are the richest of the countries considered in this study and the diets consist of a large proportion of seafood. It can be concluded that sample X2 is likely to have originated from either UAE or Oman based on the samples measured in this study.

Sample X3 falls within the ellipse of Yemen to the left of the plot. This individual is likely to have been consuming only a small proportion of meat and a high proportion of cereals or vegetables. It can be concluded based on the samples measured in this study that the individual is likely to have originated from Yemen (95 % confidence limit).

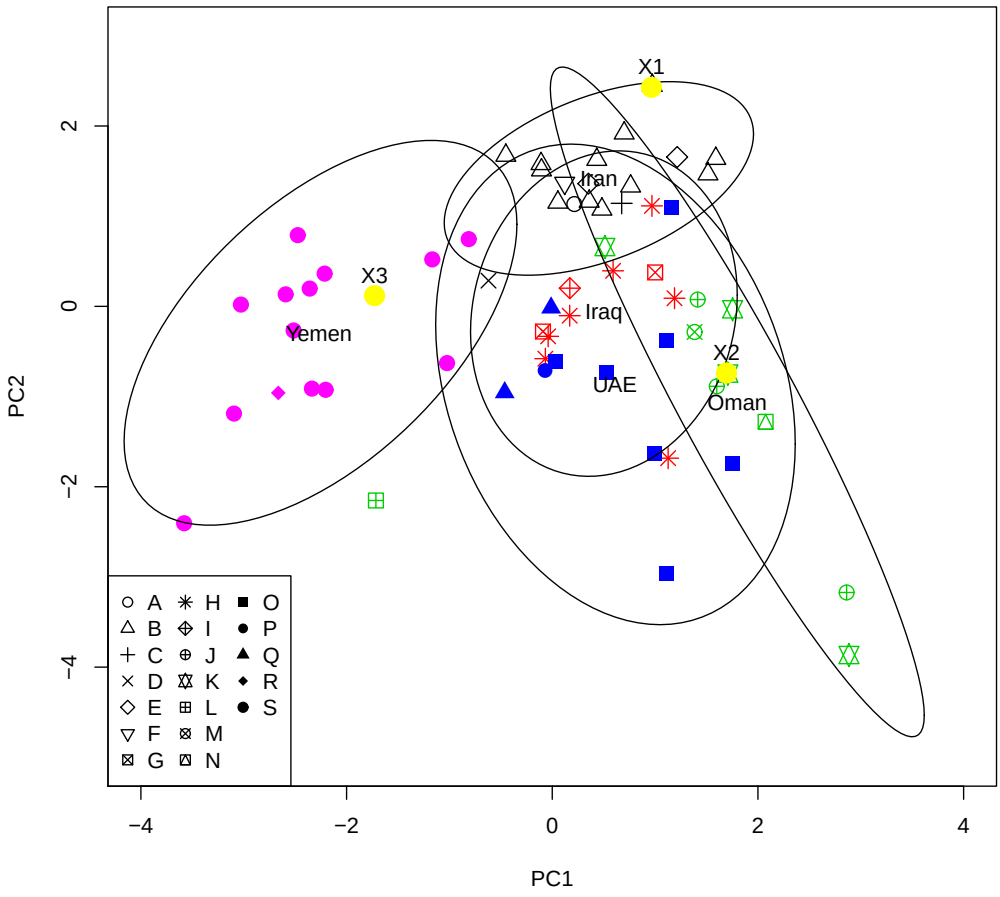


Figure 61: Ellipsoid plot of the principle components of the Middle East human tooth samples. Ellipsoids show the 95 % confidence extent for each of the locations of origin where n >1 and were calculated using the ordiellipse functionality in the VEGAN package for R. Points are coloured so that the country of origin can be clearly seen, black = Iran, red = Iraq, blue = UAE, green = Oman and pink = Yemen. Yellow = unknown samples.

## 4.4 Conclusions

LA-ICP-MS has been used to determine the trace element concentrations of 14 trace elements in the tooth enamel of 63 human teeth from the Middle East. Laser ablation has proven to be an ideal technique for this study as minimal sample is required and minimal damage is produced. This method is limited by the lack of suitable certified reference materials which meant that results are only semi-quantitative, calibrated to NIST 610 and 612 glass standards and normalised to $^{43}$Ca. In order for this technique to be used in official forensic investigations, a suitable standard shall need developing and a number of studies have worked towards that end as described in Section 4.1.4.

Analysis of variance using the location of origin of the teeth as the grouping variable determined that 8 of the measured elements, K, V, Ni, Cu, Zn, Sr, Mo and Pb showed significant difference in the concentrations between the locations. The reason for the observed differences in the populations is most likely due to dietary differences between the different locations. The 8 elements showing significant difference between the groups were subsequently used as the variables in a multi-variate PCA model. There is considerable overlap between the locations except for the samples from Al Ghail and Taiz in Yemen which were significantly different from the other samples at the 95 % confidence limit. From the PCA plots (Figures 58 and 59) it is clear that the main differences are between countries and this is likely due to cultural and economic differences in diet. Yemen for example is characterised by low meat, high grain diet which would be expected in this poorer country. The ellipse plot (Figure 60) shows the 95 % confidence limits of each of the 5 countries from the study. There is significant overlap between Iran, Iraq, Oman and UAE although there are also areas for each country that can be differentiated. Samples from Yemen were almost completely differentiated from the other countries.

It should be noted that the model is based on a limited number of samples and may not be representative of the overall population of each country. As more samples are included the overlap between the countries is expected to increase. Also this model only takes into

account the Middle East. It is highly likely that samples from other areas of the world may overlap with those in this model. Therefore there must be some indication that the questioned individual originated form within the study region to justify using this model for comparison.

The trace element PCA model was applied to three samples, treated as questioned samples. It was not possible to pinpoint the origin of the unknown samples to one location due to the overlap between locations. It could be determined that sample X1 is most likely to have originated in Iran, X2 from Oman or UAE and X3 from Yemen. This information may be useful if there is no previous intelligence as to the origin of the questioned individual, or to support a previous forensic hypothesis. However it is not possible to refine the possible location to a smaller scale than 'national' as the trace element concentrations are largely defined by national or cultural eating habits. Trace elements may however be useful for gathering information on individuals based on elevated or reduced levels of certain elements. Exposure to anthropogenic elements such as lead or cadmium for example may indicate someone who works or lives in close proximity to industry. Elevated strontium and very low zinc may be indicative of someone consuming a vegetarian diet.

Table 25: Measured trace element concentrations ($\mu$g g$^{-1}$) of the Middle East tooth enamel samples (n=63)

| **Sample ID** | **Mg** | $\pm1\sigma$ | **K** | $\pm1\sigma$ | **Ti** | $\pm1\sigma$ | **V** | $\pm1\sigma$ | **Cr** | $\pm1\sigma$ | **Mn** | $\pm1\sigma$ | **Fe** | $\pm1\sigma$ |
|---|---|---|---|---|---|---|---|---|---|---|---|---|---|---|
| TE064 | 988 | ±92 | 214 | ±9 | 9 | ±3 | 0.14 | ±0.47 | 0.62 | ±0.26 | 5 | ±4 | 3 | ±1 |
| TE065 | 748 | ±48 | 75 | ±4 | 10 | ±2 | 0.33 | ±0.21 | 0.46 | ±0.15 | 2 | ±0 | 4 | ± 1 |
| TE066 | 719 | ±76 | 182 | ±15 | 6 | ±7 | 0.26 | ±0.19 | 0.41 | ±0.19 | 1 | ±1 | 4 | ±2 |
| TE067 | 855 | ±35 | 88 | ±2 | 17 | ±5 | 0.17 | ±0.23 | 0.68 | ±0.44 | 2 | ±1 | 5 | ±2 |
| TE068 | 3896 | ±1120 | 118 | ±4 | 8 | ±2 | 0.12 | ±0.26 | 0.43 | ±0.21 | 1 | ±0 | 6 | ±1 |
| TE069 | 1033 | ±22 | 225 | ±9 | 12 | ±5 | 0.20 | ±0.09 | 0.41 | ±0.14 | 3 | ±1 | 3 | ±1 |
| TE070 | 723 | ±27 | 240 | ±87 | 9 | ±2 | 0.00 | ±0.26 | 0.39 | ±0.25 | 19 | ±11 | 5 | ±5 |
| TE071 | 709 | ±24 | 89 | ±8 | 11 | ±2 | 0.17 | ±0.30 | 0.37 | ±0.25 | 1 | ±0 | 6 | ±2 |
| TE072 | 769 | ±8 | 172 | ±4 | 5 | ±1 | 0.17 | ±0.10 | 0.64 | ±0.19 | 3 | ±0 | 3 | ±2 |
| TE073 | 763 | ±15 | 173 | ±4 | 9 | ±2 | <DL | | 0.29 | ±0.28 | 3 | ±1 | 2 | ±1 |
| TE074 | 638 | ±32 | 101 | ±3 | 11 | ±3 | 0.27 | ±0.22 | 0.34 | ±0.23 | 2 | ±1 | 0 | ±0 |
| TE075 | 969 | ±24 | 111 | ±3 | 11 | ±3 | <DL | | 0.57 | ±0.15 | 1 | ±0 | 4 | ±1 |

Continued on Next Page...

Table 25 – Continued

| Sample ID | Mg | ±1σ | K | ±1σ | Ti | ±1σ | V | ±1σ | Cr | ±1σ | Mn | ±1σ | Fe | ±1σ |
|---|---|---|---|---|---|---|---|---|---|---|---|---|---|---|
| TE076 | 1329 | ±22 | 131 | ±3 | 14 | ±2 | <DL | | 0.36 | ±0.18 | 2 | ±0 | 2 | ±1 |
| TE077 | 1007 | ±26 | 182 | ±4 | 10 | ±1 | <DL | | 0.23 | ±0.34 | 3 | ±1 | 0 | ±2 |
| TE078 | 924 | ±35 | 107 | ±6 | 12 | ±2 | <DL | | 0.38 | ±0.12 | 2 | ±0 | 3 | ±1 |
| TE079 | 1063 | ±61 | 153 | ±12 | 10 | ±2 | <DL | | 0.76 | ±0.43 | 2 | ±0 | 4 | ±1 |
| TE080 | 1086 | ±37 | 255 | ±3 | 16 | ±2 | <DL | | 0.78 | ±0.81 | 10 | ±6 | 1 | ±2 |
| TE081 | 979 | ±61 | 198 | ±7 | 11 | ±2 | <DL | 0.82 | ±0.53 | 10 | ±3 | 2 | ±1 | |
| TE082 | 1396 | ±110 | 330 | ±45 | 22 | ±5 | <DL | 0.65 | ±0.34 | 14 | ±3 | 4 | ±3 | |
| TE039 | 1160 | ±20 | 119 | ±5 | 0 | ±5 | 0.31 | ±0.34 | 0.76 | ±0.41 | 6 | ±2 | 4 | ±6 |
| TE040 | 1584 | ±110 | 139 | ±4 | 4 | ±2 | 0.48 | ±0.13 | 0.92 | ±0.64 | 5 | ±3 | 7 | ±7 |
| TE041 | 910 | ±38 | 94 | ±6 | 6 | ±2 | 0.31 | ±1.09 | 0.75 | ±0.54 | 9 | ±1 | 14 | ±3 |
| TE042 | 997 | ±11 | 200 | ±10 | 4 | ±3 | 1.17 | ±1.09 | 0.78 | ±0.49 | 7 | ±1 | 31 | ±17 |
| TE043 | 1108 | ±14 | 164 | ±5 | 4 | ±2 | 0.36 | ±0.41 | 0.34 | ±0.37 | 4 | ±1 | 5 | ±2 |
| TE044 | 1123 | ±48 | 277 | ±9 | 3 | ±7 | 0.25 | ±0.64 | 0.68 | ±0.29 | 2 | ±1 | 12 | ±3 |
| TE045 | 985 | ±12 | 159 | ±11 | 6 | ±4 | 0.26 | ±0.93 | 0.45 | ±0.55 | 6 | ±1 | 3 | ±3 |

Continued on Next Page...

Table 25 – Continued

| **Sample ID** | **Mg** | ±1$\sigma$ | **K** | ±1$\sigma$ | **Ti** | ±1$\sigma$ | **V** | ±1$\sigma$ | **Cr** | ±1$\sigma$ | **Mn** | ±1$\sigma$ | **Fe** | ±1$\sigma$ |
|---|---|---|---|---|---|---|---|---|---|---|---|---|---|---|
| TE046 | 861 | ±13 | 224 | ±7 | 4 | ±5 | 0.28 | ±0.55 | 0.96 | ±0.74 | 2 | ±1 | 2 | ±3 |
| TE047 | 1103 | ±32 | 234 | ±18 | 5 | ±8 | 0.09 | ±0.52 | 1.09 | ±0.45 | 94 | ±27 | 4 | ±6 |
| TE048 | 1089 | ±22 | 247 | ±7 | <DL | | 0.13 | ±0.23 | 0.37 | ±0.51 | 6 | ±3 | 4 | ±1 |
| TE027 | 951 | ±35 | 126 | ±28 | 11 | ±7 | <DL | | 0.86 | ±0.53 | 22 | ±5 | 7 | ±3 |
| TE028 | 941 | ±18 | 204 | ±4 | 13 | ±8 | <DL | | 1.65 | ±1.35 | 2 | ±1 | 4 | ±1 |
| TE029 | 2154 | ±26 | 459 | ±26 | 8 | ±3 | <DL | | 0.81 | ±0.46 | 1 | ±1 | 2 | ±1 |
| TE030 | 975 | ±32 | 182 | ±20 | 10 | ±5 | <DL | | 0.32 | ±0.51 | 2 | ±1 | 2 | ±3 |
| TE031 | 904 | ±30 | 157 | ±10 | 10 | ±4 | <DL | | 0.46 | ±0.64 | 2 | ±0 | 0 | ±3 |
| TE032 | 801 | ±22 | 160 | ±7 | 9 | ±3 | <DL | | 0.41 | ±0.97 | 1 | ±1 | 3 | ±1 |
| TE033 | 1069 | ±156 | 130 | ±14 | 9 | ±3 | <DL | | 0.80 | ±0.72 | 1 | ±1 | 1 | ±2 |
| TE034 | 898 | ±118 | 140 | ±14 | 8 | ±2 | <DL | | 0.94 | ±0.85 | 2 | ±1 | 6 | ±2 |
| TE035 | 993 | ±5 | 206 | ±3 | 14 | ±5 | <DL | | 1.28 | ±0.60 | 9 | ±2 | <DL | |
| TE037 | 983 | ±23 | 157 | ±25 | 15 | ±4 | <DL | | 0.19 | ±0.86 | 5 | ±2 | 5 | ±3 |
| TE038 | 888 | ±29 | 179 | ±0 | 8 | ±4 | <DL | | 0.93 | ±0.46 | 4 | ±3 | 8 | ±10 |

Continued on Next Page...

Table 25 – Continued

| **Sample ID** | **Mg** | ±1$\sigma$ | **K** | ±1$\sigma$ | **Ti** | ±1$\sigma$ | **V** | ±1$\sigma$ | **Cr** | ±1$\sigma$ | **Mn** | ±1$\sigma$ | **Fe** | ±1$\sigma$ |
|---|---|---|---|---|---|---|---|---|---|---|---|---|---|---|
| TE016 | 841 | ±19 | 194 | ±37 | 0 | ±3 | 0.59 | ±0.55 | <DL | | 3 | ±2 | 5 | ±1 |
| TE017 | 923 | ±30 | 224 | ±12 | 9 | ±4 | <DL | | 1.21 | ±0.36 | 4 | ±1 | 3 | ±4 |
| TE018 | 1108 | ±92 | 177 | ±11 | 13 | ±7 | <DL | | 0.96 | ±0.44 | 2 | ±1 | 3 | ±7 |
| TE019 | 1096 | ±45 | 252 | ±6 | 8 | ±3 | <DL | | 1.46 | ±0.54 | 10 | ±1 | 7 | ±1 |
| TE020 | 7713 | ±810 | 274 | ±34 | 17 | ±17 | <DL | | 0.24 | ±0.66 | 2 | ±2 | 5 | ±23 |
| TE021 | 894 | ±22 | 195 | ±9 | 9 | ±5 | <DL | | 0.97 | ±0.76 | 1 | ±1 | 1 | ±1 |
| TE022 | 1408 | ±53 | 323 | ±15 | 16 | ±3 | <DL | | 1.72 | ±0.45 | 1 | ±2 | 0 | ±3 |
| TE023 | 957 | ±28 | 208 | ±9 | 12 | ±16 | <DL | | 1.46 | ±0.59 | 2 | ±2 | 1 | ±1 |
| TE024 | 1036 | ±43 | 211 | ±14 | 10 | ±1 | <DL | | 2.27 | ±2.13 | 1 | ±1 | 4 | ±1 |
| TE025 | 991 | ±47 | 255 | ±18 | 9 | ±3 | <DL | | 0.73 | ±0.12 | 1 | ±2 | 2 | ±1 |
| TE049 | 1392 | ±43 | 271 | ±19 | 9 | ±3 | 0.05 | ±0.40 | 0.33 | ±0.23 | 2 | ±0 | 3 | ±1 |
| TE050 | 1302 | ±89 | 247 | ±25 | 15 | ±16 | 0.09 | ±0.40 | 0.67 | ±0.44 | 8 | ±1 | 3 | ±1 |
| TE051 | 1453 | ±29 | 240 | ±11 | 10 | ±9 | <DL | | 0.60 | ±0.51 | 3 | ±1 | 3 | ±1 |
| TE052 | 1801 | ±58 | 321 | ±12 | 7 | ±3 | 0.22 | ±0.28 | 0.57 | ±0.79 | 5 | ±1 | 3 | ±2 |

Continued on Next Page...

Table 25 – Continued

| **Sample ID** | **Mg** | ±1$\sigma$ | **K** | ±1$\sigma$ | **Ti** | ±1$\sigma$ | **V** | ±1$\sigma$ | **Cr** | ±1$\sigma$ | **Mn** | ±1$\sigma$ | **Fe** | ±1$\sigma$ |
|---|---|---|---|---|---|---|---|---|---|---|---|---|---|---|
| TE053 | 1242 | ±43 | 236 | ±3 | 6 | ±3 | <DL | | 0.36 | ±0.24 | 1 | ±1 | 3 | ±1 |
| TE054 | 1587 | ±39 | 310 | ±16 | 5 | ±2 | 0.06 | ±0.77 | 0.66 | ±0.38 | 5 | ±2 | 1 | ±2 |
| TE055 | 1978 | ±182 | 248 | ±20 | 6 | ±2 | 0.15 | ±0.50 | 0.57 | ±0.23 | 3 | ±1 | 3 | ±1 |
| TE056 | 1705 | ±65 | 178 | ±6 | 9 | ±4 | 0.05 | ±0.37 | 0.20 | ±0.44 | 3 | ±1 | 2 | ±1 |
| TE057 | 1664 | ±84 | 301 | ±26 | 20 | ±3 | 0.51 | ±0.28 | 0.93 | ±0.32 | 3 | ±2 | 4 | ±3 |
| TE058 | 2064 | ±57 | 551 | ±33 | 10 | ±2 | 0.73 | ±1.02 | 0.91 | ±0.43 | 4 | ±1 | 0 | ±1 |
| TE059 | 1666 | ±100 | 258 | ±7 | 16 | ±1 | 0.36 | ±1.12 | 0.64 | ±0.21 | 4 | ±1 | 5 | ±3 |
| TE060 | 1442 | ±21 | 278 | ±4 | 8 | ±2 | 0.10 | ±0.14 | 0.53 | ±0.26 | 3 | ±0 | 7 | ±1 |
| TE061 | 1495 | ±75 | 193 | ±16 | 12 | ±4 | <DL | | <DL | | 9 | ±3 | 2 | ±1 |
| TE062 | 1383 | ±126 | 171 | ±8 | 13 | ±2 | 0.16 | ±0.14 | 0.59 | ±0.32 | 1 | ±0 | 0 | ±1 |
| TE063 | 1397 | ±57 | 156 | ±21 | 14 | ±9 | 0.20 | ±0.23 | 0.48 | ±0.33 | 5 | ±3 | 3 | ±2 |

Table 26: Measured trace element concentrations ($\mu$g g$^{-1}$) of the Middle East tooth enamel samples (n=63)

| **Sample ID** | **Ni** | $\pm1\sigma$ | **Cu** | $\pm1\sigma$ | **Zn** | $\pm1\sigma$ | **Se** | $\pm1\sigma$ | **Sr** | $\pm1\sigma$ | **Mo** | $\pm1\sigma$ |
|---|---|---|---|---|---|---|---|---|---|---|---|---|
| TE064 | <DL | | 2.51 | ±0.87 | 1011 | ±32 | 8 | ±6 | 192 | ±4 | 0.07 | ±0.26 |
| TE065 | <DL | | 2.84 | ±0.82 | 1200 | ±74 | 18 | ±7 | 141 | ±3 | <DL | |
| TE066 | <DL | | 2.14 | ±0.74 | 1069 | ±38 | 11 | ±±15 | 150 | ±4 | <DL | |
| TE067 | <DL | | 2.16 | ±0.95 | 1274 | ±66 | 17 | ±9 | 134 | ±4 | 0.32 | ±0.95 |
| TE068 | <DL | | 1.95 | ±0.58 | 805 | ±15 | 15 | ±11 | 140 | ±3 | 0.09 | ±0.20 |
| TE069 | <DL | | 2.20 | ±0.23 | 602 | ±35 | 8 | ±10 | 187 | ±6 | <DL | |
| TE070 | <DL | | 2.46 | ±0.12 | 1181 | ±86 | 12 | ±12 | 129 | ±3 | <DL | |
| TE071 | <DL | | 2.38 | ±0.51 | 1201 | ±45 | 4 | ±17 | 236 | ±4 | <DL | |
| TE072 | <DL | | 1.63 | ±0.80 | 1057 | ±60 | 8 | ±9 | 301 | ±4 | <DL | |
| TE073 | <DL | | 2.48 | ±1.04 | 942 | ±43 | 14 | ±8 | 313 | ±6 | 0.11 | ±0.20 |
| TE074 | <DL | | 2.40 | ±0.72 | 842 | ±35 | 15 | ±8 | 126 | ±1 | <DL | |
| TE075 | <DL | | 2.39 | ±0.35 | 704 | ±23 | 8 | ±6 | 261 | ±4 | <DL | |

Continued on Next Page...

Table 26 – Continued

| **Sample ID** | **Ni** | $\pm1\sigma$ | **Cu** | $\pm1\sigma$ | **Zn** | $\pm1\sigma$ | **Se** | $\pm1\sigma$ | **Sr** | $\pm1\sigma$ | **Mo** | $\pm1\sigma$ |
|---|---|---|---|---|---|---|---|---|---|---|---|---|
| TE076 | 0 | ±1 | <DL | | 665 | ±29 | 7 | ±5 | 298 | ±5 | <DL | |
| TE077 | 0 | ±0 | <DL | | 805 | ±14 | 4 | ±4 | 182 | ±6 | <DL | |
| TE078 | 0 | ±0 | <DL | | 1262 | ±86 | 9 | ±4 | 181 | ±2 | 0.15 | ±0.12 |
| TE079 | 1 | ±1 | <DL | | 1192 | ±82 | 9 | ±8 | 203 | ±3 | <DL | |
| TE080 | 0 | ±1 | 0.35 | ±0.97 | 1150 | ±57 | 10 | ±6 | 220 | ±6 | 0.26 | ±0.34 |
| TE081 | 1 | ±1 | <DL | | 1120 | ±45 | 8 | ±2 | 256 | ±8 | 0.04 | ±0.15 |
| TE082 | 0 | ±1 | 1.54 | ±3.75 | 797 | ±54 | 8 | ±6 | 136 | ±4 | <DL | |
| TE039 | 4 | ±3 | 0.51 | ±2.10 | 848 | ±39 | 20 | ±12 | 126 | ±5 | 0.52 | ±0.23 |
| TE040 | 3 | ±3 | 0.09 | ±1.34 | 514 | ±25 | 11 | ±13 | 159 | ±3 | 0.56 | ±0.37 |
| TE041 | 2 | ±3 | 0.17 | ±0.91 | 1206 | ±63 | 17 | ±17 | 226 | ±6 | 0.77 | ±0.31 |
| TE042 | 6 | ±2 | 0.63 | ±1.03 | 713 | ±21 | 14 | ±10 | 185 | ±2 | 0.35 | ±0.67 |
| TE043 | 3 | ±1 | <DL | | 992 | ±24 | 16 | ±17 | 215 | ±1 | 0.77 | ±0.32 |
| TE044 | 4 | ±2 | <DL | | 987 | ±22 | 31 | ±21 | 165 | ±4 | 1.01 | ±0.27 |
| TE045 | 5 | ±1 | <DL | | 992 | ±22 | 9 | ±18 | 173 | ±4 | 0.51 | ±0.41 |

Continued on Next Page…

Table 26 – Continued

| **Sample ID** | **Ni** | $\pm1\sigma$ | **Cu** | $\pm1\sigma$ | **Zn** | $\pm1\sigma$ | **Se** | $\pm1\sigma$ | **Sr** | $\pm1\sigma$ | **Mo** | $\pm1\sigma$ |
|---|---|---|---|---|---|---|---|---|---|---|---|---|
| TE046 | 3 | ±3 | 1.06 | ±1.14 | 823 | ±23 | 20 | ±15 | 142 | ±3 | 0.67 | ±0.62 |
| TE047 | 4 | ±2 | <DL | | 593 | ±13 | 26 | ±15 | 238 | ±8 | 0.42 | ±0.40 |
| TE048 | 4 | ±2 | <DL | | 758 | ±35 | 34 | ±8 | 162 | ±4 | 0.35 | ±0.47 |
| TE027 | 5 | ±3 | 6.42 | ±8.30 | 735 | ±23 | 5 | ±24 | 144 | ±8 | 0.07 | ±0.57 |
| TE028 | 2 | ±2 | 2.40 | ±3.11 | 861 | ±17 | 17 | ±51 | 294 | ±5 | 0.17 | ±0.66 |
| TE029 | 2 | ±5 | 2.49 | ±1.65 | 265 | ±37 | 22 | ±24 | 179 | ±3 | 0.11 | ±0.40 |
| TE030 | 4 | ±2 | 15.76 | ±31.66 | 981 | ±22 | <DL | | 268 | ±4 | <DL | |
| TE031 | 3 | ±5 | 1.70 | ±1.55 | 949 | ±35 | <DL | | 73 | ±2 | <DL | |
| TE032 | 2 | ±4 | 5.20 | ±9.11 | 997 | ±57 | <DL | | 86 | ±2 | <DL | |
| TE033 | 3 | ±3 | 19.96 | ±13.63 | 819 | ±105 | <DL | | 95 | ±6 | <DL | |
| TE034 | 3 | ±3 | 3.11 | ±7.85 | 809 | ±94 | <DL | | 174 | ±6 | <DL | |
| TE035 | 4 | ±4 | <DL | | 577 | ±31 | 2 | ±34 | 275 | ±6 | 0.02 | ±0.66 |
| TE037 | 5 | ±4 | 11.03 | ±7.14 | 905 | ±41 | <DL | | 226 | ±5 | <DL | |
| TE038 | 6 | ±4 | 65.80 | ±136.18 | 847 | ±104 | <DL | | 93 | ±3 | 0.17 | ±0.37 |

Continued on Next Page…

Table 26 – Continued

| **Sample ID** | **Ni** | $\pm1\sigma$ | **Cu** | $\pm1\sigma$ | **Zn** | $\pm1\sigma$ | **Se** | $\pm1\sigma$ | **Sr** | $\pm1\sigma$ | **Mo** | $\pm1\sigma$ |
|---|---|---|---|---|---|---|---|---|---|---|---|---|
| TE016 | <DL | | 1.93 | ±0.78 | 1240 | ±19 | 30 | ±27 | 74 | ±2 | 0.31 | ±0.58 |
| TE017 | 3 | ±3 | 2.46 | ±1.87 | 855 | ±26 | <DL | | 130 | ±2 | <DL | |
| TE018 | 6 | ±6 | <DL | | 1034 | ±117 | <DL | | 289 | ±11 | <DL | |
| TE019 | 3 | ±2 | 4.31 | ±8.10 | 752 | ±36 | 0 | ± 25 | 191 | ±6 | 0.42 | ±1.65 |
| TE020 | 2 | ±3 | <DL | | 653 | ±213 | <DL | | 177 | ±7 | <DL | |
| TE021 | 4 | ±3 | 4.26 | ±3.42 | 802 | ±21 | <DL | | 177 | ±2 | <DL | |
| TE022 | 2 | ±3 | 3.59 | ±2.86 | 945 | ±75 | 5 | ±17 | 233 | ±4 | <DL | |
| TE023 | 3 | ±1 | 3.06 | ±4.02 | 891 | ±31 | 6 | ±24 | 260 | ±3 | <DL | |
| TE024 | 3 | ±4 | 1.29 | ±2.46 | 717 | ±23 | <DL | | 202 | ±3 | <DL | |
| TE025 | 1 | ±3 | 5.54 | ±3.21 | 848 | ±33 | 13 | ±27 | 231 | ±6 | <DL | |
| TE049 | 3 | ±3 | <DL | | 473 | ±20 | 23 | ±5 | 809 | ±3 | 1.06 | ±1.49 |
| TE050 | 1 | ±2 | 0.03 | ±1.99 | 626 | ±32 | 18 | ±21 | 804 | ±10 | 0.70 | ±0.19 |
| TE051 | 3 | ±1 | <DL | | 496 | ±42 | 19 | ±7 | 1073 | ±44 | 0.35 | ±0.42 |
| TE052 | 3 | ±2 | 0.10 | ±1.52 | 509 | ±24 | 21 | ±6 | 790 | ±13 | 0.54 | ±0.18 |

Continued on Next Page…

Table 26 – Continued

| **Sample ID** | **Ni** | $\pm1\sigma$ | **Cu** | $\pm1\sigma$ | **Zn** | $\pm1\sigma$ | **Se** | $\pm1\sigma$ | **Sr** | $\pm1\sigma$ | **Mo** | $\pm1\sigma$ |
|---|---|---|---|---|---|---|---|---|---|---|---|---|
| TE053 | 0 | ±10 | <DL | | 499 | ±18 | 4 | ±10 | 868 | ±19 | 0.31 | ±0.41 |
| TE054 | 3 | ±1 | <DL | | 360 | ±25 | 5 | ±5 | 588 | ±21 | 0.38 | ±0.16 |
| TE055 | 4 | ±2 | <DL | | 620 | ±42 | 19 | ±8 | 411 | ±26 | 0.69 | ±0.91 |
| TE056 | 1 | ±2 | 0.12 | ±0.89 | 410 | ±34 | 10 | ±33 | 322 | ±9 | 0.52 | ±0.27 |
| TE057 | <DL | | 2.98 | ±0.73 | 344 | ±55 | 1 | ±15 | 889 | ±34 | 1.07 | ±1.17 |
| TE058 | <DL | | 2.69 | ±0.65 | 201 | ±72 | 0 | ±7 | 642 | ±87 | 0.32 | ±0.23 |
| TE059 | <DL | | 2.84 | ±0.71 | 437 | ±16 | 15 | ±8 | 570 | ±8 | 0.16 | ±0.24 |
| TE060 | <DL | | 2.10 | ±0.49 | 473 | ±18 | 2 | ±13 | 933 | ±81 | <DL | |
| TE061 | <DL | | 3.19 | ±0.66 | 257 | ±23 | 15 | ±12 | 788 | ±14 | 0.11 | ±0.39 |
| TE062 | <DL | | 2.48 | ±0.95 | 310 | ±12 | 11 | ±3 | 1273 | ±35 | 0.14 | ±0.31 |
| TE063 | <DL | | 2.96 | ±0.40 | 538 | ±83 | 5 | ±13 | 600 | ±66 | <DL | |

Table 27: Measured trace element concentrations ($\mu$g g$^{-1}$) of the Middle East tooth enamel samples (n=63)

| **Sample ID** | **Cd** | $\pm1\sigma$ | **Pb** | $\pm1\sigma$ |
|---|---|---|---|---|
| TE064 | 0.87 | $\pm$0.24 | 5 | $\pm$0 |
| TE065 | 1.03 | $\pm$0.23 | 7 | $\pm$1 |
| TE066 | 0.97 | $\pm$0.12 | 5 | $\pm$1 |
| TE067 | 1.13 | $\pm$0.19 | 5 | $\pm$0 |
| TE068 | 0.92 | $\pm$0.11 | 3 | $\pm$0 |
| TE069 | 0.98 | $\pm$0.14 | 5 | $\pm$1 |
| TE070 | 0.93 | $\pm$0.10 | 3 | $\pm$1 |
| TE071 | 1.08 | $\pm$0.10 | 3 | $\pm$0 |
| TE072 | 1.04 | $\pm$0.10 | 4 | $\pm$0 |
| TE073 | 1.26 | $\pm$0.11 | 5 | $\pm$1 |
| TE074 | 0.98 | $\pm$0.12 | 8 | $\pm$1 |
| TE075 | 0.95 | $\pm$0.08 | 11 | $\pm$1 |

Continued on Next Page...

Table 27 – Continued

| **Sample ID** | **Cd** | $\pm 1\sigma$ | **Pb** | $\pm 1\sigma$ |
|---|---|---|---|---|
| TE076 | 0.09 | ±0.05 | 11 | ±1 |
| TE077 | 0.06 | ±0.08 | 10 | ±0 |
| TE078 | 0.05 | ±0.05 | 10 | ±1 |
| TE079 | 0.05 | ±0.07 | 9 | ±1 |
| TE080 | 0.11 | ±0.07 | 9 | ±1 |
| TE081 | 0.04 | ±0.06 | 13 | ±2 |
| TE082 | 0.01 | ±0.07 | 2 | ±0 |
| TE039 | 0.26 | ±1.48 | 18 | ±3 |
| TE040 | 0.81 | ±0.21 | 3 | ±3 |
| TE041 | 0.69 | ±0.09 | 9 | ±2 |
| TE042 | 1.29 | ±0.25 | 12 | ±1 |
| TE043 | 0.75 | ±0.21 | 18 | ±1 |
| TE044 | 0.77 | ±0.17 | 10 | ±2 |
| TE045 | 0.77 | ±0.23 | 21 | ±5 |

Continued on Next Page…

Table 27 – Continued

| **Sample ID** | **Cd** | $\pm 1\sigma$ | **Pb** | $\pm 1\sigma$ |
|---|---|---|---|---|
| TE046 | 0.70 | ±0.18 | 15 | ±1 |
| TE047 | 0.85 | ±0.14 | 46 | ±10 |
| TE048 | 1.06 | ±0.38 | 5 | ±2 |
| TE027 | 0.49 | ±0.24 | 11 | ±1 |
| TE028 | 0.53 | ±0.05 | 29 | ±2 |
| TE029 | 0.38 | ±0.21 | 1 | ±0 |
| TE030 | 0.54 | ±0.19 | 20 | ±2 |
| TE031 | 0.50 | ±0.33 | 18 | ±1 |
| TE032 | 0.39 | ±0.28 | 6 | ±0 |
| TE033 | 0.57 | ±0.16 | 3 | ±2 |
| TE034 | 0.43 | ±0.29 | 15 | ±4 |
| TE035 | 0.99 | ±0.98 | 3 | ±1 |
| TE037 | 0.56 | ±0.09 | 20 | ±3 |
| TE038 | 0.53 | ±0.17 | 3 | ±1 |

Continued on Next Page…

Table 27 – Continued

| **Sample ID** | **Cd** | $\pm 1\sigma$ | **Pb** | $\pm 1\sigma$ |
|---|---|---|---|---|
| TE016 | 0.14 | ±0.67 | 11 | ±1 |
| TE017 | 1.67 | ±0.30 | 18 | ±1 |
| TE018 | 0.73 | ±1.58 | 3 | ±3 |
| TE019 | 1.01 | ±1.12 | 8 | ±1 |
| TE020 | 0.33 | ±1.37 | 4 | ±1 |
| TE021 | 0.38 | ±0.75 | 7 | ±0 |
| TE022 | 0.63 | ±0.41 | 1 | ±0 |
| TE023 | 0.47 | ±0.19 | 5 | ±1 |
| TE024 | <DL | | 4 | ±1 |
| TE025 | 0.40 | ± 0.19 | 4 | ±2 |
| TE049 | 0.68 | ±0.31 | 3 | ±0 |
| TE050 | 0.87 | ±0.20 | 14 | ±3 |
| TE051 | 0.73 | ±0.12 | 9 | ±5 |
| TE052 | 0.67 | ±0.07 | 8 | ±1 |

Continued on Next Page...

Table 27 – Continued

| **Sample ID** | **Cd** | $\pm 1\sigma$ | **Pb** | $\pm 1\sigma$ |
|---|---|---|---|---|
| TE053 | <DL | | 13 | ±2 |
| TE054 | 0.43 | ±0.16 | 1 | ±0 |
| TE055 | 1.05 | ±0.45 | 7 | ±1 |
| TE056 | 0.60 | ±0.27 | 13 | ±2 |
| TE057 | 1.45 | ±0.39 | 9 | ±2 |
| TE058 | 1.11 | ±0.23 | 2 | ±1 |
| TE059 | 1.11 | ±0.22 | 9 | ±0 |
| TE060 | 1.03 | ±0.14 | 6 | ±0 |
| TE061 | 1.24 | ±0.18 | 2 | ±0 |
| TE062 | 0.75 | ±0.25 | 2 | ±0 |
| TE063 | 1.07 | ±0.17 | 24 | ±3 |

# Chapter 5

# ‘Probability scapes’: A model for the prediction of origin of human remains in the Middle East

## 5.1 Introduction

One of the aims of this study to determine the spatial $\delta^{18}$O and $^{87}$Sr/$^{86}$Sr isotopic variation of human tooth enamel and to provide a new spatial prediction tool for application in forensic human identification investigations. In Chapters 2 and 3, empirical isotopic data collected from samples of known origin were combined with environmental and geological variables to produce oxygen and strontium isoscapes of the Middle East study region. Isoscapes have proven a useful tool for the understanding of spatial isotopic variation in a number of biological, environmental and geological systems [14]. The use of isoscapes as a forensic tool is still in its infancy and as such there are a number of limitations to be overcome. One limitation of this method is the nature of the output produced. As seen in Chapters 2 and 3, an isoscape can be used to highlight the bands of isotopic space that relate to the measured value from a questioned sample ($\pm$95 % C.I.). This can be useful

for intelligence gathering in a forensic invesitigation, particularly if there is no prior information available as to the victims origin. However the highlighted band may often cover a large geographical region with no indication of which areas might be the most likely origin. The isoscape may also be interpreted to mean there is no possibility of an individual originating outside of the highlighted band. There may only be a small probability of the individual originating outside of the isotopic band but ignoring this possibility may result in an individual remaining unidentified. It would be more useful to determine the likelihood of a person coming from a location based on their isotopic composition, firstly to offer more information than a band of isotopic space and secondly, by presenting the data as a likelihood or probability of origin, it is more likely to be understood in a court of law, which is vital when presenting expert witness data.

In this chapter, a probabilistic approach that has been introduced recently for the tracking of bird migration will be adapted as a possible method for presenting forensic isotopic data ([19, 224, 225]). The chapter also presents the first example of a multi isotope probability scape for identification of human provenance and proposes a method for the use of human population density information to further resolve the prediction of origin of unidentified human remains.

### 5.1.1 Expert witness reporting: Why would a probabilistic approach to isotope analysis help in the court room

'There are important differences between the the quest for truth in the courtroom and the quest for truth in the laboratory', [226]. It is the responsibility of forensic scientists to ensure that the methods used in forensic investigations are performed with the greatest care and yield reproducible results with high precision and accuracy. Failure to do so could potentially lead to false conviction of innocent individuals, or the release of a guilty party if substandard evidence is deemed inadmissible in court. The UK currently has no legal documentation controlling the admissibility of expert scientific evidence in court. The UK

Law Commission published a consultation paper in 2009 and a draft Criminal Evidence (Experts) Bill was submitted in March 2011 advising that reliability based admissibility tests should be applied to expert witness evidence. The bill is currently awaiting a response from the government. The proposed measures are based upon the American criminal justice system and the Daubert standard (Daubert v. Merrell Dow Pharmaceuticals [226]). This set of legal guidelines ensures that expert witness evidence submitted to court is reliable, relevant to the case and based on a scientific method that is widely accepted by the scientific community [227].

Stable isotope analysis is not yet used frequently as expert evidence in the courtroom. However, as analytical techniques improve, and as understanding of global and local isotopic variation of materials of interest increases, allowing for more accurate and precise models to be produced, it is expected to become more common [227]. As described by Ehleringer and Matheson in the Utah Law Review 2010 ([227]) it is essential that when stable isotope analysis becomes more commonplace in the court of law, a framework is in place to ensure that data is reproducible, reliable and therefore admissible in court. Isotope analysis is a relatively mature technique and operating protocols for more common samples such as water are now fairly routine. A number of research groups work towards a better understanding of spatial isotopic variation of forensically interesting samples and to ensure that suitable reference materials are available. Therefore isotope analysis should be easily transferable to the courtroom as long as suitable guidelines are in place. One major difficulty that is foreseen by the author is that stable isotope fractionation is a complex process and presentation of isotopic data to a jury of laymen will not be trivial. Rule 403 of the US rules of evidence states: ‘Although relevant, evidence may be excluded if its probative value is substantially outweighed by the danger of unfair prejudice, confusion of the issues or misleading the jury, or by considerations of undue delay, waste of time, or needless presentation of cumulative evidence’. Explaining specialist scientific areas to a non-scientific audience is always challenging; an audience can be quickly lost if too much specialist terminology is used. Rule 403 is vitally important to the justice system as if a

jury are presented with evidence from an 'expert' or 'specialist' there is a danger that if the science presented is too complex, the jury are likely to defer to the experts opinion and do not have the experience to assess the reliability of the evidence. This again may lead to false conviction. In a study of the common factors associated with 86 cases of wrongful conviction it was shown that forensic science testing error occurred in 63 % of the cases and false or misleading testimony by forensic scientists was a factor in 27 % [228].

DNA typing is one of the most commonly used methods for human identification and is often referred to as the 'gold standard' of forensic science. The great strength of DNA typing is that results are presented to the jury as a probability of two samples being from the same source based on a database. By presenting the data in this way the jury are able to get a clear indicication of the scientific conclusions without being blinded by a stream of scientific jargon. The techniques presented in this chapter may prove invaluable for the presentation of isotopic data in a court of law.

### 5.1.2 Literature review: Applications of isoscape based probability surfaces

The idea to use Bayes probability inversion for the presentation of forensic isotopic data was inspired by a number of recent bird migration studies ([224, 19, 20, 225]). Monitoring bird migration patterns can be challenging as extrinsic markers such as ringing and radio collars tend to be inefficient due to low recapture rates. By measuring the stable isotope ($\delta^2$H, $\delta^{13}$C) composition of avian feather keratin, spatial information about the origin of a bird can be inferred. The limitation of using isotopic data to infer migration patterns is that unlike ringing, isotopic models do not produce an exact observation. Due to natural isotopic variation the isotopic signature of avian breeding grounds may overlap, making it difficult to differentiate between populations from these sites. Royle and Rubenstein [225] suggested calculating the conditional probability of a bird feather with isotopic composition y originating from a population b ($f(y|b)$) based on the population distribution of a

breeding site. The aim was to infer the breeding ranges of black-throated blue warblers from the northern United States. The study region was split into three breeding ranges (NW, NE and S). The average isotopic composition ($\delta^2$H, $\delta^{13}$C) and the isotopic variance for each of the breeding ranges was calculated from empirical data measured from bird feathers (n=266) collected from breeding sites within the three ranges. A normal population distribution was assumed for the three breeding ranges. The probability density (referred to as likelihood in the paper) for a bird feather with a $\delta^2$H isotopic composition y* originating from breeding range b can be calculated using the normal distribution function (Equation 41):

$$f(y*|\mu_b, \sigma_b^2) = \frac{1}{\sqrt{2\pi\sigma_b^2}} \exp - \left( \frac{(y* - \mu_b)^2}{2\sigma_b^2} \right) \tag{41}$$

where $\mu_b$ is the population average isotopic composition for breeding range b and $\sigma_b^2$ is the isotopic variance for breeding range b. Using this method breeding regions were correctly assigned to 50.8 % of the birds using $\delta^{13}$C and 53.5% using $\delta^{18}$O. By using both sets of data simultaneously 58.7% of the birds were correctly assigned which shows slight inprovement over the single isotopic predictions. It may be useful to combine isotope systems in this study for improved assignment of origin. Royle and Rubenstein combine the two isotope systems by calculating the covariance between them This assumes that there is some correlation between $\delta^2$D and $\delta^{13}$C which is not necessarily true. For the purpose of this thesis $\delta^{18}$O and $^{87}$Sr/$^{86}$Sr isotope composition of tooth enamel will be considered to be independent events and the combined probability calculated accordingly. Royle and Rubenstein also consider the effect of relative abundance on likelihood predictions. Consider two populations, A and B. If A contains 90 individuals and B contains 10 individuals and an individual is selected at random, it is reasonable to suggest that there is a 90% chance that the sample will originate from population A. By using Baye's rules for conditional probability Royle and Rubenstein are able to take into account the effect of the *a priori* relative abundance inforamtion on the isotope based likelihood predictions. Relative abundance could be applied to human studies such as this thesis, as population

density information is readily available. However until now, population density information has not been considered in support of human isotopic studies.

Wunder and Norris [224] present a study on the population assignment of American Redstarts using stable isotope analysis of bird feather keratin. The aim of the study was to consider the effect of analytical and spatial interpolation error on assignment probability for the birds breeding ground. It was shown that by modeling the analytical error associated with each individual sample had a significant affect on the assignment of origin. This is to be expected due to the overlapping isotopic composition of the defined breeding regions. In this paper the breeding regions were defined by splitting the breeding range into 5 geographical regions and the mean and standard deviation of $\delta^2$H for each of the 5 breeding regions were calculated from the precipitation isoscape defined by Bowen and Revanaugh [59]. This method is limited as the average and standard deviation of the $\delta^2$H composition calculated from the isoscape grid may not be representative of the drinking water consumed by the bird population. This method assumes that each of the grid squares provides an equal contribution to the average isotopic composition of the region when in actuality this may not be the case. However, where there is limited empirical data available for defining the regional isotopic composition, a basic modeling approach may be the only option available.

## 5.2 Method: Development of a $\delta^{18}$O and $^{87}$Sr/$^{86}$Sr based probability-scape

The $\delta^{18}$O and $^{87}$Sr/$^{86}$Sr isoscapes developed in Chapter 2 and 3 can be considered to be an estimate of the mean isotopic composition of tooth enamel carbonate at each grid location $j$ in the study region. If the isotopic composition of an unknown sample is measured ($\delta^{18}O_{vsmow}$ =$x_{ij}$ or $^{87}$Sr/$^{86}$Sr = $z_{ij}$), the isoscapes can be used to show the isotopic bands from which it may have originated. However the isoscapes provides no indication of the likelihood that the unknown sample originated at a give location. Nor do they take into account possible population heterogeneity at each location $j$ which could result in false negative result. Here, the $\delta^{18}$O and $^{87}$Sr/$^{86}$Sr isoscape models generated in Chapters 2 and 3 are used as the basis for two probability-scapes, based on the Bayesian approach described by Royle and Rubenstein [225] and more recently modified by Wunder [19]. Using the new probability scape models it is possible to determine the likelihood of tooth $i$ originating from a given location $j$.

### 5.2.1 Structure of the probability model

The tooth enamel $\delta^{18}$O and $^{87}$Sr/$^{86}$Sr probability models consist of two components. The first component being the oxygen and strontium isoscapes described in Chapters 2 and 3. The $\delta^{18}$O isoscape is defined by Equation 34 (see Chapter 2). The strontium isoscape is defined by empirical data based on underlying geological units (see Chapter 3). The isoscapes can be considered to be an estimate of the mean isotopic composition (($\delta^{18}O_{vsmow}$ =$\bar{x}_{ij}$ or $^{87}$Sr/$^{86}$Sr = $\bar{z}_{ij}$) at each grid location $j$.

The second component (referred to as the stochastic component by Wunder [19]), ($\sigma^2$) represents the variance around the mean isotopic composition observed for each grid location $j$ and can be considered to be an indication of the limitations of the model. For example it can take into consideration the error in the isoscape model based on analyt-

ical precision, interpolation error, sample heterogeneity and also represents the range in isotopic composition of the population at location $j$. In an ideal situation the stochastic component would be small and the deterministic isoscape would describe almost all of the variation in isotopic space for the study region [19]. As discussed in Section 2.7 this is not the case due to limitations of sample size and lack of information about some variables (such as dietary input of oxygen). The mean isotopic composition and stochastic component can be combined to define a probability density structure based on a sample of interest. The probability density function for a normal distribution is defined by Equation 42:

$$f(y|\mu,\sigma^2) = \frac{1}{\sqrt{2\pi\sigma^2}} \exp - \left( \frac{(y-\mu)^2}{2\sigma^2} \right) \tag{42}$$

where y is the measured isotopic composition of a measured sample, $\mu$ is the average isotopic composition of the population and $\sigma^2$ is the expected variance in the population.

For the $\delta^{18}$O isoscape, $\hat{\epsilon}$ (Equation 34) represents the residual 'error' in the carbonate model at a given location. This residual error is due to the limits of the current understanding of the oxygen isotope variation in human tooth enamel in the study region. The residuals from the TEC model show an approximately normal distribution around the mean (0 ‰). The variance of the residuals ($\sigma^2$) is 0.99 ‰. In order to further understand the local variance structure, information about diet and sources of water is required that are not available for this study. Until this information becomes available, the model residual variance (0.99 ‰) shall be considered to represent the isotopic variance for each grid location $j$ in the isoscape, and a normal distribution will be assumed as given by Equation 43:

$$P(J=j|y_i,\sigma^2) = \frac{1}{\sqrt{2\pi\sigma^2}} \exp - \left( \frac{(y_i-\bar{y}_j)^2}{2\sigma^2} \right) \tag{43}$$

where $y_i$ is the measured $\delta^{18}O$ isotopic composition of sample $i$, $\bar{y}_j$ is the mean $\delta^{18}O$ isotopic composition at location $j$ given by Equation 34 (see Section 2.7.2) and $\sigma^2$ is the

expected population variance predicted based on the model residuals (0.99 ‰).

The stochastic component in the $^{87}$Sr/$^{86}$Sr probability scape is defined by the calculated variance ($\sigma^2$) of the measured tooth and soil samples for each of the geological units as shown in Table 16 and Figure 62 (see Chapter 3). The probability density distribution for strontium is given by Equation 44:

$$P(J = j|z, \sigma^{2'}) = \frac{1}{\sqrt{2\pi\sigma^{2'}}} \exp - \left( \frac{(z - \bar{z}])^2}{2\sigma^{2'}} \right) \tag{44}$$

where $z_i$ is the measured $^{87}$Sr/$^{86}$Sr isotopic composition of sample $i$, $\bar{z}_j$ is the mean $^{87}$Sr/$^{86}$Sr isotopic composition at location $j$ and $\sigma^2$ is the population variance at each location.

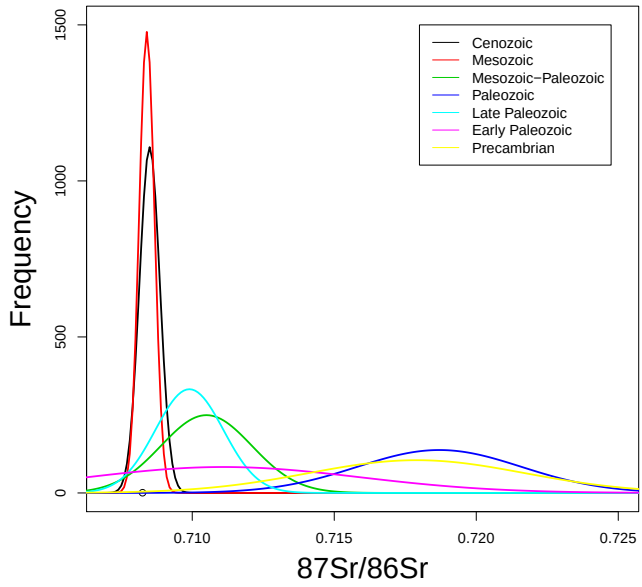


Figure 62: A histogram illustrating the $^{87}$Sr/$^{86}$Sr isotopic composition of the different geological units in the Middle East study region.

By substituting the measured isotopic composition of an unknown tooth into the $\delta^{18}$O or $^{87}$Sr/$^{86}$Sr probability model, a probability density layer is returned that can be visualised as a probability density map or 'probability scape'. It is useful to normalise the probability density ($P_{norm} = P_j/P_{max}$) to return a scale from 0 - 1, with 1 being the areas from

which it is most likely the tooth will have originated. This makes easier to visualise the most likely regions of origin. However, for the presentation of results in a court room environment it might be more useful to report the probability of a sample occurring at a given location. The probability that a tooth with an isotopic composition $y$ originated at a given grid location $j$ can be calculated by integration of the probability density function $f(y|\mu, \sigma)$ between limits $y + \sigma^*$ and $y - \sigma^*$ (where $\sigma^*$ is the intra-sample standard deviation calculated from replicate measurements) to give:

$$P(A) = \int_{y-\sigma^*}^{y+\sigma^*} f(y|\mu, \sigma) \tag{45}$$

This can be achieved relatively easily using the pnorm functionality in the R base package.

#### 5.2.1.1 Combined isotope model

Royle and Reubenstein [225] demonstrated that by combining two or more isotope systems, it is possible to improve the likelihood of a correct geographical assignment. They included a parameter for the covariance between $\delta^2$H and $\delta^{13}$C to combine the likelihood. However this method suggests that there is some correlation between isotope systems which is not the case. For the purpose of this study, $\delta^{18}$O and $^{87}$Sr/$^{86}$Sr are considered to be independent events. That is the $\delta^{18}$O isotopic composition is not influenced in any way by the $^{87}$Sr/$^{86}$Sr isotopic composition and vice versa. This is a valid assumption as the two isotope systems are influenced by different factors during the formation of tooth enamel. Plotting $\delta^{18}$O against $^{87}$Sr/$^{86}$Sr clearly shows that there is no correlation between these variables. The probability of a sample at a given grid location $j$ having a given $\delta^{18}$O composition $x$ shall be called P(X) and the probability of a sample at a given grid location $j$ having a given $^{87}$Sr/$^{86}$Sr composition $z$ shall be called P(Z). The intersection of the independent events X and Z (X∩Z), that is the event where both X and Z occur, can be given by the multiplication rule for independent events given in Equation 46:

$$P(X \cap Z) = P(X)P(Z) \tag{46}$$

Again, the results can be normalised to produce a map with a scale from 0 - 1, with 1 being the areas from which it is most likely that the tooth originated.

#### 5.2.1.2 Including human population density information to further aid identification

As was shown by Royle and Reubenstein [225], consideration of the relative abundance of a population can further help to determine the potential origin of an unknown sample (see Section 5.1.2). In case study 2 (Section 5.3.1.3), the population density of the study region shall be considered as supporting *a priori* information for the measured isotopic data to further improve the likelihood of identifying the unidentified individual.

A population density grid for the Middle East was prepared from the Global Population of the World data set (CIESIN) [229] using ArcGIS desktop (ESRI, CA), shown in Figure 63. From the population density map it is clear that the majority of the human population of the study region is concentrated into three main areas; the east coast of Oman and UAE, the west coast of Yemen and Saudi Arabia and finally Iran and Iraq with most of the larger cities situated near to the border between the two. A large portion of the Arabian peninsula has a population density of $<$10 individuals per km$^2$ due to the arid environment. The Rub' al Khali (Empty quarter) desert in the south of the peninsula is largely unpopulated.

The multi-isotope probability model Equation 46 can be considered the probability of an individual from the population at location $j$ exhibiting both the $\delta^{18}$O composition $x$ and the $^{87}$Sr/$^{86}$Sr composition $z$. If this information is combined with the *a priori* knowledge about the population density distribution of the sample region the number of people who would be expected to exhibit both $x$ and $z$ per square kilometer can be inferred by the equation:

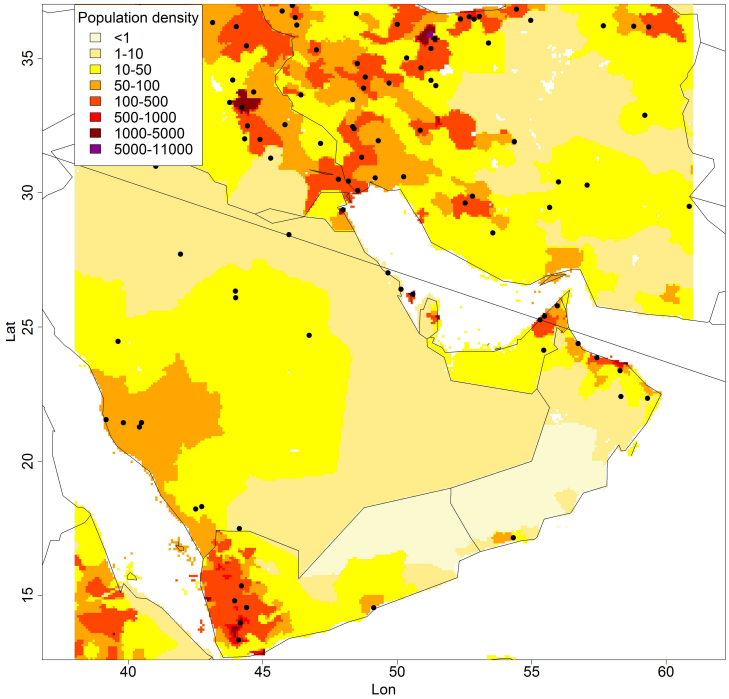


Figure 63: A map of the human population density of the Middle East. The values are in individuals per km$^2$. The population density grid used is from the Global Population of the World dataset (CISEN 2005) [229] using ArcGIS desktop (ESRI, CA). Black circles represent the major cities whose populations are $>$100,000 (UN 2002).

$$n_{xz} = n_j * P(X \cap Z) \tag{47}$$

where $n_j$ is the population density at location $j$. By using the population density information areas areas expected to contain $<1$ person per square kilometer with the expected isotope signature can be excluded. It must be noted that the probability of a person coming from a region is not increased where the population density is higher. However it is logical for investigating officers to begin preliminary investigation in areas with higher population density.

## 5.3 Results

The performance of the $\delta^{18}O$, $^{87}Sr/^{86}Sr$ and combined probability scapes was assessed by considering the results for 53 measured tooth enamel samples from the Middle East tooth collection for which both isotopic systems had been measured. The teeth originated from 19 cities within the study region (Figure 5). In order to test the efficiency of the model it is assumed that the teeth can only have originated from one of the 19 known locations. The measured $\delta^{18}O$ and $^{87}Sr/^{86}Sr$ values for each tooth were inserted into the respective models. The (normalised) probability that the tooth originated from each of the 19 cities was extracted from the probability scape using the overlay function in R [223] and ranked according to the likelihood of the sample occurring at a given location. There is a 5.3 % chance that the correct origin could be selected at random without considering any other information (1/19).

Using the $\delta^{18}O$ probability scape, only 1 sample (2 %) could be solely assigned to the correct city of origin based on probability. 9 other samples could be assigned to the correct city of origin or 5 other cities that also shared the highest likelihood of origin to give a total of 10 of the 53 samples (19 %) assigned. If more samples were available so that the population structures of the individual cities could be calculated rather than assuming a homogeneous variance across the study region, this could be further improved.

Using the $^{87}Sr/^{86}Sr$ probability scape , 4 samples (8 %) could be solely assigned the correct city of origin. 2 samples could be assigned to the correct city of origin or 2 other cities that shared the highest likelihood of origin to give a total of 6 of the 53 samples (11 %) assigned. 13 samples also resulted in cities of origin with the highest likelihood of origin, but these could not be differentiated from 13 other locations and so were not included as successful assignments.

Combining the probabilities using the rules for independent events (Section 5.2.1.1) resulted in significant improvement to the assignments. 6 samples (11 %) could be solely assigned to the correct city of origin, 1 sample could be assigned to their city of origin

or one other location with similar likelihood, 5 samples could be assigned to their city of origin or 2 other possible locations and 1 sample could be assigned to their correct city of origin or 4 other possible locations. This gives a total of 13 samples (25 %) correctly assigned to their city of origin. Two samples resulted in very low likelihood of originating from their known origin. There is a possiblity that these samples are outliers in the population, or an incorrect origin was supplied.

Consider the performance of this model in the gathering of forensic intelligence. In a hypothetical case where the unknown individual originated from one of a possible 19 locations, with no further information, a forensics team may have to make inquiries to all 19 cities about possible missing people before a location of origin can be determined. However if the strontium and oxygen isotope ratios of the individual are measured then the number of possible locations of origin can be drastically reduced. Of the 53 samples tested with the combined probability model, 96 % could be assigned to the correct city of origin upon enquiring to the 8 cities with the highest returned probability (Figure 64). Origin could be assigned to 11 % of the sample population by investigating only 1 city. By using this technique the number of possible origins can be reduced by 68 % or more which could greatly improve the possibility of identifying an unknown individual.

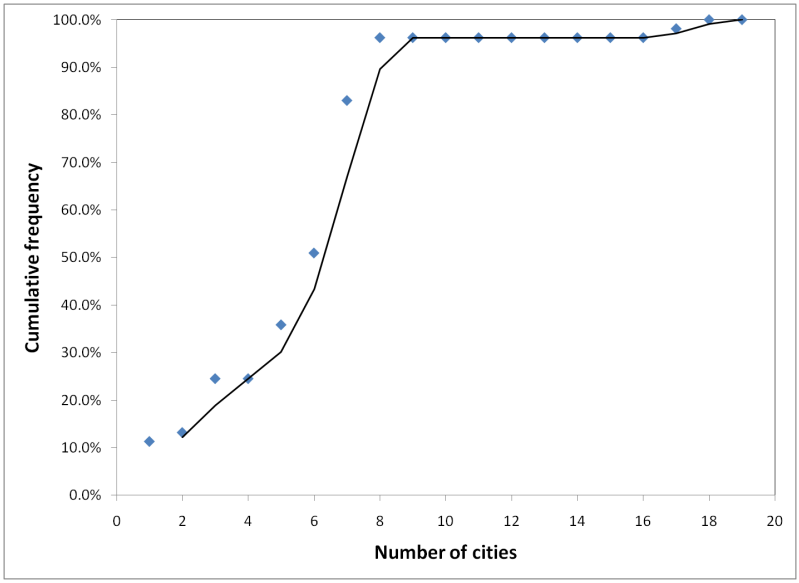


Figure 64: Cumulative frequency curve illustrating the number of cities that need to be investigated to ensure that the origin of the unknown sample is determined.

### 5.3.1 Example case studies

In this section the probability models are applied to some real samples to illustrate their potential to provide forensic intelligence that may aid in the identification of human remains. Interpretation of the model will depend on the question being asked by the forensic investigation but it is assumed that there is some suggestion that the remains in question have originated from within the study region. The first example was taken from an actual forensic case involving the remains of an unidentified female found in the United Arab Emirates. The woman was expected to be Indian by origin and in this case, the model is used to determine whether it is likely that the woman could have originated from Abu Dhabi. The second and third case studies are based on samples selected from the Middle East tooth collection as hypothetical examples to illustrate how the models might be used in a forensic case to constrain the possible regions of origin. The study region covers approximately 6.4 million square kilometers. In the case of unknown samples it is possible that the individual could have originated from anywhere within that area. It is the aim of these models to reduce the area that a forensic investigation needs to cover in order to improve the likelihood of identifying remains.

#### 5.3.1.1 Case study 1

The first example (X3) is taken from an official forensic case from the Abu Dhabi Police Forensic Services. Measurements were performed at the University of Dundee and the University of East Anglia. The new Middle East prediction model was not completed in time to use in this case, but here it is demonstrated how the model would have been useful were it available. The remains of a human female, expected to be of Indian origin were found in Abu Dhabi, UAE. The aim of the investigation was to determine whether or not the individual could have originated from Abu Dhabi. The $\delta^{18}O_{vpdb}$ composition of the tooth enamel carbonate from the remains was 28.7 $\pm$ 0.6 ‰. The $^{87}Sr/^{86}Sr$ composition was 0.71137 $\pm$ 0.00002.

The $\delta^{18}$O probability density grid for sample X3 was calculated from Equation 43 and is shown in Figure 65a. The maximum probability density for the sample area was 0.15. The probability density model was integrated between limits $28.73 \pm 0.55$ ($1\sigma$) to produce a layer of probability as shown in Figure 65b. Almost 90 % of the study region has a probability of $< 5$ %. The maximum probability of origin was 17 % for the south coast of the Arbian peninsula. From the model it can be concluded that there is less than a 5 % chance that the sample originated in the United Arab Emirates. The probability that the sample originated in Abu Dhabi is 1.1%. If the sample originated from within the study region it would most likely have originated on the Southern Arabian coast.

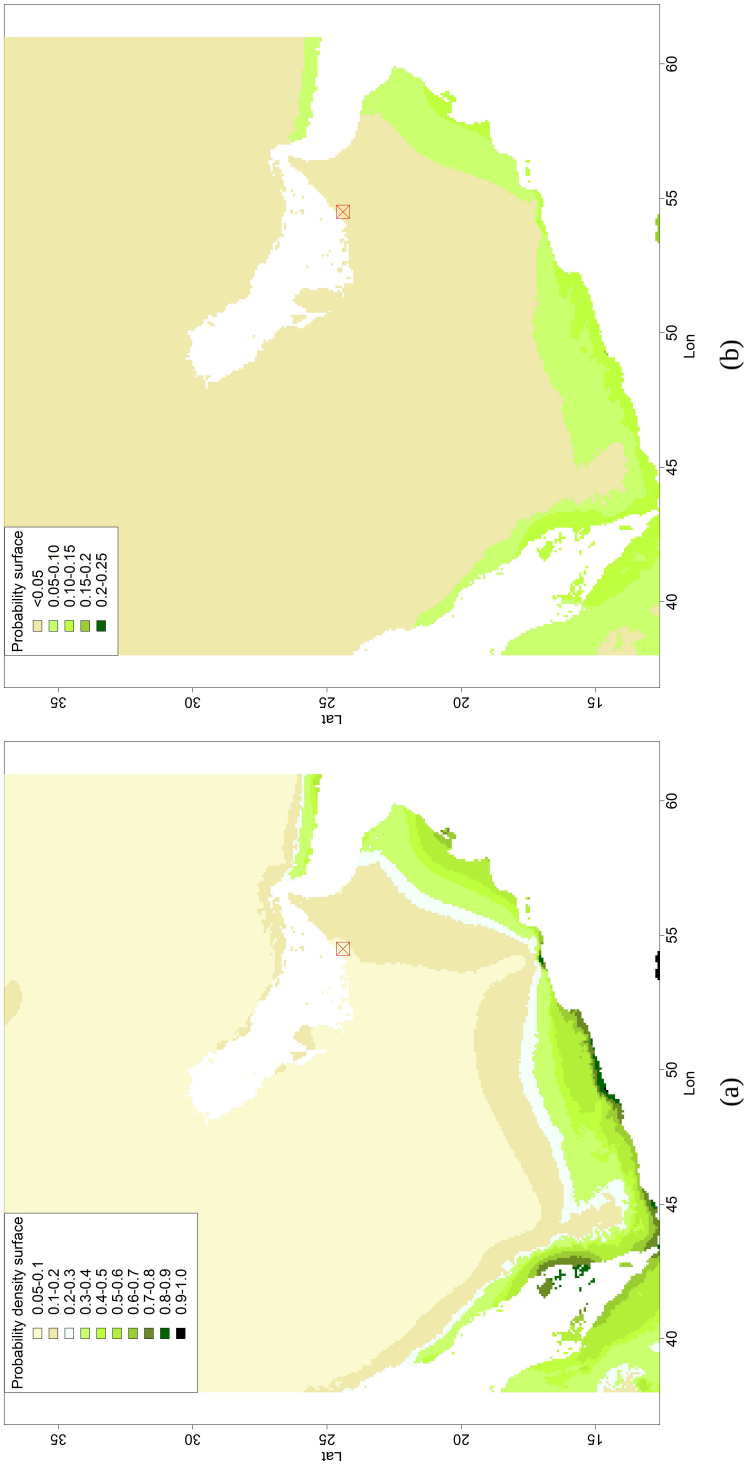


Figure 65: a) Normalised probability density scape and b) Probability scape based on the $\delta^{18}O$ composition of a tooth enamel carbonate sample (X3) from the remains of an unknown individual discovered in Abu Dhabi, UAE. Abu Dhabi is highlighted on the maps (red square)

An $^{87}Sr/^{86}Sr$ probability density layer was prepared (Figure 66a). The maximum returned probability density was 51.8 but if the scale is normalised as in Figure 66a it is clear that there is little differentiation between geological units in the study region. The probability of this strontium isotope composition was calculated by integrating between limits as with the previous examples. The resulting probability layer is shown in Figure 66b. It is unlikely that the woman originated from the Middle East as less than 5 % of the population for the majority of the study region would be expected to have a similar isotopic composition. The probability that the woman originated in Abu Dhabi which overlies Cenozoic bedrock is much less than 1 % (6E(-14) %). If the woman had originated from within the study region it is most likely (8.5 %) that she originated from an area on or near to Paleozoic-Mesozoic bedrock or Late Paleozoic bedrock (6.3 %). The remainder of the geological units in the study region are unlikely to have resulted in the isotopic composition observed ($< 5$ %).

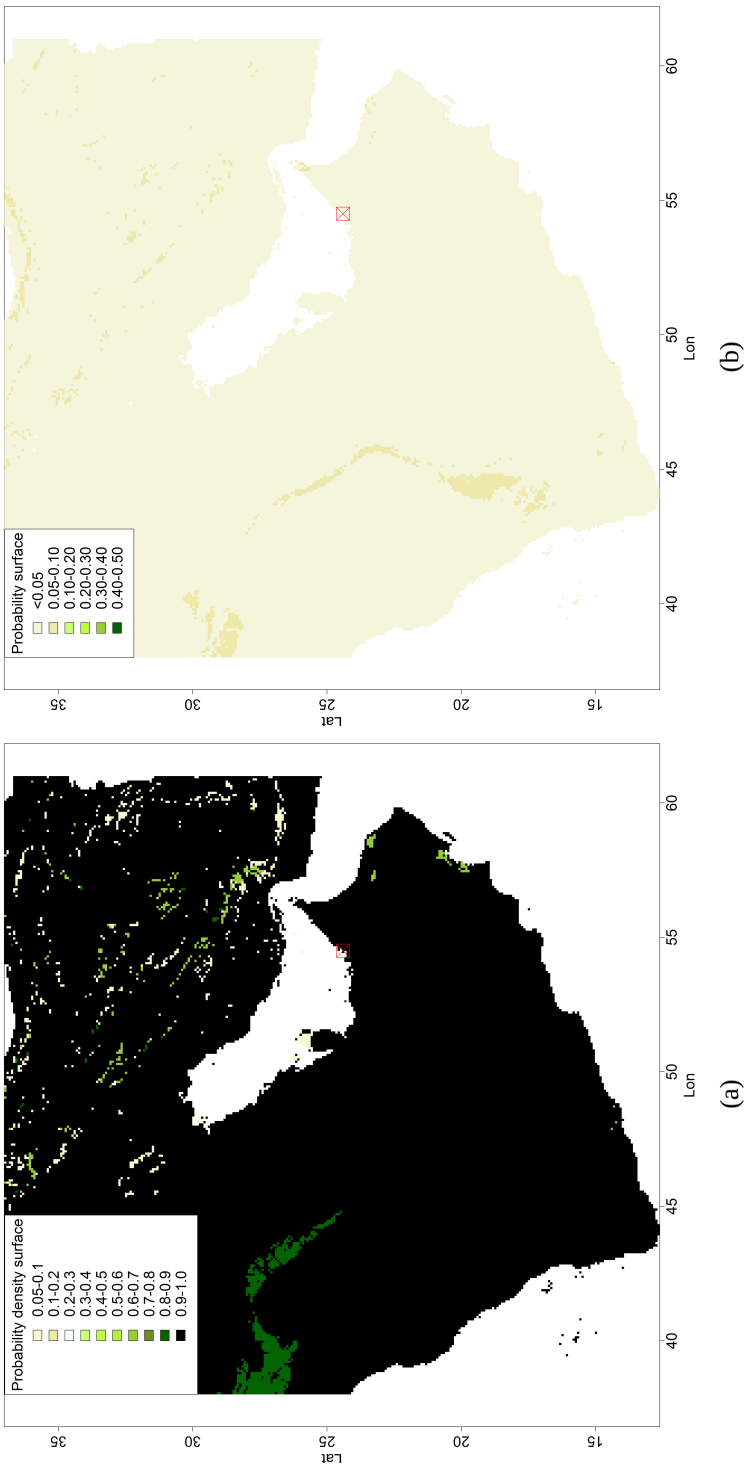


Figure 66: a) Normalised probability density scape and b) Probability scape based on the $^{87}Sr/^{86}Sr$ isotope composition of a tooth enamel carbonate sample (X3) from the remains of an unknown individual discovered in Abu Dhabi, UAE. Abu Dhabi is highlighted on the maps (red square)

At this stage it can be concluded that it is highly unlikely that the unidentified woman originated from Abu Dhabi. The likelihood of an individual from Abu Dhabi having the measured $\delta^{18}O_{carb}$ isotope composition is 1.1 %. The likelihood of an individual having the measured strontium isotopic composition is $<<$1%. It must be noted that is not impossible for the individual to have originated in Abu Dhabi but it is highly unlikely ($<$1%). Meier-Augenstein and Hoogewerff concluded that the woman had an oxygen isotope composition consistent with Sri Lanka or India. Currently there are no global models for the relationship between $\delta^{18}O_{carb}$ and $\delta^{18}O_{dw}$. This would be a possible area of interest that could expand on this thesis.

#### 5.3.1.2 Case study 2

The second example is a tooth taken from the Middle East tooth collection (referred to here as X1), known to have originated in Muscat, Oman. In this hypothetical example it is assumed that no further information about the sample is known other than it has originated from within the study region. The $\delta^{18}O_{vpdb}$ composition of the tooth enamel carbonate was 26.70 ‰ ($\pm$ 0.3, 1$\sigma$), measured by IRMS as described in Section 2.3.4. The $^{87}Sr/^{86}Sr$ composition of the tooth enamel was 0.71035 ($\pm$ 0.0002), measured using MC-ICP-MS as described in Section 3.2.2.

Firstly the measured oxygen isotopic composition of sample X1 was inserted into the $\delta^{18}O$ probability model given by Equation 43 to return the probability density at all locations ($j$) within the study region. The maximum probability density returned was 0.40. The results were normalised to this maximum value ($P_{norm} = P_j/P_{max}$) to return a probability layer with a scale from 0 - 1 as shown in Figure 67a. The probability density model was integrated between limits 26.70 $\pm$ 0.3(1$\sigma$), returning a layer showing the probability of the tooth originating from each location ($j$) in the study region (Figure 67b). 50 % of the study area can be excluded from the preliminary investigation as the probability or origin is less than 5 %. The highest returned probablility of origin is 24 %. An investigator can use the probability scape to show that it is most likely (20-25 %) that the remains

originated in the South of the Arabian Peninsula (Yemen, Oman or Eastern UAE), the West coast of Saudi Arabia or the South coast of Iran. This area covers 25 % of the study region. It is highly unlikely (<5 %) that the remains originated from Iran, Iraq or central Saudi Arabia.

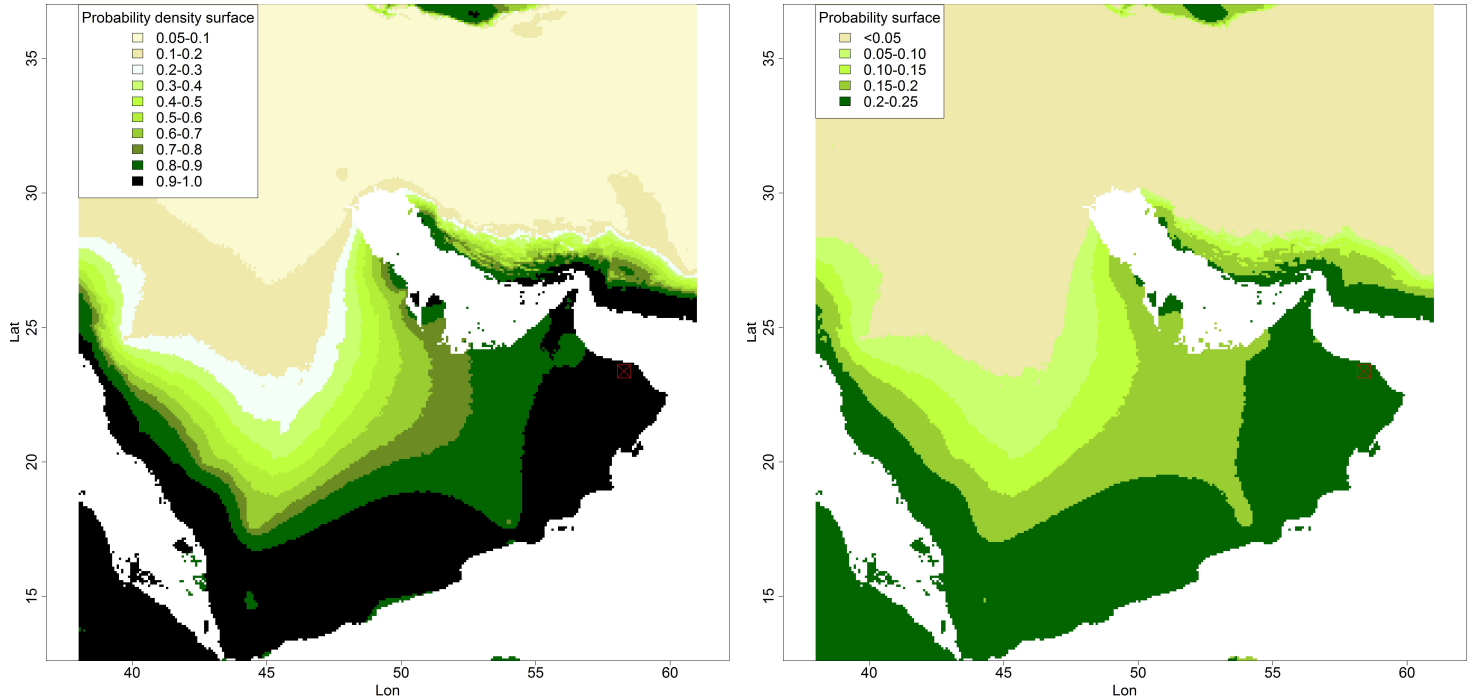


(a) (b)

Figure 67: a) Normalised probability density scape and b) Probability scape based on the $\delta^{18}$O composition of a tooth enamel carbonate sample (X1) from Muscat, Oman. The known origin of the individual is shown (red box).

Further information is required to further constrain the area of possible origin, therefore the $^{87}Sr/^{86}Sr$ isotopic composition of the tooth was measured ($0.71035 \pm 0.0002$). This value was inserted into the strontium probability model ($z$, Equation 44) a probability density grid is returned with a maximum probability density of 52.55. If the probability density is normalised to return a scale from 0 to 1 (Figure 68a) it becomes clear that there is little differentiation across the study region. By integrating between limits ($0.71035 \pm 0.0002$) the probability of an individual having the measured strontium isotope composition is returned (Figure 68b). The maximum probability returned by the model was 12.4 % which corresponds to the area of Late Paleozoic geology that defines the edge of the Arabian shield (shown in dark green on the map). The next highest probability was 9.9 %, corresponding to the small units of Paleozoic-Mesozoic sediment. The tooth originated from Muscat which lies on one of these Paleozoic-Mesozoic units as shown by the red box in Figure 68b. The probability of the tooth originating from any of the remaining geological units is less than 5 % with over three quarters of the study region returning a probability of less than 1 %. If it assumed that the tooth did indeed originate from the Middle East study region then using the probability model 98 % of the study region can be excluded from initial investigation with a probability of less than 5 %. It can be concluded that the tooth is most likely to have originated within one of the areas lying on or close to late Paleozoic or Paleozoic-Mesozoic geology with between 12.4 to 10 % of the population expected to have a similar isotopic composition.

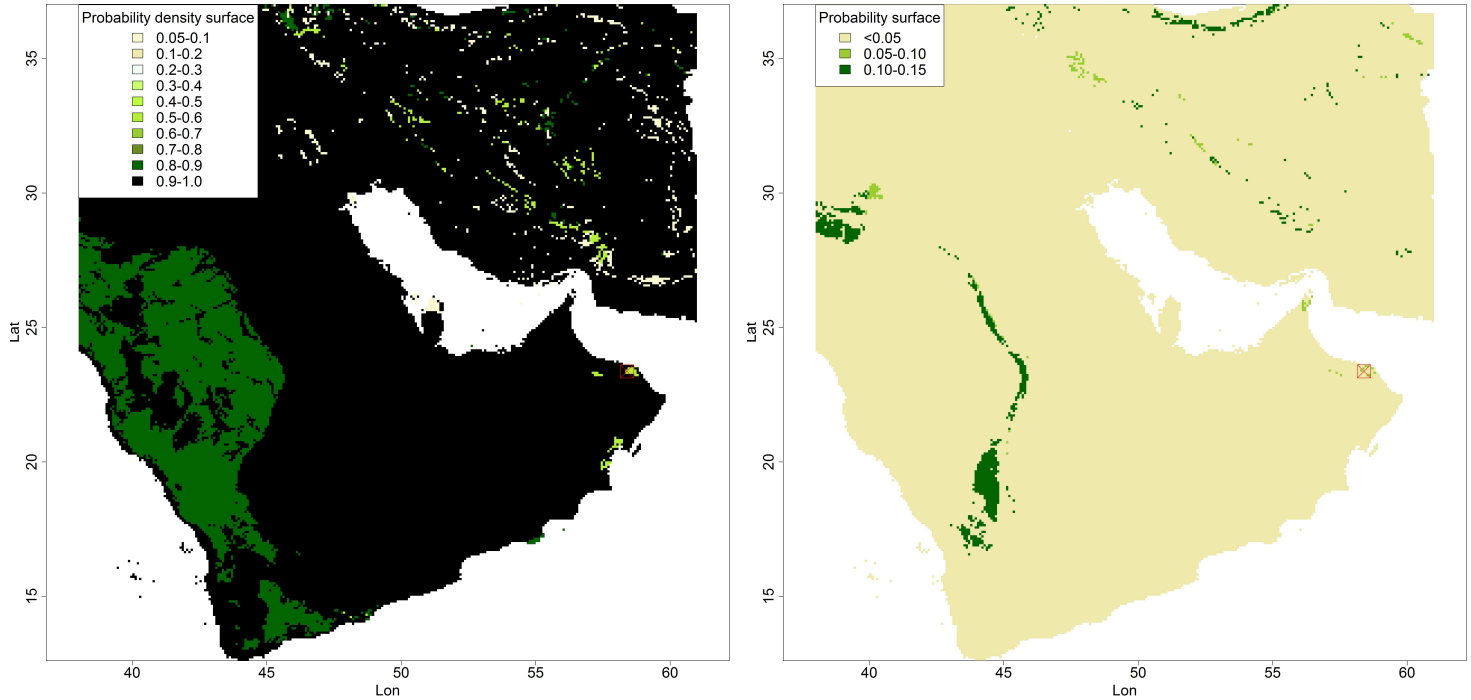


(a) (b)

Figure 68: a) Normalised probability density scape and b) Probability scape based on the $^{87}Sr/^{86}Sr$ composition of a tooth enamel sample (X1) from Muscat, Oman. The known origin of the individual is shown (red box).

Combining the two probability scapes using Equation 46 can further reduce the area of possible origin in the study region. Figure 69 shows the normalised combine probability scape for tooth X1. The combined probability describes the proportion of the population at each location $j$ expected to have the same $\delta^{18}$O and $^{87}$Sr/$^{86}$Sr isotopic composition as the unknown sample. From Figure 69 it can be seen that by combining the probability scapes the locations of possible origin have been narrowed to two regions in the south of the Peninsula; either from the small area of Paleozoic-Mesozoic geology in Oman in the East (P = 2.3 %) or, the area of Late Paleozoic geology in the northern Yemeni highlands (P = 2.8 %). These represent approximately 0.5 % of the study region (and includes the area of known origin).

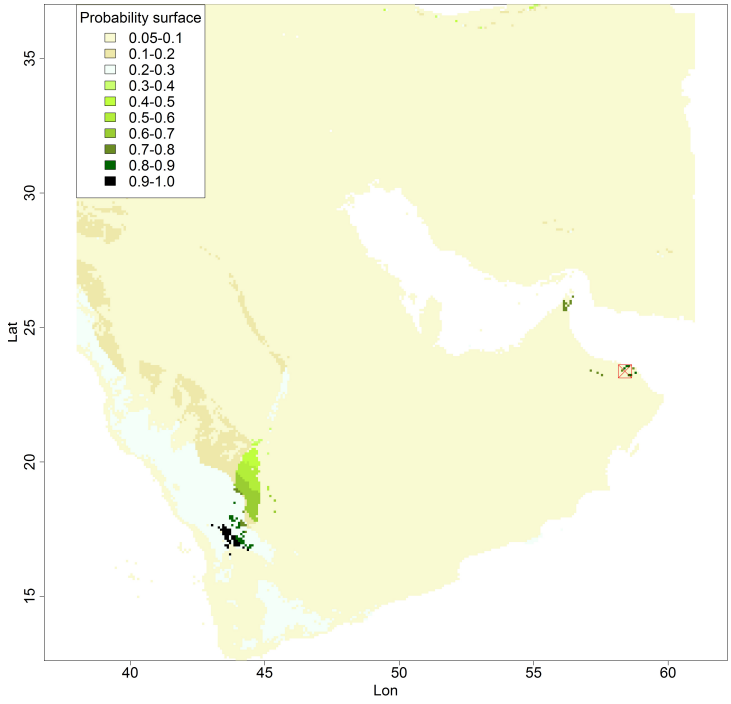


Figure 69: Normalised probability scapes based on $\delta^{18}$O and $^{87}$Sr/$^{86}$Sr composition of tooth enamel carbonate sample from Muscat, Oman. Values reported are the normalised combined probability (independent events) of the $\delta^{18}$O and $^{87}$Sr/$^{86}$Sr composition occurring at each grid location $j$. The actual origin of the sample is shown (red square)..

Using the combined $\delta^{18}O_{vpdb}$ and $^{87}$Sr/$^{86}$Sr probability scape it is possible to conclude that sample X1 of unknown origin, is most likely to have originated from either a small region on the east coast of Oman which corresponds with the capital city of Muscat or the area

in northern Yemen surrounding the capital city Sana'a. 99.5 % of the study region has been excluded for the purpose of the preliminary investigation due to the low likelihood of origin. However this does not mean that the sample could not have originated from these regions. Only that the likelihood is significantly lower than the areas not excluded.

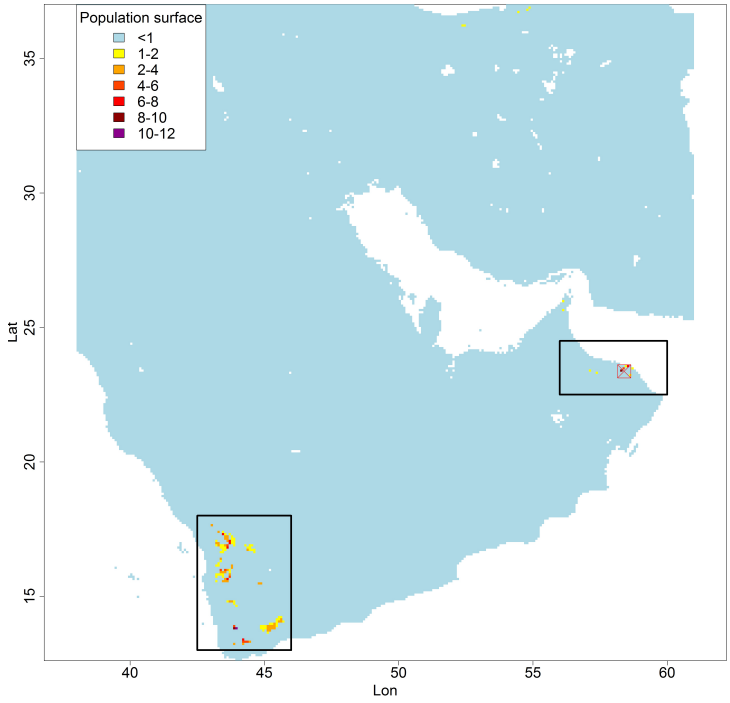


Figure 70: A human population layer based on the combined $\delta^{18}$O and $^{87}$Sr/$^{86}$Sr composition of tooth enamel carbonate sample from Muscat, Iran. Values reported are the amount of individuals per grid location $j$ likely to return the same isotopic signature as that of the measured sample.

Trace element analysis may now be useful for further refining the likely location of origin as it was shown in Chapter 4.1 that the trace element composition of Yemen was significantly different to that of Oman at the 95 % confidence level. The trace element composition of sample X1 was transformed using the principal components calculated in Section 4.3 and shown in Figure 58 and has been plotted on the principal component bi plot for comparison (Figure 71). Based on the trace element composition of the tooth enamel from sample X1 it can be concluded that the sample did not originate from Yemen (based on 95 % C.I.). The trace element composition is consistent with someone originating from Oman or the UAE. Combining this information with that from the oxygen and

strontium probability scape it is likely that the individual originated in or around Muscat, Oman.

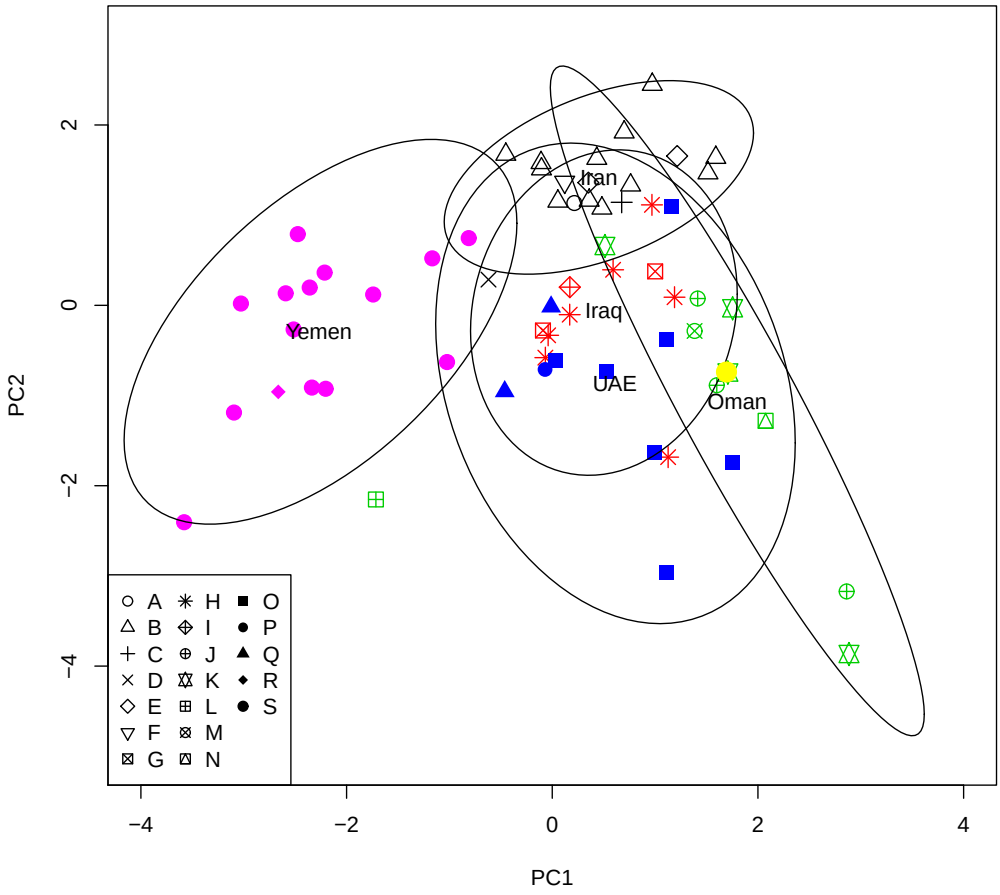


Figure 71: Ellipsoid plot of the principal components of the Middle East human tooth samples for the identification of unknown sample X1. Ellipsoids show the 95 % confidence extent for each of the locations of origin where n >1 and were calculated using the ordiellipse functionality in the VEGAN package for R. Points are coloured so that the country of origin can be clearly seen, black = Iran, red = Iraq, blue = UAE, green = Oman and grey = Yemen.

#### 5.3.1.3 Case study 3

The third example is a tooth taken from the Middle East tooth collection (referred to here as X2), known to have originated in Tehran, Iran. In this hypothetical example it assumed that the individual in question is unidentified but there has been some indication that they

may have originated in Tehran, Iran. The aim in this case is to provide the investigating officer with the likelihood of the sample originating in Tehran compared to other areas in the study region. The $\delta^{18}O_{VSMOW}$ composition of the tooth enamel carbonate was 23.99 ‰ measured by IRMS as described in Section 2.3.4. The $^{87}Sr/^{86}Sr$ composition of the tooth enamel was 0.70825 ($\pm$ 0.0002), measured using MC-ICP-MS as described in Section 3.2.2.

The measured oxygen isotope composition of tooth X2 was inserted into the $\delta^{18}O$ probability model given by Equation 43 to return the probability density at all locations ($j$) within the study region. The maximum probability density returned by the model was 0.4. A map of normalised probability density is shown in Figure 72a. The probability density model was integrated between limits 23.99 $\pm$ 0.3 ($1\sigma$), returning a layer of probability as shown by Figure 72b. The highest probability of origin was 24 %, found in areas of Iran and Iraq. Approximately 30 % of the study region (Southern and western region of the Arabian Peninsula and the south coast of Iran) has a predicted probability of $< 5$ % and can be excluded from initial investigation. 30 % of the study area (areas in Iran and Iraq) returns a predicted probability of $> 20\%$. The probability that the sample originated from Tehran based on the tooth $\delta^{18}O$ composition is 21.4 % so it can be said that it is not possible to exclude Tehran, but further information is required as the tooth could also have originated from approximately 30 % of the study region with the same or higher likelihood.

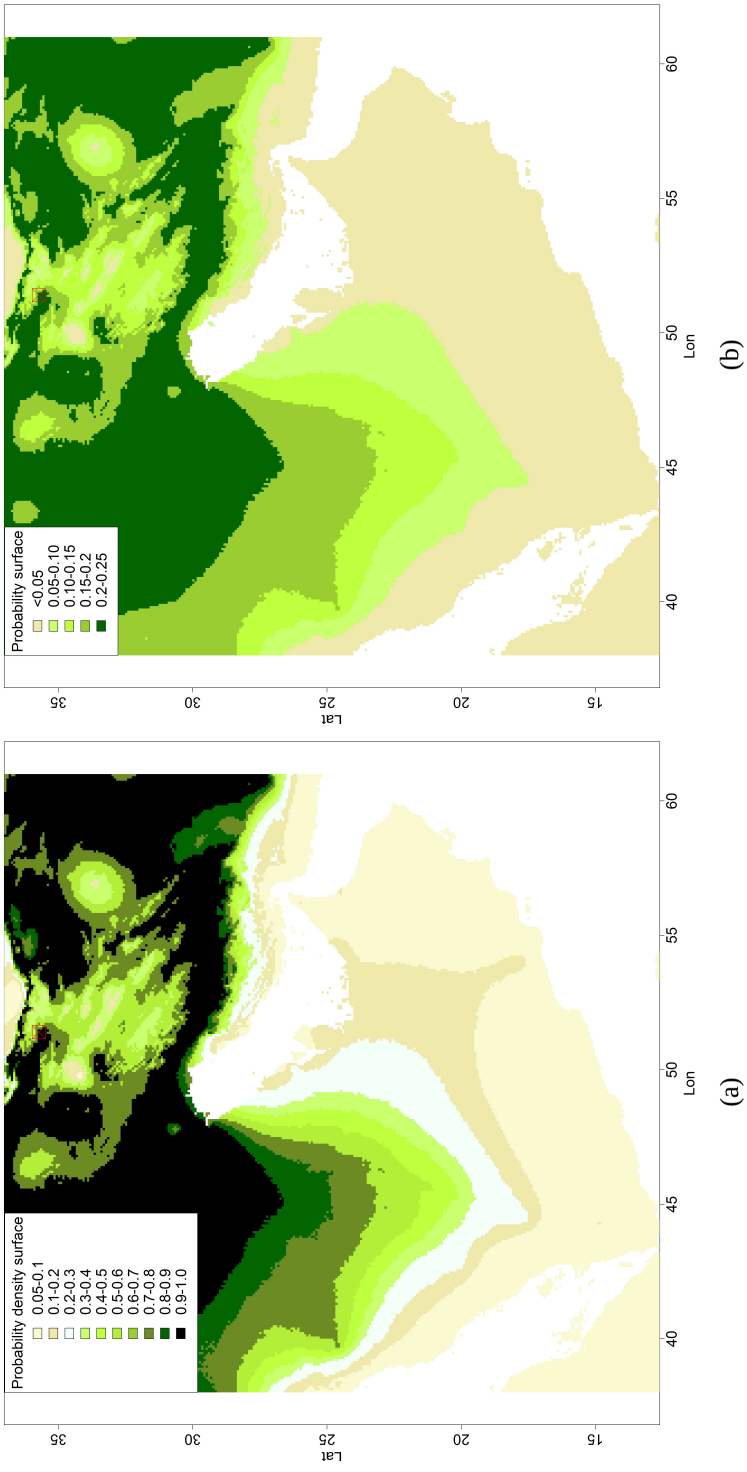


Figure 72: a) Normalised probability density scape and b) Probability scape based on the $\delta^{18}O$ composition of a tooth enamel carbonate sample (X2) from Tehran, Iran. The known origin of the individual is shown (red box).

Further information is required to further reduce the likely region of origin, therefore the $^{87}Sr/^{86}Sr$ isotopic composition of the tooth was measured ($0.70825 \pm 0.0002$). This value was inserted into the strontium probability model ($z$, Equation 44) to produce a probability density model (Figure 73a). The maximum returned probability density was 53.27. The probability density was normalised and the resulting map (Figure 73a) shows that a tooth with this isotopic composition could have potentially originated from anywhere in the study region. Integrating the probability density curve for each geological unit between limits ($0.70825 \pm 0.0002$) returns a map of the probability of the tooth originating from each location (Figure 73b). The maximum probability is returned for the Mesozoic geology (48 %, dark green). The probability of the tooth originating from an area near or on a cenozoic geological unit is 34 %. If the population structure (Figure 62) for each of the geological units is considered it is clear that there is significant overlap between the isotopic composition of the Mesozoic and Cenozoic geolgies. In this case the strontium model alone can only offer limited information about the origin of the tooth. Tehran lies on cenozoic bedrock hence the probability that the sample X2 originated from Tehran is 34 % so Tehran cannot be excluded based on the $^{87}Sr/^{86}Sr$ composition. However it cannot be differentiated from the remainder of the study region appart from the areas of older Precambrian and Paleozoic bedrock in the west of the study region ($P < 1$ %).

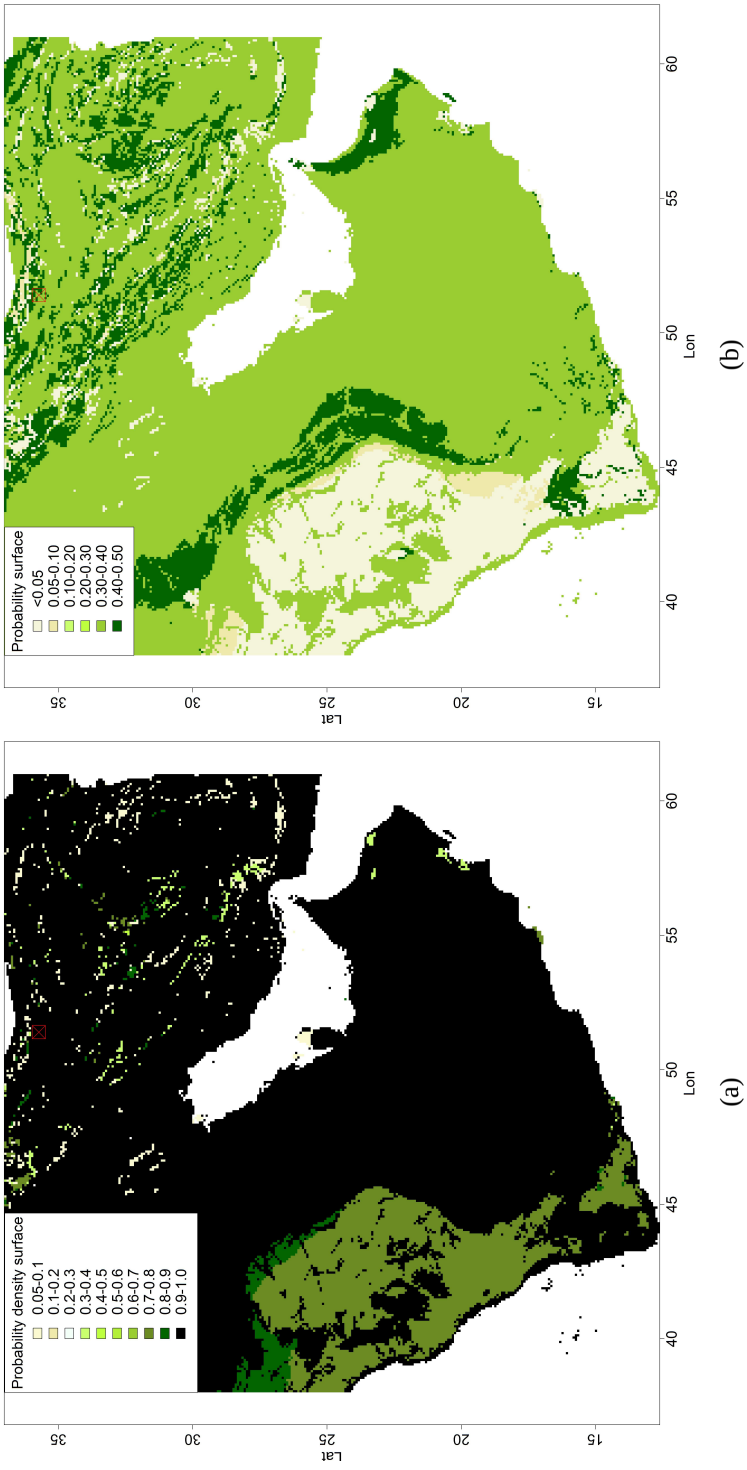


Figure 73: a) Normalised probability density scape and b) Probability scape based on the $^{87}Sr/^{86}Sr$ composition of a tooth enamel sample (X2) from Tehran, Iran. The known origin of the individual is shown (red box).

By combining the probability scapes it may be possible to exclude more of the study region. The normalised, combined probability scape is shown in Figure 74. The maximum probability returned by the model was 11 %. This is significantly higher than the previous example (X1) due to the fact that the isotopic composition of this tooth is more of an average signal for the study region hence it is expected that more individuals will fall within these isotopic ranges. Using the normalised probability map it is logical that an investigating officer would concentrate their preliminary search in the areas of highest probability. If 0.5 - 1 (, P = 5.5 - 11 %) is taken as the range considered in the initial investigation then 66 % of the study region can be preliminarily excluded, an improvement of 36 % on the $\delta^{18}$O probability scape and a 52 % improvement on the $^{87}$Sr/$^{86}$Sr probability scape when used on their own. The probability of an individual from Tehran having the same strontium and oxygen isotopic composition is 7.3 % (normalised = 0.65). It can be concluded from this information that Tehran cannot be excluded as a possible origin of the sample X2. However 25 % of the study region has an equal or higher probability of origin.

It may be useful to consider the human population distribution of the study region to further refine the model. It has been shown (Section 5.2.1.2, [225]) that the relative abundance of a species may have a significant effect on the probability of assignment. If the unknown sample X2 is considered to be a randomly selected sample that could originate from anywhere within the study region, it is clear that it is more likely that the sample will have originated from a city with a high population rather than a desert with a small or no population. Using this logic it may be possible to further reduce the area from which the tooth may have originated. Each grid location $j$ in the combined probability scape (Figure 74) for sample X2 was multiplied by the human population density (people per km$^2$) for that location, as given by the modified GPWv3 grid ([229], Section 5.2.1.2). The result is a grid showing the number of people per square kilometer ($n_{xj}$) expected to have the same oxygen and strontium isotope composition as sample X2 (Figure 75).

By considering the population density it is possible to exclude a further 5 % of the study

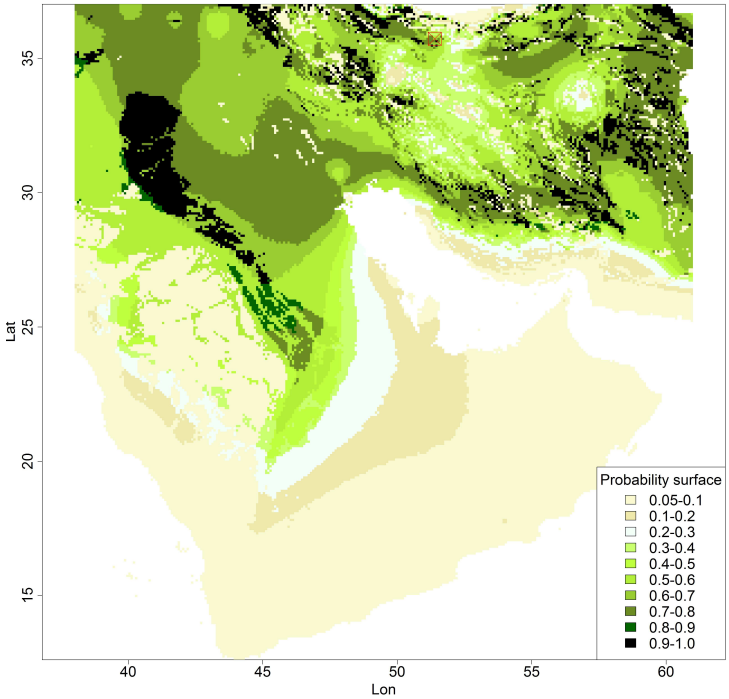


Figure 74: Normalised probability scapes based on the $\delta^{18}$O and $^{87}$Sr/$^{86}$Sr composition of tooth enamel carbonate sample from Tehran, Iran. Values reported are the normalised combined probability (independent events) of the $\delta^{18}$O and $^{87}$Sr/$^{86}$Sr composition occurring at each grid location $j$. The actual origin of the sample is shown (red square).

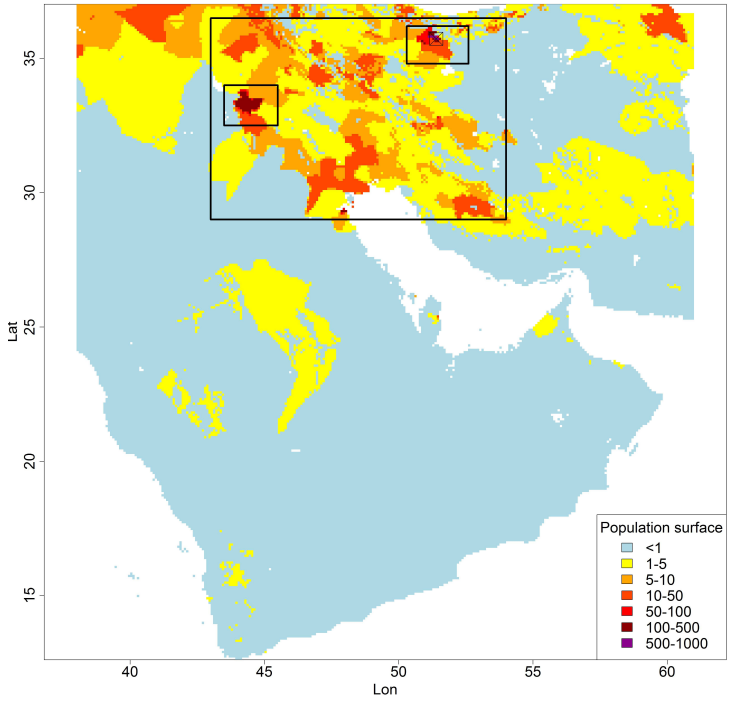


Figure 75: A human population layer based on the $\delta^{18}$O and $^{87}$Sr/$^{86}$Sr composition of tooth enamel carbonate sample from Tehran, Iran. Values reported are the amount of individuals per grid location $j$ likely to return the same isotopic signature as that of the measured sample.

region by excluding those areas with a population density of $<1$. As shown by the combined probability scape and now confirmed by the addition of the population variable it is most likely that the tooth in question originated from the north of the study region. The large box highlights the most likely region of origin which covers western Iran, eastern Iraq and Kuwait, however it is possible that the tooth originated from outside of this region the areas where the number of people per kilometer expected to exhibit the measured isotope signature is greater than 1. The major cities in the study region (population $>$100,000, UN) are shown in Table X and Figure 63. It might be useful to the investigator to determine the number of individuals (per km$^2$) expected to exhibit the measured isotopic signature in each of these cities and rank them accordingly so that the investigation may be concentrated in those areas that it is most likely that the tooth originated. The 10 most likely cities for the origin of X2 are listed in Table 28. It has been shown that Tehran is the most likely origin of the major cities (797 individuals per km$^2$). At this stage it can be reported that, in support of initial intelligence, based on the isotopic and population density information available, the sample X2 is most likely to have originated in Tehran. It may be required to report the likelihood that the sample could have originated at some other location. The next most likely city of origin was Baghdad (124 individuals per km$^2$). The likelihood that the sample X2 originated from Tehran over Baghdad can be given by the equation P$_{Tehran}$ = $n_{xz}$(Tehran)/$n_{xz}$(Tehran + Baghdad). The probability of the sample originating in Tehran is 87 % with only a 13 % (approximately 1 in 8) chance of the sample originating from Baghdad. Table 28 includes the probabilities of the sample orignating from the other major cities ranked in the top 10 most likely origins.

The trace element composition of the tooth enamel may provide supporting evidence for this conclusion. The trace element composition of sample X2 was transformed using the principal components calculated in Section 4.3 and shown in Figure 58 and has been plotted on the principal component bi plot for comparison (Figure 76). The trace element composition of sample X2 is consistent with an individual originating in Iran (95 % confidence limit). The individual is not consistent with originating in Iraq at the 95 %

Table 28: Table showing the top 10 most likely locations of origin of sample X2. $n_{xz}$ is the number of individuals per km$^2$ likely to have the same isotopic composition as sample X2. $P(X \cap Z)$ is the probability of an individual having the same isotopic composition as sample X2. P vs Tehran is the probability of the sample coming from that location compared to Tehran.

| | City | $n_{xz}$ | $P(X \cap Z)$ | P vs Tehran |
|---|---|---|---|---|
| 1 | Tehran | 797 | 7% | - |
| 2 | Baghdad | 124 | 7% | 13% |
| 3 | Kuwait City | 96 | 6% | 11% |
| 4 | Miandoab | 27 | 8% | 3% |
| 5 | Hamadan | 23 | 11% | 3% |
| 6 | Esfahan | 22 | 7% | 3% |
| 7 | Borujerd | 21 | 8% | 3% |
| 8 | Sanandaj | 20 | 8% | 2% |
| 9 | Mashhad | 20 | 10% | 2% |
| 10 | Shiraz | 15 | 8% | 2% |

confidence limit so it can be confirmed that the individual is unlikely to have originated in Baghdad and therefore is most likely to have originated in Tehran, Iran based on the oxygen and strontium isotope and trace element concentration data for the tooth enamel.

## 5.4 Conclusions

By using knowledge of the isotopic variation within the human population at each grid location $j$ within a chosen study region it is possible to calculate the probability of an unknown sample originating from each location (Section 5.2). The returned probability scape offers an investigating forensic scientist more information than a standard isoscape.

The probability models were tested by observing the amount of samples that could be assigned to the correct city of origin based on the 19 cities for which teeth were available in this study. 25 % of the samples could be assigned to the correct city of origin using the combined probability scape, an improvement of 4 % on the $\delta^{18}$O model, 17 % on the $^{87}$Sr/$^{86}$Sr model and 20 % when assignments were made randomly with no isotopic information. If it is assumed that the investigation will work logically through the cities based on the likelihood of origin and that the individuals could be identified when the location

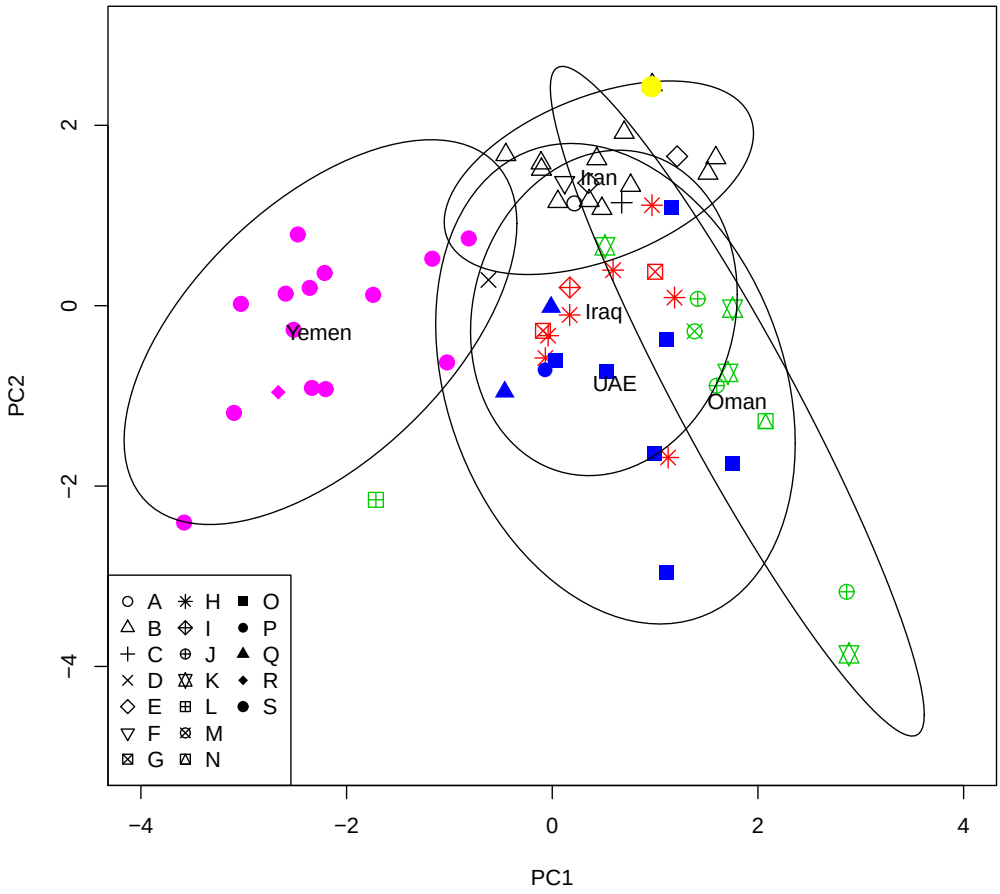


Figure 76: Ellipsoid plot of the principal components of the Middle East human tooth samples for the identification of unknown sample X2. Ellipsoids show the 95 % confidence extent for each of the locations of origin where n >1 and were calculated using the ordiellipse functionality in the VEGAN package for R. Points are coloured so that the country of origin can be clearly seen, black = Iran, red = Iraq, blue = UAE, green = Oman and grey = Yemen.

of origin is discovered, 96 % of the individuals could be identified within enquiries to 8 cities, reducing the workload of the investigating team by more than half.

Three case studies have been presented to illustrate how the probability scape models might be used to provide valuable information about the potential origin of unidentified human remains. Case study 1 (Section 5.3.1.1) was an example from a real forensic investigation. Using the combined probability scape it could be concluded that the tooth was unlikely ($P < 1$ %) to originate from Abu Dhabi. In case study 2 (Section 5.3.1.2), using the combined $\delta^{18}O$ and $^{87}Sr/^{86}Sr$ model, 99.5 % of the study region was able to be excluded from preliminary investigations leaving two main areas of likely origin, Sana'a in Yemen or Muscat in Oman. The known origin of the tooth was Muscat. In case study 3 (Section 5.3.1.3), the combine probability scape for the sample was used in conjunction with information about the human population density in the study region to exclude 80 % of the study region from preliminary investigation. Then by considering the major urban areas in the study region it could be conluded that Tehran was the most likely origin for the unknown tooth, supporting the initial intelligence. Trace element composition provided useful supporting evidence in these cases, further refining the prediction of origin of the unknown samples.

In previous studies spatial isotope data has only been used to approximate the potential area of origin for an unknown sample at large regional or international scale. In this study it has been illustrated that spatial isotopic data has the potential to narrow the origin of an unknown sample to a much smaller scale. When combined with human population density and any other *a priori* intelligence, there is the potential to differentiate between cities. There is still a significant amount of work required to further refine the isoscapes upon which the probability scape models are based, both to reduce the error in model predictions and also to provide a better understanding of the isotopic variation among the human population. The strontium model in particular is limited by the number of reference samples, hence the more samples that are measured the more representative the models can be.

# Chapter 6

# Conclusions and future directions

There is a requirement for new methods to aid in the identification of human remains in forensic studies as conventional methods leave hundreds of individuals unidentified each year. The intention of this study was to produce a new forensic tool to aid the identification of human remains. This thesis presents a number of new isoscape and probability scape models which, it is hoped will facilitate the identification of unidentified remains in the Middle East. In order to achieve this outcome, a collection of 68 modern human teeth of known origin from within the Middle East were analysed for their $\delta^{18}$O and $^{87}$Sr/$^{86}$Sr isotopic composition and their trace element concentrations. Until recently there have been no spatial prediction models available to enable forensic investigators to link the isotopic signature measured in modern human tissue to a geographic area and indeed there are currently no published examples of isoscapes for the prediction of modern human origin based on tooth enamel.

Of the limited number of modern human forensic studies that have utilised isotopic data, almost all have been conducted in the US or Europe. This thesis offer the first insight into the $\delta^{18}$O and $^{87}$Sr/$^{86}$Sr isotopic variation in the Middle East, an area which is of great interest (Section 1.6).

The results from the Middle East teeth collection have provided the framework for a

number of new tools and novel ideas that can be applied to the provenancing of human remains.

- A new drinking water isoscape for the Middle East has been developed, having concluded that current online global precipitation models do not sufficiently describe the isotopic variation observed in the study region. The new isoscape improves on the commonly used OIPC model by 42 %.
- From the new drinking water isoscape it was possible to produce a linear model relating $\delta^{18}$O of tooth enamel carbonate to the $\delta^{18}$O of drinking water. The model explained 70 % of the variation within the Middle East tooth collection and is the first example of a direct correlation between modern human tooth enamel carbonate and drinking water.
- A strontium isoscape was produced for the Middle East and although limited due to the relatively invariable geology of the study region, it has shown potential for differentiating between modern human individuals.
- The trace element data collected has shown some potential for differentiating between individuals from different regions in the Middle East and provides the foundations for a new reference database that could be developed by future studies as new samples become available.
- Finally, a probabilistic approach to isoscape modeling was applied as a potential new method for presenting isotope data in court. Using a multi-isotope approach ($\delta^{18}$O and $^{87}$Sr/$^{86}$Sr) and including population density as a prior probability this method has the potential to improve the likelihood of identifying human remains.

The merits and limitations of the new models and techniques described will be discussed in this chapter. The implications of this research for the forensic science community in the future will also be considered.

## 6.1 $\delta^{18}$O drinking water isoscape of the Middle East

In order to link the oxygen isotopic composition of human tooth enamel to a geographical region it is necessary to first have a suitable spatial model for the isotopic variation in drinking water. It was hypothesised that publically available global models of isotopes in precipitation [137, 3] would not sufficiently explain the isotopic variation in the study region due to the limited number of GNIP sample collection stations and the complex climate in the Middle East. By compiling water isotopic data from the Middle East into a small database and comparing with predictions from the global models this hypothesis was confirmed. The OIPC [137] explains only 17 % of the isotopic variation and the van Der Veer model explains none of the variation. One of the key outcomes of this thesis has been the development of a new $\delta^{18}$O in drinking water isoscape for the study region that explains almost 60 % of the isotopic variation.

### 6.1.1 Model limitations

As oxygen and hydrogen isotope signatures in most biological materials have some connection to source water, it is important that the base water isoscapes available capture as much of the isotopic variation of the area of interest as possible. Since the launch of the Online Isotopes in Precipitation Calculator (OIPC) it has become very easy to generate spatial isotope data and a number of studies use values from this source in their studies. The launch of the IsoMAP online software [230] in spring this year (2011) further facilitates the generation of spatial precipitation data, offering facilities to create isoscapes online. These facilities have made spatial precipitation isotope data accessible to the general scientific community, enabling isotope analysis to be applied to new, developing fields including (isotope) forensics. However there is a danger that blind application of these models without consideration of the associated limitations and errors could lead to false conclusions which might have repercussions in the future, particularly in the field of forensic science.

One of the main lessons from this thesis is that these global models are particularly limited in regions with low sampling density or complex climate systems such as the Middle East. Predictions from the OIPC have been shown to vary as much as 3 ‰($\delta^{18}$O) from measured water values. Ideally water samples should be available for direct measurement when conducting research in a geographical area that is poorly defined by available models. If this is not the case, an isoscape can be developed by correlating isotope values from the literature with geographical (latitude, altitude) or climatic (temperature, precipitation, relative humidity) variables. In this study the developed local isoscape explained 43 % more variation than the best global model.

### 6.1.2 Future directions: A global isotopic database

A hindrance experienced during this study was the lack of easily accessible isotope data for the study region. The GNIP database forms the basis of the publically available global models [137] but this database only includes information from GNIP collection stations of which there are three in the study region. Stable isotope analysis of water is now common across a wide range of disciplines from hydrology to forensics and as such there is a wealth of $\delta^{18}$O and $\delta$D isotopic information available in the literature. However compiling relevant data is time consuming and frustrating work for individual researchers. One of the main suggestions made during the recent Isoscapes conference held in September (2011) is the requirement for a database that compiles published isotope data. IsoMAP [230] have been developing resources to allow researchers to create spatial precipitation isoscapes online, but this is still dependent on the GNIP dataset which as previously mentioned is massively limited in some areas of the globe. One solution would be to expand the GNIP project to improve sampling density in under represented areas. However, as the IAEA depend mainly on volunteers for the collection of precipitation for the GNIP database this is not really a viable option. Another solution may be to create an open source database compiling the wealth of published isotopic data that is available so that it is more easily accessible for researchers.

## 6.2 $\delta^{18}$O carbonate isoscape for the Middle East

It is generally accepted that due to the simple sample preparation involved, $\delta^{18}$O analysis of tooth enamel carbonate would be the most efficient method of $\delta^{18}$O analysis for modern human samples in forensic cases. However there have been surprisingly few studies of tooth enamel carbonate and, other than the preliminary relationship shown by Ehleringer [50], there have been no studies describing the relationship between $\delta^{18}$O of tooth enamel carbonate and local drinking water. Previous studies have transformed carbonate $\delta^{18}$O composition into a predicted drinking water signal via the phosphate relationship described by Bryant [100], a two step process that can lead to large prediction errors.

The Middle East tooth collection was analysed for the $\delta^{18}$O composition of enamel carbonate. As information about the origin of these teeth is available, this dataset afforded the unique opportunity to directly determine the relationship between drinking water and tooth enamel carbonate:

$$\delta^{18}O_{VSMOW-carb} = 0.77 * (\delta^{18}O_{VSMOW-dw}) + 28.1 \quad (48)$$

This new model describes 70 % of the isotopic variation of human tooth enamel carbonate. The remainder is attributed to difference in diet, age, health and metabolism of individuals. This is the first time that the relationship between drinking water and tooth enamel carbonate from the Middle East has been derived, confirming the hypothesis that the $\delta^{18}$O isotopic composition of human tooth enamel is directly related to that of local drinking water. This model will facilitate future forensic human identification studies in the Middle East.

### 6.2.1 Limitations and future implications of the carbonate model

One of the main questions arising from the new carbonate - drinking water model is, can this relationship be applied to other regions of the world? As previously mentioned the $\delta^{18}O$ composition of human tooth enamel is determined by the inputs (drinking water, food and oxygen from the atmosphere) and fractionation that occurs during the carbonate formation which is a function of individual metabolism. If 100 % of the isotopic composition was provided by local drinking water one would expect a gradient of 1 in the linear regression model. In the Middle East model, the gradient is 0.77 which suggests that approximately 20 % of the isotopic signal originates from other sources. Compare this to the preliminary relationship for the US and the intercepts are comparible ([50] = 27.6 ‰) but the gradient is much shallower (0.35) suggesting that the American population gets the majority of its' isotopic composition from food or non local water. As previously suggested (Section 2.2.3) this is to be expected, as the global supermarket culture of the western world threatens to 'reduce the degree of isotopic identity of regional populations' [25].

From this observation it is clear that the relationship between drinking water and tooth enamel carbonate is dependent on the proportion of oxygen that is provided by local drinking water and hence different models are required for different populations as shown in Figure 77.

In order to use this carbonate model at a global scale in the future, it would be useful to determine an estimate for the percentage of oxygen incorporated from local drinking water for different populations around the world. Ideally this would be achieved by measurement of samples of known origin in order to create regional or national regression models as has been demonstrated with success in this study. However, it is very difficult to obtain suitable modern human teeth samples. An alternative may be to estimate the gradient of the regression based on survey data about diet. One clear conclusion of this research is that it is not satisfactory to calibrate a global precipitation or drinking water

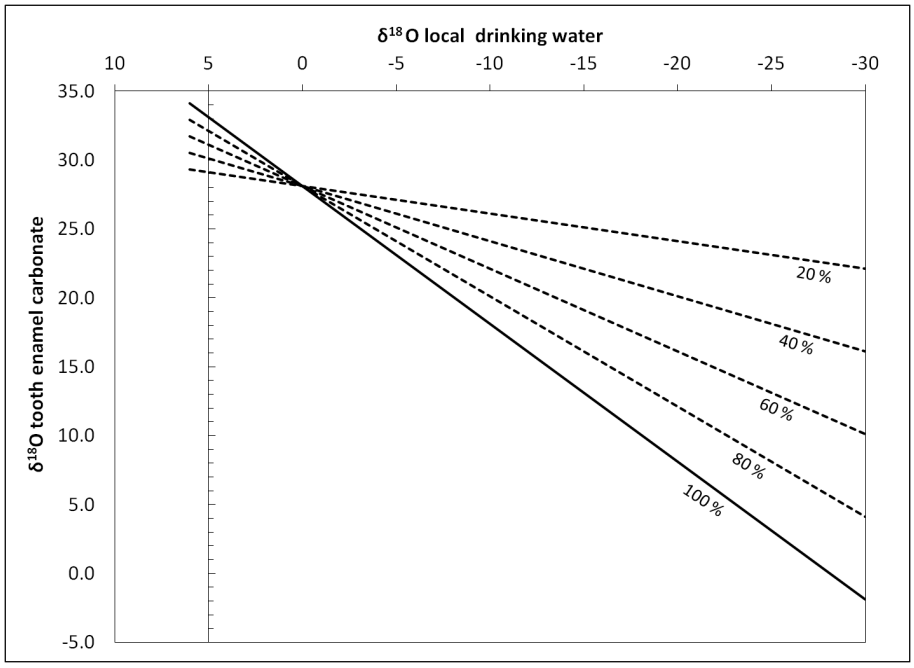


Figure 77: A model describing the relationship between $\delta^{18}$O of tooth enamel carbonate and local drinking water based on the percentage of oxygen that is incorporated from local drinking water.

isoscape to modern $\delta^{18}$O carbonate values using one global model.

## 6.3 $^{87}Sr/^{86}Sr$ isoscape for the Middle East

In one of the most influential papers concerning strontium in skeletal material Beard and Johnson [28] suggest that 'in the case of humans, the utility of using Sr isotopes to infer geographic information is probably more difficult today than it was just two or three decades ago, because of increased national and international diversity of Ca (and Sr) sources in food'.

The results presented in this thesis provide evidence that the strontium isotope composition of modern human tooth enamel from individuals from the Middle East is linked to the underlying geology and can be a useful tool for differentiating between modern populations. Although the results presented were limited due to the relative geological homogeneity of the study region (45 of 53 samples measured originated in areas overlying Cenozoic sediment), 4 samples originating in Muscat (Oman) and 2 samples from Sur (Oman) which lies on or near to an older Paleozoic-Mesozoic sedimentary unit, displayed significantly higher strontium isotope ratios than those from the younger geologies. This result has two implications. Firstly that strontium isotopic composition can be used to differentiate between locals and migrants in the modern human population in and around Muscat (Oman), a characteristic that may be useful for the identification of human remains in this large capital city. Secondly, the results suggest that the modern human population in the Middle East maintains a strontium isotopic composition that is linked to the local underlying geology as predicted in the thesis hypotheses (Section 1.4).

Using the measured strontium isotope results from human tooth enamel, and assigning strontium isotope values for the unmeasured geological regions based on European soil samples from similar underlying bedrock, it was possible to produce the first bioavailable $^{87}Sr/^{86}Sr$ isoscape of the Middle East. Further measurements of human samples are required to validate the predicted isoscape values for the geological units where no tooth enamel was available. As such the isoscape should be considered a preliminary estimate.

### 6.3.1 Application of $^{87}Sr/^{86}Sr$ isotope analysis in future human identification cases

A major point of discussion during a breakout session at the Isoscape conference this year (2011) was the requirement for better resolved isoscapes for the prediction of bioavailable $^{87}Sr/^{86}Sr$ composition, both for archaeological and forensic applications. There are very few published strontium isoscapes available and as described in Chapter 3 they are very limited and have not been validated using human samples of known origin. In this study it has been shown that predictions from the Beard and Johnson age only model are significantly lower than the strontium composition observed in human tooth enamel. A promising development in this field is the research of Batille (Purdue) who is in the process of creating a model based on rock type and mineralogy as well as age in an attempt to improve on the Beard and Johnson model [231]. This new model promises to explain more of the isotopic variation within the underlying bedrock. However it is inevitable that the model will require validating with a large number of human samples before it can be applied to forensic case work.

Important research that needs to be conducted in the near future is the measurement of human tooth or bone of known origin in other forensically interesting regions of the world. It would be particularly interesting to look at the human strontium signature from around the US or Great Britain to establish whether the global supermarket culture of the west has indeed led to the loss of local isotopic character. Further research is also required to determine the proportion of strontium that is provided by the diet. Strontium concentration is highest in plants and therefore diet is likely to provide the majority of strontium in the human body. However strontium may also be inhaled from the atmosphere as dust or pollution. It is currently uncertain as to what proportion of the strontium signal in humans is due to this atmospheric strontium. It is quite possible that strontium may only prove useful in less developed regions of the world where a higher proportion of local foods is produced and consumed.

## 6.4 Trace Elements

Recent studies have shown that trace elements are useful for differentiating between samples of forensic interest (particularly specialty food products) from different geographical regions [45]. However relatively few studies have applied trace element analysis to modern human tissue. In this study, trace element concentrations in 63 human teeth from 19 locations within the Middle East were measured in order to test the hypothesis that, it is possible to differentiate between modern human populations consuming diets from different regions based on trace element concentration.

This thesis represents the largest study of trace elements in modern human teeth to date, and the results provide the foundations of a database for comparison to future forensic samples. Of the 14 elements analysed in this study, 8 were determined to show significant difference between the human populations (ANOVA, Table 24). Of these 8 elements, 7 are good indicators of dietary sources (K, V, Ni, Cu, Zn, Sr and Mo) while lead is an indicator of environmental pollution. PCA was applied to the dataset resulting in 3 main groups (Figure 58). The first mainly contains samples from Yemen which are characterised by high strontium, low zinc content which is likely due to a low meat, high cereal diet which is common in a poorer country such as Yemen. The second group were mainly from Iran and contain higher zinc concentrations indicative of a high proportion of red meat in the diet. The third group were mainly from UAE and Oman and are characterised by higher Cu, Ni and V concentrations which are indicative of consumption of seafood and more expensive products such as chocolate and dates. Oman and UAE are the richest of the countries in the study region and have large fishing trades. They are also neighboring countries so it is reasonable that individuals from UAE and Oman should exhibit similar trace element concentrations. Trace element differentiation is limited to a national scale as the major determining factor is diet and diet is likely determined by national and cultural preferences and economy. The limited discriminating power of trace element analysis means that it is not overly useful as a technique on its own. However it may provide valuable support to other techniques such as isotope analysis as has been shown in Section

5.3.1.

### 6.4.1 Limitations of trace elements in human identification studies

The main limitation of trace element analysis in human samples is that it is not possible to model the expected trace element concentration for a population as it depends on too many variables. Instead, questioned samples must be compared to a database of measured values of known origin. Obtaining suitable reference samples of human tissue is difficult due to the invasive nature of the sampling process. This problem is exacerbated by the fact that different types of tissue contain different concentrations of trace elements so it is necessary to compile a new database for all tissues of interest. Using trace elements for human provenancing will be limited by the standard of the reference database available.

Compilation of a suitable database will be time consuming and expensive, and may only provide limited discrimination between regions as has been shown in this study. As such it is unlikely that trace element analysis will be used to entirely answer open forensic questions such as ‘where did this person come from’. Trace element analysis will be more useful in the support of other evidence to answer closed questions, for example ‘could individual A have originated at location X’ or ‘did individual A originate at location X or Y’. These questions can be answered by measuring suitable reference samples for comparison when required.

One practical limitation of this technique is that although LA-ICP-MS allows for fast analysis of samples and generates a large amount of data for comparison, there are currently no matrix matched calibration standards for hydroxy apatite samples. As such only semi-quantative results can be reported. It is necessary to develop an internationally accepted calibration standard in order for the results of LA-ICP-MS to be acceptable in a court of law.

## 6.5 Probability Scapes

One of the most important outcomes of this thesis has been the development of the multi-isotope ($\delta^{18}O$, $^{87}Sr/^{86}Sr$) probability scape of the Middle East described in Chapter 5. Applying the probabilistic approach to isotope mapping used in bird ecology [232] has an advantage over traditional isoscapes for two reasons. Firstly, presenting isotopic data as a likelihood of origin will greatly facilitate the communication of isotopic data to a jury in a court room environment. Secondly, by producing a map of probability of origin for a sample of interest, forensic investigators can focus their efforts on regions with the highest probability of origin and work systematically to the less probable regions until they reach a conclusion. This is an improvement on the traditional 'isotopic band' approach, as this band of isotopic space is often very large at a global scale if no *a priori* information is available. This also gives the false impression that the individual could not have originated from outside the given band which is not the case.

In this study the oxygen and strontium isoscapes were inverted to produce probability scapes based on a normal probability distribution. The probability scapes were then combined using the multiplication rule for independent events in order to investigate the hypothesis that combining oxygen and strontium isoscapes would improve the likelihood of a successful prediction of origin. In all of the case study scenarios tested (see Section 5.3.1), the likelihood of a successful conclusion being made was improved by combining the two isotope systems.

The probability models were applied to three case studies to illustrate their potential for answering forensic questions. There are two types of question that might be asked in a forensic investigation. The first is an open question; 'where did this person originate'? This may be asked if no other forensic intelligence is available. The second is a closed question such as 'could this person originate from location A'? These are more common and may be asked when a hypothesis has already been formed based on other evidence. Previous studies have applied isotope analysis to closed questions [23]. In this study, the

new probability scape models has been applied to both types of scenario with promising results.

In case study 1 the model was applied to evidence from an official forensic case. This is an example of a closed question scenario as there was evidence that the woman in question originated from India and the question asked was, 'could this individual have originated in Abu Dhabi'? Based on the multi-isotope probability scape it could be concluded that the tooth was very unlikely ($P < 1\%$) to have originated in Abu Dhabi. It was also highly unlikely that the woman originated from anywhere within the Middle East study region.

In case study 2 the models were applied to a simulated open forensic question where it was assumed that the sample could have originated from anywhere within the Middle East study region. 99.5 % of the study region could be excluded ($P < 5$ %) based on the multi-isotope probability scape. This is an important result for application of isotopes in forensics in the future, as it clearly shows that isotopic data can significantly reduce the possible locations of origin for an individual, even when no other forensic intelligence is available.

In case study 3 the model was applied to a simulated closed question; 'is it likely that the individual could have originated in Tehran, Iran'? Based on the multi-isotope model it was not possible to exclude Tehran as a possible origin but 25 % of the study region was shown to have the same or higher likelihood of origin. Population density was added as a prior probability variable in the model in order to strengthen this conclusion. Based on the population density it was possible to calculate the number of people (per km) expected to have the same oxygen and strontium isotopic range as the unknown sample. Using this approach it could be shown that it was 8 times more likely that the individual originated in Tehran than any of the other major populated areas in the study region. This is the first time that population density has been used to support isotopic data.

The advantage of this new method is that a list can be produced of the most likely cities/ towns of origin so that an investigation can work systematically based on the probability

of origin. This should reduce the workload of the police, cutting the time taken to identify human remains and hence increase the number of identifications possible, even when no prior evidence is available to guide the investigation. By considering the 53 teeth samples measured in this study as a set of unidentified individuals, it has been shown that using the multi-isotope approach (assuming that an individual can be identified once their origin is determined) 11 % of individuals coul be identified by enquiring to the most probable location of origin. In 96 % of cases, the workload involved in the identification of unidentified remains could be reduced by 68 % or more by using oxygen and strontium isotope evidence alone. Based on these figures, using oxygen and strontium isotopes in human identification could help to identify hundreds of individuals worldwide who would have remained unknown using conventional methods.

### 6.5.1 Limitations

The main limiting factor of the probability scape models is the quality of the underlying isoscapes. The discriminatory power of an isoscape will always be limited by the natural isotopic variation observed in the system of interest for a given region. By improving the general understanding of the processes leading to the isotopic variation observed, isoscape model error can be reduced. By reducing the isoscape model error and hence the stochastic component of the probability model ($\sigma$), it will be possible to exclude more of the study region as the location of origin for unknown samples, increasing the likelihood of identification.

A current limitation of the model is that due to lack of suitable reference materials it must be assumed that the local isotopic variation is normally distributed. Variation from a normal distribution may be caused by a number of factors such as, the proportion of wealthy individuals who can afford to eat imported food, the amount of desalinated water consumed in a region or the health and age distribution of the population. As more samples become available these variations can be incorporated into the model in order to improve

predictions.

A further limitation of the approach taken in this study is the 'centralisation' effect of using population density as a prior in the prediction model. Large cities will always be highlighted as having the highest probability of origin due to the significantly higher population, even if suburban towns and villages fall within the same probability band in the initial probability scape. As has been shown in this thesis, population density is a useful prior predictor in regions such as the Middle East where, due to the arid environment, the human population tends to be concentrated into urban areas. However, in a region such as Europe where a significant proportion of the human population live in rural areas, population density may not be so useful.

Interpreting these results and deciding which technique is the most useful for forensic purposes is a matter for debate and will depend on the type of forensic question being asked. This study has shown how population density can be used to confirm (or disprove) a hypothesis formed, based on *a priori* evidence (Case study 3). Where no *a priori* evidence is available, using population density may bias the investigation to urban areas when in reality the sample comes from a small rural population. In this case it it might be more useful to present the original multi-isotope probability scape. The author suggests that by considering both the original probability scape and a population weighted probability scape, an investigating team can determine the most efficient and systematic investigative approach to individual cases.

## 6.6 The future of forensic human identification isoscapes

The number of human remains found annually that are still unidentified after investigation using conventional means is unacceptable. This thesis represents one of the first major investigations into the value of isotopic and trace element analysis of modern, 21st Century, human tooth enamel as an indicator of geographic origin in forensic studies. The methods used in this thesis are built upon the foundations laid by a number of forensic and

archaeological isotope geochemists such as Meier-Augenstein ([71, 23, 15]), Ehleringer ([1, 50, 227]), Bowen ([33]), Bell ([233]), Lee-Thorp ([234, 233]) and many other who have been mentioned throughout this thesis. By continuing to develop the understanding of isotopic and elemental signals found within the human body it is hoped that they will become a standard tool in the arsenal of the forensic investigator that will enable the identification of a larger number of bodies found who have been victims of crime or war atrocities.

One of the main concerns about using isotopic data in the forensic community is the fact that the input of dietary products from international sources may overwhelm the local isotopic signature in modern humans. However there have been no studies until now to prove this point. This thesis has clearly shown that, at least for the Middle East study region, oxygen isotopic composition is related to the local drinking water signal in a strong linear relationship and can be therefore linked to a spatial prediction isoscape to determine regions of possible origin. Strontium has also shown the potential to differentiate between individuals living on older geological bedrock indicating a link to local food sources. Trace elements have also been shown to differentiate between populations based on dietary intake. By combining this chemical intelligence with some *a priori* information about population distribution it has been possible to reduce possible ares of origin down to $< 1$ % of the study region and even produce a list of the top ten cities of origin with corresponding likelihood.

The Middle East has not been affected by 'global supermarket culture' to the extent of the United States or the UK. However it is reasonable to assume that if isotopic information can be used to determine a city of origin for unidentified remains in the Middle East, then isotopic and trace element data will be useful in more developed countries too. Most likely at a coarser resolution, but any information that could improve the likelihood of a successful identification of an individual is important. If isotope analysis of human remains resulted in the identification of one or two more of the $\sim 15$ unidentified bodies found in the UK every month, that is one or two more families who can be offered comfort

and one or two more cases that can be taken to court and resolved.

# Bibliography

[1] Ehleringer, J. R. *et al.* Hydrogen and oxygen isotope ratios in human hair are related to geography. *Proceedings of the National Academy of Sciences of the United States of America* **105**, 2788–2793 (2008).

[2] Majoube, M. Fractionnement en oxygene 18 et en deutkrium entre leau et sa vapeur. *J. Chim. Phys.* **68**, 1423–1436 (1971).

[3] Van der Veer, G., Voerkelius, S., Lorentz, G., Heiss, G. & Hoogewerff, J. A. Spatial interpolation of the deuterium and oxygen-18 composition of global precipitation using temperature as ancillary variable. *Journal of Geochemical Exploration* **101**, 175–184 (2009).

[4] Missing Persons Bureau. Missing persons: Data and analysis 2009/2010. *National Policing Inprovement Agency, Missing Persons Bureau Report* 1–33 (2010).

[5] Lemre, J. Remains of WTC worker Ernest James, 40, ID'd ten years after 9/11. *New York Daily News* **August 24,** (2011).

[6] The National Police Agency of Japan. National police agency (2011). URL `http://www.npa.go.jp/english/index.htm`.

[7] National Police Improvement Agency. National police improvement agency (2011). URL `http://www.npia.police.uk`.

[8] Cattaneo, C. *et al.* Unidentified cadavers and human remains in the EU: and unknown issue. *International Journal of Legal Medicine* **113**, N1–N5 (2000).

[9] Ritter, N. Missing persons and unidentified remains: The nations silent mass disastor. *National Institute of Justice* **256** (2007).

[10] Cattaneo, C. *et al.* Unidentified bodies and human remains: An Italian glimpse through a European problem. *Forensic Science International* **195**, 167.e1 – 167.e6 (2010).

[11] Ezzo, J. A. & Price, T. Migration, regional reorganization, and spatial group composition at Grasshopper Pueblo, Arizona. *Journal of Archaeological Science* **29**, 499–520 (2002).

[12] Price, T. D., Manzanilla, L. & Middleton, W. D. Immigration and the Ancient City of Teotihuacan in Mexico: a Study Using Strontium Isotope Ratios in Human Bone and Teeth. *Journal of Archaeological Science* **27**, 903–913 (2000).

[13] Buzon, M. R. & Bowen, G. J. Oxygen and carbon isotope analysis of human tooth enamel from the New Kingdom site of Tombos in Nubia. *Archaeometry* **52**, 855–868 (2010).

[14] West, J., Bowen, G., Dawson, T. & Tu, K. (eds.) *Isoscapes: Understanding movement, pattern and process on Earth through isotope mapping* (Springer, 2010).

[15] Meier-Augenstein, W. *Stable Isotope Forensics* (Wiley-Blackwell, 2010).

[16] Hoogewerff, J. *et al.* The Last Domicile of the Iceman from Hauslabjoch: A Geochemical Approach Using Sr, C and O Isotopes and Trace Element Signatures. *Journal of Archaeological Science* **28**, 983–989 (2001).

[17] Castro, W., Hoogewerff, J., Latkoczy, C. & Almirall, J. R. Application of laser ablation (LA-ICP-SF-MS) for the elemental analysis of bone and teeth samples for discrimination purposes. *Forensic Science International* **195**, 17–27 (2010).

[18] Schwarcz, H. P. Tracing unidentified skeletons using stable isotopes. *Forensic Magazine* **4(3)**, 28–31 (2007).

[19] Wunder, M. B. Using Isoscapes to Model Probability Surfaces for Determining Geographic Origins. In *Isoscapes*, 251–270 (Springer, 2010).

[20] Hobson, K. A., Lormée, H., Van Wilgenburg, S. L., Wassenaar, L. I. & Boutin, J. M. Stable isotopes ($\delta$D) delineate the origins and migratory connectivity of harvested animals: the case of european woodpigeons. *Journal of Applied Ecology* **46**, 572–581 (2009).

[21] Iacumin, P., Bocherens, H., Mariotti, A. & Longinelli, A. Oxygen isotope analyses of co-existing carbonate and phosphate in biogenic apatite: a way to monitor diagenetic alteration of bone phosphate. *Earth and Planetary Science Letters* **142**, 1–6 (1996).

[22] Bowen, G., Hoogewerff, J. & West, J. Editorial board. *Journal of Geochemical Exploration* **102**, IFC–IFC (2009).

[23] Meier-Augenstein, W. & Fraser, I. Forensic isotope analysis leads to identification of a mutilated murder victim. *Science & Justice* **48**, 153–159 (2008).

[24] Bentley, A. R. Strontium Isotopes from the Earth to the Archaeological Skeleton: A Review. *Journal of Archaeological Method and Theory* **13**, 135–187 (2006).

[25] Pye, K. & Croft, D. Isotope and trace element analysis of human teeth and bone for forensic purpose. In Pye, K. & Croft, D. (eds.) *Forensic Geoscience: Principles, techniques and applictaions*, 215–236 (Geological Society Publishing House, Bath, 2004).

[26] Ezzo, J. A., Johnson, C. M. & Price, T. D. Analytical Perspectives on Prehistoric Migration: A Case Study From East-Central Arizona. *Journal of Archaeological Science* **24**, 447 – 466 (1997).

[27] Pinstrup-Anderson, P. & Babinard, J. Globalisation and human nutrition: Opportunities and risks for the poor in developing countries. *African Journal of Food and Nutritional Sciences* **1**, 9–18 (2001).

[28] Beard, B. & Johnson, C. Strontium isotope composition of skeletal material can determine the birth place and geographic mobility of humans and animals. *J.For.Science* **45**, 1049–1061 (2000).

[29] Ng, F. & Ataman Aksoy, M. Who are the net food importing countries. *The World Bank Development Research Group* (2008).

[30] U.S. Department of Commerce & U.S. Department of Transportation. Commodity flow survey. *Economic Census* (2007).

[31] O'Brien, D. & Wooller, M. Tracking human travel using stable oxygen and hydrogen isotope analyses of hair and urine. *Rapid Communications in Mass Spectrometry* **21**, 2422–2430 (2007).

[32] Chesson, L. A., Podlesak, D. W., Erkkila, B. R., Cerling, T. E. & Ehleringer, J. R. Isotopic consequences of consumer food choice: Hydrogen and oxygen stable isotope ratios in foods from fast food restaurants versus supermarkets. *Food Chemistry* **119**, 1250–1256 (2010).

[33] Bowen, G. J. *et al.* Dietary and physiological controls on the hydrogen and oxygen isotope ratios of hair from mid-20th century indigenous populations. *American Journal of Physical Anthropology* **139**, 494–504 (2009).

[34] Thompson, A. *et al.* Stable isotope analysis of modern human hair collected from Asia (China, India, Mongolia, and Pakistan). *American Journal of Physical Anthropology* **141**, 440–451 (2010).

[35] Skinner, H. Minerology of Bone. In *Essentials of Medical Geology* (Elsevier, 2005).

[36] Hillson, S. *Teeth* (Cambridge University Press, 1986).

[37] Al Na'imi, K. S. *Human Geographical provenancing via enamel surface trace elements*. Master's thesis, School of Forensic and Investigative Sciences, University of Central Lancashire (2009).

[38] USGS. Earth resources observation and science (2010). URL `eros.usgs.gov`.

[39] Kennedy, C., Bowen, G. & Ehleringer, J. Temporal variation of oxygen isotope ratios ($\delta^{18}$O) in drinking water: Implications for specifying location of origin with human scalp hair. *Forensic Science International* **208**, 156 – 166 (2011).

[40] Rauch, E., Rummel, S., Lehn, C. & Bttner, A. Origin assignment of unidentified corpses by use of stable isotope ratios of light (bio-) and heavy (geo-) elementsa case report. *Forensic Science International* **168**, 215 – 218 (2007).

[41] Musaiger, A. Diet and Prevention of Coronary Heart Disease in the Arab Middle East Countries. *Medical principles and practice* **11**, 9–16 (2002).

[42] CIA. Country comparison, GDP per capita (2010). URL `www.cia.gov/library`.

[43] Iranianpedia. What is iranian diet (2011). URL `www.iranianpedia.com`.

[44] Budzikiewicz, H. & Grigsby, R. D. Mass spectrometry and isotopes: A century of research and discussion. *Mass Spectrometry Reviews* **25**, 146–157 (2006).

[45] Kelly, S., Heaton, K. & Hoogewerff, J. Tracing the geographical origin of food: The application of multi-element and multi-isotope analysis. *Trends in Food Science & Technology* **16**, 555–567 (2005).

[46] Cerling, T., Omondi, P. & Macharia, A. Diets of Kenyan elephants from stable isotopes and the origin of confiscated ivory in Kenya. *African Journal of Ecology* **45**, 614–623 (2007).

[47] Hobson, K. A., Van Wilgenburg, S. L., Larson, K. & Wassenaar, L. I. A feather hydrogen isoscape for Mexico. *Journal of Geochemical Exploration* **102**, 167–174 (2009).

[48] Meier-Augenstein, W. & NicDaeid, N. Feasibility of source identification of seized street drug samples by exploiting differences in isotopic composition at nat-

ural abundance level by GC/MS as compared to isotope ratio mass spectrometry (IRMS). *Forensic Science International* **174**, 259–261 (2008).

[49] Ehleringer, J. R., Casale, J. F., Lott, M. J. & Ford, V. L. Tracing the geographical origin of cocaine. *Nature* **408**, 311–312 (2000).

[50] Ehleringer, J. *et al.* A Framework for the Incorporation of Isotopes and Isoscapes in Geospatial Forensic Investigations. In *Isoscapes* (Springer, 2011).

[51] Fraser, I., Meier-Augenstein, W. & Kalin, R. M. Stable Isotope Analysis of Human Hair and Nail Samples: The Effects of Storage on Samples. *Journal of Forensic Sciences* **53**, 95–99 (2008).

[52] Meier-Augenstein, W. Stable Isotope Fingerprinting - Chemical element ”DNA”. In Black, S. & Thompson, T. (eds.) *Forensic Human Identification*, vol. 1, 29–55 (CRC Press, 2006).

[53] Faure, G. *Principles and applications of geochemistry* (Prentice Hall, 1998), 2nd edn.

[54] Craig, H. & Gordon, L. Deuterium and oxygen-18 varitaions in the ocean and marine atmosphere. In *Stable isotopes in oceanographic studies and paleo-temperatures* (Lab.Geol.Nucl. Pisa, 1965).

[55] IAEA. *Environmental isotopes in the hydrological cycle Volume II* (IAEA, 2000).

[56] BBC. History a cold case. Broadcast BBC1 (2010).

[57] Muller, W., Fricke, H., Halliday, A. N., McCulloch, M. T. & Wartho, J. Origin and Migration of the Alpine Iceman. *Science* **302**, 862–866 (2003).

[58] Dansgaard, W. Stable isotopes in precipitation. *Tellus (Sweden)* **16**, 436–468 (1964).

[59] Bowen, G. J. & Revenaugh, J. Interpolating the isotopic composition of modern meteoric precipitation. *Water Resources Research* **39** (2003).

[60] Yurtsever, Y. & Gat, J. Atmospheric Waters. In *Stable Isotope Hydrology*, vol. 210 of *Technical Reports* (International Atomic Energy Agency, 1981).

[61] Birks, S., Gibson, J., Gourcy, L., Aggarwal, P. & Edwards, T. Maps and animations offer new opportunities for studying the global water cycle. *Eos Trans. AGU Electron. Suppl.* **83(37)** (2002).

[62] Bowen, G. & Wilkinson, B. Spatial distribution of $\delta^{18}O$ in meteoric precipitation. *Geology* **30**, 315–318 (2002).

[63] Hijmans, R. J., Cameron, S. E., Parra, J. L., Jones, P. G. & Jarvis, A. Very high resolution interpolated climate surfaces for global land areas. *International Journal of Climatology* **25**, 1965–1978 (2005).

[64] Dutton, A., Wilkinson, B. H., Welker, J. M., Bowen, G. J. & Lohmann, K. C. Spatial distribution and seasonal variation in $\delta^{18}O$ of modern precipitation and river water across the conterminous USA. *Hydrological Processes* **19**, 4121–4146 (2005).

[65] Bowen, G. J., Ehleringer, J. R., Chesson, L. A., Stange, E. & Cerling, T. E. Stable isotope ratios of tap water in the contiguous United States. *Water Resour. Res.* **43** (2007).

[66] Bowen, G. J., Chesson, L., Nielson, K., Cerling, T. & Ehleringer, J. Treatment methods for the determination of $\delta^2H$ and $\delta^{18}O$ of hair keratin by continuous-flow isotope-ratio mass spectrometry. *Rapid Communications in Mass Spectrometry* **19**, 2371–2378 (2005).

[67] Benson, S., Lennard, C., Maynard, P. & Roux, C. Forensic applications of isotope ratio mass spectrometry–A review. *Forensic Science International* **157**, 1–22 (2006).

[68] Cordella, C., Moussa, I., Martel, A.-C., Sbirrazzuoli, N. & Lizzani-Cuvelier, L. Recent developments in food characterization and adulteration detection: Technique-

oriented perspectives. *Journal of Agricultural and Food Chemistry* **50**, 1751–1764 (2002).

[69] Chesson, L. A., Podlesak, D. W., Thompson, A. H., Cerling, T. E. & Ehleringer, J. R. Variation of hydrogen, carbon, nitrogen, and oxygen stable isotope ratios in an american diet: Fast food meals. *Journal of Agricultural and Food Chemistry* **56**, 4084–4091 (2008).

[70] Lock, C. M. & Meier-Augenstein, W. Investigation of isotopic linkage between precursor and product in the synthesis of a high explosive. *Forensic Science International* **179**, 157–162 (2008).

[71] Fraser, I., Meier-Augenstein, W. & Kalin, R. M. The role of stable isotopes in human identification: a longitudinal study into the variability of isotopic signals in human hair and nails. *Rapid Communications in Mass Spectrometry* **20**, 1109–1116 (2006).

[72] Forensic Isotope Ratio Mass Spectrometry Network. Forensic isotope ratio mass spectrometry network (2010). URL `http://www.forensic-isotopes.org`.

[73] Trace. Tracing the origin of food. URL `http://www.trace.eu.org`.

[74] Longinelli, A. Oxygen isotopes in mammal bone phosphate: A new tool for paleohydrological and paleoclimatological research? *Geochimica et Cosmochimica Acta* **48**, 385–390 (1984).

[75] Luz, B., Kolodny, Y. & Horowitz, M. Fractionation of oxygen isotopes between mammalian bone phosphate and environmental drinking-water. *Geochimica et Cosmochimica Acta* **48**, 1689–1693 (1984).

[76] Daux, V., Lécuyer, C., Adam, F., Martineau, F. & Vimeux, F. Oxygen isotope composition of human teeth and the record of climate changes in France (Lorraine) during the last 1700 years. *Climatic Change* **70**, 445–464 (2005).

[77] Daux, V. *et al.* Oxygen isotope fractionation between human phosphate and water revisited. *Journal of Human Evolution* **55**, 1138–1147 (2008).

[78] Schoeninger, M. J. & Moore, K. Bone stable isotope studies in archaeology. *Journal of World Prehistory* **6**, 247–296 (1992).

[79] White, C. D., Spence, M. W., Stuart-Williams, H. l. Q. & Schwarcz, H. P. Oxygen Isotopes and the Identification of Geographical Origins: The Valley of Oaxaca versus the Valley of Mexico. *Journal of Archaeological Science* **25**, 643–655 (1998).

[80] Bowen, G. J. *et al.* Stable hydrogen and oxygen isotope ratios of bottled waters of the world. *Rapid Communications in Mass Spectrometry* **19**, 3442–3450 (2005).

[81] Tudge, A. P. A method of analysis of oxygen isotopes in orthophosphate–its use in the measurement of paleotemperatures. *Geochimica et Cosmochimica Acta* **18**, 81–93 (1960).

[82] Urey, H. C., Lowenstam, H. A., Epstein, S. & McKinney, C. R. Measurement of paleotemperatures and temperatures of the upper Cretaceous of England, Denmark, and the southeastern United States. *Geological Society of America Bulletin* **62**, 399–416 (1951).

[83] Epstein, S., Buchsbaum, R., Lowenstam, H. & Urey, H. C. Carbonate-water isotopic temperature scale. *Geological Society of America Bulletin* **62**, 417–426 (1951).

[84] Longinelli, A. Oxygen Isotopic Composition of Orthophosphate from Shells of Living Marine Organisms. *Nature* **207**, 716–719 (1965).

[85] Longinelli, A. & Nuti, S. Oxygen-Isotope Ratios in Phosphate from Fossil Marine Organisms. *Science* **160**, 879–882 (1968).

[86] Longinelli, A. & Nuti, S. Revised phosphate-water isotopic temperature scale. *Earth and Planetary Science Letters* **19**, 373–376 (1973).

[87] Levinson, A. A., Luz, B. & Kolodny, Y. Variations in oxygen isotopic compositions of human teeth and urinary stones. *Applied Geochemistry* **2**, 367–371 (1987).

[88] Fricke, H. C. & O'Neil, J. R. Inter- and intra-tooth variation in the oxygen isotope composition of mammalian tooth enamel phosphate: implications for palaeoclimatological and palaeobiological research. *Palaeogeography, Palaeoclimatology, Palaeoecology* **126**, 91–99 (1996). Doi: DOI: 10.1016/S0031-0182(96)00072-7.

[89] Fricke, H., Clyde, W. C. & O'Neil, J. R. Intra-tooth variations in $\delta^{18}O$ ($PO_4$) of mammalian tooth enamel as a record of seasonal variations in continental climate variables. *Geochimica et Cosmochimica Acta* **62**, 1839–1850 (1998).

[90] Stuart-Williams, H. L. Q. & Schwarcz, H. P. Oxygen isotopic determination of climatic variation using phosphate from beaver bone, tooth enamel, and dentine. *Geochimica et Cosmochimica Acta* **61**, 2539–2550 (1997).

[91] Langlois, C., Simon, L. & Lécuyer, C. Box-modeling of bone and tooth phosphate oxygen isotope compositions as a function of environmental and physiological parameters. *Isotopes in Environmental Health Studies* **39**, 259–272 (2003).

[92] Kohn, M. J. Predicting animal $\delta^{18}O$: Accounting for diet and physiological adaptation. *Geochimica et Cosmochimica Acta* **60**, 4811–4829 (1996).

[93] Cerling, T. *et al.* Determining biological tissue turnover using stable isotopes: the reaction progress variable. *Oecologia* **151**, 175–189 (2007).

[94] Crowson, R. A., Showers, W. J., Wright, E. K. & Hoering, T. C. Preparation of phosphate samples for oxygen isotope analysis. *Analytical Chemistry* **63**, 2397–2400 (1991).

[95] Anbar, M., Halmann, M. & Silver, B. Determination of Oxygen-18 in Phosphate ion. *Analytical Chemistry* **32**, 841–842 (1960).

[96] Firsching, F. H. Precipitation of Silver Phosphate from Homogenous Solution. *Analytical Chemistry* **33**, 873–874 (1961).

[97] O'Neil, J., Roe, L., Reinhard, E. & Blake, R. A rapid and precise method of oxygen isotope analysis of biogenic phosphate. *Israel Journal of Earth Sciences* **43**, 203–212 (1994).

[98] Stephan, E. Oxygen Isotope Analysis of Animal Bone Phosphate: Method Refinement, Influence of Consolidants, and Reconstruction of Palaeotemperatures for Holocene Sites. *Journal of Archaeological Science* **27**, 523–535 (2000).

[99] Lécuyer, C. *Handbook of sStable Isotope Analytical Techniques*, vol. 1, chap. 22, 482–496 (Elsevier, 2004).

[100] Bryant, D., Koch, P., Froelich, P., Showers, W. & Genna, B. Oxygen isotope partitioning between phosphate and carbonate in mammalian apatite. *Geochimica et Cosmochimica Acta* **60**, 5145–5148 (1996).

[101] Vennemann, T. W., Fricke, H. C., Blake, R. E., O'Neil, J. R. & Colman, A. Oxygen isotope analysis of phosphates: a comparison of techniques for analysis of $Ag_3PO_4$. *Chemical Geology* **185**, 321–336 (2002).

[102] McCrea, J. On the Isotopic Chemistry of Carbonates and a Paleotemperature Scale. *Journal of Chemical Physics* **18**, 849–857 (1950).

[103] Swart, P. K., Burns, S. J. & Leder, J. J. Fractionation of the stable isotopes of oxygen and carbon in carbon dioxide during the reaction of calcite with phosphoric acid as a function of temperature and technique. *Chemical Geology: Isotope Geoscience section* **86**, 89–96 (1991).

[104] Land, L. S., Lundelius Jr, E. L. & Valastro Jr, S. Isotopic ecology of deer bones. *Palaeogeography, Palaeoclimatology, Palaeoecology* **32**, 143–151 (1980).

[105] Friedman, I. & O'Neil, J. Compilation of stable isotope fractionation factors of geochemical interest. *U.S. Geological Survey Proof Paper* **440-KK** (1977).

[106] Zazzo, A., Lécuyer, C. & Mariotti, A. Experimentally-controlled carbon and oxygen isotope exchange between bioapatites and water under inorganic and microbially-mediated conditions. *Geochimica et Cosmochimica Acta* **68**, 1–12 (2004).

[107] Koch, P., Tuross, N. & Fogel, M. The effects of sample treatment and diagenesis on the isotopic integrity of carbonate in biogenic hydroxylapatite. *Journal of Archaeological Science* **24**, 417–429 (1997).

[108] Bowen, G. J., West, J. B. & Hoogewerff, J. Isoscapes: Isotope mapping and its applications. *Journal of Geochemical Exploration* **102**, v–vii (2009). Doi: DOI: 10.1016/j.gexplo.2009.05.00.

[109] Bowen, G. *et al.* Isoscapes to address large-scale earth science challenges. *Eos Trans. AGU Electron. Suppl.* **90**, 109–116 (2009).

[110] Kaimal, B., Johnson, R. & Hannigan, R. Distinguishing breeding populations of mallards (Anas platyrhynchos) using trace elements. *Journal of Geochemical Exploration* **102**, 176–180 (2009).

[111] Walther, B. D. & Thorrold, S. R. Inter-annual variability in isotope and elemental ratios recorded in otoliths of an anadromous fish. *Journal of Geochemical Exploration* **102**, 181–186 (2009).

[112] Hobson, K. A., Barnett-Johnson, R. & Cerling, T. Using isoscapes to track animal migration. In *Isoscapes: Understanding movement, pattern, and process on Earth through isotope mapping* (Springer, 2010).

[113] Leavitt, S. W., Treydte, K. & Yu, L. Environment in time and space: Opportunties from tree-ring isotope networks. In *Isoscapes: Understanding movement, pattern and process on Earth through isotope mapping* (Springer, 2010).

[114] Bowen, G. J., Wassenaar, L. I. & Hobson, K. A. Global application of stable hydrogen and oxygen isotopes to wildlife forensics. *Oecologia* **143**, 337–348 (2005).

[115] Wassenaar, L. I., Van Wilgenburg, S. L., Larson, K. & Hobson, K. A. A groundwater isoscape ($\delta D$, $\delta^{18}O$) for Mexico. *Journal of Geochemical Exploration* **102**, 123–136 (2009).

[116] Sjostrom, D. J. & Welker, J. M. The influence of air mass source on the seasonal isotopic composition of precipitation, eastern USA. *Journal of Geochemical Exploration* **102**, 103–112 (2009).

[117] Bowen, G. J. Isoscapes: Spatial pattern in isotopic biogeochemistry. *Annual Review of Earth and Planetary Sciences* **38**, 161–187 (2010).

[118] Thomson, J. Further experiments on positive rays. *Philisophical Magazine Series 6* **24**, 209–253 (1912).

[119] Nier, A. A mass spectrometer for isotope and gas analysis. *Review of scientific instruments* **18**, 398 (1947).

[120] Horita, J. & Kendall, C. *Handbook of Stable Isotope Analytical Techniques*, vol. 1, chap. 1, 1–37 (Elsevier, 2004).

[121] Cohn, M. & Urey, H. C. Oxygen exchange reactions of organic compounds and water. *Journal of the American Chemical Society* **60**, 679–687 (1938).

[122] Hoefs, J. *Stable Isotope Geochemistry* (Springer, 2004), 5 edn.

[123] Brand, W. Mass Spectrometer Hardware for Analysing Stable Isotope Ratios. In *Handbook of Stable Isotope Analytical Techniques* (Elsevier, 2004).

[124] Brand, W. A., Geilmann, H., Crosson, E. R. & Rella, C. W. Cavity ring-down spectroscopy versus high-temperature conversion isotope ratio mass spectrometry; a case study on $\delta^2$H and $\delta^{18}$O of pure water samples and alcohol/water mixtures. *Rapid Communications in Mass Spectrometry* **23**, 1879–1884 (2009).

[125] Sharp, Z. *Principles of stable isotope geochemistry* (Pearson, Prentice Hall, 2007).

[126] Bol, R., Marsh, J. & Heaton, T. Multiple stable isotope analysis of human hair to identify the recent migrants in a rural community in SW England. *Rapid Communications in Mass Spectrometry* **21**, 2951–2954 (2007).

[127] Hijmans, R., Cameron, S., Parra, J., Jones, P. & Jarvis, A. Very high resolution interpolated climate surfaces for global land areas. *International Journal of Climatology* **25**, 1965–1978 (2005).

[128] Hijmans, R., Cameron, S. & Parra, J. Worldclim - global climate data (2010). URL `www.worldclim.org`.

[129] Wushiki, H. $^{18}O/^{16}O$ and D/H of the Meteoric waters in South Arabia. *Journal of the Mass Spectrometry Society of Japan* **39**, 239–250 (1991).

[130] Khademi-Moghari, H. *Stable isotope geochemistry, mineralogy, and microscopy of gypsiferous soils from central Iran*. Ph.D. thesis, University of Saskatchewan (1997).

[131] Bazuhair, A., Hussein, M. & Hamza, M. Recharge sources of some spring waters in Saudi Arabia by use of stable isotopes. *Isotope and Radiation research* **22(2)**, 99–107 (1990).

[132] Zak, I. & Gat, J. Saline waters and residual brines in the Shiraz-Sarvistan basin, Iran. *Chemical Geology* **16**, 179–188 (1975).

[133] Karimi, H. & Moore, F. The source and heating mechanism for the Ahram, Mirahmad and Garu thermal springs, Zagros Mountains, Iran. *Geothermics* **37**, 84–100 (2008).

[134] Robinson, B. W. & Al Ruwaih, F. The stable-isotopic composition of water and sulfate from the Raudhatain and Umm Al Aish freshwater fields, Kuwait. *Chemical Geology: Isotope Geoscience section* **58**, 129–136 (1985).

[135] IAEA/WMO. Global Network of Isotopes in Precipitation. The GNIP Database. Accessible at: http://isohis.iaea.org (2006).

[136] Weyhenmeyer, C. E., Burns, S. J., Waber, H. N., Macumber, P. G. & Matter, A. Isotope study of moisture sources, recharge areas, and groundwater flow paths within the eastern Batinah coastal plain, Sultanate of Oman. *Water Resour. Res.* **38**, 1184– (2002).

[137] Bowen, G. J. Online isotopes in precipitation calculator (2011). URL `http://wateriso.eas.purdue.edu/waterisotopes/index.html`.

[138] Alsharhan, A., Rizk, Z., Nairn, A., Bakhit, D. & Alhajari, S. *Hydrology of an arid region: The Arabian Gulf and adjoining areas* (Elsevier, 2001).

[139] Rozanski, K., Araguás-Araguás, L. & Gonfiantini, R. Isotopic patterns in modern global precipitation. In *Climate change in continental isotopic records* (American Geophysical Union, 1993).

[140] Nier, A. O. The Isotopic Constitution of Strontium, Barium, Bismuth, Thallium and Mercury. *Physical Review* **54**, 275 (1938).

[141] Faure, G. & Powell, J. *Strontium Isotope Geology*. Minerals, Rocks and Inorganic Materials (Springer-Verlag, Berlin-Heidelberg-New York, 1972).

[142] Aldrich, L. T., Wetherill, G. W., Tilton, G. R. & Davis, G. L. Half-Life of $Rb^{87}$. *Physical Review* **103**, 1045 (1956).

[143] Faure, G., Hurley, P. & Powell, J. The isotopic composition of strontium in surface water from the North Atlantic Ocean. *Geochimica et Cosmochimica Acta* **29**, 209–220 (1965).

[144] Sillen, A. & Kavanagh, M. Strontium and paleodietary research: A review. *Yearbook of physical antropology* **25**, 67–90 (1982).

[145] Voerkelius, S. *et al.* Strontium isotopic signatures of natural mineral waters, the reference to a simple geological map and its potential for authentication of food. *Food Chemistry* **118**, 933–940.

[146] Faure, G., Hurley, P. & Powell, J. The isotopic composition of strontium in surface water from the North Atlantic Ocean. *Geochimica et Cosmochimica Acta* **29**, 209 – 220 (1965).

[147] Price, T., Burton, J. & Bentley, R. The characterization of biologically available strontium isotope ratios for the study of prehistoric migration. *Archaeometry* **41**, 117–135 (2002).

[148] Dahl, S. G. *et al.* Incorporation and distribution of strontium in bone. *Bone* **28**, 446–453 (2001).

[149] Aggarwal, J., Habicht-Mauche, J. & Juarez, C. Application of heavy stable isotopes in forensic isotope geochemistry: A review. *Applied Geochemistry* **23**, 2658–2666 (2008).

[150] Bot, B. L., Oulhote, Y., Deguen, S. & Glorennec, P. Using and interpreting isotope data for source identification. *TrAC Trends in Analytical Chemistry* **30**, 302 – 312 (2011).

[151] Almeida, C. M. R. & Vasconcelos, M. T. S. D. Does the winemaking process influence the wine 87Sr/86Sr? A case study. *Food Chemistry* **85**, 7–12 (2004).

[152] Barbaste, M., Robinson, K., Guilfoyle, S., Medina, B. & Lobinski, R. Precise determination of the strontium isotope ratios in wine by inductively coupled plasma sector field multicollector mass spectrometry (ICP-SF-MC-MS). *J. Anal. At. Spectrom.* **17**, 135–137 (2002).

[153] Pillonel, L. *et al.* Stable isotope ratios, major, trace and radioactive elements in emmental cheeses of different origins. *Lebensmittel-Wissenschaft und-Technologie* **36**, 615–623 (2003).

[154] Rossmann, A. *et al.* The potential of multielement stable isotope analysis for regional origin assignment of butter. *European Food Research and Technology* **211**, 32–40 (2000).

[155] Franke, B. *et al.* Tracing the geographic origin of poultry meat and dried beef with oxygen and strontium isotope ratios. *European Food Research and Technology* **226**, 761–769 (2008).

[156] Crittenden, R. *et al.* Determining the geographic origin of milk in Australasia using multi-element stable isotope ratio analysis. *International Dairy Journal* **17**, 421 – 428 (2007).

[157] West, J. B., Hurley, J. M., Duds, F. . & Ehleringer, J. R. The stable isotope ratios of marijuana. ii. strontium isotopes relate to geographic origin. *Journal of Forensic Sciences* **54**, 1261–1269 (2009).

[158] DEGRYSE, P., SCHNEIDER, J., KELLENS, N., WAELKENS, M. & MUCHEZ, P. Tracing the resources of iron working at ancient Sagalassos (South-West Turkey): A combined lead and strontium isotope study on iron artefacts and ores. *Archaeometry* **49**, 75–86 (2007).

[159] Hoppe, K. A., Koch, P. L., Carlson, R. W. & Webb, S. D. Tracking mammoths and mastodons: Reconstruction of migratory behavior using strontium isotope ratios. *Geology* **27**, 439–442 (May, 1999).

[160] Koch, P. L. *et al.* Isotopic tracking of change in diet and habitat use in african elephants. *Science* **267**, 1340–1343 (1995).

[161] Ericson, J. A. Strontium isotope characterization in the study of prehistoric human ecology. *Journal of Human Evolution* **14**, 503 – 514 (1985).

[162] Price, T. D., Johnson, C. M., Ezzo, J. A., Ericson, J. & Burton, J. H. Residential Mobility in the Prehistoric Southwest United States: A Preliminary Study using Strontium Isotope Analysis. *Journal of Archaeological Science* **21**, 315 – 330 (1994).

[163] White, C. D., Price, T. D. & Longstaffe, F. J. Residential histories of the human sacrifices at the Moon Pyramid, Teotihuacan. *Ancient Mesoamerica* **18**, 159–172 (2007).

[164] Sillen, A., Hall, G., Richardson, S. & Armstrong, R. $^{87}Sr/^{86}Sr$ ratios in modern and fossil food-webs of the Sterkfontein Valley: implications for early hominid habitat preference. *Geochimica et Cosmochimica Acta* **62**, 2463–2473 (1998).

[165] Evans, J., Montgomery, J., Wildman, G. & Boulton, N. Spatial variations in biosphere $^{87}Sr/^{86}Sr$ in Britain. *Journal of the Geological Society* **167**, 1–4 (2010).

[166] Hedman, K. M., Curry, B. B., Johnson, T. M., Fullagar, P. D. & Emerson, T. E. Variation in strontium isotope ratios of archaeological fauna in the midwestern united states: a preliminary study. *Journal of Archaeological Science* **36**, 64–73 (2009).

[167] Montgomery, J., Evans, J. A. & Cooper, R. E. Resolving archaeological populations with Sr-isotope mixing models. *Applied Geochemistry* **22**, 1502 – 1514 (2007).

[168] Budd, P., Montgomery, J., Evans, J. & Chenery, C. Combined Pb, Sr and O isotope analysis of human dental tissue for the reconstruction of Archaeological residential mobility. *Plasma Source MAss Spectrometry: The New Millennium* 300–323 (2001).

[169] Fisher, W. B. *The Middle East: A Physical, Social and Regional Geography* (Methuen & co. LTD, 1957).

[170] Pollastro, R., Karshbaum, A. & Viger, R. Maps showing geology, oil and gas fields and geologic provinces of the Arabian peninsula. *USGS Open file report 97-470B* (1998).

[171] Pollastro, R., Persits, F. & Steinshouer, D. Map showing geology, oil and gas fields, and geologic provinces of Iran. *USGS Open file report 97-470G* (1998).

[172] Weyhenmeyer, C. E., Waber, H. N., Kramers, J., Burns, S. J. & Matter, A. Strontium Isotope Ratios ($^{87}Sr/^{86}Sr$) as Tracers for Recharge Areas, Groundwater Movement and Mixing in an Arid Coastal Region of the Sultanate of Oman. *AGU Fall Meeting Abstracts* D260+ (2001).

[173] Chiesa, S., Civetta, L., Fino, M. D., Volpe, L. L. & Orsi, G. The Yemen trap series: Genesis and evolution of a continental flood basalt province. *Journal of Volcanology and Geothermal Research* **36**, 337 – 350 (1989).

[174] Rehkämper, M., Schönbächler, M. & Stirling, C. H. Multiple Collector ICP-MS: Introduction to Instrumentation, Measurement Techniques and Analytical Capabilities. *Geostandards Newsletter* **25**, 23–40 (2001).

[175] Micromass. *Isoprobe Users Guide, Code: 6666633, Issue 1*. Micromass Ltd.

[176] Rehkmper, M., Schnbchler, M. & Stirling, C. H. Multiple Collector ICP-MS: Introduction to Instrumentation, Measurement Techniques and Analytical Capabilities. *Geostandards Newsletter* **25**, 23–40 (2001).

[177] Walder, A. J. & Freedman, P. A. Communication. isotopic ratio measurement using a double focusing magnetic sector mass analyser with an inductively coupled plasma as an ion source. *J. Anal. At. Spectrom.* **7**, 571–575 (1992).

[178] Horwitz, E. *et al.* A lead-selective extraction chromatographic resin and its application to the isolation of lead from geological samples. *Analytica Chimica Acta* **292**, 263–273 (1994).

[179] Reimann, C. *et al. Agricultural soils in Northern Europe: a geochemical atlas* (E. Schweizerbartsche Verlagsbuchhandlung, 2003).

[180] Kabata-Pendias, A. & Pendias, H. *Trace Elements in Soils and Plants* (CRC Press, 2001).

[181] Schroeder, H. & Nason, A. Trace element analysis in clinical chemistry. *Clinical Chemistry* **17**, 461–474 (1971).

[182] Foth, H. Soil as a natural body. In *Fundamentals of soil science*, 11–21 (John Wiley and Sons, 1990).

[183] Taylor, S. & McLennan, S. *The continental crust: Its composition and evolution* (Blackwell Scientific Publ., 1985).

[184] Faure, G. *Principles and applications of inorganic geochemistry* (Macmillan Publishing Company, 1991).

[185] Hunt, C. Minerology and geochemistry. In *Geology of Soils: Their evolution, classification and uses*, 253–285 (1972).

[186] Adriano, D. *Trace elements in the terrestrial environment* (Springer-Verlag, 1986).

[187] Zimmermann, M. *Micronutrients in health and disease* (Thieme, 2001).

[188] Doyle, J. & Spaulding, J. Toxic and essential trace elements in meat - a review. *J ANIM SCI* **47**, 398–419 (1978).

[189] Webb, E. *et al.* Inductively coupled plasma-mass (ICP-MS) and atomic emission spectrometry (ICP-AES): Versatile analytical techniques to identify the archived elemental information in human teeth. *Microchemical Journal* **81**, 201 – 208 (2005).

[190] Sharma, R. & Shupe, J. Lead, cadmium, and arsenic residues in animal tissues in relation to those in their surrounding habitat. *Science of The Total Environment* **7**, 53 – 62 (1977).

[191] Iyengar, V. & Woittiez, J. Trace elements in human clinical specimens: evaluation of literature data to identify reference values. *Clin Chem* **34**, 474–481 (1988).

[192] Balluz, L. S., Kieszak, S. M., Philen, R. M. & Mulinare, J. Vitamin and Mineral Supplement Use in the United States: Results From the Third National Health and Nutrition Examination Survey. *Arch Fam Med* **9**, 258–262 (2000).

[193] Amr, M. & Helal, A. Analysis of trace elements in teeth by ICP-MS: Implications for caries. *Journal of Physical Science* **21(2)**, 1–12 (2010).

[194] Mertz, W. The essential trace elements. *Science* **213**, 1332–1338 (1981).

[195] Blott, S. J., Croft, D., Pye, K., Saye, S. E. & Wilson, H. Particle size analysis by laser diffraction. In *Forensic Geoscience: Principles techniques and applications*, vol. 232, 63–73 (Geological Society, London, Special Publications, 2004).

[196] Pye, K. Forensic examination of rocks, sediments, soils and dust using scanning electron microscopy and x-ray chemical microanalysis. In *Forensic Geoscience: Principles, techniques and applications*, vol. 232, 103–121 (Geological Society, London, Special Publications, 2004).

[197] Jarvis, K., Wilson, H. & James, S. Assessing element variability in small soil samples taken during forensic investigation. vol. 232, 171–182 (Geological Society, London, Special Publications, 2004).

[198] Pye, K. & Blott, S. J. Comparison of soils and sediments using major and trace element data. In *Forensic Geoscience: Principles, techniques and applications*, vol. 232, 183–196 (Geological Society, London, Special Publications, 2004).

[199] Pye, K., Blott, S., Croft, D. & Carter, J. Forensic comparison of soil samples: Assessment of small-scale spatial variability in elemental composition, carbon and nitrogen isotope ratios, colour, and particle size distribution. *Forensic Science International* **163**, 59–80 (2006).

[200] Concheri, G. *et al.* Chemical elemental distribution and soil dna fingerprints provide the critical evidence in murder case investigation. *PLoS ONE* **6** (2011).

[201] Day, M. P., Zhang, B. & Martin, G. J. Determination of the geographical origin of wine using joint analysis of elemental and isotopic composition. iidifferentiation of the principal production zones in France for the 1990 vintage. *Journal of the Science of Food and Agriculture* **67**, 113–123 (1995).

[202] Watling, J. *et al.* The applictaion of solution and laser ablation based ICP-MS and solution based AES for the provenance determination of selected food and drink produce. *THe Open Chemical and Biomedical Methods Journal* **3**, 179–196 (2010).

[203] Pilgrim, T. S., Watling, R. J. & Grice, K. Application of trace element and stable isotope signatures to determine the provenance of tea (Camellia sinensis) samples. *Food Chemistry* **118**, 921 – 926 (2010). Food Authenticity & Traceability.

[204] Posey, R. *Multi-element analysis of a selection of European olive oils by ICP-MS and a newly proposed LA-ICP-MS technique*. Master's thesis, University of East Anglia, School of Chemistry (2008).

[205] McGaw, E. A., Szymanski, D. W. & Smith, R. W. Determination of Trace Elemental Concentrations in Document Papers for Forensic Comparison Using Inductively Coupled PlasmaMass Spectrometry. *Journal of Forensic Sciences* **54**, 1163–1170 (2009).

[206] May, C. & Watling, R. A comparison of the use of refractive index (RI) and laser ablation inductively coupled plasma mass spectrometry (LA-ICP-MS) for the provenance establishment of glass bottles. *Forensic Science, Medicine, and Pathology* **5**, 66–76 (2009).

[207] Koons, R. & Buscaglia, J. Forensic significance of bullet lead compositions. *Journal of Forensic Sciences* **50**, 341–351 (2005).

[208] Cucina, A., Tiesler, V., Sierra Sosa, T. & Neff, H. Trace-element evidence for foreigners at a Maya port in Northern Yucatan. *Journal of Archaeological Science* **38**, 1878–1885 (2011).

[209] Ezzo, J. A. Zinc as a paleodietary indicator: An issue of theoretical validity in bone-chemistry analysis. *American Antiquity* **59**, pp. 606–621 (1994).

[210] Cucina, A., Dudgeon, J. & Neff, H. Methodological strategy for the analysis of human dental enamel by LA-ICP-MS. *Journal of Archaeological Science* **34**, 1884–1888 (2007).

[211] Hirata, T. & Miyazaki, Z. High-Speed Camera Imaging for Laser Ablation Process:For Further Reliable Elemental Analysis Using Inductively Coupled Plasma-Mass Spectrometry. *Analytical Chemistry* **79**, 147–152 (2007).

[212] Dolphin *et al.* Variation in elemental intensities among teeth and between pre- and postnatal regions of enamel. *American Journal of Physical Anthropology* **128**, 878–888 (2005).

[213] Dolphin, Alexis, E., Goodman & Alan, H. Maternal diets, nutritional status, and zinc in contemporary mexican infants' teeth: Implications for reconstructing paleodiets. *American Journal of Physical Anthropology* **140**, 399–409 (2009).

[214] Kang, D., Amarasiriwardena, D. & Goodman, A. Application of laser ablationinductively coupled plasma-mass spectrometry (LAICPMS) to investigate trace metal spatial distributions in human tooth enamel and dentine growth layers and pulp. *Analytical and Bioanalytical Chemistry* **378**, 1608–1615 (2004).

[215] Chavagnac, V. *et al.* Towards the development of a fossil bone geochemical standard: An inter-laboratory study. *Analytica Chimica Acta* **599**, 177–190 (2007).

[216] Russo, R. & Mao, X. *Laser ablation and Desorption*. 8 (Academic Press, 1998).

[217] Thomas, R. A beginner's guide to ICP-MS: Part 1. *Spectroscopy* **16(4)**, 38 – 42 (2001).

[218] Technologies, A. *ICP-MS: A primer* (Agilent Technologies, 2005). URL `www.chem.agilent.com`.

[219] Neufeld, L. Introduction to Laser Ablation ICP-MS for Analysis of forensic samples. *Agilent Technologies* (2004).

[220] Haglund, R. *Laser Ablation and Desorption* (Academic Press, 1998).

[221] Flyvholm, M.-A., Nielsen, G. D. & Andersen, A. Nickel content of food and estimation of dietary intake. *Zeitschrift fr Lebensmitteluntersuchung und -Forschung A* **179**, 427–431 (1984).

[222] Pate, F. Bone chemistry and paleodiet. *Journal of archaeological method and theory* **1**, 161–209 (1994).

[223] R Development Core Team. *R: A Language and Environment for Statistical Computing*. R Foundation for Statistical Computing, Vienna, Austria (2010). URL `http://www.R-project.org/`. ISBN 3-900051-07-0.

[224] Wunder, M. B. & Norris, D. R. Improved estimates of certainty in stable-isotope-based methods for tracking migratory animals. *Ecological Applications* **18**, 549–559 (2008).

[225] Royle, J. & Rubenstein, D. The role of species abundance in determining breeding origins of migratory birds with stable isotopes. *Ecological Applications* **14(6)**, 1780–1788 (2004).

[226] U.S. supreme court. Daubert v. Merrell Dow Pharmaceuticals, INC. *509 U.S.* 596–597 (1993).

[227] Ehleringer, J. & Matheson, S. Stable isotopes and courts. *Utah law review* **2** (2010).

[228] Saks, M. J. & Koehler, J. J. The coming paradigm shift in forensic identification science. *Science* **309**, 892–895 (2005).

[229] Gridded population of the world version 3 (gpwv3): Population density grids (2005). URL `http://sedac.ciesin.columbia.edu/gpw/`.

[230] Bowen, G., West, J., Liu, Z. & Miller, C. Isomap (2011). URL `http://isomap.org`.

[231] Batille, C. P. & Bowen, G. Mapping $^{87}Sr/^{86}Sr$ variations in bedrock and water for regional migration studies. *Isoscapes conference proceedings* (2011).

[232] Wunder, M. *Isoscapes*, chap. 12e, 251–272 (Springer, 2010).

[233] Bell, L., Lee-Thorp, J. & Elkerton, A. The sinking of the Mary Rose warship: A medieval mystery solved. *Journal of Archaeological Science* **36**, 166–173 (2009).

[234] Lee-Thorp, J. A. On isotopes and old bones. *Archaeometry* **50**, 925–950 (2008).